PROGRAMA DE DOCTORADO EN BIOMEDICINA

UNIVERSIDAD DE GRANADA

Tesis Doctoral

◊

Development and Evaluation of Smart Polymeric and Lipidic Nanoparticles for Theranosis of Breast and Pancreatic Cancer

Memoria presentada por Don. SAÚL ABENHAMAR NAVARRO MARCHAL para optar a la mención de Doctor Internacional por la Universidad de Granada

Granada, 2020

Editor: Universidad de Granada. Tesis Doctorales
Autor: Saúl Abenhamar Navarro Marchal
ISBN: 978-84-1117-323-0
URI: http://hdl.handle.net/10481/74728

A Raquel e Ismael

Eso desean los que viven en estos tiempos, pero no nos toca a nosotros decidir qué tiempo vivir, solo podemos elegir qué hacer con el tiempo que se nos ha dado.

Palabras de Gandalf a Frodo en las profundidades de Khazad-dûm.

INDEX

ABSTRACT

ABSTRACT

Nanomedicine is playing a growing part in pharmaceutical research and development, primarily in the form of nanoparticle-based delivery systems for drugs and imaging agents. The development of targeted therapies, especially for cancer, is one of the main goals of nanomedicine today. Conventional chemotherapy usually prompts modest tumor response and provokes undesirable side effects due to the nonspecific action of drugs on proliferating tissues. To avoid these and other disadvantages, drug nanocarriers should be formulated to deliver the antitumor drug directly to the cancerous cells. The main objective of the application of nanomedicine in cancer is to have a better therapeutic effect, to increase the bioavailability and to allow the administration of lower doses of drug while obtaining lower toxicity rates and improving the patient's quality of life. Another objective is to overcome the multiple mechanisms of drug resistance that make this treatment ineffective in a high percentage of cancer cases since some subpopulations of tumor cells have the ability to evade drug associated cytotoxicity.

However, to have a real translation of nanomedicine in patients it is necessary the interdisciplinary collaboration of different scientist areas since there is too many variables to be properly controlled. These variables include the use of biocompatible materials, with simple but robust processes for biomaterial assembly, usually requiring different conjugation chemistries followed by some purification processes. Therefore, current formulations based on complex nanostructures such as polymer conjugates, polymeric micelles, liposomes, carbon nanotubes, or nanoparticles, must be superficially modified to provide carriers with vectorization properties. Moreover, our research group has developed several strategies for preparing functionalized polymeric cross-linked polystyrene nanoparticles (NPs), which are covalently conjugated to cargoes of different nature. On the other hand, in recent years, lipid liquid nanocapsules (LLNCs) have been developed as potential nanocarriers. The inner hydrophobic domain, surrounded by an amphiphilic shell, has been used to encapsulate hydrophobic drugs that are protected during their transport to the target cells.

Thus, the main objective of this thesis has been the development and evaluation of two different nanosystems in its composition, for the diagnosis and treatment of

breast and pancreatic cancer. One of the nanosystems used has been polystyrene NPs. A novel chemical-based orthogonal bioconjugation strategy to produce tri-functionalized NPs carrying doxorubicin (DOX), near-infrared cyanine dye (Cy7) and a homing peptide CRGDK, a peptide specifically binds to neuropilin-1 (Nrp-1) overexpressed on triple negative breast cancer (TNBC) cells, has been validated. These theranostic NPs have been evaluated *in vitro* and *in vivo* using an orthotopic xenotransplant mouse model using TNBC cells. *In vitro* assays show that theranostic NPs improve the therapeutic index in comparison with free DOX. Remarkably, *in vivo* studies showed preferred location of theranostic NPs in the tumor area reducing the volume at the same level than free DOX while presenting lower side effects. Another of the nanosystems used have been LLNCs, specifically olive oil liquid nanocapsules (O^2LNC). These LLNCs have been modified to evaluate several biological properties against cancer. In this sense, LLNCs covered by the human serum albumin (HSA) protein and loaded with curcumin as a hydrophobic model drug have been successfully developed. A cross-linking procedure with glutaraldehyde (GAD) was performed to further strengthen the protective protein layer. Physicochemical properties and release kinetics of the nanocapsules were investigated, and cellular uptake and killing capacity were evaluated on the MCF-7 human breast-cancer line. The nanocapsules exhibited a cytotoxic capacity (IC_{50}) similar to that of free curcumin, but avoiding the problems associated with excipients, and displayed an outstanding uptake performance, entering cells massively in less than 1 min. On the other hand, O^2LNC functionalized by covalent coupling of an anti-CD44-FITC antibody (αCD44) that can specifically target pancreatic cancer stem cells (PCSCs) overexpressing the CD44 receptor have been successfully developed. Firstly, O^2LNCs formed by a core of olive oil were surrounded by a shell containing phospholipids (Epikuron®), a non-ionic surfactant (Pluronic® F68) and deoxycholic acid molecules to provide a surface enriched in solvent-exposed free carboxylic acid functional groups. Then, O^2LNCs were coated with an αCD44 antibody to the optimized formulation of immuno-nanocapsules (αCD44-O^2LNC). The optimization of an αCD44 coating procedure, a complete physico-chemical characterization of these functionalized nanosystems, as well as clear evidence of their efficacy *in vitro* and *in vivo,* were demonstrated. Our results indicate the high targeted uptake of these αCD44-O^2LNCs and the increased antitumor efficacy (up to four times) of paclitaxel-loaded

αCD44-O^2LNC compared to free paclitaxel in PCSCs. Also, αCD44-O^2LNCs were able to selectively target PCSCs in an orthotopic xenotransplant *in vivo* model.

RESUMEN

RESUMEN

La nanomedicina está desempeñando un papel cada vez más importante en la investigación y el desarrollo farmacéutico, principalmente en forma de sistemas de administración de fármacos y agentes de imagen basados en nanopartículas. El desarrollo de terapias dirigidas, especialmente contra el cáncer, es uno de los principales objetivos de la nanomedicina en la actualidad. La quimioterapia convencional generalmente provoca una respuesta tumoral modesta y produce efectos secundarios indeseables debido a la acción inespecífica de los medicamentos sobre los tejidos en proliferación. Para evitar estas y otras desventajas, los nano-transportadores de fármacos deben formularse para administrar el fármaco antitumoral directamente a las células cancerígenas. El objetivo principal de la aplicación de la nanomedicina en el cáncer es tener un mejor efecto terapéutico, aumentar la biodisponibilidad y permitir la administración de dosis más bajas de fármaco mientras se obtienen tasas de toxicidad más bajas y se mejora la calidad de vida del paciente. Otro objetivo es superar los múltiples mecanismos de resistencia a los medicamentos que hacen que este tratamiento sea ineficaz en un alto porcentaje de casos de cáncer, ya que algunas subpoblaciones de células tumorales tienen la capacidad de evadir la citotoxicidad asociada a la quimioterapia.

Sin embargo, para conseguir una traslación real de la nanomedicina a los pacientes, es necesaria la colaboración interdisciplinar de diferentes áreas científicas, ya que existen demasiadas variables que deben ser controlarlas adecuadamente. Estas variables incluyen el uso de materiales biocompatibles, obtenidos mediante el ensamblaje de biomateriales mediante procesos simples pero robustos, y que generalmente requieren diferentes químicas de conjugación seguidas de algunos procesos de purificación. Por lo tanto, las formulaciones actuales basadas en nanoestructuras complejas tales como conjugados poliméricos, micelas poliméricas, liposomas, nanotubos de carbono o nanopartículas, deben modificarse superficialmente para proporcionar nano-transportadores con propiedades de vectorización. Además, nuestro grupo de investigación ha desarrollado varias estrategias para preparar nanopartículas de poliestireno que luego se conjugan covalentemente con moléculas de diferente naturaleza. Del mismo modo, en los últimos años, se han desarrollado

nanocápsulas lipídicas liquidas (LLNC) como potenciales nano-transportadores. El dominio hidrofóbico interno, rodeado por una corteza anfifílica, se ha utilizado para encapsular medicamentos hidrofóbicos que están protegidos durante su transporte a las células diana.

Por lo tanto, el objetivo principal de esta tesis ha sido el desarrollo y la evaluación de dos nanosistemas diferentes en su composición, para el diagnóstico y tratamiento del cáncer de mama y de páncreas. Uno de los nanosistemas utilizados han sido las nanopartículas (NPs) de poliestireno. Se ha validado una nueva estrategia de bioconjugación ortogonal basada en productos químicos para producir NPs trifuncionalizadas, vehiculizando doxorrubicina (DOX), un colorante que emite en el infrarrojo cercano (Cy7) y un péptido específico CRGDK, que se une específicamente a la neuropilina-1 (Nrp-1, la cual se encuentra sobreexpresada en células de cáncer de mama triple negativo (TNBC). Estas NPs teranósticas se han evaluado *in vitro* e *in vivo* utilizando un modelo de xenotrasplante ortotópico en ratones de células TNBC. Los ensayos *in vitro* muestran que las NPs teranósticas mejoran el índice terapéutico en comparación con la DOX libre. Sorprendentemente, los estudios *in vivo* mostraron la ubicación preferida de las NPs teranósticas en el área del tumor, reduciendo el volumen al mismo nivel que la DOX libre pero presentando efectos secundarios más bajos. Otro de los nanosistemas utilizados han sido las LLNC, específicamente las nanocápsulas líquidas de aceite de oliva (O^2LNCs). Estas LLNC han sufrido varias modificaciones. Por un lado, se han desarrollado con éxito O^2LNCs cubiertas por la proteína albúmina sérica humana (HSA) y cargadas con curcumina como fármaco modelo de tipo hidrofóbico. Se realizó un procedimiento de reticulación con glutaraldehído (GAD) para fortalecer aún más la capa proteica protectora. Además, se investigaron las propiedades fisicoquímicas y la cinética de liberación de las nanocápsulas, y se evaluó la absorción celular y citotoxicidad en la línea de cáncer de mama humano MCF-7. Las nanocápsulas exhibieron una capacidad citotóxica (IC_{50}) similar a la de la curcumina libre, pero evitando los problemas asociados con los excipientes, y mostraron un rendimiento de absorción altísimo, internalizándose en las células de forma masiva en menos de 1 minuto. Por otro lado, se han desarrollado con éxito O^2LNC funcionalizadas mediante el acoplamiento covalente de un anticuerpo anti-CD44-FITC (αCD44) que puede dirigirse

específicamente a las células madre cancerígenas pancreáticas (PCSC), que sobreexpresan el receptor CD44. En primer lugar, las O^2LNC formados por un núcleo de aceite de oliva fueron recubiertos por una cubierta que contenía fosfolípidos (Epikuron®), un tensioactivo no iónico (Pluronic® F68) y moléculas de ácido desoxicólico para proporcionar una superficie enriquecida en grupos funcionales de ácido carboxílico libre expuesto al medio de dispersión. Luego, las O^2LNC se funcionalizaron con un anticuerpo αCD44 para la formulación optimizada de inmuno-nanocápsulas (αCD44-O^2LNC). Se demostró la optimización de un procedimiento de funcionalización αCD44, mediante una caracterización fisicoquímica completa de estos nanosistemas funcionalizados, así como una clara evidencia de su eficacia *in vitro* e *in vivo*. Nuestros resultados indican la alta captación selectiva de estas αCD44-O^2LNC y la mayor eficacia antitumoral (hasta cuatro veces) de αCD44-O^2LNC cargadas con paclitaxel en comparación con paclitaxel libre en PCSCs. Además, los αCD44-O^2LNC pudieron dirigirse selectivamente a las PCSCs y acumularse en el tumor en un modelo *in vivo* de xenotrasplante ortotópico de cáncer de páncreas.

INTRODUCTION

1. CANCER

1.1. Definition

Cancer encompasses a heterogeneous group of disorders with very different biological properties, applying this general term to define those diseases characterized by abnormal and uncontrolled growth of the cells of a tissue or organ that extend beyond their usual limits and can invade adjacent parts of the body or spread to other organs through the lymphatic system and blood circulation through a process known as metastasis[1].

Cancer is also referred to as a malignant tumor or malignant neoplasm. The Greek term "*neoplasia*" means new growth, and refers to the abnormal and uncontrolled proliferation of cells in a tissue or organ. Most neoplasms proliferate to form distinct masses, tumors, with malignant neoplasms or malignant tumors being characterized by a high degree of anaplasia and invasiveness[1]. Within the process of the development of cancer or carcinogenesis, it is called tumorigenesis or oncogenesis to the transition from a normal cell to a tumor cell capable of initiating a tumor, while it is called tumor progression to the transition of the tumor to metastasis and, often , the acquisition of cancer resistance to treatment[2].

1.2. Epidemiology

According to the latest data compiled by GLOBOCAN, in 2018 there were approximately 18.1 million new cases of cancer in the world (**Figure 1**), and 9,6 million deaths were due to this disease (**Figure 2**). The most frequent types of cancer differ between developed and developing countries, as well as between men and women. However, globally, the five types of cancer with the highest incidence in the world population are: lung, breast, colorectal, prostate and stomach represented in **Figure 1.**

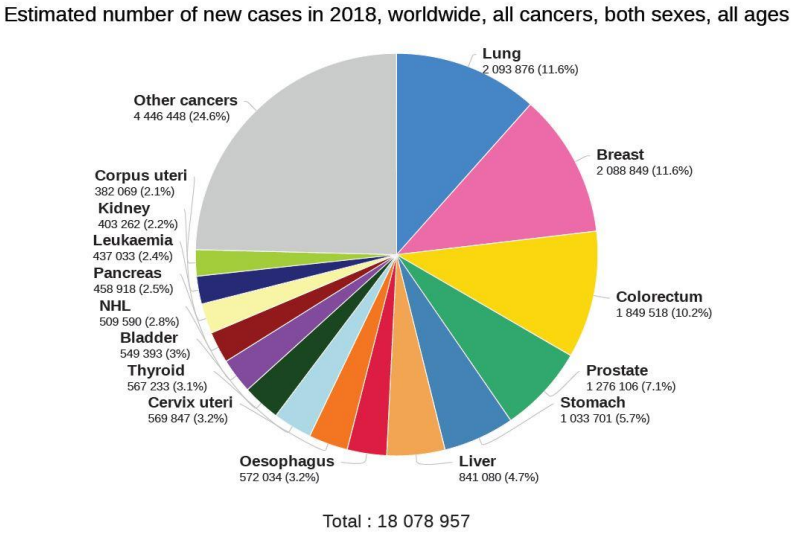

Figure 1: Pie chart present the distribution of new cases of cancers in 2018 for both sexes worldwide. GLOBOCAN 2018.

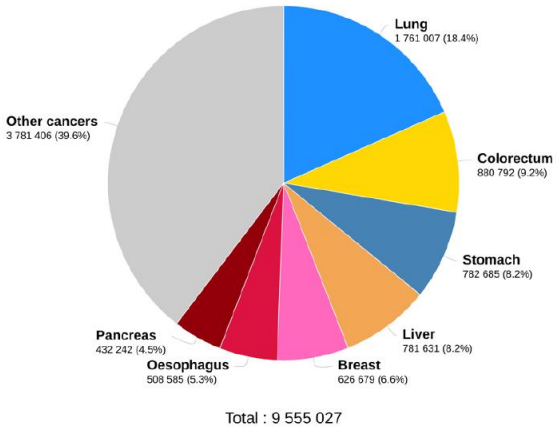

Figure 2: Pie chart present the distribution of deaths for the 10 most common cancers in 2018 for both sexes worldwide. GLOBOCAN 2018.

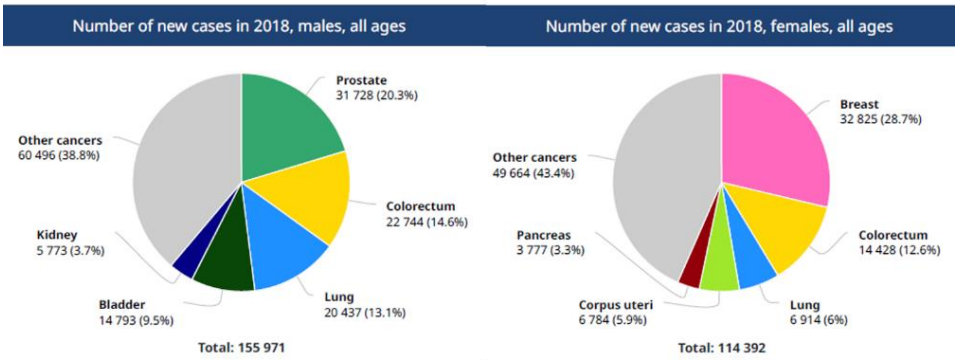

Figure 3: Pie chart present the distribution of cases for the 10 most common cancers in 2018 for males and females in Spain. GLOBOCAN 2018.

In Spain, the neoplasms constitute the second cause of mortality, representing 33.1% of the total deaths registered in 2018 according to the latest data published by the National Statistics Institute, reaching 45% of the total when considering the Age group between 40 and 79 years. The types of cancer with the highest incidence among men in our country are prostate, with 20,3% of the total cases registered in 2018; the colorectal, with 14,6% and the lung with 13,1%; while the most frequent in women are breast cancer, which represents 28.7% of all registered cancers; the colorectal, with 12,6%; and the lung, with 7% (**Figure 3**). On the other hand, lung cancer is the leading cause of mortality from this disease in both sex in Spain, followed by colorectal and breast (**Figure 4**).

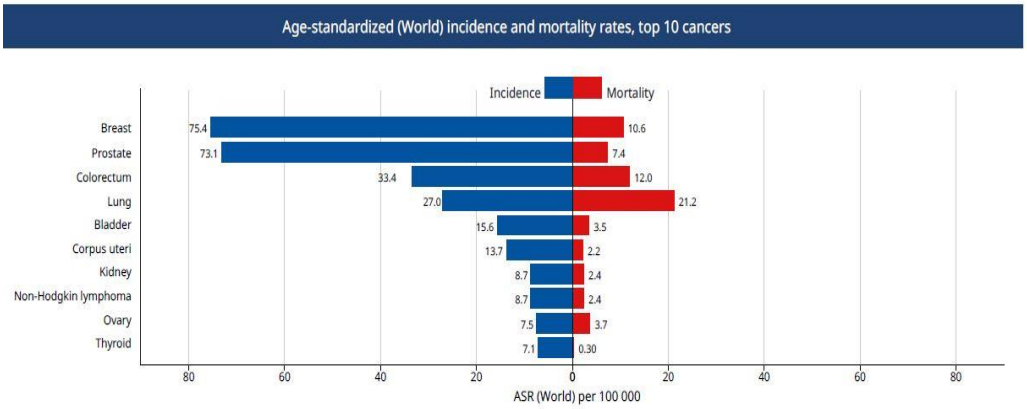

Figure 4: Dual bars present the incidence and mortality rates of the top 10 cancers in Spain. GLOBOCAN 2018.

Aging is another fundamental factor for the development of cancer. The incidence of cancer increases dramatically with age, probably due to an accumulation of risks of specific cancers, combined with the tendency of cell repair mechanisms to lose their effectiveness when the person ages[1]. The expected population increase for the coming years also foresees an aging population, with an annual increase of 2.44% of people over 60 years of age and an annual increase of 3.35% of the number of people for the next decades exceed 80 years old. This increase will be greater in developing countries for both age groups. These data imply an increase from the current 12.7% to 25.8% of the population over 60 years of age in the world by 2050 (UN, 2011). In

addition, regardless of the population increase and the aging population, an augment in the incidence rates of this disease has also been observed, which implies a progressive increase in the occurrence of new cancer cases in the future[1].

1.3. Etiology

Transformation from a normal cell to a tumor cell is a staggered process, which typically involves a progression from a precancerous lesion to a malignant tumor. These changes are the result of the interaction between the person's genetic factors and environmental factors[3]. These environmental factors include chemicals, complex mixtures, occupational exposures, physical agents, biological agents and lifestyle-related factors (International Agency for Research on Cancer. IARC, 2012). Especially important are the so-called carcinogens, external agents that increase the risk of developing cancer, which can be subdivided into three main categories: i) physical carcinogens, ii) chemical carcinogens and iii) biological carcinogens[4].

Different types of ionizing and non-ionizing radiation are included among physical carcinogens. The main non-ionizing radiations are ultraviolet (UV) radiation, visible radiation and infrared radiation, all of which have the sun as their main source. This type of radiation shows a low penetration power, so they represent a real danger to the eyes and skin[4]. UV radiation is the one with the greatest carcinogenic power, and it has been shown that exposure to this type of radiation significantly increases the risk of skin cancer (IARC, 2012).

Regarding chemical carcinogens, they were initially identified by observing the existence of a relationship between certain types of cancer and certain occupations that involved exposure to certain substances, such as soot or tar[4]. At present, several studies have corroborated the carcinogenic effect of many substances such as aflatoxins, arsenic, asbestos, formaldehyde and benzene among many others (IARC, 2012).

Tobacco smoke is the most common source of chemical carcinogens for humans, and it is estimated that smoking is responsible for approximately 30% of cancer cases in high-income countries. Tobacco smoke contains about 4,800 different compounds, of which 66 are carcinogens. Of these, polycyclic aromatic hydrocarbons and tobacco-specific nitrosamines are the most important, although it also has other carcinogenic

substances such as aromatic amines, heavy metals and benzene. Tobacco use causes 13 types of cancer, although lung cancer is the most relevant among all cancers attributable to smoking.

Biological carcinogens include infections by certain viruses, bacteria or parasites[1]. Approximately 95% was associated with Helicobacter pylori infections, hepatitis B and C viruses, and human papillomavirus[5].

Different studies show that obesity and alcohol consumption increase the risk of certain types of cancer. On the other hand, physical activity reduces the incidence of different types of cancer, and also counteracts some of the adverse effects of cancer treatments, attenuates the progression of the disease and reduces the risk of recurrence, apart from providing other benefits for health[6]. In addition, other factors related to cancer risk are certain reproductive factors and hormones, both endogenous and exogenous. These are strongly involved in the etiology of breast, endometrial, ovarian and cervical cancers in women[1].

On the other hand, it has been observed that some cancers have a hereditary component and tend to show family aggregation, although it is estimated that only 5-10% of cancer cases are due to inherited germline mutations[3]. Genetic susceptibility to cancer is focused on the study of inherited genetic variations and their association with cancer risk. In this sense, many studies show that some genetic polymorphisms in certain genes increase the risk of certain types of cancer[7]. These cancer susceptibility genes are usually mainly oncogenes, tumor suppressor genes or cancer risk modifying genes. Various susceptibility genes have been identified and related to the risk of suffering from various types of cancer such as breast, colorectal, prostate, lung or bladder, among others[7].

1.4. Carcinogenesis

Carcinogenesis is a staggered process, during which cells undergo profound metabolic and behavioral changes that lead to excessive and premature proliferation, allowing them to escape the action of the immune system and eventually invade distant tissues to form metastases[1,8]. The development of cancer is driven by the accumulation

of alterations that affect the structure and function of the genome, while genetic alterations and epigenetic changes are equally important in this process.

In order for a cell to become cancerous, it has to acquire certain characteristics, among which are mainly: i) the maintenance of proliferative signaling, ii) the evasion of growth suppressing mechanisms, iii) resistance to cell death, iv) the replicative immortality, v) the induction of angiogenesis, vi) and the activation of its invasion and metastasis capacity[9] (**Figure 5**). In addition, in recent years two new characteristics of cancer cells that can bind to those mentioned above have been described, such as: vii) reprogramming of energy metabolism, viii) and the ability to evade their destruction by the immune system[10] (**Figure 5**). In addition to these characteristics, several studies have shown that, in the early stages of the neoplasms, the cells show certain characteristics that, in turn, allow the acquisition of the characteristics mentioned above, such as: ix) genomic instability and increase in mutation rates[11]; x) and the induction of inflammatory processes[12] (**Figure 5**).

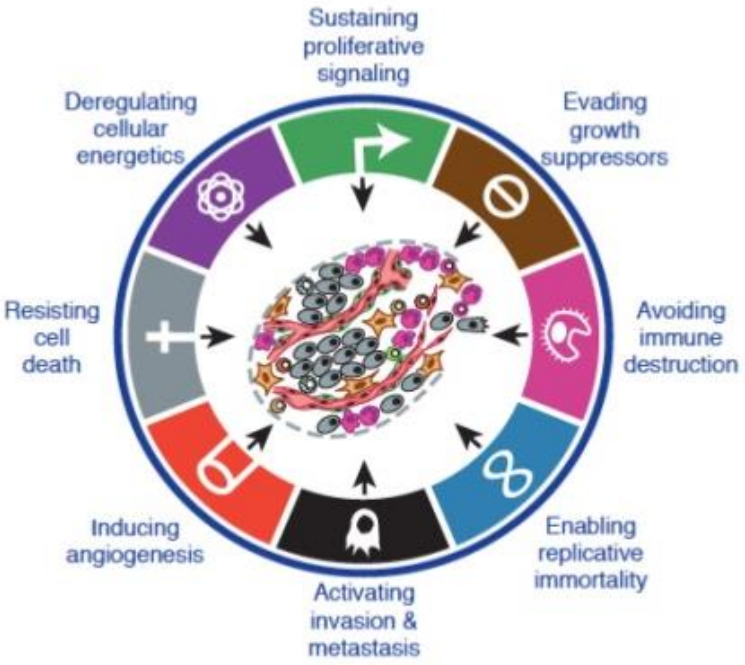

Figure 5. Main characteristics of cancer cells (Image modified from Hanahan and Weinberg[9])

1.4.1. Maintenance of proliferative signaling.

Cancer cells can acquire high proliferative capacity through different pathways. One possibility is the production of mitogenic growth factors by the tumor cell itself that stimulate its proliferation in an autocrine way[13]. Alternatively, the interactions of cancer cells with normal cells, which support the tumor, can stimulate them to provide growth factors to cancer cells[14]. Another mechanism consists in increasing the expression levels of surface receptor proteins in cancer cells, making them more sensitive to growth factors.

Within the human genome, there are a large number of genes involved in the process of cell proliferation, known as protooncogenes. These genes are referred to as oncogenes, and their oncoprotein products, when they appear mutated or expressed incorrectly, accelerating progression through the cell cycle and producing an uncontrolled proliferation of cells[15].

1.4.2. Evasion of growing suppressing mechanisms.

In addition to the ability of cancer cells to induce and keep growth stimulating signals activated, these cells must also bypass powerful programs that negatively regulate cell proliferation. Many of these programs depend on the action of genes called tumor suppressors[9]. Epigenetic mutations or alterations that inactivate these genes cause an increase in mutation rates, favoring the appearance of mutations in other tumor suppressor genes and protooncogenes and, therefore, promoting carcinogenesis[16].

1.4.3. Resistance to cell death.

Apoptosis is a strictly regulated form of cell death that plays a fundamental role in normal development and tissue homeostasis by eliminating unnecessary or harmful cells[17]. There are two main apoptotic pathways: i) the extrinsic pathway, which receives and processes apoptosis-inducing extracellular signals, ii) and the intrinsic route, which detects and integrates a variety of signals of intracellular origin.[9,17,18]Apart from apoptosis, there are other mechanisms of cell death, including autophagy, necrosis and mitotic catastrophe[19].

1.4.4. Angiogenesis induction.

Like normal tissues, tumors require food in the form of nutrients and oxygen, as well as the ability to evacuate metabolic wastes and CO_2. The neovasculature associated with the tumor, generated by the angiogenic process, is aimed at meeting these needs[9]. However, tumor vessels are disorganized and heterogeneous, showing certain structural and functional differences with those of normal vasculature[20].

1.4.5. Replicative immortality.

Most normal cell lineages in the body have a limited number of growth and division cycles. This limitation has been associated with two distinct barriers that restrict proliferation: i) senescence, which entails an entry, usually irreversible, into a non-proliferative, but viable state; ii) and the crisis, which implies cell death. On some occasions, cells in culture arise from a population in crisis and show unlimited replication potential, thanks to a process known as cell immortalization, a characteristic feature of established cell lines. Regarding cancer cells, it is widely accepted that these cells require unlimited replication potential in order to be able to generate macroscopic tumors[9].

1.4.6. Activation of the capacity of invasion and metastasis.

As the neoplasms progress in their pathological degree and malignancy, cancer cells acquire the ability to spread from the primary tumor to other organs, which is reflected in local invasion and distant metastasis[9]. This process can be subdivided into several steps, which are collectively known as the invasion-metastasis cascade: i) vascularization and progressive growth of the primary tumor, ii) local invasion through the extracellular matrix (ECM) and cell layers of the surrounding stroma; iii) the intravasation of cancer cells to the lumen of the lymphatic and blood vessels, iv) survival to transport, v) the arrest of these cells in distant organs, vi) the extravasation to the parenchyma of these tissues, vii) the formation of micrometastases and, viii) the growth of these cancer cell nodules to cause macroscopic tumors, a process that is referred to as "metastatic colonization"[21,22] **(Figure 6).**

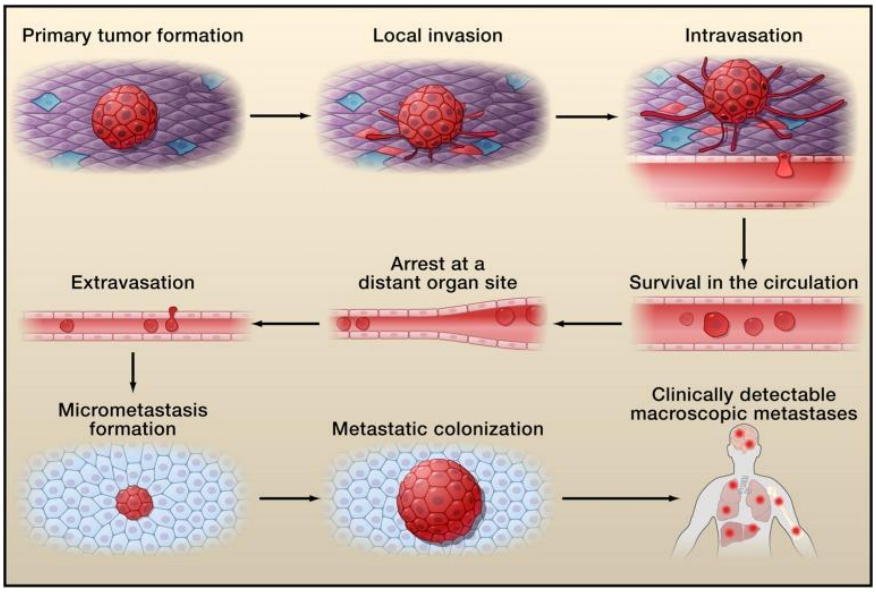

Figure 6. Schematic representation of the invasion-metastasis cascade.[21,22]

When circulating tumor cells adhere to the capillary beds, they pass through the vessel wall through a process called extravasation, entering the parenchyma of the target organ and causing micrometastases[21]. Regarding metastatic colonization, it has been observed that angiogenesis plays a crucial role in the growth of micrometastases[23].

1.4.7. Other characteristics of cancer cells.

The acquisition of the characteristics listed above, which allow cancer cells to survive, proliferate and spread, depends largely on a succession of alterations in the genomes of these cells. It has been observed that cancer cells show an increase in mutation rates compared to the rest of the body's cells. This genomic instability is mainly due to: i) the appearance of defects in the DNA maintenance and repair machinery; ii) and to a telomeric dysfunction, caused by the loss of telomeric repeats or telomere protection structures[9,11,24].

On the other hand, the tumors appear infiltrated by cells of the immune system and, therefore, reflect the inflammatory conditions that arise in non-neoplastic tissues. These inflammatory processes associated with tumors also participate in the acquisition, by incipient neoplasms, of the distinctive characteristics of cancer cells. Inflammation caused by tumors contributes to carcinogenesis primarily through the supply of bioactive molecules in the tumor microenvironment.[9,12,25].

Finally, cancer cells employ different mechanisms to evade the attack and their elimination by cells of the immune system. These cells show low immunity, although some are recognized and eliminated by immune cells. This fact reveals the double role that the immune system plays in tumorigenesis since, on the one hand, it participates in tumor development and progression and, on the other hand, it plays an active protective role in the elimination of cancer cells[9,26].

2. TYPES OF CANCER

2.1. General Classification

There are multiple classifications of tumors, however a simplified way of classifying them, widely used, is the application of a nomenclature depending on their location. Thus, there is usually talk of cancer of the colon, breast, brain, lung, prostate, ovary, larynx, liver, etc. However, each of these tumor types encompasses a set of subtypes that differ in their molecular profile, morphology or the expression of specific markers, something known as intertumoral heterogeneity[27].

Depending on the tissue from which the cancer originates, three main types are distinguished: i) carcinomas, which represent solid tumors that originate from epithelial cells that line the internal and external surfaces of the body; ii) sarcomas, solid tumors that develop from connective tissue cells, such as muscles or bones; iii) and lymphomas and leukemias, which are cancers of white blood cell cells. In addition to these, depending on the tissue of origin, other types of cancer can also be distinguished, such as blastomas, which are derived from embryonic tissues of the organs, or myelomas, which develop from the bone marrow tissue[28].

2.2. Breast Cancer

2.2.1. Incidence and Mortality.

Breast cancer is, by far, the most frequent cancer among women with an estimated number, in 2018, of 2,09 million new cases of cancer diagnosed worldwide. It represents 11,6% of all cancers that develop in women (**Figure 1**), and ranks second overall. Although it is the most common cancer in women in both developed and developing regions, the incidence rates are much higher in the former. The risk of suffering from this type of cancer appears mainly from the age of 40, and it increases as

the age progresses. In our country, the incidence of breast cancer among women is estimated at 28.7% compared to the total number of registered cancers (**Figure 7**) (GLOBOCAN 2018).

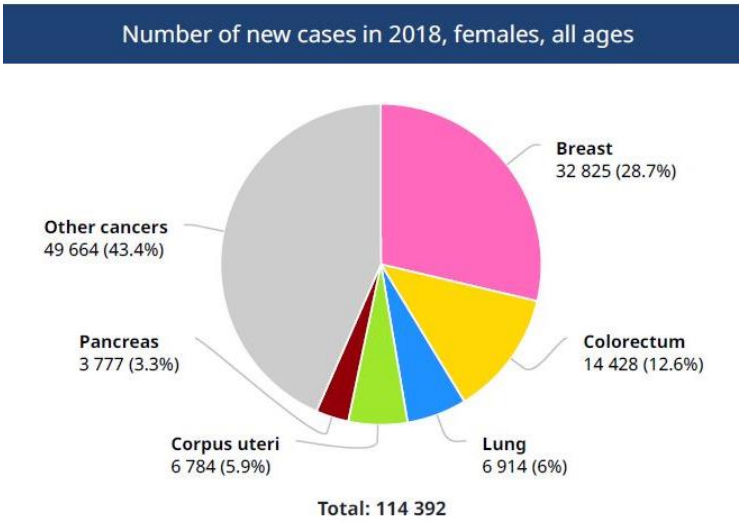

Figure 7: Pie chart present new cases of breast cancer in 2018, females. Spain. (GLOBOCAN 2018)

The mortality rate range is much smaller because of the greater survival in developed regions (GLOBOCAN). This decreasing in breast cancer mortality in developed countries in the last two decades is mainly due to the improvement of diagnostic techniques, such as mammograms, and of the treatments applied.[1] As a result, breast cancer is ranked as the fifth leading cause of cancer death globally, representing a mortality rate of 6.6% of the total **(Figure 2)**.

2.2.2. Etiology

The main external agents involved in the development of breast cancer in humans are alcoholic beverages, drugs such as diethylstilbestrol, contraceptives and menopausal therapies that combine estrogen and progesterone, as well as X and gamma radiation. All these factors are classified within group 1 according to the IARC carcinogen classification[29] (IARC, 2012).

Another important risk factor is that due to genetic predisposition. Thus, for example, certain alleles of genes such as BRCA1, BRCA2, TP53 or PTEN, confer a high risk of breast cancer, while certain genetic variations that affect genes such as PALB2, BRIP, ATM or CHEK2, are related to a risk moderate[30]. Of all of them, the best known are the tumor suppressor genes BRCA1 and BRCA2.

2.2.3. Subtypes.

The WHO classifies the different tumors that affect the breast, from the histological point of view, into eight main groups: i) epithelial tumors, ii) myoepithelial lesions, iii) mesenchymal lesions, iv) fibroepithelial tumors, v) nipple tumors, vi) malignant lymphomas, vii) metastatic tumors, viii) and male breast tumors. The vast majority of these tumors are adenocarcinomas. Regarding men, there are two subtypes of breast tumors: gynecomastia and carcinomas, which in turn are divided into *in situ* or invasive[31].

Another classification of this type of cancers, of great clinical relevance, is based on the molecular study of tumors. This molecular classification provides valuable information when choosing the most appropriate therapy in each case, as well as serving as a prognostic value of the disease. The molecular markers traditionally used are the estrogen (ER) and progesterone (PR) receptors, and the type 2 EGF receptor (HER2), also known as ERBB2[32]. According to this classification, four main intrinsic molecular subtypes of breast cancer are distinguished, which are referred to as: i) luminal A, ii) luminal B, iii) HER2, iv) and basal type[33–35].

The luminal A and luminal B subtypes are characterized by expressing luminal cell markers[34]. Tumors of the luminal subtype A express ER and/or PR, but do not overexpress HER2 (ER and/or $PR^+/HER2^-$), while those of luminal subtype B do overexpress HER2 (ER and/or $PR^+/HER2^+$). The HER2 subtype is characterized by not expressing hormonal receptors, so its growth is independent of both hormones, and by an overexpression of the HER2 protooncogen ($ER^-/PR^-/HER2^+$). On the other hand, the so-called basal type cancer is characterized by being $ER^-/PR^-/HER2^-$, being also referred to as triple negative[35]. Of all the subtypes identified, the basal type is the most undifferentiated breast cancer and the worst prognosis for the patient. This subtype is the most frequent in women who present mutations in the BRCA1 gene in the germ line.

2.3 Pancreatic Cancer

2.3.1. Incidence and Mortality.

In 2018, 458,918 new cases of pancreatic cancer were diagnosed worldwide. It represents 2.5% of all cancers that develop in both sexes **(Figure 1)**, and ranks 11th overall. Although it is a fairly common cancer in women and men, both in developed and developing regions, the incidence rates are much higher in the former. The risk of suffering from this type of cancer appears mainly after the age of 35, and it increases as the age progresses. In our country, the incidence of pancreatic cancer among the population is estimated at 2,9% compared to the total number of registered cancers (**Figure 8**) (GLOBOCAN 2018).

	New cases			Deaths		
Cancer	Number	Rank	(%)	Number	Rank	(%)
Breast	32 825	1	12.1	6 421	4	5.7
Prostate	31 728	2	11.7	5 793	5	5.1
Lung	27 351	3	10.1	22 896	1	20.2
Colon	24 119	4	8.9	12 423	2	10.9
Bladder	18 268	5	6.8	5 680	6	5.0
Rectum	12 570	6	4.6	4 145	9	3.6
Kidney	8 075	7	3.0	2 861	13	2.5
Non-Hodgkin lymphoma	7 811	8	2.9	3 044	12	2.7
Pancreas	7 765	9	2.9	7 279	3	6.4
Stomach	7 684	10	2.8	5 609	7	4.9

Figure 8: Incidence and mortality by cancer site in Spain. GLOBOCAN 2018.

The range of the mortality rate is much greater, approximately 4,5% for the world population (**Figure 3**). As a result, pancreatic cancer ranks as the 7th leading cause of cancer death globally, representing a death rate of 44% of the total. In Spain, it is estimated that 7.279 people died from pancreatic cancer in 2018, which represents a mortality rate of 6.4% of all deaths due to cancer and ranks as the 3th leading cause of cancer death (**Figure 8**) (GLOBOCAN 2018).

2.3.2. Etiology.

To date, the causes of pancreatic cancer are still insufficiently known, although certain risk factors have been identified. People are at higher risk to develop pancreatic

cancer with any of the risk factors such as smoking, obesity, genetics, diabetes, diet and inactivity[36–38]. Smoking is one of the most important risk factors for pancreatic cancer and the risk persists for at least 10 years after smoking cessation[39,40]. The risk of developing pancreatic cancer increases with age[37]. Over 80% of pancreatic cancers develop between the ages of 60 and 80 years. Excess weight (obesity) is also a risk factor for pancreatic cancer.[36,41] On the other hand, pancreatic cancer is more common in people with diabetes but the reason for this is unknown. The risk is mainly in people with type 2 diabetes.[42]

Patients with pancreatitis, especially the chronic or recurrent forms, had a moderate excess of pancreatic cancer risk.[43] About 4% of chronic pancreatitis patients developed pancreatic cancer.[44]

In addition, pancreatic cancer has been linked to a diet with a high consumption of red and processed meats (such as sausages and bacon) and low consumption of fruits and vegetables (vegetables).[45,46] Infections of the stomach with the bacterium Helicobacter pylori (H. pylori) that causes ulcer, or infections with Hepatitis B can also increase the risk of pancreatic cancer.[47] Other potential risk factors include aspirin use, occupational exposure to certain pesticides, and dietary factors such as carbohydrate or sugar intake[47,48].

2.3.3. Subtypes.

Pancreatic cancer consists of several histological subtypes including: **I)** Pancreatic adenocarcinoma which accounts for approximately 95% of cancers of exocrine pancreas. Generally, these cancers originate in the ducts of the pancreas (Pancreatic ductal adenocarcinoma (PDAC)). **II)** Less common types of exocrine cancer: the other less common types of exocrine pancreatic cancer include adeno-squamous carcinomas, squamous cell carcinomas, seal ring cell carcinomas, undifferentiated carcinomas, and undifferentiated giant cell carcinomas. **III)** Ampullary cancer (carcinoma of the ampulla of Vater). **IV)** Benign and precancerous tumors in the pancreas.[49–51]

3. THEORIES ABOUT INTRATUMORAL HETEROGENEITY

3.1. Stochastic Model

The stochastic model or clonal evolution model proposes that the tumors are monoclonal, that is, they come from a single abnormal cell, and that, over time, the descendants of this ancestral cell acquire several combinations of mutations, producing a clonal selection for the acquisition of certain advantages over neighboring cells. This genetic variability would be responsible both for the progression of the tumor, and for the existence of cellular differences within it, that is, intratumoral heterogeneity.[52,53]

This model maintains that all cells within a tumor are biologically equivalent and, therefore, have the same ability to regenerate the tumor. The morphological, proliferative and functional heterogeneity observed between the cells of the same tumor are due to random or stochastic influences that alter the behavior of the individual tumor cells. These stochastic events can be: i) intrinsic, such as variations in levels of transcription factors or deregulation of signaling pathways; ii) or extrinsic, such as an appropriate microenvironment or immune response. Thus, this model establishes that all tumor cells have the same potential to boost tumor growth, although only a small population develops this functionality. What determines that a cell acquires the ability to start a tumor is due to the appropriate influences, making it impossible to prospectively isolate the tumor-initiating fraction (**Figure 9**).[54,55]

3.2. Cancer Stem Cells Model or Hierarchical Model

The cancer stem cell model (CSC) or hierarchical model postulates that tumors develop from a subset of malignant cells that have stem cells (SC) characteristics, which are the only cells capable of initiating and maintaining tumor growth (**Figure 9**). These CSCs, also commonly known as tumor-initiating cells (TIC), are defined by properties as: i) its ability to initiate tumors and direct neoplastic proliferation; ii) its capacity for infinite self-renewal; iii) its ability to divide asymmetrically, leading to a more mature offspring of rapidly expanding progenitor cells, which eventually differentiate and deplete their proliferative potential, potentially causing any tumor cell to originate; iv) its resistance to apoptosis; v) or its metastatic potential. Thus, according to this model, this population of CSC shows certain differences with the rest of the tumor cells, so it should be possible to isolate them prospectively.[55]

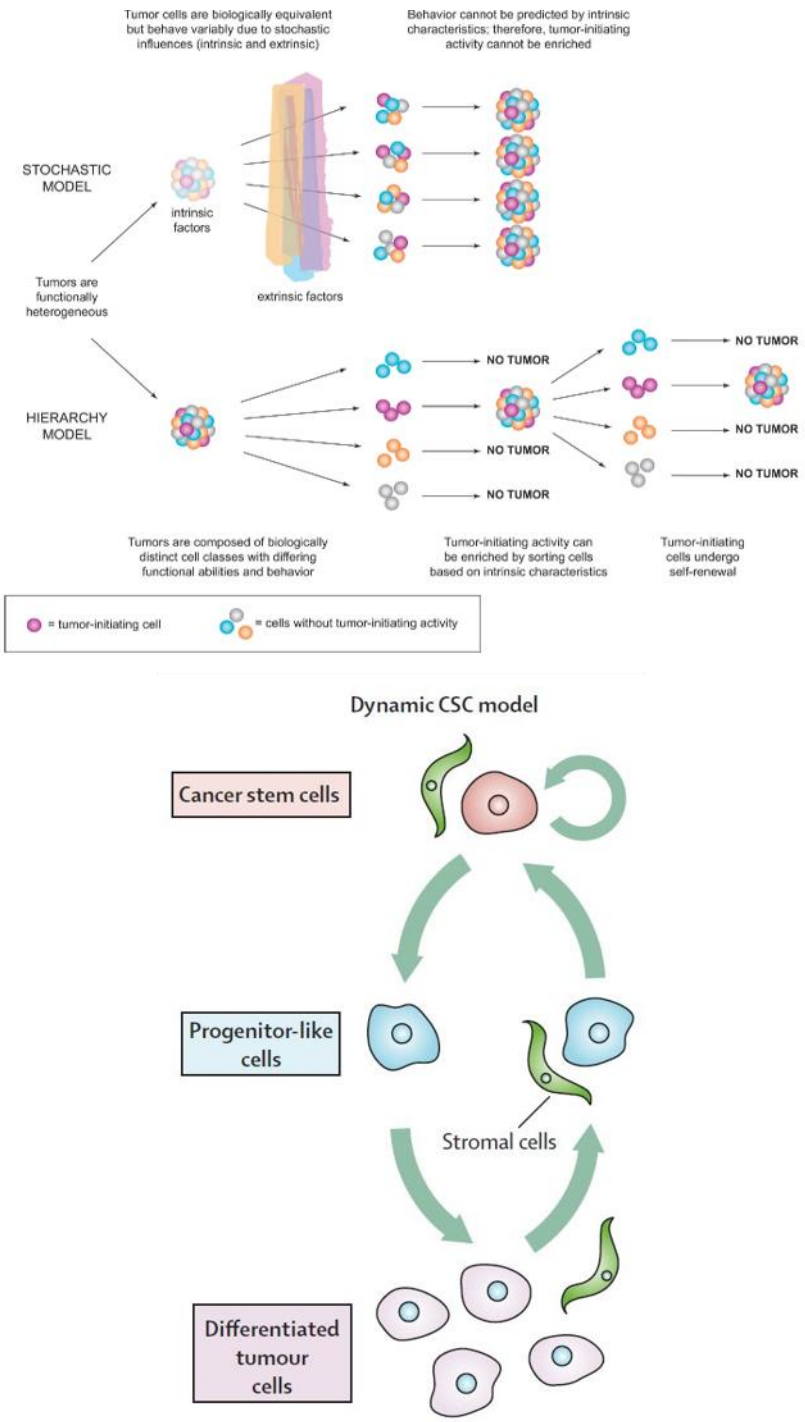

Figure 9. Theories of intratumoral heterogeneity: Stochastic, hierarchy and dynamic model (Image modified from Dick, 2009 and Vermeulen, L. et al. 2012).[54,56]

One of the first experiments that corroborated the existence of CSC was that performed by Chester M. Southam and Alexander Brunschwig in 1961. In their studies they observed that only a very small percentage of tumor cells, which had been

extracted from patients with disseminated neoplasia and, subsequently, injected subcutaneously in other parts of the body of the same patients, they had the ability to form tumors.[57] Investigations for the search for this cellular subpopulation occurred in later years, and were first identified in leukemia in 1994,[58] proposing the possibility that solid tumors were also driven by CSC.[59] Almost a decade later, these cell populations were described in solid tumors, specifically in breast cancer,[60] and have subsequently been identified in other types of cancer. However, currently it has not been shown that all cancers can be explained by this model, and it is even thought that the origin of these CSCs may follow a clonal evolution model.[61]

3.3. Dynamic Model.

In the hierarchical model, the differentiated tumor cells have lost their clonogenic capacity and only the CSCs contribute to the expansion and long-term progression of the malignancy. This model suggests that CSCs should be the target for successful therapeutic intervention. Unfortunately, CSCs seem to be more resistant than differentiated tumor cells to most of the common therapies,[56] which could explain therapeutic failure; the applied drug effectively kills most of the differentiated tumor cells, resulting in tumor shrinkage, yet the CSCs are relatively unharmed and reside in the fibrotic tissue that remains from the initial tumor bulk. After therapy is discontinued, the highly tumorigenic CSCs resume growth, which clinically manifests itself as a relapse. With this in mind, many researchers were convinced that specific and effective targeting of the CSC population could cure the patient. Crucially, this assumption relies on the idea that the CSC population is stable over time, and that CSC features are intrinsic qualities that cannot be attained by differentiated tumor cells. However, novel data, from Vermeulen, L. et al. and several others, suggest that this is not the case.[62–65] The CSC phenotype is much more fluid than anticipated and is strongly regulated by the tumor microenvironment (TME). They refer to this concept as the dynamic CSC model (**Figure 9**); this nuanced view of the nature of CSCs might settle much of the dispute between those who view CSCs as a factual entity and those who consider them an illusion. Additionally, this notion directly affects the design of novel therapies aimed at targeting the CSC population.[56]

In addition, researchers of our group have proposed a novel point of view about tumor origins based on the dynamic model. Since the development of an effective therapeutic strategy against CSCs has proved to be complex and until now, not very effective, we suggest a different approach focused on targeting those cells that could induce the CSCs appearance from non-stem tumors cells, and their subsequent migration and niche nesting. The proposed model postulates that a non-CSC (or a few number of non-CSCs) have the capacity to generate a primary tumor. While the primary tumor is growing, it promotes the malignant transformation of the surrounding tissue-associated cells to form the TME. By the action of many factors (**Figure 10**), including mRNAs (purple circles), secreted by these cells, some non-stem tumor cells located in the edge of the tumor revert their phenotype to a more undifferentiated state, turning into stem-like cells (CSCs). These CSCs can escape from the primary tumor and originate the metastatic tumor, thus the cell type of origin of the primary and metastatic tumor is different explaining the differences between both types of tumors.[66]

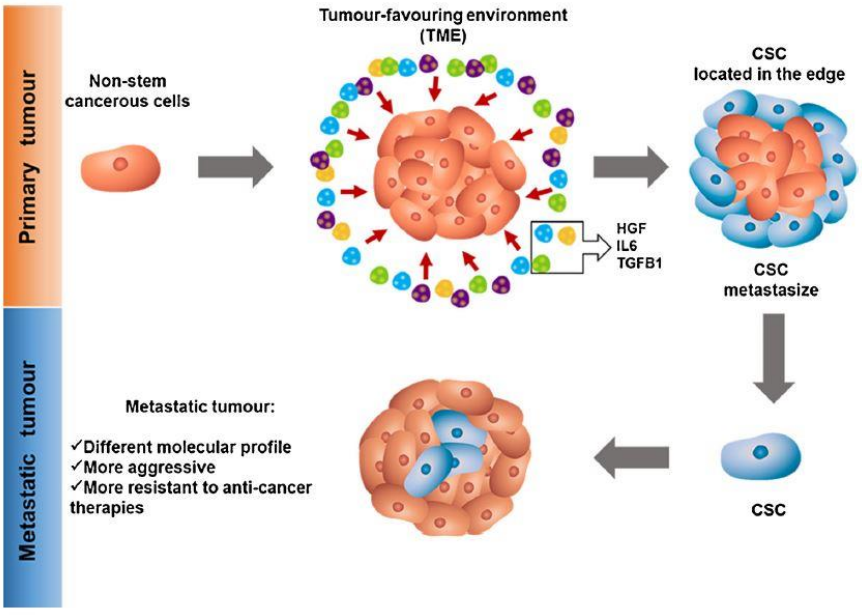

Figure 10: New model of cancer development.[66]

4. THEORIES ON INTERTUMOR HETEROGENEITY

4.1. Mutational Model

The mutational model postulates that the variability observed between tumors that arise in the same organ are due to genetic and/or epigenetic mutations, which determine the phenotype of the tumor, so that the differences in morphology and characteristics of these are the result of different mutations (**Figure 11a**). This intertumoral heterogeneity leads to the classification of the different subtypes of tumors that are located in the same organ, which are characterized by their molecular profile, their morphology and the expression of specific markers, such as growth factor and hormonal receptors.[27]

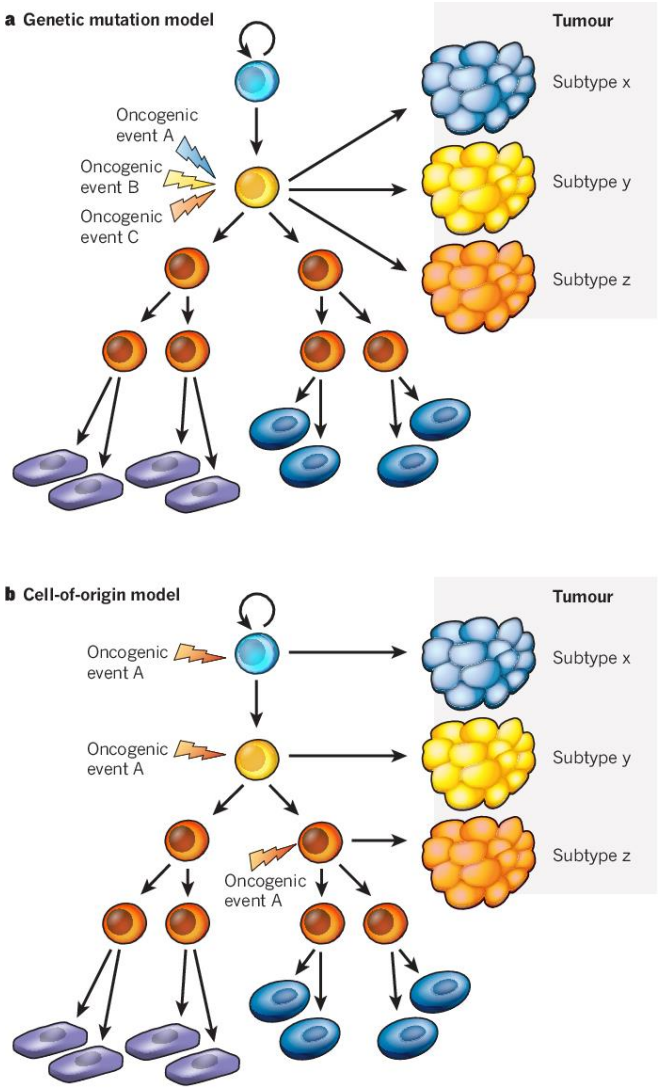

Figure 11. Theories of intertumoral heterogeneity: (A) Mutational model; (B) cell-of-origin model (Image modified from Visvader, 2011)[27]

4.2. Cell-of-Origin Model

The cell-of-origin model determines that the different cancer subtypes that arise within the same organ or tissue are due to different cell populations in the hierarchy of the cell lineage (**Figure 11b**). According to this model, each normal cell of the organism, whether SC, progenitor or differentiated, can accumulate mutations and become the cell of origin. Depending on the degree of differentiation of the cell that initially acquires the tumor phenotype, one tumor subtype or another will develop (**Figure 11b**).[27]

The concept of the cell-of origin refers to the cell that acquires tumorigenic mutations and becomes the first tumor cell, and differs from the cells responsible for the spread of the tumor after its creation. After this malignant transformation, the progression of the carcinogenesis can follow a stochastic model or a CSC model, regardless of the degree of differentiation of the cell of origin.[67] In the case that the tumor follows a CSC model, the genesis of these may require subsequent modifications in the cells descending from the origin cell (**Figure 12**). Thus, although the terms TIC and CSC are usually used interchangeably, the first one more adequately denotes the cell-of origin, while the second refers to the cells that spread cancer.[27]

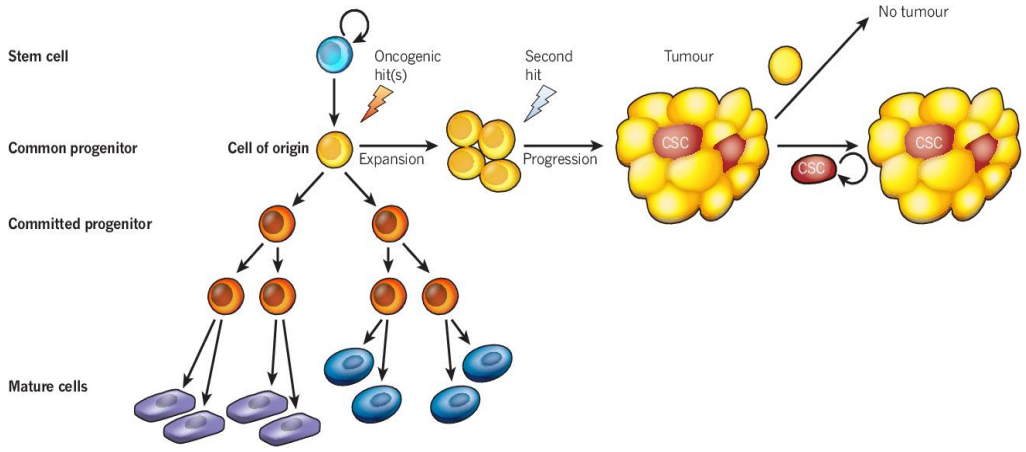

Figure 12. Possible relationship between the origin cell origin and cancer stem cells (CSC). (Image modified from Visvader, 2011)[27]

5. CANCER STEM CELLS (CSCs)

5.1. Self-renewal and Pluripotency in Cancer Stem Cells

Although the SC and the CSC share important functional similarities, such as their capacity for self-renewal and their potential for differentiation; however, they have different biological behaviors, mainly due to the profound deregulation of the CSC's capacity for self-renewal. The differences in the mode of division, the properties of the cell cycle, the replicative potential and the repair of DNA damage, in addition to the activation/inactivation of specific molecular pathways for cancer, give CSCs a malignant phenotype.[68] Some of the signaling pathways that appear deregulated in these cells are related to the self-renewal, differentiation and survival of organ-specific SCs and embryonic SC (ESCs).[69,70]

5.2. Identification of Cancer Stem Cells

5.2.1. Isolation and Characterization.

One of the main characteristics used for the identification of CSCs is the differential expression of specific surface markers by these cells. In this regard, a wide variety of surface markers have been proposed for the identification of CSCs cell populations in different tumor types, including, for example, CD133 (PROM1), CD44, CD34, CD24, CD166 (ALCAM) , CD326 (EpCAM or ESA), CD90 (THY1), CD49, CD184 (CXCR4), CD20, CD38 or CD19, among others.[67,71–76]

One of the most commonly used markers to define enriched populations of CSCs in a multitude of tumor types is the CD133. This transmembrane glycoprotein is considered as a marker of SC and progenitor cells and it is overexpressed in different cell types such as hematopoietic SC (HSC), endothelial progenitor cells (EPC) and organ-specific SC of different tissues. Its physiological function, as well as its ligands and specific secondary messengers are not known exactly, although it is believed to be involved in the organization of the plasma membrane, and some studies indicate that the expression of CD133 in CSCs may be related to cell mobility and the ability to form spheres.[67,77,78] The selection of $CD133^{+}$ cells, either by flow cytometry or by sorting (MACS), in solid tumors and/or tumor cell lines have allowed to obtain subpopulations of CSC with the capacity to restore the heterogeneity of the original tumor in immunodeficient animal models.[79,80] However, recent research shows that CD133 is also

expressed in differentiated cells, and it has also been observed that both $CD133^+$ and $CD133^-$ subpopulations of metastatic tumor cells have the ability to induce long-term carcinogenesis in immunosuppressed mice.[81]

Another surface marker widely used in the study of CSCs is CD44, a transmembrane glycoprotein involved in cell-cell and cell-ECM adhesion that regulates motility and cell proliferation, and which has also been related to tumor growth, cell invasion and metastasis.[82–84] The expression of this marker has been observed in a multitude of solid tumors, including breast, colon, pancreas, prostate, ovarian, head and neck cancer; relating in all cases to the CSC phenotype.[60,85–89]

For the correct isolation of CSC, the study of more than one biomarker is usually used, which allows a better selection of this cell population within the set of cells that constitute the tumor. In fact, different combinations of surface markers have been used depending on the tumor type, for example: i) $CD34^+/CD38^-$ in leukemia,[58] ii) $CD133^+/CD20^+$ in melanoma,[76] iii) $CD24^+/CD44^+/CD326^+$ in the pancreatic cancer ,[87] iv) or $CD44^+/CD24^-$ in the ovary and prostate cancers.[89,90]

Another method recently used for the identification and isolation of CSCs is the determination of enzymatic activities, such as ALDH activity. One of the most commonly used methods to determine this enzymatic activity is the assay with the Aldefluor™ kit. This test was designed to determine the activity of ALDH1, more specifically of the isoenzyme ALDH1A1, although recent studies indicate that it is not specific to it, and that it also allows to determine the activity of other isoenzymes such as ALDH1A2 and ALDH2.[91] The isolation of the cell population within the tumor that shows high ALDH activity through flow cytometry, has shown that it correlates with an enrichment in cells with CSC properties in different tumor types such as breast,[92] colon,[93] prostate,[94] lung,[95] head and neck,[96] as well as in various lines of sarcoma.[97] However, it has also been observed that $ALDH^-$ populations of breast cancer can generate micrometastases of the lung, which indicates, therefore, that the metastatic potential is not exclusive to the $ALDH^+$ population, and that this may represent only a fraction of CSCs.[98]

Although surface molecules, enzymes, transport proteins and proteins involved in pluripotency and self-renewal are being used for the identification of CSCs, other

more reliable tests are functional tests. These include *in vitro* proliferation assays, ability to originate colony forming units, sphere formation, adhesion, migration and invasion; and *in vivo* tests of tumorigenicity, metastatic ability and ability to recapitulate the morphological characteristics of the original tumor.[99] Of all these functional tests, the most decisive is the ability to generate high frequency tumor xenografts that restore the heterogeneity of the original tumor in animal models.

5.2.2. Specific Markers of Breast Cancer Stem Cells (BCSC).

After the initial demonstration of the existence of CSCs in hematopoietic tissue tumors,[58] breast cancer was the first solid malignant disease in which these CSCs were identified and isolated (Al-Hajj et al., 2003).[60] This first identification was based on the expression of the CD44 and CD24 surface markers. The breast CSCs (BCSC) were identified by showing a phenotype $CD44^{+}/CD24^{-/low}$, since this population showed a greater tumorigenicity.

$CD44^{+}/CD24^{-/low}$ phenotype is the most commonly used to isolate and/or identify BCSC from human tumors. Some authors have included in their studies new markers such as: CD133, CXCR4, CD49F (Integrin-α6), DLL1, DNER , ESA, PROCR, ALDH activity, the ability to exclude Hoechst 33342 dye , and even the ability to form mammospheres or adhesion capacity (**Table 1**)[100].[70,71,83,101,102] Regarding the culture of breast tumor cells as mammospheres, on non-adherent surfaces and in conditions of serum deprivation, it has been observed that this type of culture increases tumorigenicity and the expression of markers associated with the BCSC phenotype.[100]

Table 1. Some markers used for the isolation, enrichment and/or identification of breast cancer stem cells (BCSC).

MARKERS	REFERENCE
$CD44^+/CD24^{-/low}$	(Al-Hajj et al., 2003)
$CD133^+$	(Wright et al., 2008)
$CD49F^+/DLL^{high}/DNER^{high}$	(Pece et al., 2010)
$PROCR^+/ESA^+$	(Hwang-Verslues et al., 2009)
Capacity of formation of mamospheres	(Rappa et al., 2008)
Low adhesion	(Walia and Elble, 2010)

5.2.3. Specific Markers of Pancreatic Cancer Stem Cells (PCSC).

PCSC populations account for less than 1% of all pancreatic cancer cells. PCSCs populations express the cell surface markers $CD44^+$, $CD24^+$ and epithelial-specific antigen $(ESA)^+$.[103,104] When it is transplanted into NOD/SCID mice, a $CD44^+CD24^+ESA^+$ CSC subpopulation isolated from human primary pancreatic cancers readily formed tumors, while cancer cells lacking these cell surface markers are poorly tumorigenic.[103,104] The CSC marker-positive cells display a 100-fold increased capacity for the development of tumors and exhibit tumor morphology similar to primary pancreatic cancer. Moreover, these CSCs maintain their cell surface marker phenotype after repeated passages as xenografts in immunocompromised mice.[103,105] Pancreatic cancers contain 1–3% of $CD133^+$ cancer cells, some of which show high expression of CXCR4, a pro-invasive marker. These $CD133^+/CXCR4^+$ cells, but not $CD133^+/CXCR4^-$ cells, have significant metastatic capacity. Accordingly, it remains possible that there is more than one type of CSC sub-population in pancreatic cancer tissues, which would be consistent with the known heterogeneity of most human tumors.[104,106] In summary, human PCSCs are enriched in $CD44^+CD24^+ESA^+CD133^+$c-$MET^+/CD44^+$or high Aldefluor activity among others[107] (**Table 2**). Regarding the culture of pancreatic tumor cells as pancreatospheres, on non-adherent surfaces and in conditions of serum deprivation, it has been observed that this type of culture increases tumorigenicity and the expression of markers associated with the PCSC phenotype.[107]

Table 2. Some markers used for the isolation, enrichment and/or identification of pancreatic cancer stem cells (PCSC).

MARKERS	REFERENCE
$CD44^+/CD24^+$	(Dosch, JS et al., 2015)
$CD133^+$	(Kim, MP et al., 2011)
$c\text{-}MET^+/CD44^+$	(Li,C et al., 2011)
$PROCR^+/ESA^+$	(Lee, CJ et al., 2008)
Capacity of formation of pancreospheres	(Dosch, JS et al., 2015)
Low adhesion	(Walia and Elble, 2010)

6. NANOTECHNOLOGY

From ancient times, to find the most suitable way for drug administration has been a challenging issue. For example, plants and minerals were pulverized and drunk together with either milk or wine by the ancient Egyptians, as described in Ebers papyrus (circa 1500 BC). Even before, Sumerians widely used creams and lotions combining plants, oils and water for medicinal and cosmetic purposes. A Sumerian tale, recorded on a clay tablet more than four thousand years ago, describes how two friendly gods reveal to a prince the "secrets of Heaven and Earth": first, “They showed him how to observe oil on water - a secret of Anu, Enlil and Ea”, and after that “They taught him how to make calculations with numbers”.[108] This early text, specifically linking medicine and mathematics, could be considered as the first step towards the present-day science behind the study of drug delivery systems.

An ideal drug delivery system should transport the drug to the targeted organ or receptor in the required dose, preserving it intact after crossing the different physiological barriers. Developing the appropriate drug delivery system solves plenty of the complications related with drug delivery, since it will help to minimize drug degradation and loss, to prevent harmful side-effects and to increase both drug bioavailability and the fraction of the drug accumulated in the required zone.

This problem becomes even more complicated when the drug to be administered has low solubility in water. Highly potent, but poorly water-soluble drug candidates are common outcomes of contemporary drug discovery programs,[109] reaching percentages as high as 80-90% of the total of the possible candidates depending on the therapeutic area.[110] However, frequently these promising drugs are dismissed in the first stages of the selection because of the difficulties related with their administration. As a way of example, their very low solubility hinders dissolution and therefore limits drug concentration at the target site, often to an extent that the therapeutic effect is not achieved. This could be overcome by increasing the dose; however, this dose escalation would cause local toxicity, increased risk of side effects or even drug precipitation.

The term "Nanotechnology" refers to the design, characterization and application of structures, devices and systems by controlling shape and size at atomic, molecular and supramolecular level.[111] Advances in nanotechnology have led to the development of new nanomaterials whose physico-chemical properties differ from those of their larger counterparts due to their higher surface-to-volume ratio. These novel properties make them excellent candidates for biomedical applications. Nanotechnology is a new discipline of science and engineering that has led to innovative approaches in many areas of medicine. Its applications in the screening, diagnosis, and treatment of diseases are collectively referred to as "nanomedicine", an emerging field that has the potential to revolutionize individual and population-based health this century.[112] In contrast to conventional therapies, where the basic approach is to remove diseased cells faster than healthy cells, nanomedicine attempts to use sophisticated approaches to either kill specific cells or repair them, one cell at a time.[113] It is now possible to provide therapy at a molecular level with the help of NPs, treating diseases and adding light to our understanding of their pathogenesis. Nanomedicine can be considered a refinement of molecular medicine, integrating innovations in genomics and proteomics on the road to a more personalized medicine, so as to allow improved treatment efficacies for many diseases.

6.1. Nanomedicine: Origin and Advantages.

The coming of nanomaterials was forecast as long ago as 1959 by Richard P. Feynman, "the man who dared to think small".[114] Feynman proposed using machine tools to make smaller machine tools and so on until the atomic level.[115] Nowadays, over fifty years later, nanomedicine is playing a growing part in pharmaceutical research and development, primarily in the form of NP-based delivery systems for drugs and imaging agents, connecting a broad range of disciplines as engineering, biology, physics and chemistry and leading to numerous publications and patents (**Figure 13**).

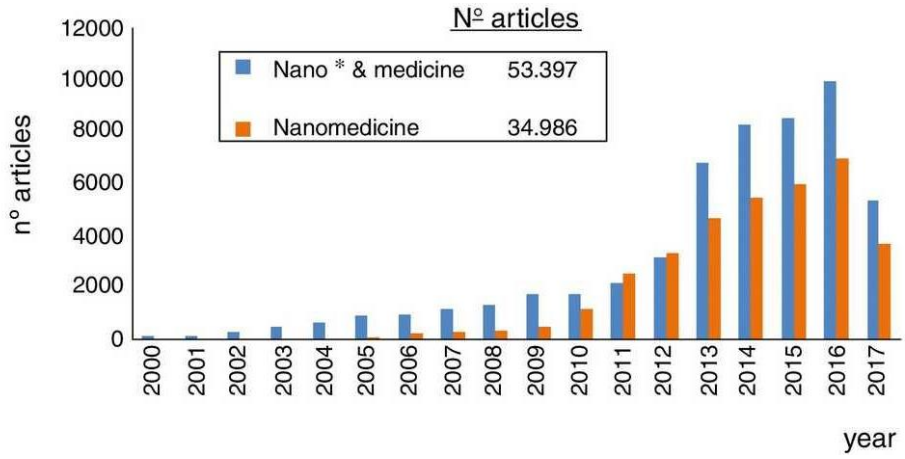

Figure 13: Evolution of the number of papers published annually indexed in the WOS during the XXI century on nanomedicine using two different search terms.[116]

Nanomedicine applications are grouped in three interrelated areas: regenerative medicine, analytical/diagnostic tools and drug delivery.

6.1.1. Regenerative Medicine.

Tissue engineering brings together principles and innovations from engineering and the life sciences for the improvement, repair or replacement of tissue/organ function. Nanotechnology has the potential to provide instruments that can accelerate progress in the field of tissue engineering and reconstruction, which will greatly enhance and contribute to the field of regenerative medicine.[117] There have been great strides made in using nanomedicine to enhance the functions of cells necessary to regenerate a diverse number of tissues (such as bone, blood vessels, skin, teeth, the nervous

system, cornea and the heart among others). In this context, Liu et al. explored the use of silver nanoparticles (AgNPs) on skin excisional wound healing. The *in vitro* and *in vivo* experiments revealed that AgNPs could increase the rate of wound closure through the promotion of proliferation and migration of keratinocytes and by driving the differentiation of fibroblasts into myo-fibroblast for wound contraction.[118] Moreover, the mechanical function in healed skin after treatment with AgNPs had similar elastic force, collagen deposition, as well as collagen fibrils alignment to normal skin.[119] These results indicated that AgNPs could regulate remodeling process during skin tissue regeneration.

Other applications of nanotechnology in regenerative medicine include the design and development of nanomaterials to mimic extracellular matrices and form scaffolds, an artificial extracellular matrix suitable for tissue formation, using various materials, such as collagen, calcium sulfate and chitosan hydroxyapatite[120–123] or superparamagnetic iron oxide NPs developed to track the migration of mesenchymal stem cells.[124] Moreover, Ortega-Oller et al. reported the use of nano/microparticles of PLGA as a delivery system of one of the most commonly used growth factors in bone tissue engineering, the bone morphogenetic protein 2 (BMP2).[125]

6.1.2. Nanodiagnostic Tools.

Nanomolecular diagnostics is the use of nanobiotechnology in molecular diagnostics[126] and can be termed 'nanodiagnostics'. Nanodiagnostic tools are developed to meet the rigorous demands of the clinical laboratory for sensitivity, and therefore earlier disease detection and cost-effectiveness.

In a diagnostic assay usually a recognition element (e.g. nucleic acid, enzyme, antibody, receptor, tissue, cell, aptamer) interacts with a compound or microorganism of interest and the physico-chemical property of a label (such as pH, electron transfer, heat, electric or chemical potential, mass, optical properties) is used to detect this event. In heterogeneous formats, a support might be used to immobilize the recognition element.[127] Nanostructures are deployed either as a label or as a support. Due to their small sizes, they can detect very few molecules in solution offering lowest limits of detection and thereby improving sensitivity. Furthermore, conventional labels (such as fluorescent dyes) can be immobilized on nanostructures improving the detection signal

and thus the sensitivity of the diagnostic assay. Some examples of nanostructures as diagnostic tools that bring in marked improvements over prevalent classical assays are nanobiosensors, microarrays, latex immunoaggregation assays, biochips of different elements (DNA, proteins or cells) and lab-on-a-chip devices.[112]

It is noteworthy that metal-based NPs are the most promising nanocarriers for theranosis. Thus, there are a lot of reports using this type of NPs such as dually functionalized manganese-based layered double hydroxide nanoparticles (Mn-LDH) as an effective anticancer drug/gene delivery system and for T1 -weighted magnetic resonance imaging (MRI) in brain cancer theranostics,[128] Gadolinium-based NPs for theranostic MRI-radiosensitization,[129] Gold-based nanospheres and nanorods particles used as theranostic agents[130] or theranostics based on iron oxide and gold nanoparticles for imaging-guided photothermal and photodynamic therapy of cancer,[131] among many others.

6.1.3. Drug Delivery.

The pharmaco-dynamic and pharmaco-kinetic of drugs can be modulated by using nanocarriers. In this way, one of the main objectives of Nanomedicine is the efficient delivery of drugs on pathologic cells or tissues. For this, is essential the use of vectorized nanocarriers for a directed delivery on a target site. The potential of eliminating a tumorous outgrowth without any collateral damage through nanomaterial-based drug delivery has created significant interest and NPs form the basis for bio-nano-materials[132]. A major efforts in designing drug delivery systems are based on functionalized NPs.[133,134]

The biological activity of a substance therapeutically active (a drug or biomolecules) depends, above all, on the nature of the interaction with the target tissue or organ. The interaction occurs when the drug is in the desirable place and in the right quantity to achieve the desired response, which means that the therapeutic agent should be released at a specific location in the body and at a controllable speed. This can be achieved if the active ingredient is suitably formulated prior to administration.

Typically, drugs are orally taken, because oral is the most convenient route and usually the safest and least expensive,[135] but a large number of drugs cannot be

administered by this route because the absorbed amount through the gastrointestinal membrane is too small to produce a therapeutic effect. For these and other problems, many drugs should be administered by alternative routes such as intravenous, topical or inhaled route, among others. Parenteral route is particularly important because it avoids many of the problems associated with oral drug delivery. But intravenous injection of poorly soluble drugs may cause embolization of blood vessels due to drug aggregation, and it often shows local toxicity as a result of high drug concentrations at the site of deposition.[136]

Frequently, conventional dosage forms require repeated administration in order to maintain the drug concentration in the blood to a level high enough to ensure a therapeutic effect. Chronic administration may be inconvenient for the patient, leading to poor compliance with the prescribed dosing regimen. A tool to fix this and other problems associated with repeated administration of a drug is the medical application of nanotechnology.

The greatest advantage of nanotechnology lies in its potential to create novel structures with enhanced abilities to translocate through cell membranes, thereby, enhancing their delivery efficiency. The benefits of developing NPs as drug delivery systems include enhancement of pharmacological activity,[137] solubility (many drug molecules can be incorporated in the particle matrix),[138] stability and bioavailability (designing NPs with optimal size and surface characteristics to increase their circulation time in the bloodstream),[139] protection from toxicity and physical and chemical degradation, sustained delivery,[140] feasibility of variable routes of administration,[141] facilitation of the drug transport across critical and specific barriers,[142] etc. Engineering materials on this scale allow for novel medical therapies which are able to release the associated drug to the target tissue in a controlled manner, improving the specificity and resulting in decreased side effects for patients.[143] Moreover, the diverse platforms of nanotechnology can be utilized to combine different drugs into a single nanotherapeutic agent for synergistic therapeutic benefits.

7. NANOPARTICLES FOR THERAPEUTIC MOLECULES DELIVERY IN CANCER THERAPY. CLASSIFICATION OF THE DIFFERENT NANOPLATFORMS.

The main objective of the application of nanomedicine in cancer is to have a better therapeutic effect, to increase the bioavailability and to allow the administration of lower doses of drug while obtaining lower toxicity rates and improving the patient's quality of life.[144] Another objective is to overcome the multiple mechanisms of drug resistance that make this treatment ineffective in a high percentage of cancer cases since cancer cells have the ability to evade cytotoxicity.[145,146]

Anti-cancer nanomedicines require the vehiculization of drugs on nanostructured platforms. These nanoplatforms are particles of submicron size (10-1000 nm in diameter),[147] nanosystems that can be manufactured using a variety of materials (including polymers, lipids, viruses and organometallic compounds, among others).[148] In addition, all NP-based drug delivery vectors must be able to transport and release the drug at a specific location. They can be classified by their physical form or functional properties, which must be adapted to the specific needs of the drug to be administered and to the intended therapeutic use.[149] (**Figure 14**)

There are four denominations for nanosystems according to their composition/structure. Thus, according to its composition we can find Nanoparticles (solid interior), Nanoemulsions (liquid interior, not miscible, stabilized by surfactant), Nanocapsules (same as nanoemulsions but surrounded by membrane/polymer) and Nanocrystals (Crystalline, inorganic interior). According to its structure we can find organic nanosystems (polymers, proteins, liposomes, micelles and lipids) and inorganic (metals, semiconductors, carbon and oxides) (**Figure 15**).

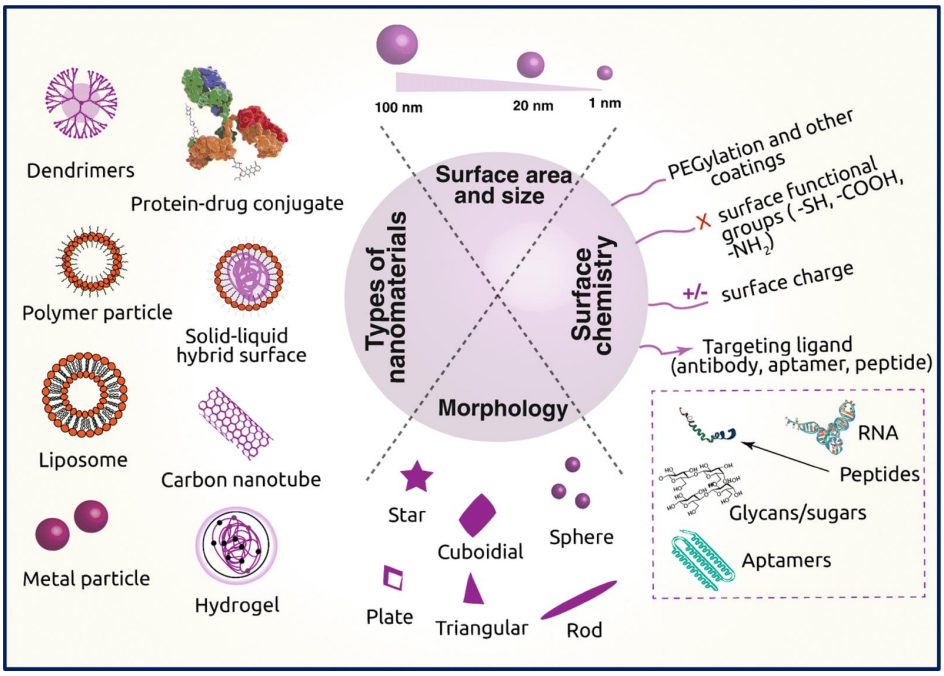

Figure 14: Schematic representation of different types of nanomaterials employed in cancer therapy, their important physical properties and surface chemistry required to carry drugs.[150]

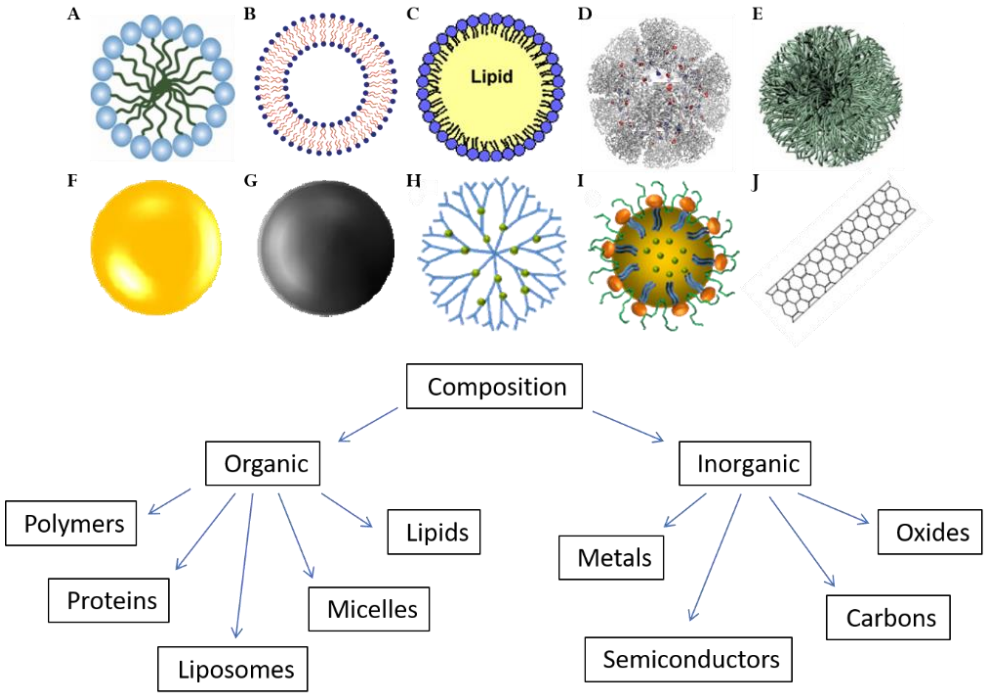

Figure 15: Examples of drug delivery platforms: A) Micelle. B) Liposome C) Lipid. D) Proteins. E) Polymeric. F) Gold nanoparticle. G) Magnetic. H) Dendrimer. I) Nanoemulsion. J) Carbon nanotube.

7.1. Polymer-based Drug Nanocarriers

Polymer therapeutics have been extensively investigated as therapeutic carriers. They encompass polymer–protein conjugates, drug-polymer conjugates and supramolecular drug-delivery systems. Many polymers have been proposed as drug delivery carriers, but only a few of them have been accepted into clinical practice.

The polymers of choice are biodegradable and bioavailable due to their better encapsulation, control release and less toxic properties. The incorporation of hydrophobic drugs into polymer chains improves their solubility in water and changes their biodistribution.[151] Mucoadhesive materials such as chitosan can be used to increase contact between the polymer containing the drug and cell membranes.[152] Several types of polymer-based drug carriers have been tested as possible drug delivery systems, including polymeric NPs, dendrimers, hydrogels and micelles.

7.1.1. Polymeric Nanoparticles.

The polymeric NPs are designed from biocompatible and biodegradable polymers and in their synthesis several methods are used based on the needs of their application and the type of drugs to be encapsulated.[153] These particles are solid matrix systems in which the drug is dispersed within the particle or conjugated with the polymeric skeleton. Polymeric NPs are formulated to vehicle small hydrophilic or hydrophobic drug molecules, as well as proteins and nucleic acids. Numerous NPs are in preclinical or clinical development.[154] For example, NPs comprising hydrophobic copolymers such as poly (lactic-co-glycolic acid) (PLGA) and polyalkylcyanoacrylate (PACA) have been used to co-encapsulate chemotherapeutic agents and multi-drug resistance (MDR) mechanism inhibitors for administration in various types of cancer.[155] Because part of our research focuses on the use of polystyrene NPs, a section of this introduction (11.1) have devoted themselves to extensive analysis of this nanosystem.

7.1.2. Hydrogels.

Hydrogels are networks of hydrophilic polymers that vary in their structure. The first one, known as the first network, has a linear structure, while the second network, called last, is a polymer network with three-dimensional covalent cross-linking. Covalent bonds between chains affect the properties of the polymer and, therefore, make these polymers suitable for use as carriers of drugs in the form of micro or NPs. They can

absorb from 10 to 20% (an arbitrary lower limit) up to thousands of times their dry weight in water, a property attributed to the presence of hydrophilic groups in their structure.[156] Some hydrogels have fluid transport characteristics and stimulus response characteristics (for example, pH, temperature and light).[157] Several synthetic hydrogels have also been studied for the purpose of chemotherapeutic drug administration.[158]

7.1.3. Dendrimers.

Dendrimers are synthetic polymers that have a highly branched structure consisting of an initiator core and multiple layers with active end groups. Each layer is called a generation and they consist of repetitive units.[159] Due to this specific structure, the bioactive agents can be encapsulated inside the dendrimers,[160] chemically adhered or physically adsorbed on the surface of the dendrimer.

Dendrimers show a growing promise as drug delivery vectors and can be generated with a wide range of scaffolding structures, sizes and surface functionalities. There are studies where dendrimers are used for simultaneous administration of chemotherapy agents (5-fluorouracil) and gene therapy (antisense microRNA miR-21).[161] Synchronous administration of the two therapeutic agents resulted in synergistic anticancer efficacy.

7.1.4. Micelles.

Polymeric micelles are formulated through a self-assembly process using block amphiphilic copolymers consisting of two or more polymer chains with different hydrophilicity. These copolymers are spontaneously assembled in a core-shell structure in an aqueous environment. The hydrophobic blocks form the nucleus where the medicine is transported, while the hydrophilic blocks conform the cover. Due to the unique properties they possess, polymeric micelles have proven to be effective drug transporters. For example, specific binding to the target cells (MCF-7 breast cancer cell line) of paclitaxel-loaded micelles directed with a specific phage protein of MCF-7 cells[162] has been demonstrated. In addition, micelles loaded with thioridazine (effective drug against BCSCs) and doxorubicin have been designed, providing a promising combined strategy for the treatment of breast cancer by targeting both cancer cells and BCSCs.[163]

7.2. Lipid-based Drug Carriers

7.2.1. Liposomes.

Liposomes are spherical lipid vesicles formed by an aqueous liquid trapped by one or more bilayers of natural or synthetic amphiphilic lipid molecules.[164] Liposomes became one of the first nanoplatforms for drug administration due to their unique characteristics. Both hydrophilic and hydrophobic therapeutic agents can be encapsulated and protected from external conditions and can be coated with polymers and functionalized with specific ligands to attack specific cells.[165] In liposomes, drugs can be encapsulated in the phospholipid bilayer, in the aqueous liquid nucleus or in the bilayer interface. Among the "first generation" vectors (not specifically targeted), the supply of liposomal drugs is certainly the most used successfully in the clinic. Doxil®, a pegylated liposomal formulation with doxorubicin, was the first liposomal drug formulation approved by the Food and Drug Administration, USA. UU. (FDA) for the treatment of AIDS associated with Kaposi's sarcoma in 1995.[166]

7.2.2. Solid Lipid Nanoparticles.

Solid lipid nanoparticles (SLNPs) developed in the early 1990s. They are 50 to 1000 nm in size, formed by a biocompatible/biodegradable lipid matrix made of solid lipids (i.e., lipids that are solid at room temperature and also at body temperature) and stabilized by surfactants.[167] SLNPs have many advantages for drug administration, such as the ability to encapsulate hydrophilic and hydrophobic drugs, good tolerability, biodegradability and high bioavailability by ocular administration.[168,169] The application of SLNPs formulations for the administration of anti-cancer drugs has overcome many obstacles commonly seen in conventional cancer chemotherapy. Several anticancer drugs have been incorporated and evaluated, including etoposide,[170] methotrexate[171] and idarubicin.[172] Conventional routes of administration (for example, the intravenous route) have shown relatively low tumor absorption.[173]

7.2.3. Lipid Liquid Nanoparticles or Nanoemulsions.

Lipid-based nanoemulsions are colloidal oil and water dispersions that typically have a dispersed phase distributed within a continuous phase that is stabilized by surfactants and co-surfactants in the oil/water interface.[174] Thermodynamically stable nanoemulsions form spontaneously with the minimum mechanical energy required.

Because part of our research focuses on the use of nanoemulsions, a section of this introduction (11.2) have devoted themselves to extensive analysis of this nanosystem.

7.3. Virus based Nanoparticles

Viruses can be considered as living NPs with a core-shell structure. Infectious agents are in the nucleus surrounded by a shell composed of proteins or proteins embedded in lipid membranes.[165] They range in sizes from 10 nm to more than one micron and can be found in a variety of distinctive forms (more abundantly icosahedra, spheres and tubes).

Virus-like particles offer the great advantages of morphological uniformity, biocompatibility and easy functionalization, and have been widely used for the administration of drugs, vaccines and gene therapy due to their high efficiency of gene transfection and receptor binding properties of spherogenic cells.

7.4. Ceramic Nanoparticles.

Ceramic NPs are typically composed of inorganic compounds such as alumina, silica and titania.[175] However, the NP core is not limited only to these materials; instead of metals, metal oxides and metal sulphides can also be used.[176] They are generally bioinert and have porous structures. These NPs have been proposed as medicament delivery vehicles for transporting drugs for various cancer therapies because these particles can be easily manipulated with the desired size, shape and porosity.[177,178] They can also be easily functionalized by several molecules due to the presence of negative charge on the surface.[179]

7.5. Metal-based Nanoparticles.

Metal NPs can be synthesized in extremely small sizes of about 20 nm and, therefore, the large surface area provides the ability to transport a relatively higher dose of medications. One of the most used are gold NPs (AuNP) because they are biocompatible, easy to synthesize, characterize and modify the surface. Therefore, gold nanoparticles are new agents that are being evaluated for biological detection, medication administration and cancer treatment.[180]

Other typical metal NPs are the magnetic core and shell NPs. They consist of a metal or metal oxide core coated with an inorganic or polymeric shell to improve its

stability and make the particle biocompatible.[181] Metal NPs can be used as thermal release triggers when irradiated with infrared light or excited by an alternating magnetic field. In the magnetic orientation of drugs, the magnetic carrier particles with surface bound drugs are injected into the vascular systems and then captured in the tumor through a locally applied magnetic field. Several studies have demonstrated the application of magnetic NPs for drug administration.[182,183]

Currently, many other metal-based nanosystems, as well as several surface functionalized hybrid NPs, are being widely used for drug delivery applications, such as platinum,[184] silver and palladium NPs.[185] Quantum dots, fluorescent semiconductor nanocrystals, have also been thoroughly investigated for the administration of drugs and images.[186] They combine a small size, a versatile surface chemistry and excellent optical properties.[187]

7.6. Carbon Nanotubes.

Carbon nanotubes (CNT) are carbon allotropes with a cylindrical nanostructure. The nanotubes have been built with a length-diameter ratio of up to 28,000,000: 1.[188] CNT can be imaginatively produced by winding a single layer of graphene sheet (single-wall CNT; SWNT) or by winding many layers to form concentric cylinders (multi-wall CNT; MWNT).[189]

Although the CNT has several unique properties, the non-functionalized (pristine) CNT is poorly soluble and highly cytotoxic. Its functionalization with more soluble and biocompatible materials has been studied, which shows that it allows to improve water solubility with the consequent improvement of its biocompatibility. Functionalized CNTs have been successfully investigated for several biomedical applications, such as proteins, nucleic acids and drug carriers.[190] The potential of CNTs for the administration of anticancer agents could be attributed to their exclusive physicochemical properties, especially to their ability to cross several biological barriers without generating an immunogenic response and toxic effects. The application of CNTs for the supply of medicines to its site of action has become one of the main areas of interest for different research groups.[191]

8. DRUG DELIVERY STRATEGIES.

It is well-known that the activity of the anticancer drugs is greatly attenuated by the time drug reaches the target, which can render the treatment to be ineffective and increase off-target effects. The effectiveness of anticancer drug treatment can be achieved only when the administered drug is of proper dosage and display maximal activity in the cancer cells. Thus, the nanomaterials used for targeting tumor cells should have the capability of increasing local concentration of the drugs in and around tumor cells, thereby reducing the potential toxicity toward healthy cells.[150] The efficient delivery of nanomaterials to the target tissues can be classified as passive and active targeting.

8.1. Passive Targeting.

The most common route of administration of nanomaterial-based anticancer drugs is intravenous injection. This approach bypasses the absorption step across the intestinal epithelium required after oral administration.[192] At tumor sites, the vascular barrier is disrupted, and this enables nanocarriers to accumulate in the tumor tissue[193] as shown in **Figure 16.** The gaps between the endothelial cells in the tumor vasculature can range from 200 to 2000 nm depending on the tumor type, localization, and environment. Moreover, due to the poor lymphatic function, the NPs are not rapidly cleared and accumulate in the tumor interstitium.[194] This is known as enhanced permeability and retention (EPR) effect, which is the basis of passive targeting.[195] This accumulation of the drug at the tumor sites is a passive process, and it requires prolonged circulation of the drug for appropriate drug delivery.

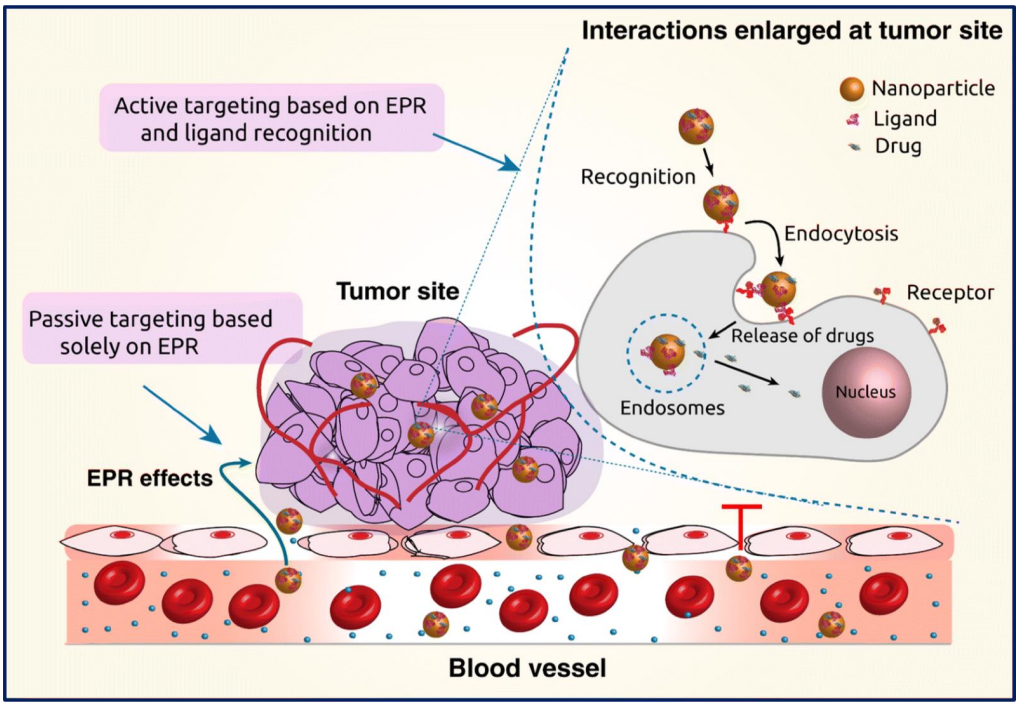

Figure 16: Graphical illustration of passive and active drug targeting strategies. In passive targeting, the nanocarriers pass through the leaky walls and accumulate at the tumor site by the enhanced permeability and retention (EPR) effect. Active targeting can be achieved using specific ligands that bind to the receptors on the tumor cells.[150]

The accumulation of the nanocarriers is essentially dependent of physicochemical properties such as size, shape (morphology), surface charge and surface chemistry.[196] The extent and kinetics of nanomaterial accumulation at the tumor site are influenced, among all these properties, by their size. The nanocarriers need to be smaller than the cutoff of the proportions in the neovasculature, with the extravasation to the tumor acutely affected by the size of the vehicle. Further, the biodistribution of the nanomaterial–drug formulation is influenced by blood perfusion, passive interactions with biomolecules along the route, and immunological clearance processes such as phagocytosis or renal clearance.[150,197]

8.2. Active Targeting.

Active targeting, also known as the ligand-mediated targeted approach, involves affinity-based recognition, retention and uptake facilitated by the target cells[196] (**Figure 16)**. The chemical affinity for active orientation is based on different specific molecular

interactions, such as receptor-ligand-based interactions, load-based interactions and motif-based interactions facilitated with substrate molecules.[198] Various biomolecules can constitute a ligand, which includes antibodies, proteins, nucleic acids, peptides, carbohydrates and small organic molecules such as vitamins.[199,200] The target substrates can be surface molecules expressed in diseased cells, proteins, sugars or lipids present in the organs, molecules present (or secreted by tumor cells) in the microenvironment of diseased cells or even the physicochemical environment in the vicinity.[201]

Intelligent and targeted systems based on nanomaterials exploit the multivalent nature of ligand interactions with the target antigens. When multiple ligand molecules accumulate in nanosystems, there is a general increase in the avidity of nanoparticles for their related objective.[200] In addition, the binding of a ligand molecule generally facilitates the binding of consequent molecules through cooperative effects, collectively improving binding efficiency and subsequent actions.[150] Generally, covalent conjugation methods have been utilized, but systems with physical absorption using affinity complexes can also be used effectively.[202] The critical aspect to this conjugation is to maintain the stability of the conjugated ligands during the adverse environment presented by the physiological environment, and various approaches have been undertaken to achieve it.[196]

The main angiogenic targets, explored by NP systems for therapeutic benefit, include the vascular endothelial growth factor receptors (VEGFRs), αvβ3 integrins, matrix metalloproteinase receptors (MMPs), and vascular cell adhesion molecule-1 (VCAM-1).[198]

Monoclonal antibodies (mAb) were the first and are still the preferred class of targeting molecules. The first mAb to gain FDA approval for the treatment of cancer was Rituximab in 1997, a chimeric mAb for the treatment of B-cell non- Hodgkin's lymphoma. Trastuzumab, in 1998, a humanized mAb for the treatment of HER2 expressing breast cancer, quickly followed. Cetuximab, which binds to epidermal growth factor receptors (EGFR), was approved for treating colorectal cancer in 2004 and head/neck cancer in 2006. Bevacizumab, a tumor angiogenesis inhibitor that binds to vascular endothelial growth factor (VEGF), was approved for treating colorectal cancer in 2004. Recent studies have tried to encapsulate chemotherapeutic drugs into NPs and then

functionalize the particle surface with mAbs to maintain targeting efficacy.[203–205] The conjugated antibodies enhance uptake and cytotoxic potency of the NPs.

Peptide-based targeting of tumor-associated receptors has emerged as potential tumor-specific chemotherapeutic agents. Peptides are attractive ligands because high-affinity sequences can be discovered through screening of combinatorial libraries. Cell permeating and fusogenic peptides from pathogens or toxins and peptides, randomly derived from technologies such as phagedisplay, are also commonly used for targeting purposes.[206] Among single nuclear localization (SNL) peptides, trans-activating transcriptional activator (TAT) peptide has been shown to be an efficient molecule for translocating NPs into cell nuclei *via* the binding import receptors, importin α and β. In a recent publication a peptide has been used to conjugate onto mesoporous silica NPs for nuclear-targeted drug delivery of doxorubicin for the first time.[207] Lipid and polystyrene NPs functionalized with targeting peptides such as RGD peptides are among the most often studied.[208]

8.2.1. Influence of Nanoparticle Engineering in Active Targeting.

The conjugation of ligands on the NPs surface changes the properties of the directed molecules and the nanomaterial.[209,210] At the same time that the ligands bind to the NP they lose the rotational and translational freedom they presented to release molecules, but the conjugate that is formed has a greater orientation capacity due to a greater presence of ligands.[211,212] Similarly, the size, geometry, surface properties (charge and hydrophobicity) and the composition of the NPs can also be altered. In some cases, NPs have demonstrated benefits that go beyond simple drug release. For example, greater resistance to degradation by nucleases by chains of nucleic acids immobilized on the surface of nanomaterials.[213] To fully understand the properties of actively targeted NPs, it is essential to determine how the physicochemical properties of NPs affect interactions with their targets (**Figure 17**).

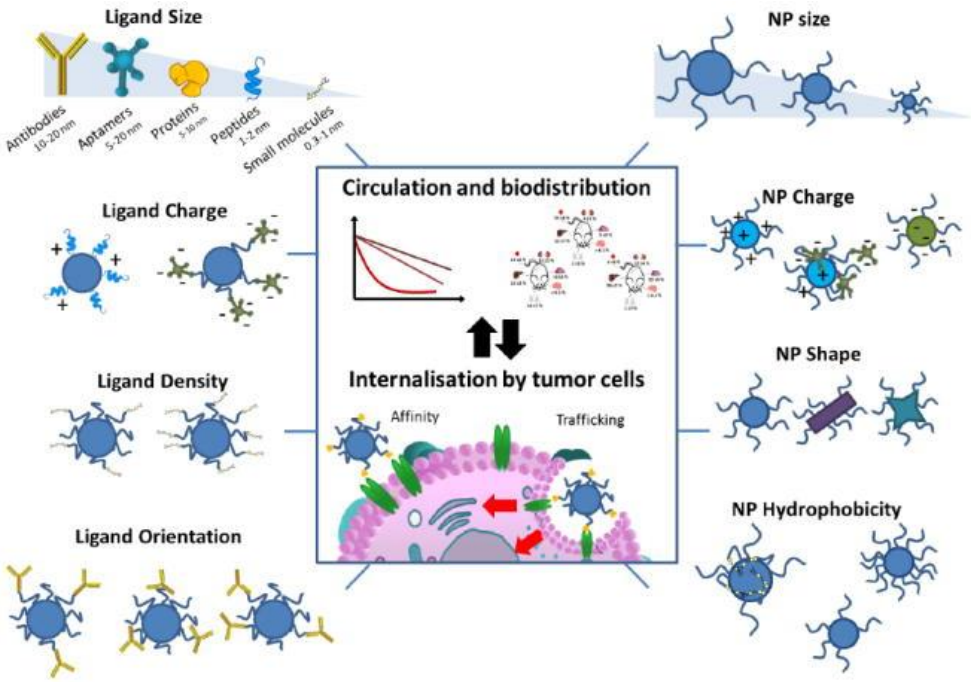

Figure 17: The physicochemical properties of the ligand and the nanoparticles affect their blood circulation profiles, their biodistribution and their ability to be internalized by cancer cells.[196]

A. Ligand Density. Because the increase in the number of antibodies per NP allows cooperative effects, the density of the molecules on the surface of the NPs affect their affinity for the substrate. Thermodynamically, the binding of a ligand to its substrate facilitates the subsequent binding of its neighboring ligands.[212] Biologically, the multiple interactions of the NP with the cell membrane forces the clustering and local concentration of receptors. This triggers the membrane envelope and leads to internalization.[214]

This allows the use of multiple ligands of relatively low affinity to bind their target efficiently and with great appetite.[200] However, this increase in affinity is not always linear. In some cases, the cooperative effect of the ligand can saturate and further increase the density of the ligand causing harmful effects on cell binding.[215,216] This effect can be explained by an incorrect orientation of the ligand, steric impediments caused by neighboring molecules or competitive behaviors with other molecules for binding with the receptor.

B. **Size and shape of the nanoparticle.** The size and shape of the nanomaterial should be taken into account at the beginning of the design of the targeted NPs as it affects the way in which the cells "see" them and, therefore, determine their distribution, toxicity and ability to select.[217] For spherical particles, smaller sizes represent higher curvatures that may be problematic for ligand functionalization after synthesis along with increased toxicity.[218] In addition to the effect on circulation properties and accumulation in the aforementioned tumors,[219] the shape of the NP seems to influence the kinetics of cell internalization and internalization pathways by modulating the interactions between the nanomaterial and the cell surface.[220]

C. **Ligand surface and charge.** From a synthetic perspective, the charge of the non-functionalized NP and that of the ligand can affect the conjugation performance and the spatial visualization of the ligand on the surface.[221] Repulsive or attractive forces between the surface of the NPs and the ligand can interfere with conjugation[222] or affect the structure and conformation of the final ligand. A chemical spacer with a reasonable length, such as those based on PEG units, can help reduce this effect, but can simultaneously complicate the synthesis and increase the final particle size.[215] In addition, the final surface charge will affect the effectiveness of the directed NPs. Since most ligands are charged molecules, the final surface charge of the NP is determined by combinations of ligand densities, materials and NP formulation strategies.

D. **Hydrophobic/Hydrophilic surface.** In addition to surface loading, hydrophobicity can also affect the engineering of the presentation of ligand.[223] This can have serious effects since most polymeric NPs have hydrophobic nuclei (e.g., polyesters, polyamides)[224] thus producing the ligand get trapped inside and not properly exposed on the surface.

9. INTRAVENOUS ADMINISTRATION OF NANOPARTICLES

For drugs administered parenterally, interactions with blood components, systemic distribution and pharmacodynamics are of great importance. In a successful intravenous treatment, therapeutic agents must pass a series of biological barriers that

include liver and kidney clearance, enzymolysis and hydrolysis, as well as cell uptake, endosomal/lysosomal degradation and spleen filtration.

Nanomaterial carriers can improve biodistribution and prolonged blood circulation of therapeutic products, which significantly increases pharmaceutical efficacy and decreases the dose of use. The fate of the drug in parenteral administration is no longer determined by the properties of the drug, but by the type of drug nanocarrier.

The kidneys effectively remove, by blood filtration, NPs with diameters smaller than 10-20 nm, and filtration through inter-endothelial slits in the walls of the splenic sinus removes particles of more than 200 nm. These filters suggest that the size of the nanoparticles should not be less than 20 nm and not more than 200 nm if prolonged circulation within the body is desired.

The mononuclear phagocyte system (MPS), composed of phagocytic cells, mainly monocytes and macrophages, plays an important role in the removal of NPs from the bloodstream. The recognition of NPs by these cells occurs after a process called opsonization. The opsonization process is the adsorption of protein entities capable of interacting with specific plasma membrane receptors in monocytes and several subsets of tissue macrophages, thus promoting the recognition of particles by these cells,[225] while the absence of opsonins in the adsorption pattern and the presence of dysopsonins lead to the circulation of particles in the bloodstream. Properties such as NP size, surface charge, hydrophobia/hydrophilicity and steric effects of particle coating can determine the compatibility of NPs with the immune system.

9.1. Protein Corona Formation.

When nanosystems are in a physiological environment, they quickly adsorb biomolecules such as proteins and lipids on their surface forming a “protein corona” (**Figure 18**), a biomolecular interface organization that can be freely divided into two components called “hard” and “soft” corona respectively. The protein corona will change the composition if the NP moves to another compartment or fluid.[226]

This crown surrounding the particle changes its original surface charge, size, solubility, aggregation and, therefore, changes the interaction of NPs with cells, influencing traffic, biodistribution and cellular absorption.[227]

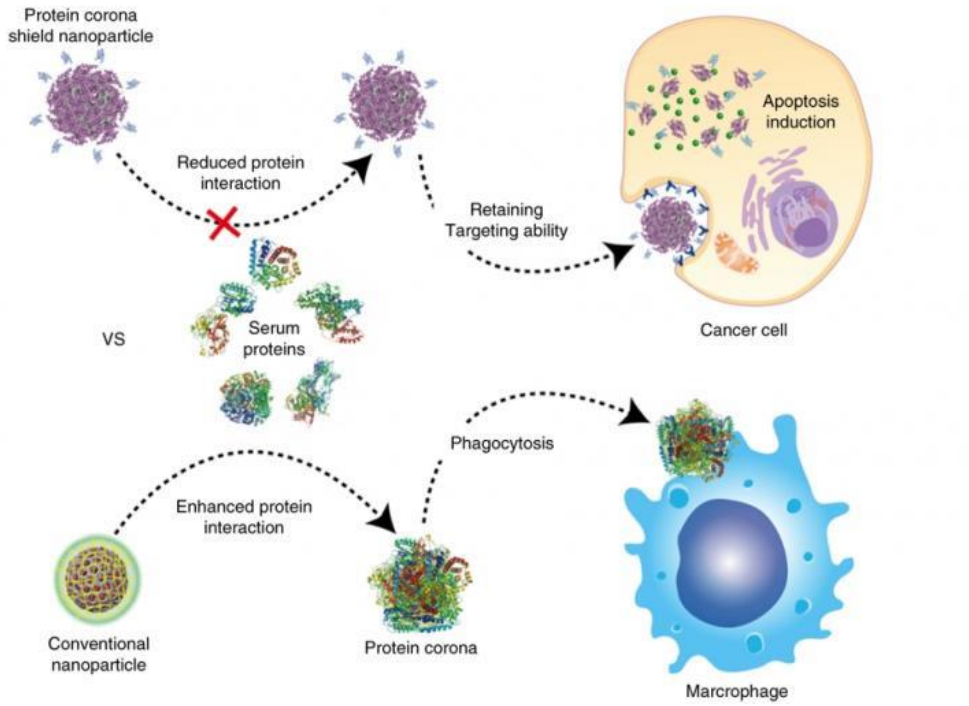

Figure 18: Schematic representation of protein corona developed on the surface of NPs in the presence of serum proteins.[228]

The protein corona influences macrophage uptake. Macrophage-killing receptors are a large group of phagocytic receptors that are responsible for the elimination of pathogens and negatively charged ligands that circulate in the blood. For example, opsonins such as IgG, complement factors and fibrinogen promote phagocytosis, removal of NPs from the bloodstream and concentration in the liver and spleen, while dyopsonins such as albumin and apolipoprotein help a longer circulation of NPs in the body.[168] It was reported that polystyrene microparticles with human serum albumin adsorbed on its surface, inhibit their phagocytosis by dendritic cells.[229]

For many nanosystems, while extraction from bloodstream is a question of minutes, interaction with distant cells is effective hours or days after exposure.

Nanoparticles functionalized with hydrophilic polymers such as polyethylene glycol (PEG) and poloxamers show better lifetime circulation properties and lower recognition of macrophages of many types of NPs by preventing protein adsorption.[230] In the case of PEGylated NPs, the adsorption of plasma proteins is influenced by the length and density of the polymer.

It has been claimed that the protein corona can cover targeting surface of nanosystems and, therefore, strongly reduces the ability to target and recognize the specific ligand by cellular receptors.[231] Therefore, understanding the interaction of the cellular plasma membrane and the protein corona around the NPs is essential to design their synthesis, drug delivery and administration.

9.2. How to Avoid Immune System Clearance.

Nanoparticles can be designed to prevent the immune system elimination and increase the circulating half-life in the blood. An important reason for seeking this is to provide a long-circulating drug vehicle from which the drug can be released in the vascular compartment continuously and in a controlled manner.

A relatively successful approach to prolong the circulation times of NPs in the blood is to create a steric/hydrophilic surface barrier of sufficient density. The poloxamer and poloxamines have been investigated to reduce the adsorption of blood proteins and opsonins and, therefore, increase the half-life of nanosystems.

Poloxamers, also known as Pluronic®, and poloxyamines or Tetronic®, are non-ionic block polymers of hydrophobic propylene oxide (PO) and hydrophilic ethylene oxide (EO). The poloxamers consist of a central hydrophobic polypropylene oxide (PPO) molecule, which is flanked on both sides by two hydrophilic polyethylene oxide (PEO) chains as shown in **Figure 19**. Poloxamines are tetrafunctional block copolymers with four coupled PEO-PPO blocks by a central bridge of ethylenediamine.[232] The adsorption of these molecules on the surface of the NPs through their hydrophobic PPO fragments provides stability to the suspension of particles by a repulsion effect through a steric stabilization mechanism, because this type of absorption leaves the hydrophilic PEO extended towards outside from the surface of the particle in a mobile state. The NPs designed with poloxamers and poloxamines exhibit reduced adsorption of blood

proteins and opsonins[233] and, as a result, resist ingestion of scavenger phagocytic cells and remain in the systemic circulation for a prolonged period.

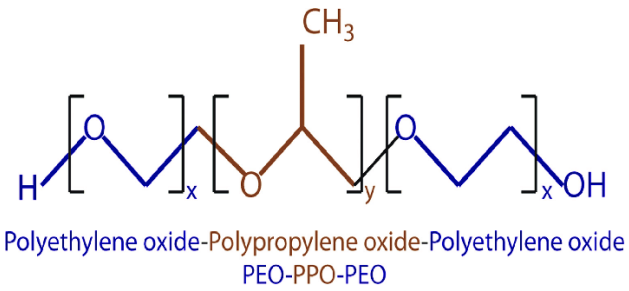

Figure 19: Structure of Pluronics.

The addition of poly (ethylene glycol) (PEG) has been widely used to increase the circulating half-life of NPs and is the preferred method of "masking" the NPs of immune system recognition. This process is also known as PEGylation.[234] PEG is a linear diol polyether that exhibits a low degree of immunogenicity and antigenicity.[235] The polymer main chain is essentially chemically inert, and the terminal primary hydroxyl groups are available for derivatization. The modification of the surface of the NPs with PEG and its derivatives can be carried out by adsorption, incorporation during the production of NPs or by covalent binding to the surface of the particles.[225] The addition of PEG can add protein resistance/opsonization properties by preventing interactions between the surface of the particle and plasma proteins, although adsorption is not completely avoided. Several studies have been conducted to determine how a change in the thickness and density of a PEG coating affects opsonization and biodistribution, showing that the degree of protein adsorption depends on the size of the PEG and graft density.[236,237]

10. CLINICAL TRIALS. SO MANY PAPERS AND SO FEW COMMERCIAL PRODUCTS.

Approval of drugs for human use by the Food and Drug Administration (FDA) through the Center for Drug Evaluation and Research (CDER) is an expensive and time-consuming process, and approval rates are low.[238] In general, the drug approval process by the FDA can be separated into preclinical, clinical and post-marketing phases. To date,

there are five clinically approved NP chemotherapeutics for cancer and many more in preclinical and clinical research[239,240] (**Table 3**).

Liposomal anthracyclines were the first NP therapies approved for clinical use. Anthracyclines (which include doxorubicin, daunorubicin, epirubicin and idarubicin) are highly effective against a wide range of cancers. Today, there are three liposomal formulations of clinically approved anthracyclines: pegylated liposomal doxorubicin (PLD; DOXIL in the United States, Caelyx elsewhere), non-pegylated liposomal doxorubicin (NPLD; Myocet) and liposomal daunorubicin (DaunoXome).[241]

In addition, Abraxane was approved by the FDA for the treatment of breast cancer. It is a 130 nm NP paclitaxel formulation bound to albumin; a non-water-soluble drug effective against different types of cancer.[242]

Finally, another clinically accepted nanosystem is the formulation of polymeric micelles of paclitaxel (Genexol-PM), with a diameter of 20-50 nm and composed of block copolymers of PEG and poly- (D, L-lactic acid).[243]

Table 3: Some of the nanomedicines approved by one or more regulatory bodies.[240]

Product	Nanoplatform/agent	Indication	Status	Company
Doxil	PEGylated liposome/doxorubicin hydrochloride	Ovarian cancer	Approved 11/17/1995 FDA50718	Ortho Biotech (acquired by JNJ)
Myocet	Non-PEGylated liposomal doxorubicin nanomedicine	Metastatic breast cancer	Approved in Europe and Canada, in combination with cyclophosphamide	Sopherion Therapeutics, LLC in North America and Cephalon, Inc. in Europe
DaunoXome	Lipid encapsulation of daunorubicin	First-line treatment for patients with advanced HIV-associated Kaposi's sarcoma	Approved in the USA	Galen Ltd.
ThermoDox	Heat-activated liposomal encapsulation of doxorubicin	Breast cancer, primary liver cancer	Received Fast Track Designation, approval expected by 2013	Celsion
Abraxane	Nanoparticulate albumin/paclitaxel	Various cancers	Approved 1/7/2005 FDA21660	Celgene
Rexin-G	Targeting protein tagged phospholipid/microRNA-122	Sarcoma, osteosarcoma, pancreatic cancer, and other solid tumor	Fully approved in Philippine Phase II/III (Fast Track Designation, Orphan Drug Status Acquired) in USA	Epeius Biotechnologies Corp.
Oncaspar	PEGylated asparaginase	Acute lymphoblastic leukemia	Approved 24/06/2006	Enzon Pharmaceuticals, Inc.
Resovist	Iron oxide nanoparticles coated with carboxydextran	Liver/spleen lesion imaging	In 2001, approved for the European market	Bayer Schering Pharma AG
Feridex	Iron oxide nanoparticles coated with dextran	Liver/spleen lesion imaging	Approved by US-FDA in 1996	Berlex Laboratories
Endorem	Iron oxide nanoparticles coated with dextran	Liver/spleen lesion imaging	Approved in Europe	Guerbet

Many other therapies are being clinically investigated. Most of them are liposomes, polymeric NPs, micelles and lipid NPs, which carry different cancer medications such as platinum drugs (cisplatin, carboplatin and oxaliplatin), alkaloids (vincristine, camptothecin derivatives and taxanes), or small interfering RNA (itRNA) among others.[239]

11. POLYSTYRENE NANOPARTICLES AND NANOEMULSIONS

The research reported in this thesis is based on the use of two nanosystems (polystyrene NPs and nanoemulsions) as a vehicle for drug delivery to treat breast and pancreatic cancer. The specific development as well as the background of each type of nanosystem is detailed in Chapter 1 for polystyrene NPs and in Chapters 2 and 3 for nanoemulsions. The characteristics of each nanosystem and its use in cancer therapy will be discussed below in a general way.

11.1 Polystyrene Nanoparticles

The NanoChemBio team has designed and developed a chemical methodology for the preparation of a wide range of functionalized, monodispersed and cross-linked polystyrene NPs, available in various sizes depending on the biological application (100 nm-2µm) (**Figure 20**). The synthesis and characterization of polystyrene NPs will be detailed in Chapter 1. These particles are chemically and biologically compatible and, therefore, can be used in different applications in the biomedical field.

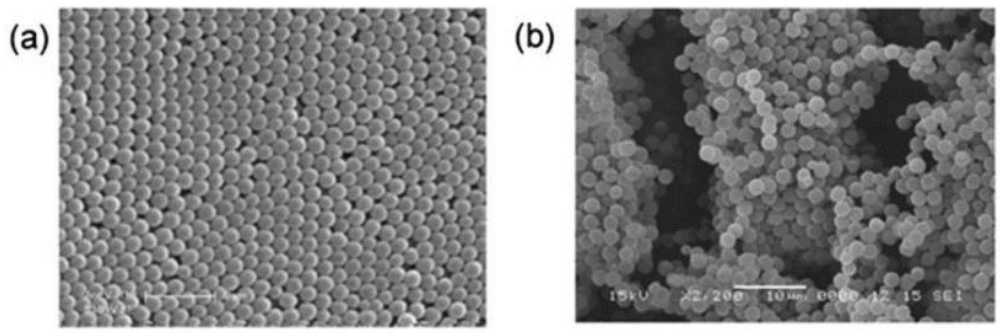

Figure 20: Scanning electron microscopy image of nanoparticles. a) 500 nm b) 200 nm

An important aspect of these nanoparticles is the ease and speed with which they are able to efficiently enter all cell lines studied to date, including adherent cells, suspension cells, stem cells and primary cells.[244] Possibly, because they have a mechanism of passive cellular input based on direct penetration (**Figure 21**), which has been previously verified by chemical and microscopic techniques for polystyrene NPs of various sizes (200 nm and 500 nm).

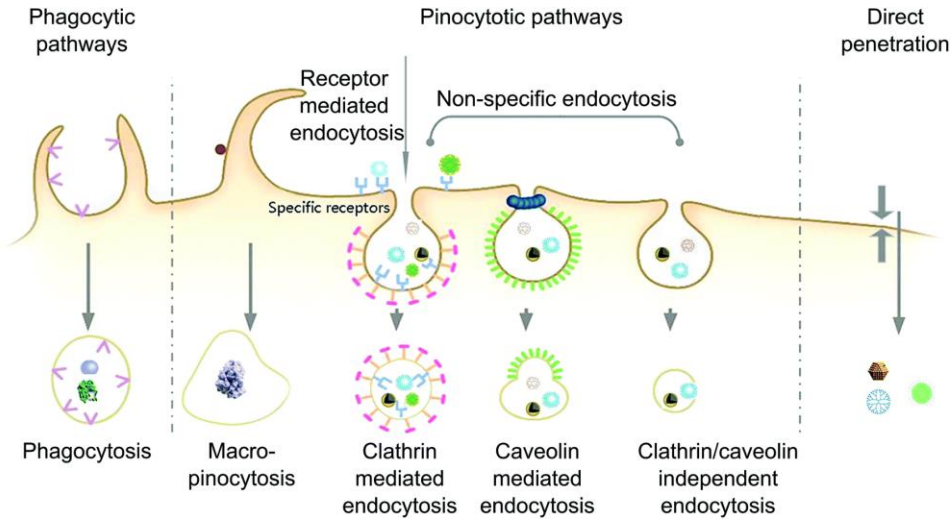

Figure 21: Schematic demonstrating the main mechanisms by which NPs are uptaken and subsequently intracellularly processed by cells. The exact mechanism taken by a particular particle is highly dependent on the precise NP characteristics, polypeptide coating layers, target cell type, and environment. The situation is further complicated by the ability of particles to exploit multiple different uptake pathways in parallel.[245]

Positive results of cellular internalization of polystyrene NPs in ESC have been reported.[246] It is important to note that these NPs do not show cellular cytotoxicity in any of the studied cell lines.[247] In this sense, perhaps the most rigorous study that has been carried out has been the generation of live and viable mice from mouse ESC previously incubated with fluorescent NPs, revealing the absence of cytotoxicity of the NPs.[248]

In addition, to corroborate the absence of cellular cytotoxicity, deep studies have been carried out on the levels of gene expression[247] and protein[249] after cellular

internalization of polystyrene NPs of various sizes (200 nm and 500 nm) in human embryonic kidney cells (HEK-293T) and murine fibroblasts (L929). The evaluation of changes in gene expression levels after internalization of 200 nm NPs was examined in both cell lines and no significant and conserved changes in gene expression were found. Therefore, examination of the gene expression profile induced by the internalization of the NPss revealed no significant transcriptional changes compared to the untreated control cells.[247] To identify differentially expressed proteins, a comprehensive proteomic analysis was performed after internalization of the 200 nm and 500 nm NPs. According to the previously obtained genomic data, the internalization of the NPs did not induce a significant variation in protein expression levels, only two significant changes were detected in the total proteome of murine fibroblasts, and none in human cells. Affected proteins were mainly involved in transcription, cell metabolism and cytoskeleton activities, therefore, important processes such as cell survival, proliferation and death, which were differentially expressed after treatment, confirming the high biocompatibility were not affected. of these nanotransporters.[249]

These NPs have been efficiently conjugated to a wide variety of materials with biological and/or therapeutic activity without affecting their nanofection capacity and have been used for different purposes as pH or calcium sensors, for the controlled release of macromolecules such as proteins and oligonucleotides, among others. Dr. Sánchez Martín, who is one of my thesis directors has developed some biological applications of these NPs, such as their use as intracellular calcium sensors.[250]; the use of fluorescent NPs as pH sensors in living cells[251]; the cellular internalization of fluorescent NPs with biotin-streptavidin[252]; the transport and intracellular release of siRNA by NPs[246,253,254]; the transport and release of proteins by NPs[255,256]; the transport and release of DNA by NPs[256]; the use of cells as "catalytic reactors", the use of palladium NP catalysis in living cells.[257] or the use of NPs as intracellular sensors of caspase-3/7 in apoptotic living cells[258] among others.

Here are two examples of these biological applications:

1. **Cellular internalization of fluorescent nanoparticles with biotin-streptavidin.**

   The use of streptavidin-conjugated NPs as a transport system capable of entering living cells using a biotinylated fluorophore (**Figure 22**) has been demonstrated by fluorescence microscopy and flow cytometry. In addition, cell internalization of a biotinylated oligonucleotide was efficiently carried out. The fact that there are several biotinylation strategies to bind different molecules such as peptides, proteins, antibodies and nucleic acids to streptavidin-loaded nanoparticles opens the door to numerous applications such as intracellular detection of a variety of macromolecular targets.[252]

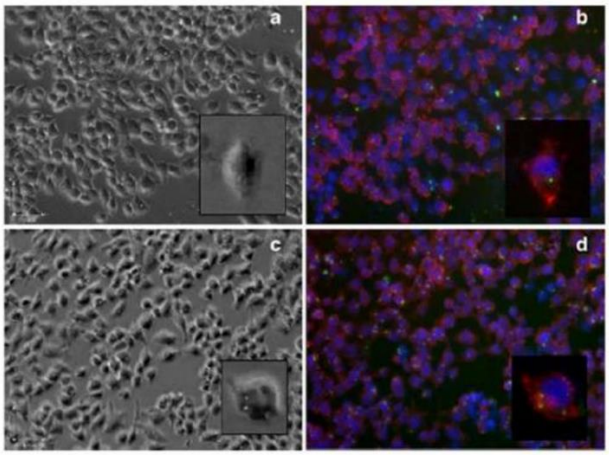

Figure 22. Analysis by confocal microscopy of the cellular internalization of 0.5 and 2 µm nanoparticles (a and b) and streptavidin-conjugated nanoparticles labeled with fluorescent biotin (c and d) in the HeLa cell line. The images a and c are taken in differential interference contrast. The cytoskeleton was stained with a red fluorescent marker (AlexaFluor® 568-phalloidin) and the core with Hoechst 33342 (b and d).

2. **Transport and release of proteins by nanoparticles.**

   Nanoparticles have been used to facilitate the release of several functional proteins within different cell lines (including mouse ESCs) (**Figure 23**) demonstrating that several functional proteins such as β-galactosidase and green fluorescent protein (GFP) can be released into

cells and quantified. In addition, the marking of the NPs with fluorescence allows the identification and subsequent isolation of the selected cells.[255,256]

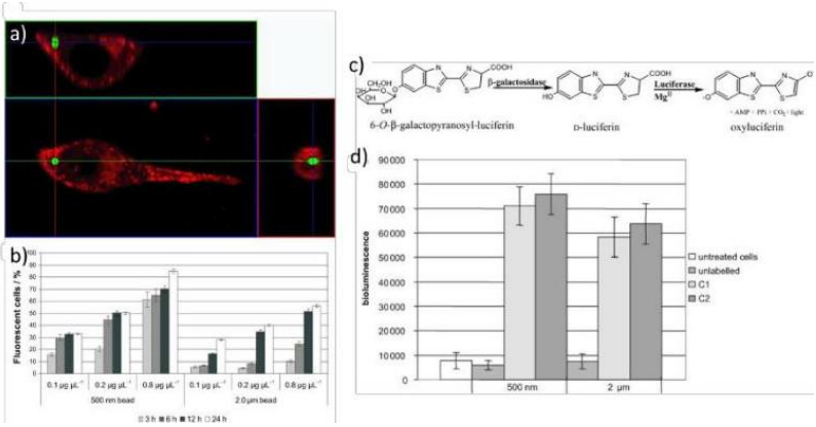

Figure 23 a): Image obtained by confocal microscopy of a mouse melanoma cell (B16F10) with a NP conjugated to EGFP protein after 24 hours of incubation. b) Flow cytometric analysis of the efficiency of cell entry of nanoparticles in B16F10 cells. c) Principle of bioluminescence detection of β-galactosidase activity d) Results of β-galactosidase activity in HeLa cells incubated with NPs bound to β-galactosidase.

The two main advantages of polystyrene NPs compared to nanoemulsions are that (i) their cross-linked structure allows obtaining NPs in the nanometric range compatible with aqueous and organic media (such as dimethylformamide or methanol) so they can follow traditional protocols of organic solid phase synthesis, allowing to carry out multiple chemical reactions, differing from the rest only compatible with aqueous media; and (ii) that the cells can be isolated with the NPs inside, this would allow defining the content of the transported load. Cells can be separated with NPs of two different colors, allowing the monitored release of two independent biomolecules within the same cell.

11.2 Nanoemulsions

An emulsion can be defined as a heterogeneous mixture of at least two immiscible liquids, that is, a dispersion of one liquid (dispersed phase) as drops in another (continuous phase). Depending on the nature of the dispersed and continuous phase, different types of emulsions can be distinguished. For example, an oil-in-water

dispersion is known as an oil-in-water (O/W) emulsion, while the opposite case will be called a water-in-oil (W/O) emulsion. If the dispersed phase represents an emulsion in itself, the systems formed are called multiple emulsions (O/W/O, W/O/W, and so forth) (**Figure 24**).

The interface of emulsions is stabilized by the presence of an emulsifier or surfactant (surfactants), which remains immobilized between the different phases that act as film formers, reducing interfacial tension and/or providing a mechanical barrier against coalescence, stabilizing the emulsion. Surfactants are molecules that have a polar (hydrophilic) and a non-polar (hydrophobic) region. This type of structure with a water insoluble fragment and a water-soluble moiety is called amphiphilic or amphipathic.

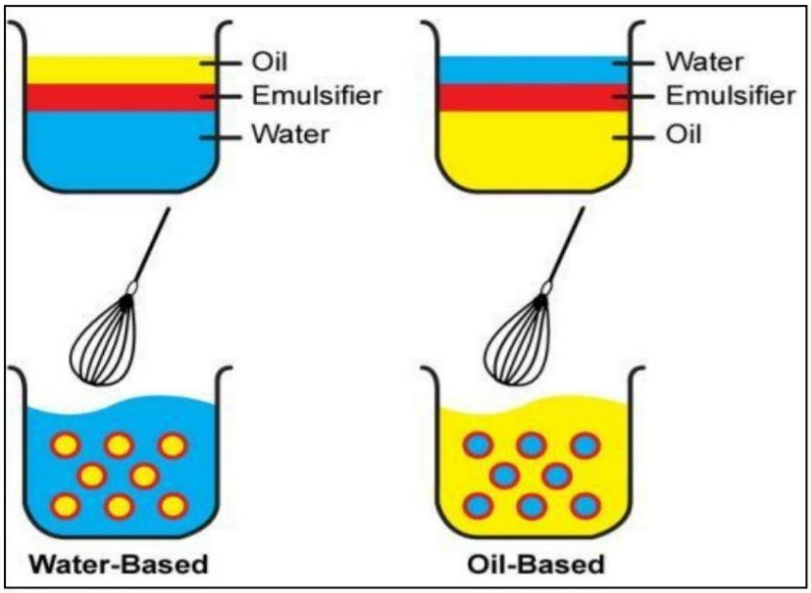

Figure 24: Different types of emulsions according to the nature of the dispersed and continuous phases.[259]

Nanoemulsions are emulsions with a drop size on the nanometric scale, and typically with a diameter less than 500 nm.[260,261] Some authors consider 200 nm or even 100 nm as the upper limit,[262] since they correlate with the word "nanotechnology" as defined by the US government's National Nanotechnology Initiative, i.e., "the

understanding and control of matter in dimensions of approximately 1–100 nm". Even within that definition, there is no unanimity about whether size should refer to radius or diameter. Although this use may coincide with current language trends, it establishes an arbitrary size limit because the emulsion properties do not change instantly when crossing the 100 nm threshold,[260] as will be seen throughout the explanation of the main properties of nanoemulsions.

It should be noted that the terminology used in this thesis has been, mainly, lipid nanocapsules because morphologically they are formed by an oily core surrounded by a polymeric shell (thick amphiphilic mechanical barrier at the droplet interface),[263] but other general terms have also been employed as nanoemulsions, nanocarriers or nanosystems.

The distinction between conventional emulsions and nanoemulsions is not arbitrary. Due to the small droplet size of nanoemulsions, new interesting properties arise, especially those related to the use of nanoemulsions as drug delivery systems. Some of these properties are:

1. **Large surface area:** for a given volume of dispersed phase, the smaller the droplet size, the greater the total surface area. In many cases, a large amount of surface is related to a high absorption of a medicine. For example, if topical administration is considered, the large surface area of the nanoemulsion allows rapid penetration of the assets.[264]
2. **Great stability against the formation of creams/sedimentation:** due to the different densities between the oil and water phases, in conventional emulsions the drops tend to float (forming creams) or to sink (sedimentation). However, in nanoemulsions the small droplet size causes a large reduction in the force of gravity, and the Brownian movement becomes sufficient to overcome gravity.[265]
3. **Intravenous administration:** it has been documented that for intravenous applications the drops should not be larger than the diameter of the capillaries (approximately 5 μm) to avoid blockage. It is known that conventional emulsions that have a drop size of about 4-6 μm or more increase the incidence of emboli and may cause changes in blood pressure.[266] In fact, the United States Pharmacopoeia has recently established that the average droplet size should be

<500 nm for injectable emulsions,[267] therefore, they belong to the nanoemulsion range.

11.2.1 Nanoemulsion Stability.

The stability of nanoemulsions is a key issue for most of its applications. This ability to remain unchanged becomes of paramount importance when nanoemulsions are to be used as medication delivery systems, since a change in their properties could render them useless or even harmful. Therefore, the mechanisms of destabilization of the nanoemulsion must be thoroughly understood and understood to avoid them. These mechanisms are quite similar to those of conventional emulsions, although some particularities must be highlighted. The main mechanisms of destabilization of nanoemulsions, represented in **Figure 25**, are:

1. **Coalescence:** nanoemulsions are not a thermodynamically stable system. If two drops are allowed to come into close contact, they will fuse to form a larger drop, as this brings a reduction in the total interfacial area and, therefore, a reduction in the total free energy of the system. This new drop could be fused with another and so on, which would lead to the final phase separation. It is an irreversible process and changes several properties of emulsions, such as droplet size, number of drops, total surface area or monodispersity. For these reasons, it is one of the worst destabilizing effects that affect nanoemulsions. Fortunately, with the right method of preparation, the type and amount of surfactant can be avoided for long periods of time, even for years.[262]
2. **Flocculation:** is the aggregation of drops without merging, that is, the drops retain their individual integrity (in contrast to emulsions destabilized by coalescence). It is a reversible process and can be prevented if the appropriate type and amount of surfactant is used.
3. **Ostwald ripening:** is the process by which the greater Laplace pressure within the small droplets drives the transfer of dispersed oil from small to large droplets through the dispersion medium. As a result, larger drops grow at the expense of smaller ones. It requires a high solubility of the dispersed phase in the continuous phase and, therefore, is only noticeable in emulsions of low molecular weight

oils. It is claimed that an emulsion is stable to Ostwald ripening when at least 50% of the oil phase is an insoluble triglyceride.[268]

4. **Creaming:** due to the different densities, the dispersed phase floats to the top of the continuous phase, according to the Stokes equation. In emulsions, this means that the oil droplets accumulate on top. However, in nanoemulsions, this destabilization is reduced sufficiently due to the small droplet size, which allows the Brownian movement to overcome the forces of gravity, since the diffusion rate becomes faster than the cremation rate.[269]
5. **Sedimentation:** it is the opposite of the last mechanism, that is, in this case the dispersed phase has a higher density than the continuous phase, and therefore sinks to the bottom. In addition, this destabilization would be avoided in nanoemulsions due to the small droplet size, analogously to cremation destabilization.

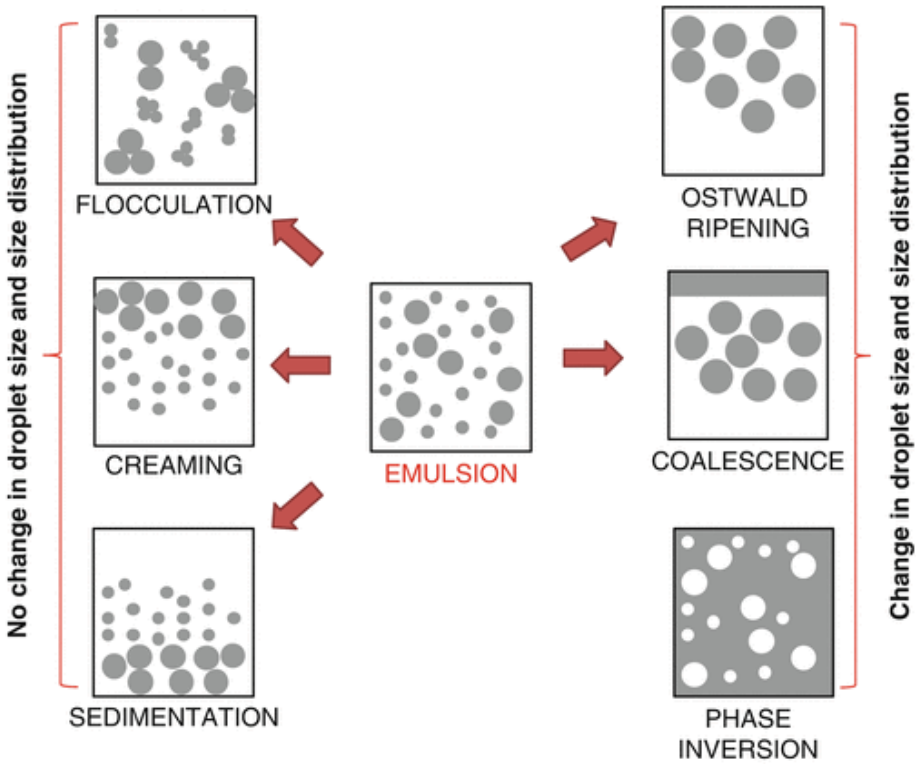

Figure 25: Schematic representation of the main destabilization mechanisms of emulsions.[270]

As mentioned above, the interface of emulsions is stabilized by the presence of an emulsifier or surfactant (surfactants). Surfactants may include nonionic block copolymers, lecithin (charged) and alcohols. Traditionally, nanoemulsions have been prepared using phospholipids as emulsifying molecules. They are ionic surfactants that offer electrostatic stabilization.[271,272] Droplets repel each other because they are composed of the same phospholipids that provide particles with net charges of the same sign. When two different phases are in contact, if one of the phases is a charged NP and the other is an electrolytic solution, ions dissolved in the medium with charge opposite to the surface of the particle tend to surround the particle to maintain neutrality of the solution. The arrangement of the charges located in one phase and those fixed on the surface of the particle form what is called the electrical double layer.[273]

Electrokinetic phenomena is a generic term applied to the effect associated with the relative movement of the ionic solution near the charged interfaces. One of these electrokinetic phenomena is the electrophoresis that appears when a uniform electric field is applied and the velocity of the particles in the steady state is measured. The electrophoretic mobility of a particle is proportional to the zeta potential, which is the potential existing in the cutting plane of the moving particles.[274]

The stability of nanoemulsions stabilized with ionic surfactants is compromised in the presence of high ionic strength media. That is the case of physiological conditions. At high salt concentrations, the accumulation of counterions near the interface filters the particle charge, causing a decrease in the zeta potential value caused by double layer compression and subsequently reducing the stability of nanoemulsions because repulsion decreases between particles.[274,275] The use of non-ionic surfactants has attracted special attention to solve these problems, although the stability they cause does not have an electrical origin.

Non-ionic surfactants are also called steric surfactants because when they are absorbed on the surface of the particles, the nanoparticles are stabilized by avoiding other particles by steric/hydrophilic repulsion.[276] Steric surfactants have bulky groups that protrude into the dispersed/continuous medium, which creates a brush-shaped barrier around the drops. When two drops approach each other, the free movement of these flexible groups is hindered by the interpenetration of the adsorbed layers,

resulting in an entropic repulsion.[277] Among others, triblock copolymers, such as poloxamers, already described above to prevent immune clearance, are a well-known example of steric surfactants. Poloxamers, unlike ionic surfactants, are not affected by high concentrations of electrolytes and, therefore, their nanoemulsions can be safely used in many industrial and pharmaceutical applications where high ionic strength values are needed.[278]

11.2.2. Advantages as Drug Delivery Carriers.

Last years, more innovative nanoemulsion formulations have been developed that vary the different components, such as the emulsifier and/or the nature of the emulsified oil.[279] The Oil phase (O-phase) dispersed in most nanoemulsions is generally composed of vegetable oils (fatty acyls) or medium chain triacylglycerols. The combination of the advantages of traditional parenteral emulsions (mainly biocompatibility and biodegradability) with the new functionalities has led to the first commercialized drug delivery systems based on nanoemulsions and several formulations are currently marketed. Examples include etomidate (Etomidat-Lipuro®) and diazepam (Diazepam-Lipuro®).[280]

Nanoemulsions have demonstrated great potential for the administration of drugs in the treatment of cancer, being able to administer a high concentration of chemotherapy drugs to cancerous tissues, improving their bioavailability. The oil phase of the nanoemulsion acts as a solubilizer for the lipophilic compound, thus improving the solubility of the drug in an emulsion system. Therefore, a smaller amount of the drug should be administered compared to an aqueous solution. By exposing the tissue to a lower concentration of the drug and by avoiding an irritating tissue vehicle, pain associated with intravenously administered drugs can be minimized.[281] In addition, because lipophilic drugs are incorporated into the innermost oil phase, they are sequestered from direct contact with body fluids and tissues, which can help overcome the pharmacokinetic mismatch associated with that particular chemotherapeutic agent.[282]

The main advantages of nanoemulsions in the field of drug delivery systems for hydrophobic drugs are: inexpensive and easy-to-scale production, low toxicity, independence of dilution, high content of the lipid phase and reduced side effects.[262]

HYPOTHESIS

HYPOTHESIS

The development of targeted therapies, in particular for cancer treatment, is one of the main goals of nanomedicine today. Conventional chemotherapy usually prompts modest tumor response and provokes undesirable side effects due to the nonspecific action of drugs on proliferating tissues. To avoid these and other disadvantages, drug nanocarriers should be formulated to deliver the antitumor drug directly to the cancerous cells. This is a complex interdisciplinary task with too many variables to be properly controlled. These variables include the use of biocompatible materials, with simple but robust processes for biomaterial assembly, usually requiring different conjugation chemistries followed by some purification processes. Therefore, current formulations based on complex nanostructures such as polymer conjugates, polymeric micelles, liposomes, carbon nanotubes, or nanoparticles, must be superficially modified to provide nanocarriers with vectorization properties. On the one hand, our group has developed several strategies for preparing functionalized polymeric cross-linked polystyrene NPs which are then covalently conjugated to cargoes of different nature. On the other hand, in recent years, lipid liquid LLNCs have been developed as potential nanocarriers. The inner hydrophobic domain, surrounded by an amphiphilic mechanical barrier, has been used to encapsulate hydrophobic drugs that are protected during their transport to the target cells.

Thus, we hypothesized that:

1. The multifunctionalization of polystyrene NPs with a ligand, such as CRGDK peptide that specifically recognize Nrp-1 membrane integrin, together with a fluorophore would be a good target delivery strategy against overexpressing Nrp-1 TNBC. In addition, the conjugation *via* pH cleavable linker of Doxorubicin (a drug of election to treat TNBC in clinical use but avoid due to side effects) and a tracker to monitor response to treatment and metastasis would make this nanodevice a good diagnostic tool and therapeutic agent to treat this cancer subtype.
2. LLNCs have an external shell which can be physico-chemically modified by proteins, such as HSA which is considered a disopsonin, i.e. a molecule that can avoid clearance by the reticulo-endothelial system and it accumulates in

malignant and inflamed tissues, and serves as the main nutrient for tumor growth. In addition, vehicularizing curcumin, which has been shown to have a cytotoxic effect on tumor cells, in the oily core of these modified LLNCs could result in a good nanosystem to target and kill breast cancer tumor cells *in vitro*.

3. LLNCs have an external shell which can be engineered by phospholipids, by surfactants as poloxamers and by molecules that provide free functional groups (e.g. Deoxycholic acid) for conjugation with ligands such as anti-CD44 antibody which is overexpressed in PCSCs. In addition, carrying paclitaxel, which is a drug used in clinic to treat pancreatic cancer, and a fluorophore, which allow to track the LLNCs *in vivo*, in the oily core of these modified LLNCs would make this nanosystem a good theranostic agent to target and kill PCSCs *in vitr*o and *in vivo*.

OBJECTIVES

OBJECTIVES

The main goal of this study was to evaluate the potential of different nanosystems (Polystyrene NPs and Nanoemulsions) to transport and deliver anticancer drugs such as Doxorubicin, Curcumin and Paclitaxel, with the aim of improving the targeting delivery in breast and pancreatic cancer cells enhancing at the same time their therapeutic efficiency.

To achieve this goal several steps were followed:

1. To trifunctionalize polystyrene NPs using a chemical-based orthogonal strategy in order to conjugate a tracker (Cy7 fluorophore), Doxorubicin (*via* pH cleavable linker) and a specific ligand (CRGDK peptide) to these NPs
2. To carry out a physico-chemical characterization of these NPs as well as to evaluate their uptake *in vitro* in the MDA-MB-231 TNBC cell line.
3. To evaluate the antitumoral effect of these modified polystyrene NPs *in vitro* and *in vivo* by generating an orthotopic TNBC xenotransplant as well as to carry out a tracking in order to verify their specific targeting delivery.
4. To develop colloidally stable nanocapsules (LLNCs) with an olive-oil core surrounded by a GAD cross-linked HSA and to perform a physico-chemical characterization of these modified nanocapsules loaded with curcumin.
5. To evaluate the uptake of LLNCs cross-linked with GAD with different modifications in their shell such as the addition of poloxamers or oleic acid by the MCF-7 BC cell line.
6. To evaluate the cytotoxic effect of curcumin-loaded LLNCs cross-linked with GAD in MCF-7 BC cell line.
7. To synthesize lipid nanocapsules (O^2LNC) based on an olive oil core surrounded by a shell structure composed of different amphiphilic molecules
8. To covalently bind an anti-CD44 antibody to their surface (immuno-O^2LNC), with the desire properties such as colloidal stability, particle size, monodispersity, and surface charge and to carry out a complete physico-chemical characterization of these modified O^2LNC.

9. To encapsulate in the oily core of the immuno-O^2LNC a hydrophobic dye (Nile Red or IR 780 iodide) and an anticancer drug (paclitaxel) in order to study the uptake and cytotoxic effect in both BxPC-3 PCC and PCSCs.

10. To generate an *in vivo* pancreatic orthotopic xenotansplant model by inoculation of BxPC-3 PCSCs transduced with SELWP LV.

11. To evaluate the specific targeting by bioluminescence and fluorescence of the immuno-O^2LNC in this *in vivo* PCSCs model.

CHAPTER 1

A VERSATILE THERANOSTIC NANODEVICE BASED ON AN ORTHOGONAL BIOCONJUGATION STRATEGY FOR EFFICIENT TARGETED TREATMENT AND MONITORING OF TRIPLE NEGATIVE BREAST CANCER

BACKGROUND

Theranostic nanodevices are capable of both delivering therapy and tracking disease through imaging. To produce these nanodevices combining cancer therapy and disease monitoring, synthetic methods for the effective multifunctionalization of NPs with a therapeutic cargo together with a ligand for selective delivery and a fluorophore to allow efficient tracking using fluorescence based imaging detection have to be developed, being this issue one of the challenges to produce theranostic nanodevices.[283,284] Most common approaches used for preparing theranostic NPs comprise drugs and trackers to be heterogeneously encapsulated in the core of the NP while ligands for targeted delivery are conjugated to the surface of the NP.[285,286] However, the versatility of these systems can be compromised due to incompatibilities between the conjugation chemistries and the encapsulation protocols. Consequently, there is still a gap to improve the loading efficiency of each component of the theranostic nanodevices.

Over the last decade, our group has developed several strategies for preparing functionalized polymeric cross-linked polystyrene NPs which are then covalently conjugated to cargoes of different nature (fluorophores, small drugs, proteins, nucleic acids and their mimics).[287,288] The main benefits of using polystyrene NPs are their robustness and stability in the biological environment, their lack of cellular toxicity during long term incubations[289] and their compatibility with standard multistep chemistries, allowing different orthogonal conjugation strategies. All of these features allow their easy entry in a broad range of cell types.[246,287,288,290,291] Remarkably, gene-expression profiling studies showed that these NPs did not induce any significant alteration in nanofected cell transcriptomes.[247] Proteomic studies showed that no key regulators of cell cycle were affected by the internalization of these NPs (their intracellular localization has been proven).[292]

Recently, the development of an efficient nanotechnology fluorescence-based method to track cell proliferation to avoid the limitations of current cell-labelling dyes has been reported.[293] Additionally, the design of a straightforward strategy to conjugate drugs via click chemistry to NPs as a novel tool to study target engagement and/or

identification inside living cells was recently presented.[294] All of these properties make NPs promising candidates for cancer theranostic applications.

Herein, we report a chemical-based orthogonal strategy for NPs multifunctionalization that opens the door for the design of a versatile nanodevice that allows the covalent conjugation of a therapeutic cargo, a ligand and a tracker in a controlled manner. This strategy allows tuning the ratio between the amounts of each one of the components. This highly controlled strategy increases the possibilities of developing more effective and reproducible nanodevices for controlled released at the desired location, with minimal off-target release that may compromise healthy tissue together with monitoring in real time. A significant advantage in covalently linking therapeutic cargoes to a vehicle system over conventional encapsulation approaches is the ability to have better control over loading and drug release. In addition, the covalent binding of the drug to the nanosystem tackle another problem faced by current treatments, low water solubility and leaking from the nanoencapsulation. The presence of a fluorophore tracker on the theranostic NP allows monitoring tumor location, disease evolution and treatment efficiency. The tri-functionalized NPs carrying doxorubicin (DOX), near-infrared cyanine dye (Cy7) and a homing peptide (CRGDK), which can actively recognize the neuropilin-1 (Nrp-1) receptor (overexpressed in triple negative breast cancer[295]) were evaluated *in vitro* using MDA-MB-231 tumor cell line and *in vivo* using an orthotopic breast cancer xenotransplant mouse model.

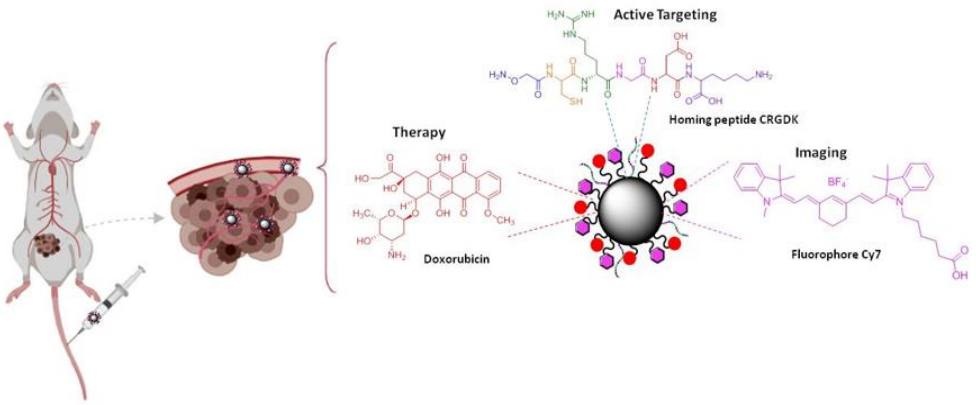

MATERIALS AND METHODS

MATERIALS AND METHODS

1. Preparation of theranostic nanoparticles (HP-Cy7-DOX-NPs)

All solvents and chemicals were purchased from Sigma-Aldrich. Double PEGylated and bifunctionalized NPs (Fmoc-Dde-NPs, 6) were obtained by using protocols previously described[296] (**see Annexes, S.I. Chapter 1**). Next, DOX-NPs (9) were obtained by carboxy functionalization and hydrazine treatment followed by DOX conjugation (**see Annexes, S.I. Chapter 1**) Then trifunctionalized NPs were generated by treatment with Fmoc-lysine-Dde (OH) (15 equiv), Fmoc deprotection and fluorophore conjugation (**see Annexes, S.I. Chapter 1**). Finally, COOH-Cy7-DOX-NPs (13) were activated with oxyma (15 equiv) and DIC (15 equiv) and were functionalized with a solution of CRGDK homing peptide (**see Annexes, S.I. Chapter 1**) in DMF and DIPEA at 25 °C for 15 hours to obtain (HP-Cy7-DOX-NPs (14)).

2. Characterization of theranostic nanoparticles

Particle mean size, size distribution and zeta potential of HP-Cy7-DOX-NPs (14) were determined by dynamic light scattering (DLS) and were measured on a Zetasizer Nano ZS ZEN 3500 (Malvern Panalytical) (**see Annexes, S.I. Chapter 1**). The shape and morphology of the NPs were observed using transmission electron microscopy (TEM)and atomic force microscopy (AFM) (Park Systems) using Xei data acquisition software. The conjugation of the Cy7 fluorophore to the NPs was checked by flow cytometry using FACS Canto II (Becton Dickinson & Co.) and Flowjo® 10 software for data analysis.

3. Doxorubicin release profile

To analyze efficiency of hydrolysis of the hydrazone bond of the HP-Cy7-DOX-NPs (14), 500 µL NPs samples (5.2 x 107 NPs/µL) were incubated in a phosphate solution at pH 5.2 and in phosphate solution at pH 7.4 for 168 hours (7 days) in an incubator at 37 °C. The supernatants were collected by centrifugation of the corresponding sample at 1, 3, 6, 24, 48, 72 and 168 hours were analyzed by high performance liquid chromatography (HPLC).

4. Cell cultures

Cell line was provided by the cell bank of the CIC of the University of Granada. For this study we used the triple negative human breast cancer cell line MDA-MB-231. This cell line was cultured in DMEM base medium (Gibco) supplemented with 10% (v/v) fetal bovine serum, 1% L-glutamine and 1% penicillin/streptomycin in a humidified incubator at 5% CO2 and 37°C.

5. Nanofection of MDA-MB-231 cell line

MDA-MB-231 cells were incubated with different ratio cell/NPs of HP-Cy7-DOX-NPs (14) at the established incubation times. Aminomethyl NPs calls Naked NPs (1) and DOX-Cy7-NPs (11) were used as control (at the specific ratio cell/NPs), and cells without NPs treatment. After that, it was detached and washed with PBS 1×. Then, samples were fixed in 2% paraformaldehyde and analyzed by flow cytometry and confocal microscopy (**see Anexes, S.I. Chapter 1**).

6. Cell viability

The cellular cytotoxicity of NPs was evaluated using 0.1 M sodium resarzurin, this quantitative fluorometric method is based on the ability of living cells to convert resarzurin (a redox dye) into a fluorescent end product, which is measured at 570 nm directly from 96-well plates (NanoQuant Plate reader Infinite 200 PRO Tecan). Cells were seeded in 96-well plates at a density of 2 x 103 cells per well and incubated for 15 hours. Then, the medium was replaced with fresh medium containing the tested samples at various concentrations. After incubation for 96 hours, the medium containing NPs was removed and replaced with phenol red free fresh complete medium. The results were evaluated according to the manufacturer's protocol, and the amount of fluorescence obtained was proportional to the number of viable cells. Viability was expressed with respect to the percentage of untreated cells (100%). Control wells were included in each plate to measure the fluorescence of the culture medium with NPs added in the absence of cells.

7. Orthotopic xenotransplant mouse model

All in vivo experiments were performed in female NOD scid gamma mice (NSG, NOD.Cg-Prkdcscid Il2rgtm1Wjl/SzJ). Animal welfare and experimental procedures were carried out in accordance with institutional (Research Ethics Committee of the

University of Granada, Spain) and international standards (European Communities Council directive 86/609). All animals (n= 5 per group) were maintained in a micro-ventilated cage system with a 12h light/dark cycle, and they were manipulated in a laminar air-flow cabinet to keep on the specific pathogen-free conditions. To establish orthotopic xenograft tumors, six-to eight-week old female mice were used. Mice were anesthetized by inhalation of isofluorane and the tumors were generated in the right breast by subcutaneous injections of 5×10^5 cells/mouse mixed with Corning ®Matrigel® Matrix and using 26-gauge needles. Intravenous administration in the vein tail of the mice of PBS, Free DOX and NPs was performed every three days for a period of 43 days, as well as the evaluation of fluorescence by IVIS® (Perkin Elmer). Tumor growth was assessed twice weekly using a digital caliper and the tumor volume was calculated by the formula $V=(length)^2\times width\times\pi/6$. The weight of the mice was also measured every three days. The end-point of the experiment was at day 44. The mice were left untreated for a month in order to eliminate the NPs that were not specifically bound to the tumor tissue. During that month, the fluorescence of the mice was analyzed in the IVIS® once a week. Finally, mice were euthanized by cervical dislocation and tumors were excised, photographed and analyzed by IVIS®.

8. Statistical analysis

The data are presented as the mean ± the standard deviation in the error bars. The sample size (n) indicates the experimental repeats of a single representative experiment, with 3 being unless otherwise specified. The results of the experiments were validated by independent repetitions. Graphs and statistical difference data were made with GraphPad Prism 6.0 (Graphpad software Inc.). Statistical significance was determined using Student's t-test in paired groups of samples with known median and 2-way repeated measures ANOVA followed by Bonferroni test compared to more than two groups of samples. A p-value of ≤ 0.05 was considered significant.

RESULTS

RESULTS

1. Preparation and characterization of NPs (HP-Cy7-DOX-NPs) as theranostic probes.

A chemical strategy was developed by the NanoChemBio team to prepare multifunctionalized polymeric NPs. A monodisperse population of aminomethyl polystyrene cross-linked NPs were prepared by dispersion polymerization using a previously reported protocol.[297] Size distribution was determined by DLS showing homogeneous size and low polydispersity (460 nm with a PDI of 0.042). Zeta potential value was 81.2 ± 0.1 mV. The concentration of NPs (4×10^6 NP/µL ± 1.44×10^{-5}) was calculated according to the method developed by our research group (see Anexes, S.I. Chapter 1).[298] After coupling reactions, their efficiencies were monitored by Kaiser colorimetric test.[299] Loading of starting aminomethyl NPs (1) (54 µmol/g) was calculated using the Fmoc test[300] following coupling of Fmoc-Gly-OH amino acid to these NPs (1).

To achieve the efficient covalent functionalization of three different chemical structures to NPs an orthogonal strategy had to be designed. The NanoChemBio team strategy is based on the fully orthogonality between Dde and Fmoc protecting groups.[301,302] Aminomethyl NPs (1) were thus trifunctionalized as describe in **Figure 26**. Firstly, NPs were double PEGylated.[303] Subsequently, these NPs were bifunctionalized as previously described, then double PEGylation was again carried out to achieve Fmoc-Dde-NPs (6) **(see Annexes, S.I. Chapter 1.).**[301] Then, drug conjugation was carried out to hydrazine functionalized nanoparticle through a pH labile hydrazone bond obtaining the conjugates DOX-NP (9). Then, a second Fmoc-Lys (Dde)–OH unit was coupled to the DOX-NPs (9) to yield trifunctional NPs (10). Then, a near infrared cyanine fluorophore (Cy7, λexc=750nm, λem=773nm) was conjugated using its NHS derivative to give rise to the COOH-Cy7-DOX-NPs (13), which can be tracked in vivo. Finally, CRGDK peptide was coupled to NPs via chemo-selective conjugation. In order to do so, the N-terminal end of the CRGDK peptide was modified with an aminooxy acetyl group (**see Annexes, S.I. Chapter 1**), which allows immobilization of the peptide to the COOH-Cy7-DOX-NPs (13), through the formation of an N-alkoxyamide bond following activation of the carboxylic group of the NPs with oxyma/DIC to obtain the final HP-Cy7-DOX-NPs(14). Control NPs without conjugation of CRGDK for targeted delivery were prepared (Cy7-DOX-NPs (11) **(see Annexes, S.I. Chapter 1).**

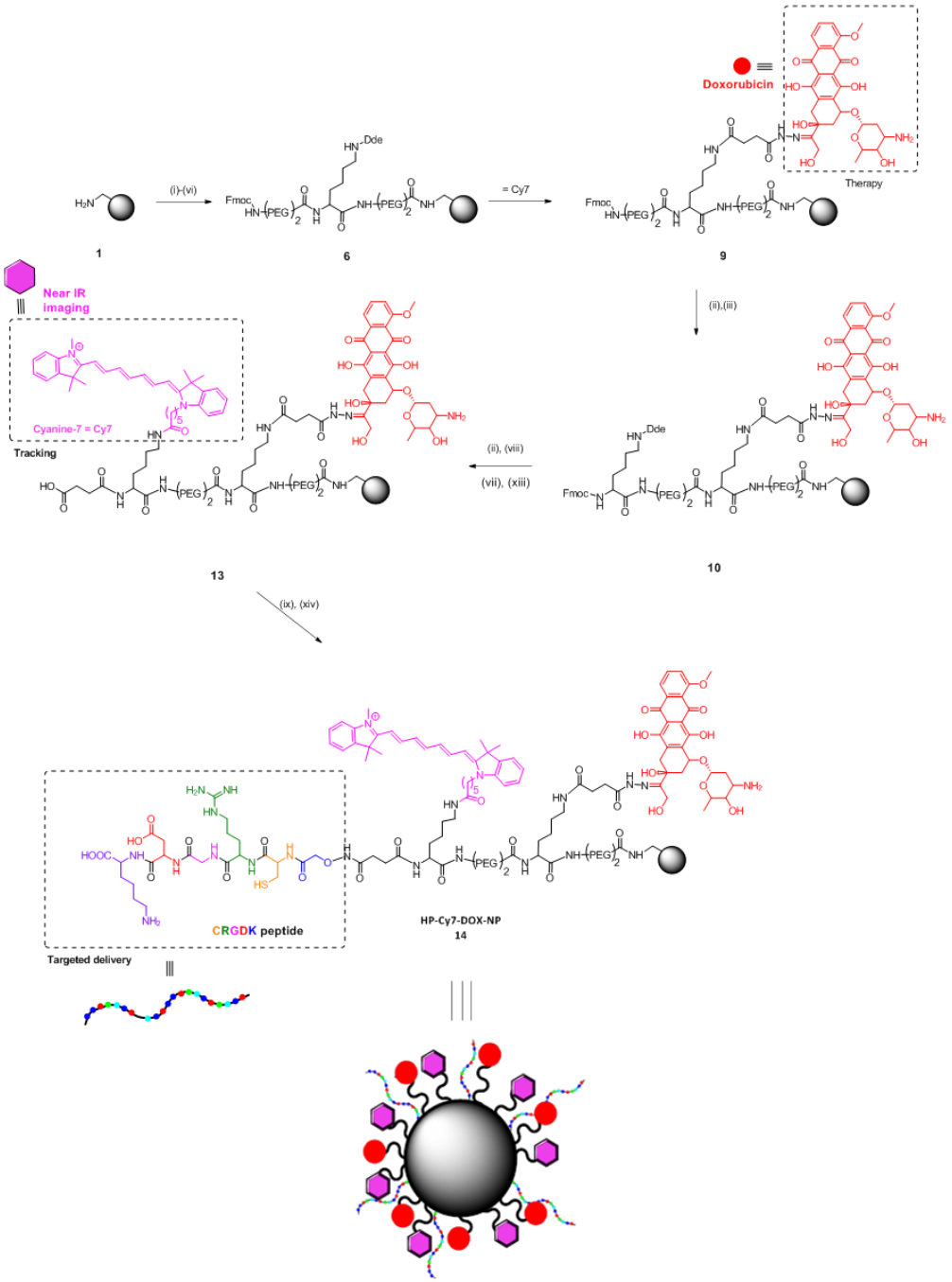

Figure 26. **General scheme of synthesis of theranostic nanoparticles (HP-Cy7-DOX-NPs (14).** Reagents and conditions (i) Fmoc-PEG-OH (15 equiv), Oxyma (15 equiv), DIC (15 equiv), DMF. 2 h, 60 °C; (ii) 20% piperidine, DMF, 3 x 20 min; (iii) Fmoc-Lys (Dde) -OH, oxyma (15 equiv), oxyma (15 equiv), DIC (15 equiv), DMF. 2 h, 60 °C; (vii) Hydroxylamine HCl, Imidazole, NMP, 2x 1 h, 25 °C; (viii) Succinic anhydride (15 equiv), DIPEA (15 equiv), 2 h., 60 ºC; (ix) Activation COOH group with oxyma (15 equiv), DIC (15 equiv), 2 h, 25 ºC; (x) hydrazine, 55% v/v (15 equiv), 15 h, 25°C; (xi) DOX, PBS pH 6, 15 h, 25 °C (xii) 20% piperidine, DMF, 3 x 20 min; (xiii) Cy7-NHS (1 equiv), DIPEA (0.1 equiv), 15 h, 25 °C; (xiv) CRGDK (7 equiv), DIPEA (0.1 equiv), 15 h, 25 °C.

Size distributions of the NPs were controlled after each key conjugation step by DLS (**Figure 27A, see Annexes, S.I. Chapter 1. Table S1**). It can be observed that this multifunctionalization strategy did not affect the NP size. These results confirm that trifunctionalized NPs were stable and aggregation did not occur. These DLS size results were corroborated by TEM analysis (**Figure 27B**) and by AFM (**Figure 27C**).

Figure 27A shows the zeta potential values in aqueous environments at pH 7.4 which shown negative values of HP-Cy7-DOX-NP (14). These results also confirm the ability of zeta potential measurements to monitor the success of the chemical modifications of NPs.[304] In order to measure the labelling level of the theranostic nanoparticles, HP-Cy7-DOX-NPs (14) was analyzed by flow cytometry, confocal microscopy (**Figure 27D and 27E**) and UV spectroscopy **(see Annexes, S.I. Chapter 1. Figure S1**). The conjugation efficiency was 74.1%. Taking into account the number of NPs used in this assay (5.2 x 10^7 NPs/µL), we can estimate a final concentration of 9.5 x 10^{-8} nmol of Cy7/NP that correspond to 5.7 x 10^7 molecules of Cy7/NP. The efficiency of conjugation of the CRGDK homing peptide to the theranostic NPs (HP-Cy7-DOX-NPs (14)) was determined by measuring the initial and final peptide concentration in the reaction vessel by BCA test.[305] The absorbance values obtained at 562 nm were translated into concentration using a standard calibration curve (**see Annexes, S.I. Chapter 1. Figure S2**). The obtained results show a conjugation efficiency of 80.7%. Taking into account the number of NPs used (1.83 x 10^8 NPs/µL), we can estimate a final concentration of 8 x 10^{-9} nmol of CRGDK/NP that correspond to a density of 5.23 x 10^7 CRGDK molecules/NP.

In order to evaluate the conjugation efficiency of DOX to theranostic NPs (HP-Cy7-DOX-NPs (14)) the unconjugated drug which remain in the supernatant of the reaction was measured by UV spectroscopy. A calibration curve, with lineal ratio between the optic density of DOX and its concentration, was previously performed (**see Annexes, S.I. Chapter 1. Figure S3**). The conjugation efficiency was calculated to be 72%. As the number of NPs used in this assay were 5.2 x 10^7 NPs/µL, we can estimate a final concentration of 1.4 x 10^8 nmol DOX per NP that correspond to 8.4 x 10^7 molecules of drug per NP. It is remarkable the fact that the final amount of each component is in the

same range (10^7 molecules per nanoparticle) to achieve each of the specific functions of this nanosystem.

The efficiency of DOX release from HP-Cy7-DOX-NPs (14) was determined by performing UV spectroscopy of the buffers in which HP-Cy7-DOX-NPs (14) were incubated and using a HPLC system (**see Annexes, S.I. Chapter 1. Figure S4**). HP-Cy7-DOX-NPs (14) where incubated at pH 5.2 (phosphate buffer) at which pH sensitive hydrazone bonds are reversible cleaved. A significant drug release of 44% ± 0.1 after 24 hours of incubation at pH 5.2 was observed. Then, a sustained release occurs up to 168 hours incubation, achieving a maximum release value of 73%. In contrast, there is no significant loss of DOX conjugated to NPs when incubation is carried out in 7.4 pH PBS (**Figure 27F**). Consequently, an efficient and selective drug release at acidic pH has been achieved.

a)

NPs	Diameter Mean (nm)	PDI	Zeta potencial (mV)
Amino methyl NP (**1**)	460 ± 0.4	0.042	81.2 ± 0.2
Fmoc-Dde-NP (**6**)	462.3 ± 1	0.1	-37.8 ± 0.62
Fmoc-Hydrazide-NP (**8**)	463 ± 0.5	0.085	31.4 ± 0.3
COOH-Cy7-DOX-NP (**13**)	462.8 ± 1.2	0.013	-17 ± 1.4
HP-Cy7-DOX-NP (**14**)	467 ± 1.6	0.015	-18.6 ± 0.6

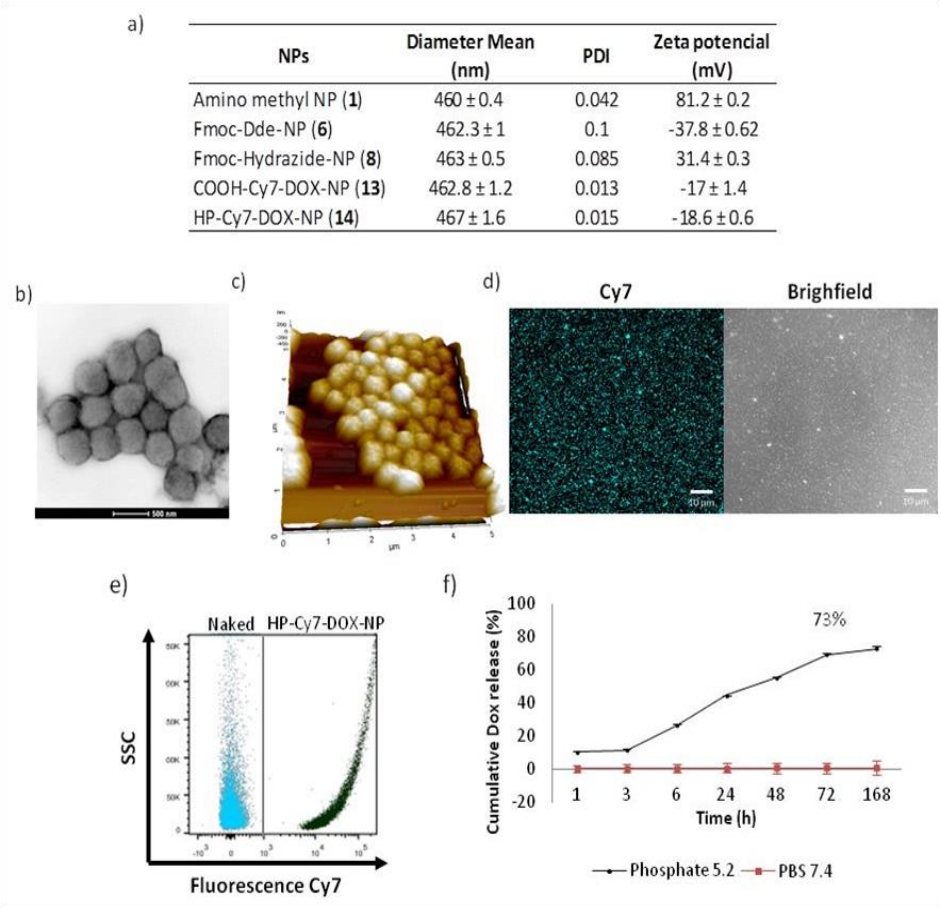

Figure 27. **Physico-chemical characterization of theranostic NPs (HP-Cy7-DOX-NPs (14)).** A) Table with particle size distribution (nm) and zeta potential of DOX-HP-Cy7-NP (14); B) TEM of HP-Cy7-DOX-NPs(14); C) AFM of HP-Cy7-DOX-NPs (14); D) Confocal microscopy of HP-Cy7-

DOX-NPs (14), Scale bar, 10 µm; E) Representative overlay dot plot obtained after flow cytometry analysis of naked NPs (1) (blue) and HP-Cy7-DOX-NPs (14) (green); F) Cumulative DOX release of HP-Cy7-DOX-NPs (14). NPs were incubated in two phosphate solutions at different pH, phosphate solution at pH 5.2 and PBS at pH 7.4, for 168 hours at 37 C. The results have been expressed with the values of the mean ± SEM.

All this preparation and characterization of NPs (HP-Cy7-DOX-NPs) as theranostic probes has been developed by Dr. Victoria Cano Cortés belonging to the NanoChemBio team.

2. Cellular uptake of theranostic nanoparticles is due to a receptor-mediated binding mechanism

To initially investigate the effect of conjugation of the different bioactive cargoes on cellular uptake, these theranostic NPs (HP-Cy7-DOX-NPs (14)) were evaluated using a triple negative breast cancer cells (MDA-MB-231) that are characterized by rapid grow rate and to be remarkable aggressive and metastatic. These cells are thus a perfect candidate to evaluate these theranostic nanodevices for two reasons: (i) they overexpress Nrp-1, which is the targets of the CRGDK homing peptide[306] and, (ii) DOX is a drug of choice for the treatment of triple negative breast cancer.[307]

Several assays were carried out to determine the number of HP-Cy7-DOX-NPs (14) required to achieve an efficient uptake by flow cytometry analysis. As a first approach, a range of concentrations of NPs from 50 to 20,000 NPs/ cells were evaluated following 24 h of incubation. Then, cells were detached, fixed and analyzed by flow cytometry. Untreated cells and cell treated with Naked NPs (1) and NPs without CRGDK, Cy7-DOX-NP (11) were used as controls. **Figure 28** shows results obtained by flow cytometry. It can be observed that uptake of theranostic NPs (HP-Cy7-DOX-NPs (14)) is very efficient and concentration dependent (**Figure 28A and 28B**). Efficient uptake was corroborated by confocal microscopy (**Figure 28F**). It is interesting to highlight the lower internalization of HP-Cy7-DOX-NPs (14) compared to Cy7-DOX-NP (11). Additionally, when the mean fluorescence intensity is analyzed (**Figure 28B**), we can observe that

nanofection keep increasing until cell saturation is reached (when 10,000 NPs are added per cell).

To evaluate the influence of the incubation time on the internalization, HP-Cy7-DOX-NPs (14) were compared with Cy7-DOX-NPs (11) (without ligand) for selective release during a period of 72 hours, at different time intervals (3, 6, 24, 48 and 72 hours), using 5,000 NPs/cell. As we can see in **Figure 28C and 28D**, after 3 hours of incubation, maximum nanofection was achieved, with a clear difference between both types of NPs, with Cy7-DOX-NPs (11) reaching 75% of the nanofection compared to 15% of the HP-Cy7-DOX-NPs (14). These results corroborate the nonspecific entry of NPs in absence of CRGDK.

Although the data reported so far could suggest a selective uptake of these theranostic NPs (HP-Cy7-DOX-NPs (14)) due to specific cell targeting, we also proceed with a deeper study that could provide more relevant information. Hence, the specificity of the cellular uptake was further investigated by competitive binding experiments with free CRGDK homing peptide. Cells were pre-incubated with CRDGK for 6 hours and afterwards treated with HP-Cy7-DOX-NPs (14) and Cy7-DOX-NPs (11) for 15 hours. Cell binding sites were effectively blocked by the free homing peptide, reducing significantly the uptake of the theranostic NPs (HP-Cy7-DOX-NPs (14)) (**Figure 28E**). Furthermore, uptake levels of tested Cy7-DOX-NPs (11) remained consistent despite free homing peptide treatment. These data also support the specific and receptor-mediated binding mechanism of HP-Cy7-DOX-NPs (14) and its significantly enhanced targeting activity with Nrp-1 overexpressing cancer cells.

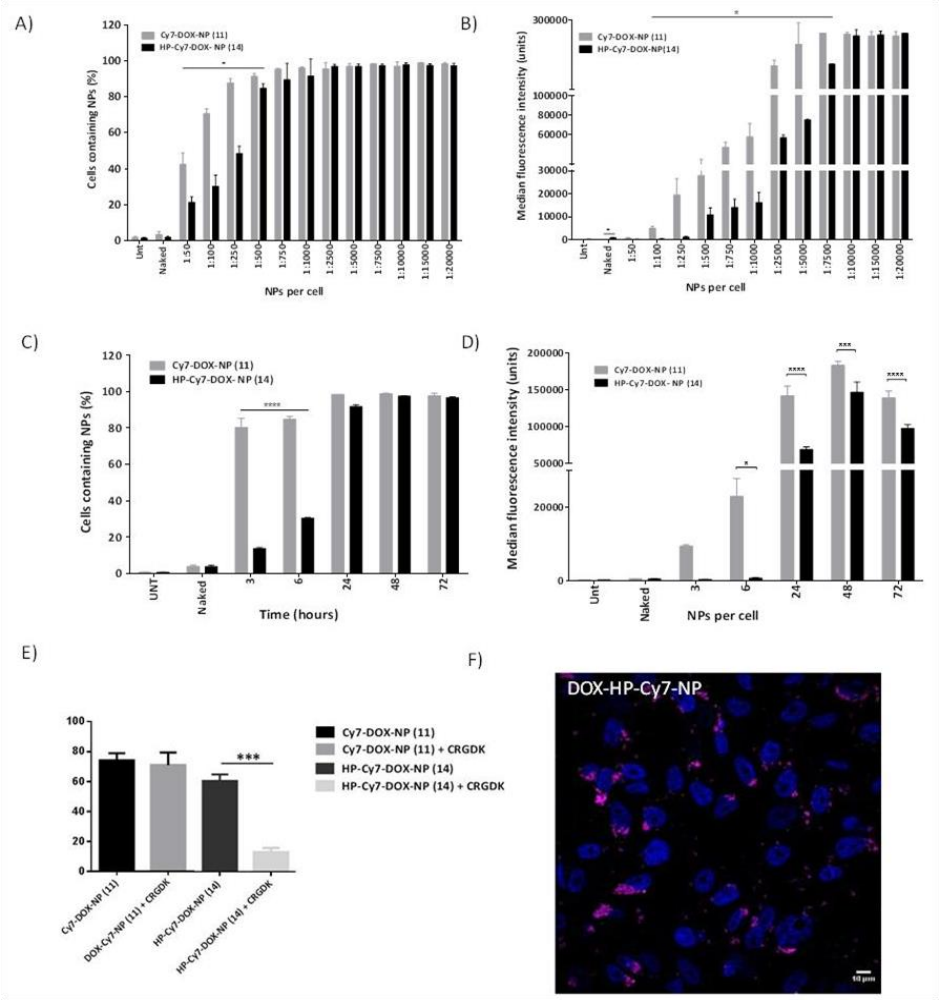

Figure 28. Evaluation of cellular uptake of theranostic NPs (HP-Cy7-DOX-NPs (14)) and control NPs without homing peptide (Cy7-DOX-NPs (11)) in the MDA MB 231 cell line. A) Bar representation to compare cellular uptake between theranostic NPs (HP-Cy7-DOX-NPs (14)) and control NPs without homing peptide (Cy7-DOX-NPs (11)). B) Bar representation to compare ΔMFI between theranostic NPs (HP-Cy7-DOX-NPs (14)) and control NPs (Cy7-DOX-NPs (11)). C) Bar representation to compare nanofection cellular between theranostic NPs (HP-Cy7-DOX-NPs (14)) and control NPs (Cy7-DOX-NPs(11)) at different times; D) Bar representation to compare ΔMFI between theranostic NPs (HP-Cy7-DOX-NPs (14)) and Cy7-DOX-NPs (11) at different times. Statistical significance was determined by two-way analysis of variance (ANOVA) with a Bonferroni's multiple comparison post-hoc between the same treatments of the different cell lines, n = 6, (*p value < 0.05, **** p value <0.0001. The results have been expressed with the values of the mean ± SEM; E) Competitive binding assay with CRGDK homing peptide; F) Confocal microscopy of the cellular uptake behavior of theranostic NPs (HP-Cy7-DOX-NPs (14)).

3. Theranostic NPs increase in vitro therapeutic efficacy of doxorubicin in triple negative breast cancer cells.

The cytotoxic effect of DOX conjugated to theranostic NPs (HP-Cy7-DOX-NPs (14)) was evaluated by measuring the cell-mediated reduction of sodium resarzurin, a standard colorimetric and quantitative method that determines the cell viability on MDA-MB-231 cells.[308] Half maximal inhibitory concentration (IC_{50}) was determined and compared with cell incubation with free DOX. A range of different NPs concentrations were incubated for 96 hours with MDA-MB-231 cells. IC_{50} value for theranostic NPs (HP-Cy7-DOX-NPs (14)) was calculated to be 41 nM (**Figure 29A**), which correspond to 2,250 NPs/cell (**see Annexes, S.I. Chapter 1. Figure S5B**). As previously reported, free DOX completely inhibited cell growth at 1000 nM, having an IC_{50} of 120 nM in MDA MB 231 cells (**see Annexes, S.I. Chapter 1. Figure S5A**). These values indicated that DOX conjugated to the NPs reduced the IC_{50} value with respect to free DOX. As result, this nanosytem offers a three-fold reduction of the amount of DOX required to have the same effect than free DOX in tumor cells. These finding demonstrate that HP-Cy7-DOX-NPs (14) could effectively target tumor cells overexpressing Nrp-1 receptors and subsequently enhance the tumor selective therapeutic effect of DOX.

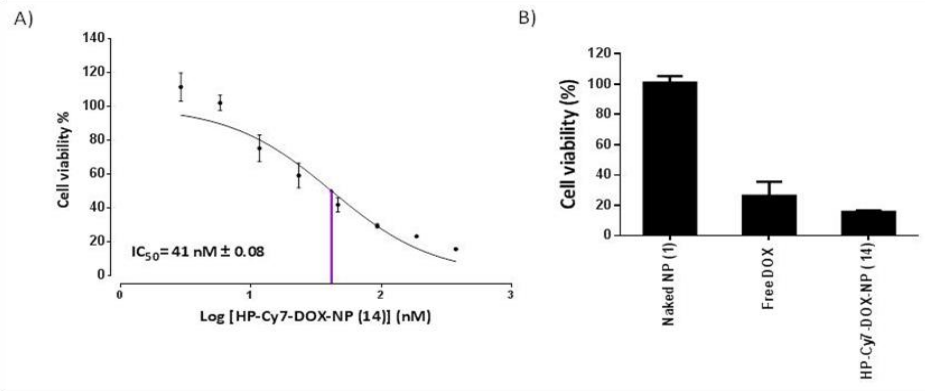

Figure 29. **Evaluation of theranostic NPs (**HP-Cy7-DOX-NPs (**14**)**) as targeted drug delivery by the CRGDK homing peptide in the MDA MB 231 cell line**. A) Half maximal inhibitory concentration (IC_{50}) of the theranostic NPs (HP-Cy7-DOX-NPs (**14**)) (nM); B) cytotoxic effect on cell viability of cells incubated when added 500nM of theranostic NPs (HP-Cy7-DOX-NPs (**14**)) compared to control NPs (Naked NPs (**1**)) and free DOX (500nM). The experiments have been carried out in triplicate and the results have been expressed with the values of the mean ± SEM.

Finally, the IC_{90} of HP-Cy7-DOX-NPs (14) against MDA-MB-231 cells was determined. The value of IC_{90} was 500 nM that correspond to 20,000 NPs/Cell. It was observed that the reduction of cell viability was enhanced by using HP-Cy7-DOX-NPs (14) when compared to free DOX (**Figure 29B**). Cell viability was reduced from 26% to 15% by using NPs. It is important to remark that the Naked NPs (1) without DOX have no effect on the cell viability of the MDA MB 231 cell line (**Figure 29B**).

4. Theranostic NPs have in vivo targeted therapeutic efficiency against triple negative breast cancer avoiding side effects of doxorubicin and tracking treatment response in real time.

To investigate in vivo therapeutic and tracking efficiency of these theranostic NPs (HP-Cy7-DOX-NPs (14)), comparative efficacy studies were carried out. An orthotopic xenotransplant of the triple-negative human breast cancer cell line MDA-MB231 was performed in immunosuppressed female NSG mice. The mice (5 per group) were divided into 3 groups and treated in accordance with the protocol approved by the Institutional Committee for Animal Care and Use (IACUC) of the University of Granada and the Andalusian Regional Government in accordance with the European Directive for the protection of animals used for scientific purposes (2010/63/EU) and the Spanish law (Royal Decree 53/2013).

The treatment with PBS, free DOX and theranostic NPs (HP-Cy7-DOX-NPs (14)) was administered during 43 days, considering time zero when the tumor reached a size of 100 mm^3. Periodic intravenous administrations were done to each group of mice every 3 days. **Figure 30A** represents the changes in the relative tumor volume as a function of the treatment time. Mice treated with free DOX showed a significant tumor growth inhibition after 3 weeks. This therapeutic effect was evident for theranostic NPs after 28 days, where a decrease in tumor volume was observed arriving on day 43 to be similar to mice treated with free DOX (**Figure 30A and 30B**). These results show that HP-Cy7-DOX-NPs (14) have a clear therapeutic effect similar to that of free DOX. Remarkably, fluorescence intensity analysis by IVIS showed that the trifunctionalized NPs (HP-Cy7-DOX-NPs (14)) were effectively tracked in vivo thanks to the conjugation of the fluorophore onto the nanoparticle and selectively accumulated in the mammary

tumor mass and not in the rest of organs thanks to the functionalization with the CRGDK homing peptide (**Figure 30C**).

Histological analysis of orthotopic xenograft tumor tissues further confirmed the therapeutic efficacy of HP-Cy7-DOX-NPs (14). As shown in **Figure 31**, xenograft tumors of the control group were composed of tightly packed and proliferative tumor cells (**Figure 31A**). However, in xenograft tumors from treatment groups, the cellularity was significantly decreased, with typical apoptotic features such as small nuclear fragments surrounded by a rim of clear cytoplasm were observed more frequently in theranostic NPs-treated than DOX-treated tumors (**Figure 31B and 31C**).

These in vivo findings demonstrate the efficient targeted delivery and enhanced therapeutic activity of these theranostic NPs in Nrp-1 overexpressing triple negative breast cancer tumors. Previously, CRGDK peptide-functionalized nanomedicines were also reported to afford good targetability to MDA-MB-231 cells in vitro and in vivo.[309,310]

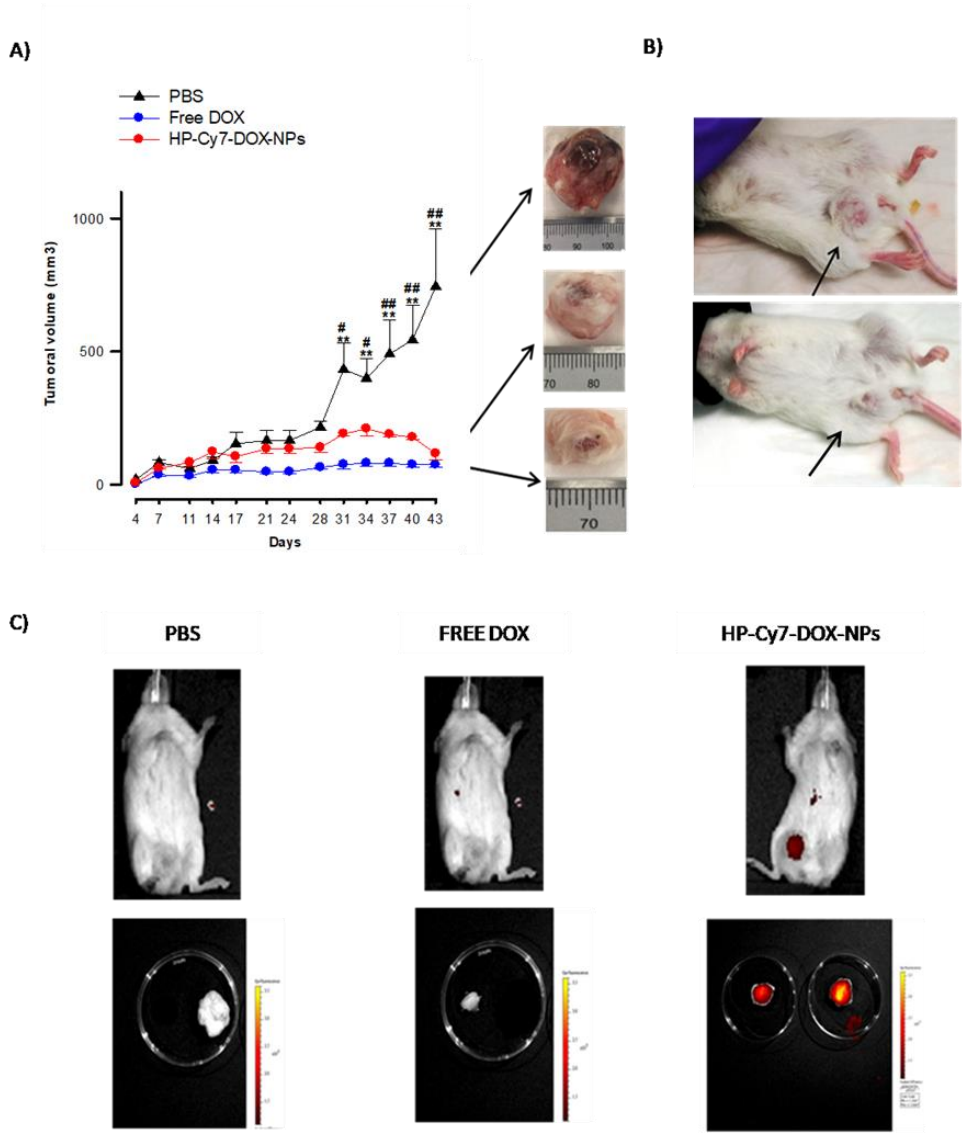

Figure 30. In vivo evaluation of therapeutic efficacy of intravenous administration of theranostic NPs (HP-Cy7-DOX-NPs (14)) in comparison with doxorubicin in solution and PBS in NSG mice with tumors induced in the breast by inoculation of MDA-MB-231 cells in matrigel. A) Representation of relative change of tumor volume (mm3) over time of each group of mice during 43 days of treatment. Each point and vertical line represent the mean ± SEM (n=5 per group). Statistically significant differences between PBS and free DOX treated groups *P≤ 0.05; **P≤ 0.01; and PBS vs. HP-Cy7-DOX-NPs #P ≤ 0.05; ##P ≤ 0.01 on the same day after treatment (2-way repeated measures ANOVA followed by Bonferroni test).Time zero was considered when the tumor reached a size of 100 mm3. Periodic administrations are made intravenously to each group of mice every 3 days. B) Images of orthotopic tumors in the breast of untreated mice (top image) and those treated with trifunctionalized NPs (bottom image) where a lower tumor volume is observed. C) In vivo fluorescence analysis (IVIS) of nanoparticle detection compared to negative controls in mice and isolated tumors.

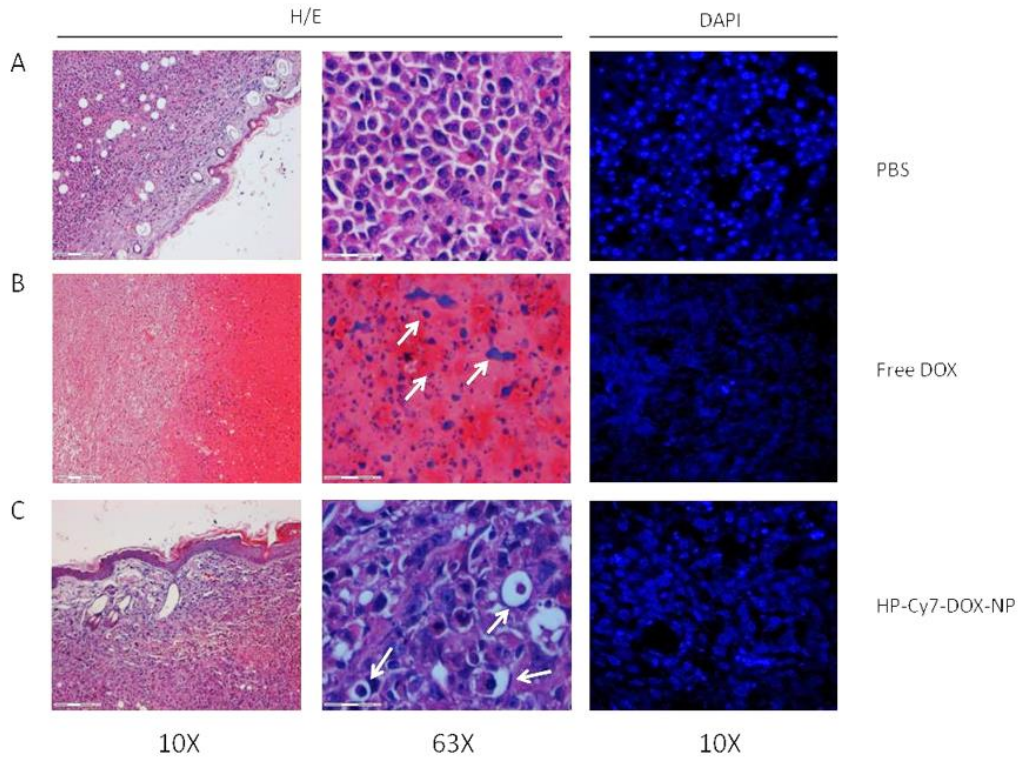

Figure 31. Histological analysis with Hematoxylin/eosin and DAPI staining of tumors extracted after treatment with PBS (A), Free DOX (B) and HP-Cy7-DOX-NPs (C).

Additionally, a series of experiments were carried out to monitor the in vivo toxicity of the treatment. First, a comparative analysis of the survival of mice treated with the theranostic nanoparticles (HP-Cy7-DOX-NPs (14)) versus mice treated with free DOX and untreated control mice (PBS) was carried out during the treatment period (43 days). In **Figure 32A** it can be observed as the percentage of survival during the treatment period was 100% for both the mice treated with NPs and those that control group. However, treatment with DOX caused a high impact on survival. After 30 days of treatment there was a drastic decrease in the percentage of survival (30%). This effect could be attributed to the inherent systemic toxicity of this antitumor drug[311] and to the serious side effects of this conventional chemotherapy treatment. Indeed, an analysis of the physical appearance of the treated mice corroborates this result. **Figure 32B** shows a representative image of a mouse treated with free DOX where evident external signs of toxicity are observed in comparison with a mouse form the group treated with theranostic nanoparticles (HP-Cy7-DOX-NPs (14)).

The main external side effects observed in mice treated with free DOX were weight loss, piloerection, behavior disorders and damaged tail, among others. The most striking side effect was the high cutaneous toxicity produced in the tail of the mice treated with DOX (**Figure 32B, top image**). Also, a significant weight reduction was found in mice treated with free DOX in comparison to weight in both control untreated or theranostic NPs-treated mice (**Figure 32C**). Additionally, to observe the toxic effect of the treatment at the level of the central nervous system, a standardized protocol to test movement was carried out at day 30 in a cage with a camera prepared for this purpose. This camera analyzes the distance travelled by the mouse during 24 hours. Treatment with HP-Cy7-DOX-NPs (14) did not affect the motor activity being comparable to that of the untreated mice; however, free DOX caused a significant decrease of mice mobility (**Figure 32C**). In metastatic breast cancer, DOX treatment has several adverse effects including cardiotoxicity, skin and hematological toxicities due to lack of selectivity, which subsequent provoke the therapeutic failure.[312] Our results suggest that DOX loaded to theranostic NPs significantly avoids important side effects.

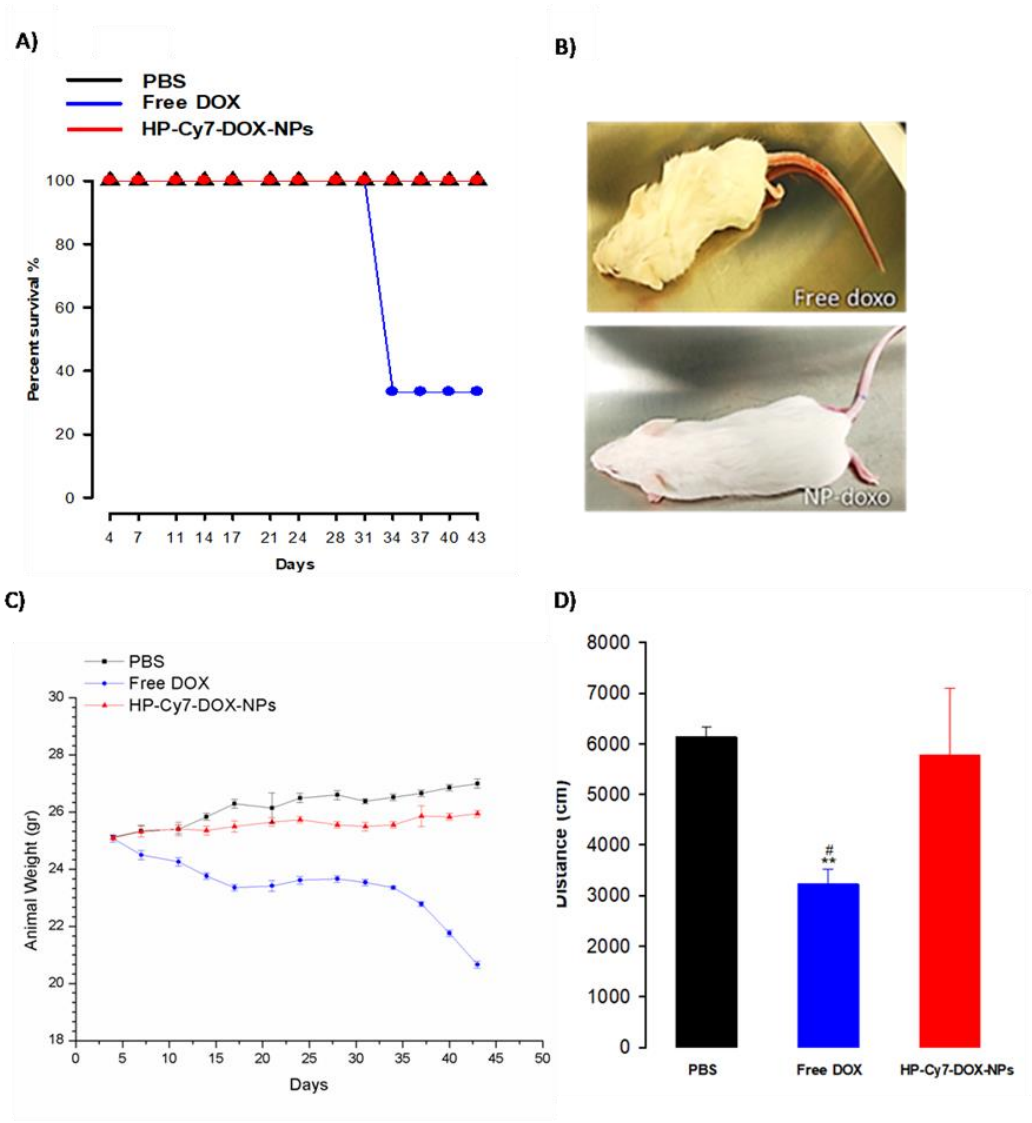

Figure 32. Evaluation of the toxicity of the theranostic nanosystem. A) Kaplan-Meier survival curve B) Comparative study of external signs of toxicity in mice treated with free DOX or treated with theranostic NPs. C) Analysis of weight variation during treatment. Each point and vertical line represent the mean ± SEM (n=5 per group). D) Analysis of activity based on the movement capacity (24 hours) of the treated mice versus control mice without treatment. Statistically significant differences between PBS and free DOX treated groups **P≤ 0.01; and HP-Cy7-DOX-NPs vs. Free DOX#P ≤ 0.05 (2-way repeated measures ANOVA followed by Bonferroni test).

DISCUSSION

DISCUSSION

In this study, a successfully developed theranostic nanodevice based on orthogonal conjugation strategies for the multifunctionalization of polymeric NPs is reported for the first time. Theranostic NPs (HP-Cy7-DOX-NPs (14)) containing controlled amount of each one of the components has been successfully prepared. A selective receptor-mediated release of DOX has been successfully achieved in TNBC cells overexpressing Nrp-1 by CRGDK peptide conjugation. Moreover, the fluorescent labeling (Cy7 tracker) allows *in vitro* and *in viv*o tracking of the nanodevice.

An orthogonal strategy to achieve the efficient covalent tri-functionalization of NPs have been developed. This included PEGylation to increase the half-life of the circulating NPs and to reduce the unfavorable interactions between the different molecules conjugated to the NPs, but also to evade opsonisation and subsequent phagocytosis.[303] Moreover, DOX was bound to the NPs through a pH labile hydrazone bond to allow the release of DOX via the pH sensitive hydrazine linker in a sustained manner in both tumor cells (lysosomes: pH 4-5, endosomes: pH 5-6) and tumor microenvironments (pH 6.5-7.2), which present lower pH values due to hypoxia if compared with that in bloodstream (pH 7.4).[313] The sustained drug release of HP-Cy7-DOX-NPs (14) up to 168 h at pH 5.2 suggests that in acidic tissues such as tumoral tissues could be a very beneficial feature to prolong and improve the therapeutic efficacy of NPs and validates the drug release strategy selected for this study.

In addition, CRGDK (Cys-Arg-Gly-Aps-Lys) homing peptide was coupled the NPs via chemo-selective conjugation to target TNBC cells overexpressing Nrp-1. This transmembrane receptor glycoprotein is involved in nervous system development and angiogenesis and, also, is overexpressed on the surface of a wide variety of tumors and it has a crucial role in TNBC tumorigenesis and metastasis. Nrp-1 is a useful targeting site for tumor-specific drug delivery and selective anti breast cancer strategies.[314] In fact, CRGDK-mediated targeting has been widely demonstrated to be able to increase the affinity for tumor cells and facilitate the drug-loaded NPs to efficiently enter the cells through ligand-receptor mediated endocytosis.[315–317] Our *in vitro* results showed the nonspecific entry of NPs in absence of the homing peptide and after the selective blockage of receptor, supporting the specific and receptor-mediated binding mechanism

of HP-Cy7-DOX-NPs (14) and its significantly enhanced targeting activity with Nrp-1 overexpressing cancer cells. Moreover, cytotoxicity assays showed three-fold reduction of the amount of DOX required to have the same effect than soluble DOX in MDA-MB-231 cells, which indicate the ability of our targeted theranostic nanosystem to increase the antitumor potency of DOX.

In agreement with these results, CRGDK peptide-functionalized nanomedicines were also reported to afford good targetability to MDA-MB-231 cells *in vitro* and in *vivo*.[309,310]. Nowadays, several reports have demonstrated that attaching this peptide to different types of NPs, they are capable of specifically recognize the Nrp-1 receptor and increase the in vivo cytotoxic effect of vehicularized drugs [35,38–40].[315,318–320]

To investigate the *in vivo* therapeutic and tracking efficiency of these theranostic NPs (HP-Cy7- DOX-NPs (14)), comparative efficacy studies were carried out. An orthotopic xenotransplant of the MDA-MB-231 TNBC cell line was performed in immunosuppressed female NSG mice while not appreciable side effects were observed. These *in vivo* experiments demonstrate the efficient targeted delivery and enhanced therapeutic activity of these theranostic NPs in Nrp-1 overexpressing TNBC tumors. Remarkably, *in vivo* fluorescence tracking analysis showed the preferable location of theranostic NPs in the tumor area reducing the volume in a similar grade than free DOX. The choice of a near infrared tracker (Cy7 fluorophore) allowed an efficient monitoring by fluorescence analysis with low background and high signal-to-noise ratio. These properties make near infrared fluorescent dyes of great interest for bioimaging applications.[321] A comparative analysis of the survival of mice treated with the theranostic nanoparticles (HP-Cy7-DOX-NPs (14)) versus mice treated with free DOX and untreated control mice (PBS) was carried out during the treatment period, showing lower survival rates for free DOX (30%) than those treated with theranostic NPs (100%). The effect of free DOX could be attributed to the inherent systemic toxicity of this antitumor drug[311] and to the serious side effects of this conventional chemotherapy treatment. Indeed, an analysis of the physical appearance of the treated mice corroborates this result. In metastatic breast cancer, DOX treatment has several adverse effects including cardiotoxicity, skin and hematological toxicities due to lack of

selectivity, which subsequent provoke the therapeutic failure.[312] Our results suggest that DOX loaded to theranostic NPs significantly avoids important side effects.

CHAPTER 2

ALBUMIN-COVERED LIPID NANOCAPSULES EXHIBIT ENHANCED UPTAKE PERFORMANCE BY BREAST-TUMOR CELLS

BACKGROUND

Controlled drug delivery may be considered a frontier area of pharmaceutical science and technology, involving a multidisciplinary scientific approach and contributing significantly to human health care. New delivery systems, compared to conventional ones, can improve efficacy and patient compliance and convenience. Due to the poor solubility of most anticancer drugs, current therapies must use solubilizer agents for intravenous administration, which provoke unpleasant secondary effects. Nanoparticle-based drug-delivery systems are suitable to overcome this solubility problem while offering other advantages, such as a high degree of biocompatibility and versatility,[322] sustained delivery,[323] and protection from chemical and physical degradation.[324]

An important restriction for the use of NPs in drug delivery is their potential toxicity.[325] A proposed solution for this limitation is to adopt, as nanocarriers, proteins that exit in the human body, such as albumin. Human serum albumin (HSA), adsorbed onto polystyrene NPs, reportedly inhibits their phagocytosis and promotes prolonged circulation time in blood.[229,326,327] Therefore, HSA is considered a disopsonin, i.e. a molecule that can avoid clearance by the reticule-endothelial system. On the other hand, albumin accumulates in malignant and inflamed tissues, and serves as the main nutrient for tumor growth.[328] For these properties, HSA has been proposed as an important tool to develop drug vehicles.[329–331]

Lipid-based nanocarriers are being widely used for drug delivery, with some already passed for clinical use.[332] Examples for such lipid nanovehicles are solid lipid NPs, nanostructured lipid carriers, and liquid lipid nanocapsules (LLNCs). LLNCs are colloidal systems consisting of an oily core covered by a protective polymeric shell. They can reach high drug-encapsulation efficiency due to their hydrophobic nature[333] and reduce tissue irritation at the deposition site due to their polymeric shell.[334] Surfactants and hydrophilic molecules such as chitosan, polyethylene glycol (PEG), poly(lactide-co-glycolide) (PLGA) or poloxamers, have been used to coat LLNCs.[335]

Features such as the pharmacokinetics, biodistribution, and the colloidal stability of NP in biological media are governed largely by their surface properties. Most NP formulations are rapidly sequestered by cells of the mononuclear phagocyte system

after intravenous administration. The choice of an appropriate coating polymer to decrease the interaction of the NP with serum components is important to achieve long blood-circulation time.[336,337] Recent studies have shown that the synthetic identity of NP plays an important role in the phagocytic cell uptake.[338,339] In addition, the physicochemical properties of the NP shell should influence the drug-release pattern. Human-serum albumin is a good candidate to be employed as external polymeric shell as it is a natural material with biocompatibility, biodegradability, and non-toxicity. This protein shell can be further strengthened by covalent cross-linking with glutaraldehyde (GAD), and specific targeting molecules that can recognize markers on the surface of cancer cells may be attached by reaction with carbodiimide.

In a previous publication, we presented an extensive study concerning the influence of processing parameters on the properties of olive-oil nanocapsules stabilized by HSA.[340] The present study describes the development of nanocapsules with an olive-oil core covered by a GAD-cross-linked HSA shell. We evaluate how the physico-chemical properties of these nanocapsules can influence their colloidal stability, drug release profile, and cellular uptake. For a hydrophobic drug model, we have chosen curcumin, a natural product with low intrinsic toxicity but recognized medicinal properties such as anti-oxidant,[341] anti-inflammatory,[342] anti-Alzheimer's disease,[343] and anti-tumoral activity.[344]

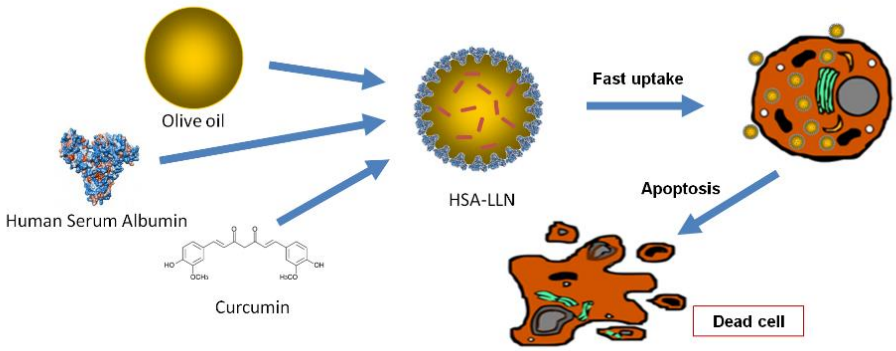

MATERIALS AND METHODS

MATERIALS AND METHODS

1. Materials

Curcumin, coumarin-6, human serum albumin (HSA), olive oil, oleic acid, glutaraldehyde (GAD), poloxamer F-127, MTT assay reactive [3-(4, 5-dimethylthiazol-2-yl)-2,5-diphenyltetrazolium bromide], 4',6-Diamidino-2-phenylindole dihydrochloride (DAPI), dimethyl sulphoxide (DMSO), L-glutamine, sodium bicarbonate, Hepes buffer, and penicillin/streptomycin solution were purchased from Sigma-Aldrich (Madrid, Spain). DMEM (Dulbecco's modified Eagle medium), MEM (minimum essential medium), and FBS (heat-inactivated fetal bovine serum) were purchased from Thermo Fisher Scientific (Gibco, Grand Island, NY, USA). The human breast-cancer MCF-7 cell line was obtained from American Type Culture Collection (ATCC) and cultured following ATCC recommendations. All aqueous solutions were prepared using ultrapure water from a Millipore Milli-Q Academic pure-water system.

2. Preparation of LLNCs

LLN were prepared using a solvent-displacement method as previously described.[340] Briefly, as a general working scheme, a solution containing 300 µl of olive oil, 37.5 ml of ethanol and different amounts of curcumin was poured into 40 ml of an aqueous phase containing HSA to form an emulsion. The dispersion became turbid immediately because of the formation of nanocapsules. After 10 min of stirring, 250 µl of a 0.16% solution of GAD was added to the dispersion to cross-link the HSA coating molecules. The mixture was left under continuous stirring over a time period of 15 min at 25ºC. Subsequently, the ethanol was evaporated under vacuum at a temperature of 34ºC in a rotary evaporator and the dispersion thoroughly dialyzed against and low-ionic-strength phosphate buffer at pH 7.

Similar LLNCs were prepared without curcumin to be used as blanks, as well as without the GAD cross-linking process for comparison purposes.

The amount of encapsulated curcumin in the nanocarriers was determined by UV-vis spectrophotometry after their disaggregation with propanol. Upon centrifugation at 14000 rpm for 10 min, the supernatant was collected and the amount of curcumin determined by absorption at 430 nm using a UV-vis spectrophotometer (BioSpectronic Kinetic Spectrophotometer, Eppendorf, Germany). The curcumin

concentration was calculated by appropriate calibration curve of free curcumin in propanol (R^2>0.999). Each batch sample was measured in triplicate.

LLNCs loaded with the fluorophore coumarin 6 were also prepared to compare the uptake efficiency of nanocapsules with different shells (protein, poloxamer, and a mixture of poloxamer and oleic acid). The preparation method in all cases was the same as previously described, changing curcumin to 0.1 mg of coumarin 6 in the three samples. HSA was replaced by 200 mg of Poloxamer F127 in the PL-C sample, and by 100 mg of Poloxamer F127 and 125 mg of oleic acid in the PLOA-C sample.

3. Morphology of nanocapsules

The aspect of LLNCs was assessed by Cryo-Transmission Electron Microscopy (Cryo-TEM) technique. Five microliters of sample were placed on a glow-discharged holey-type carbon-coated grid (Quantifoil R2/2), and vitrified in liquid ethane using a Vitrobot Mark IV (FEI), under controlled conditions. Samples were maintained at a temperature of approximately -170ºC in liquid nitrogen until they were transferred into a cryo-holder (Gatan), using a cryo-transfer stage. Imaging was carried out using FEI Tecnai G2 20 TWIN transmission electron microscope operating at 120 kV and at a nominal magnification of 100,000-150,000x under low-dose conditions. Images were recorded with a 2k x 2k MP side-mounted CCD camera (Olympus Veleta). Measurements were performed in the Andalusian Centre for Nanomedicine and Biotechnology, BIONAND (Málaga, Spain).

4. Measurement of size and surface potential of LLNCs

The particle-size distribution and zeta potential of LLNCs were determined by dynamic light scattering (DLS) using a Zetasizer Nano-S system (Malvern Instruments, UK). The self-optimization routine in the Zetasizer software was used for all measurements, and the zeta-potential calculated according to the Smoluchowsky theory. After a 100-fold dilution with a low ionic strength (2 mM) phosphate buffer at pH 7, measurements were performed at 25ºC in triplicate.

5. Determination of drug-release kinetics

The *in vitro* release kinetics of the curcumin-loaded LLNCs was undertaken by a dialysis method. For this, 2 ml of nanocapsule suspension was stuffed into a dialysis sac

and placed in a 200-ml flask containing phosphate buffer at pH 7.4 in a water bath at 37ºC under magnetic stirring at 300 rev/min. At predetermined time intervals, 50 µl aliquots were extracted from the LLNCs suspension. The remaining amount of curcumin loaded in the nanocapsules was determined as previously described.

6. Cell line and culture conditions

The human breast-cancer MCF-7 cell line was grown at 37°C in an atmosphere containing 5% CO_2 with DMEM supplemented with 10% (v/v) FBS, 2% l-glutamine, 2.7% sodium bicarbonate, 1% Hepes buffer, and 1% penicillin/streptomycin solution.

7. Uptake studies

With the aim of comparing the effectiveness entering cells of different nanocapsule shells, an initial study was performed with coumarin 6-labeled nanocapsules. For this, MCF-7 (5×10^3) cells were seeded into 6-well plates under the culture conditions detailed above. After 24 h, cells were fed with fresh medium and treated with coumarin 6-loaded nanocapsules. Cells were incubated with the particles for 30 min and 3 h and then washed twice with phosphate saline buffer (PBS) to remove free nanocapsules. Fresh PBS was added and living cells were analyzed by fluorescent microscopy (Nikon Eclipse Ti-S). Just before the examination, DAPI was added at ambient temperature and in the dark to stain nuclei DNA. Cells treated with empty nanoparticles were used as controls.

In a later stage, after the observation of the enhanced uptake performance of protein-covered nanocapsules, the uptake of Curcumin-LLNCs was analyzed by fluorescence confocal microscopy at 1 min and 3 h after exposure of cells to nanocapsules with and without GAD cross-linking. MCF-7 cells (3×10^3/well) were seeded in a µ-Slide 8 Well chambers (ibiTreat, IBIDI) using DMEM as culture medium. After 24 h, LLN with a 10 µM concentration of curcumin were diluted in 200 µl of DMEM and added to the cells. Imaging experiments were conducted with a Zeiss LSM 710 laser-scanning microscope using the tissue culture chamber (5% CO_2,37ºC) with a Plan-Apochromat 63×/1.40 Oil DIC m27. Images were processed with Zen Lite 2012 software.

8. Proliferation assays

The effect of curcumin-loaded LLNCs on cell viability was assessed using the MTT assay. MCF-7 breast-cancer cells were seeded into culture flasks with 75 ml DMEM and 10% of FBS. When confluence was optimal (80%), cells were detached with trypsin/EDTA and seeded into 96-well plates at a concentration of 3000 cells per well. The cells were then treated with curcumin-loaded LLNCs with and without GAD cross-linking, and free curcumin for three days. Free curcumin was dissolved in DMSO and curcumin LLNCs were diluted in PBS. Curcumin concentrations of all samples were 0.2, 0.5, 1, 3, 5 and 10 µM in 200 µl of DMEM.

The toxicity evaluation was performed by MTT assay according to the protocol. Briefly, the MTT solution was prepared at 5 mg/ml in 1x PBS and then diluted to 0.5 mg/ml in MEM without phenol red. The sample solution in the wells was removed and 100 µl of MTT dye was added to each well. Plates were shaken and incubated for 3 h at 37°C. The supernatant was removed and 100 µl of DMSO were added. The plates were gently shaken to solubilize the formed formazan. The absorbance was measured using a plate reader at a wavelength of 570 nm. The inhibitory concentration 50 (IC_{50}) values were calculated from dose-response curves by linear interpolation. All of the experiments, plated in triplicate wells, were carried out twice.

9. Cytotoxicity confocal fluorescence microscopy assays

MCF-7 cells were seeded at a concentration of 3000, 2000, and 1000 cells per well in two µ-Slide 8 Well. Then each plate was treated with curcumin LLNCs with and without GAD, respectively, at a concentration of 10 µM. The samples were analyzed after 24, 48, and 72 h by confocal fluorescence microscopy. The wavelengths of excitation and emission employed were 405 and 555 nm, respectively. Images were taken with a Zeiss LSM 710 laser-scanning microscope and processed with Zen Lite 2012 software.

10. Statistical analysis

SPSS 7.5 software (IBM, Chicago, IL, USA) was used for all data analyses. Results were compared with Student's t test. All data were expressed as means $\pm$ standard deviation (SD). Differences were considered statistically significant at a P value of < 0.05.

RESULTS

RESULTS

1. Preparation of LLNCs.

LLNCs were prepared using a solvent-displacement method as previously described.[340] Briefly, it consists of the formation of a nanoemulsion by incorporating, with a high mechanical force, an organic phase into an aqueous phase under stirring. This produces a nanoemulsion of a certain size due to the addition of a defined amount of olive oil to the organic phase (**Figure 33**).

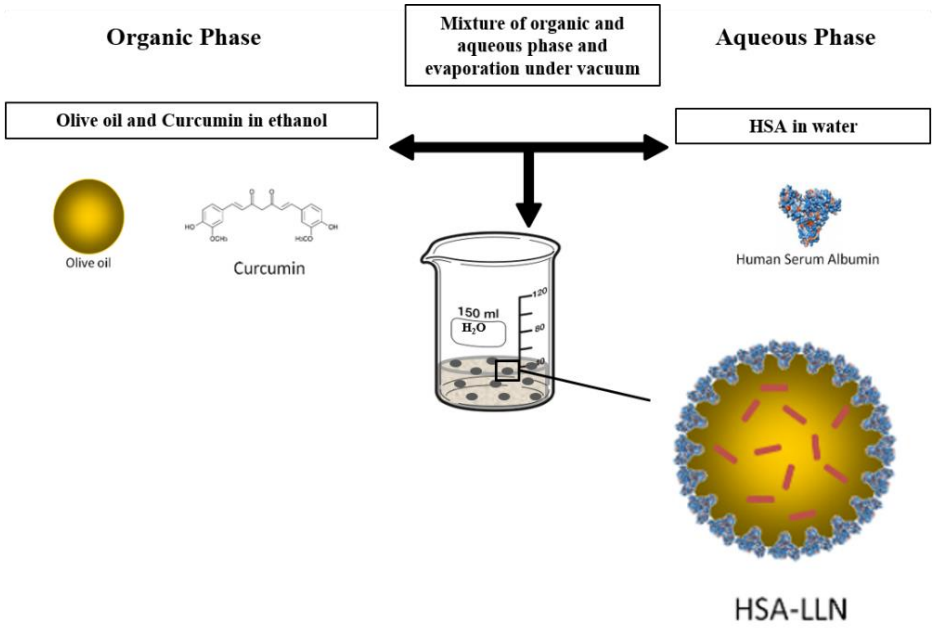

Figure 33: Scheme of synthesis of HAS-LLNCs.

2. Characterization

The nanocapsule structure was imaged by cryo-TEM (**Figure 34**). All pictures in Figure 34 correspond to LLNCs with cross-linked HSA. As can be seen in **Figures 34A and 34B**, oil nanocapsules have a spheroidal shape and are not aggregated. Arrows in **Figure 34B** indicate a break in the protein coating around the oily core.

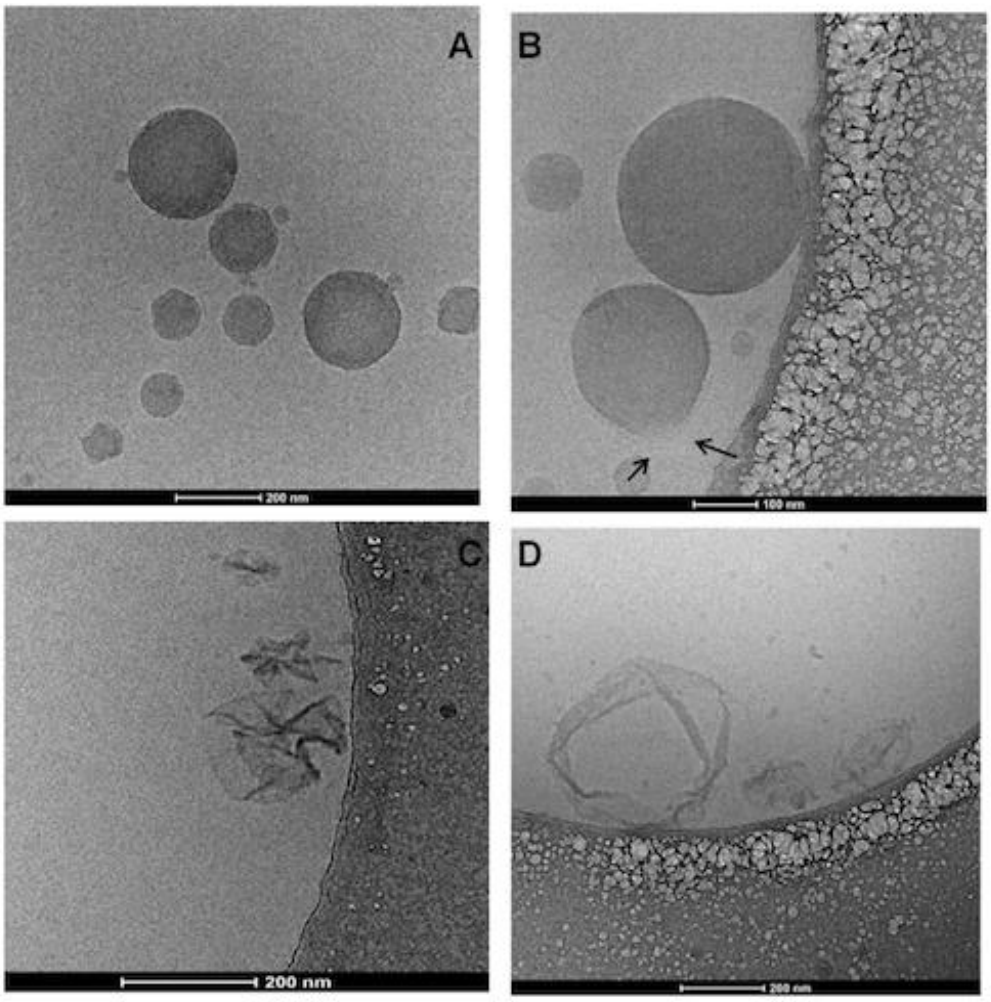

Figure 34. Cryo-TEM visualization of LLNCs stabilized by cross-linked HSA.

The cryo-electron micrographs **34C and 34D** show isolated protein shells that were covering the nanocapsules and have been broken. Clearly, the addition of GAD leads to a cross-linking of the protein shell that looks like a skin or a membrane. The LLNCs sizes are in line with DLS measurements (diameter of 169±4nm).

The effect on the nanocapsules surface charge upon treatment with GAD was analyzed by measuring the zeta potential under different experimental conditions. As a consequence of the cross-linking between the HSA molecules surrounding the oily core, the nanocapsule surface charge should significantly rise, since this covalent reaction occurs between the aldehyde groups in GAD and the protein amino residues. The number of positive charges should then diminish and, as a result, the contribution of

negatively charged carboxylic groups should become stronger and the net charge of the nanocapsules should be more negative.

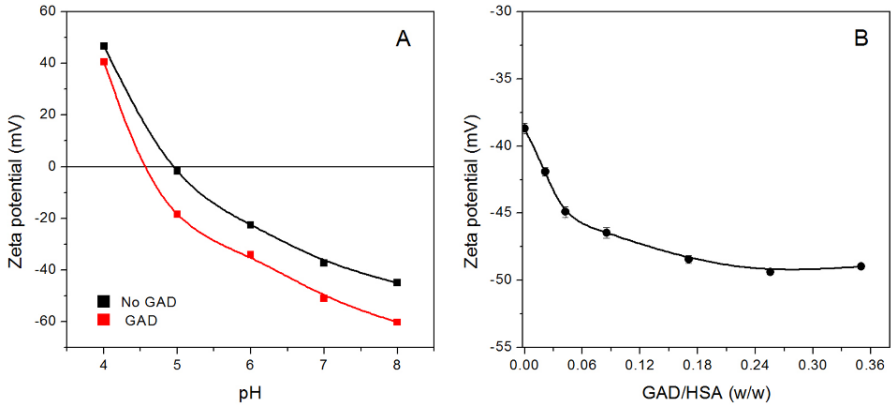

Figure 35. Zeta potential of LLNCs prepared with and without GAD. (A): Effect of pH; (B): Effect of GAD/HSA ratio (w/w).

Figure 35A presents the zeta potential as a function of pH for nanocapsules prepared with and without the GAD cross-linking treatment. As can be observed, the zeta potential of LLNCs with cross-linked HSA is more negative at all pH values studied than in the case of LLNCs not treated with GAD. An immediate consequence of this surface-charge reduction is a concomitant decrease in the isoelectric point of these nanocapsules, from around 5 to 4.6. These results clearly confirm the cross-linking between the HSA molecules.

The zeta potential is an important index for the colloidal stability of NP. It is generally accepted that zeta potential values above +30 mV or lower than -30 mV are indicative of stability.[345] Electrostatic repulsions between NP with these values of zeta potential prevent coagulation. The long-term stability of LLNCs was evaluated at 4ºC for 6 months, measuring their particle diameter and polydispersity index at different time intervals. As expected, these parameters did not differ significantly during the storage period, suggesting good colloidal stability of the LLNCs.

Another approach to verify the influence of GAD cross-linking on the nanocapsules surface charge was the evaluation of the effect of different amounts of glutaraldehyde on the zeta potential of the resulting LLNCs (**Figure 35B**). As expected, this parameter increased its negative value with the content of cross-linking agent, suggesting again that the covalent reaction with the protein amino groups was taking place while the number of positive charges decreased. The zeta potential was found to level off for a GAD/HSA relation higher than 0.20, reaching a maximum of ca. -49 mV. The extent of linking between protein molecules will depend on the number of HSA molecules on the coating shell.

Colloidal stability of the LLNCs as a function of electrolyte concentration was analyzed (**see Annexes, S.I. Chapter 2. Figure S8**)

3. Curcumin release properties

In vitro release experiments were performed at two different temperatures, namely 4ºC and 37ºC. The percentage of curcumin lost after storage (4ºC) or conditioning (37ºC) LLNCs at these two temperatures was evaluated for different time periods. The results for nanocapsules treated and not treated with GAD and kept at 4ºC are presented in **Figure 36A**. It is noteworthy that the release of curcumin from LLNCs with cross-linked HSA is retarded in comparison with non-linked LLNCs. For these nanocapsules, more than 86% of curcumin was lost after six months, while only 53% of the drug was discharged from LLNCs covered with a shell of cross-linked HSA. This marked difference suggests that the GAD cross-linked protein behaves as a “protective membrane” to hold the drug molecules inside the nanocapsules.

The effect of the curcumin-olive oil relation on drug release was also evaluated after storage of nanocapsules at 4ºC for different time intervals (**Figure 36B**). It is clear from this figure that the percentage of curcumin released increases with the initial concentration of the drug in the nanocapsule. The highest curcumin-oil relation yielded nanocapsules that released 62% of curcumin after 6 months of storage, whereas the lowest drug-oil ratio discharged only 38% of the initial drug content in the same period.

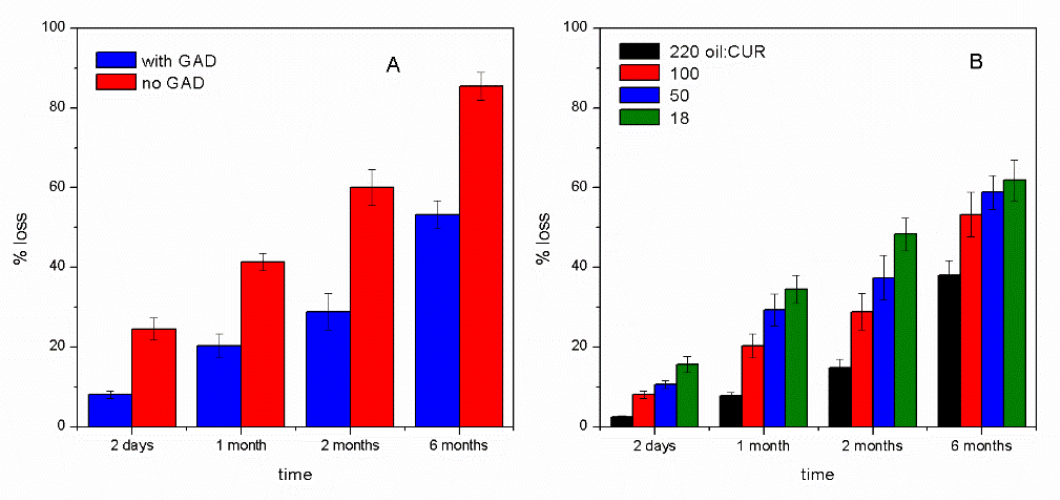

Figure 36. Percentage loss of curcumin as a function of time at 4ºC. (A): Effect of GAD treatment; (B): Effect of oil: curcumin ratio.

Another aspect of this study was the investigation of the *in vitro* curcumin release profile at 37ºC using a dialysis method. Nanocarriers are intended for drug-targeting purposes, and therefore rapid drug release or an extremely retarded one may lead to a system failure. Since Cryo-TEM images show that the LLNCs structure exhibit an oily core surrounded with a protein wall, the curcumin-release profile would be expected to be sensitive to changes in the characteristics of this protein layer. With the aim of analyzing the effect of the GAD content used in the cross-linking reaction on this parameter, the release kinetics for three LLNCs samples prepared with increasing relation GAD/HSA and with the same amount of HSA were examined. The results in **Figure 37** indicate that nanocapsules with a wall of cross-linked protein molecules retarded the discharge of curcumin at 37ºC, as happened at 4ºC. In other words, the protein cross-linking facilitated the retention of the drug in the nanocapsules.

Nanocapsules not treated with GAD exhibited an initial burst effect more pronounced than LLNCs with cross-linked HSA. This first stage involved the loss of ca. 42% and 20% of the total entrapped drug amount in the first 2 h for LLNCs non-treated and treated with GAD, respectively. It is notable that curcumin release profiles for the two GAD/HSA relations studied coincide. These observations suggest that even the smallest amount of GAD used in these experiments is adequate to generate a protective cross-linked protein membrane.

All LLNCs samples presented a rapid initial release of curcumin. This burst release could be ascribed to an immediate dissolution of curcumin deposited onto the particle surface, or to a drug accumulation near the nanocapsule surface. At a later stage, the curcumin entrapped in the inner nanocapsules core would be discharged more slowly, the rate being determined by the diffusion of the curcumin through the oily phase to the aqueous medium, and probably retarded by the physico-chemical characteristics of the surrounding shell. There was a noteworthy difference in the release kinetics patterns between the protein-covered nanocapsules presented in this study and the surfactant-covered ones described by Abdel-Mottaleb et al.[346] They reported a linear release of ibuprofen at 37ºC (zero order kinetics), with a total drug discharge after 24 h. By contrast, our system presented a more complex pattern, and drug release did not end even after 33 h. These results suggest that the release mechanism clearly depends upon the nature of the protective nanocapsule shell.

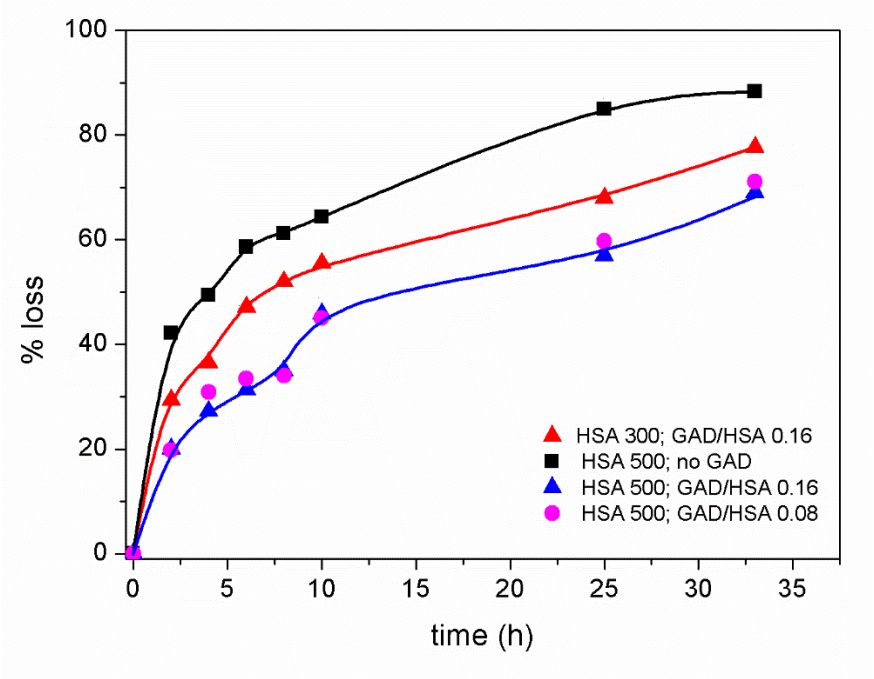

Figure 37. Percentage loss of curcumin as a function of time at 37ºC.

The effect of the HSA content (used in the synthesis of the nanocapsules) on the curcumin release profile at 37ºC is also illustrated in **Figure 37**. As can be seen, the higher the protein concentration, the slower the release kinetics. This result points out to a more compact surface monolayer, or a multilayer (or both), when protein concentration is increased, thereby hampering drug release. At the initial step, the burst release appeared stronger in the LLNCs prepared with the lower amount of HSA. From these data, we conclude that the initial burst release does not come from curcumin adsorbed at the protein surface, since in that case we would expect a higher burst release with the highest protein concentration. Given these results, it is possible that the first rapid release of the drug is due to the accumulation of curcumin near the LLNC surface.

4. Cellular uptake of coumarin 6-loaded nanocapsules

As mentioned above in the Methods section, an initial study was performed to compare the effectiveness of different nanocapsule shells entering cells. With that aim, three kinds of LLNCs were prepared with different surface coverage: HSA, Poloxamer F127, and a mixture of Poloxamer F127 and oleic acid, corresponding to the samples H10-C, PL-C, and PLOA-C, respectively.

Figure 38 shows the fluorescence detected after 30 min and 3 h of exposure of MCF-7 cells to the three samples. Green fluorescence corresponds to coumarin 6-loaded nanocapsules, while blue fluorescence highlights cell nuclei. As can be seen, the uptake was significantly faster for the H10-C nanocapsules than for the other two types. After 30 min of incubation, the coumarin 6 was localized in the cytoplasm of cells more abundantly in the case of protein-covered nanocapsules (**sample H10-C, Figure 38E**), indicating that these nanosystems are more effective vehicles to transport molecules within MCF-7 cells.

The uptake increased in all cases with a longer incubation time, but differences among the nanocapsules remained after 3 h of incubation. In **Figure 38F**, shown with a higher microscopic magnification than the other images, it is possible to appreciate an intense cytoplasmic accumulation of protein-covered LLN not observed with the other two kinds of nanocapsules.

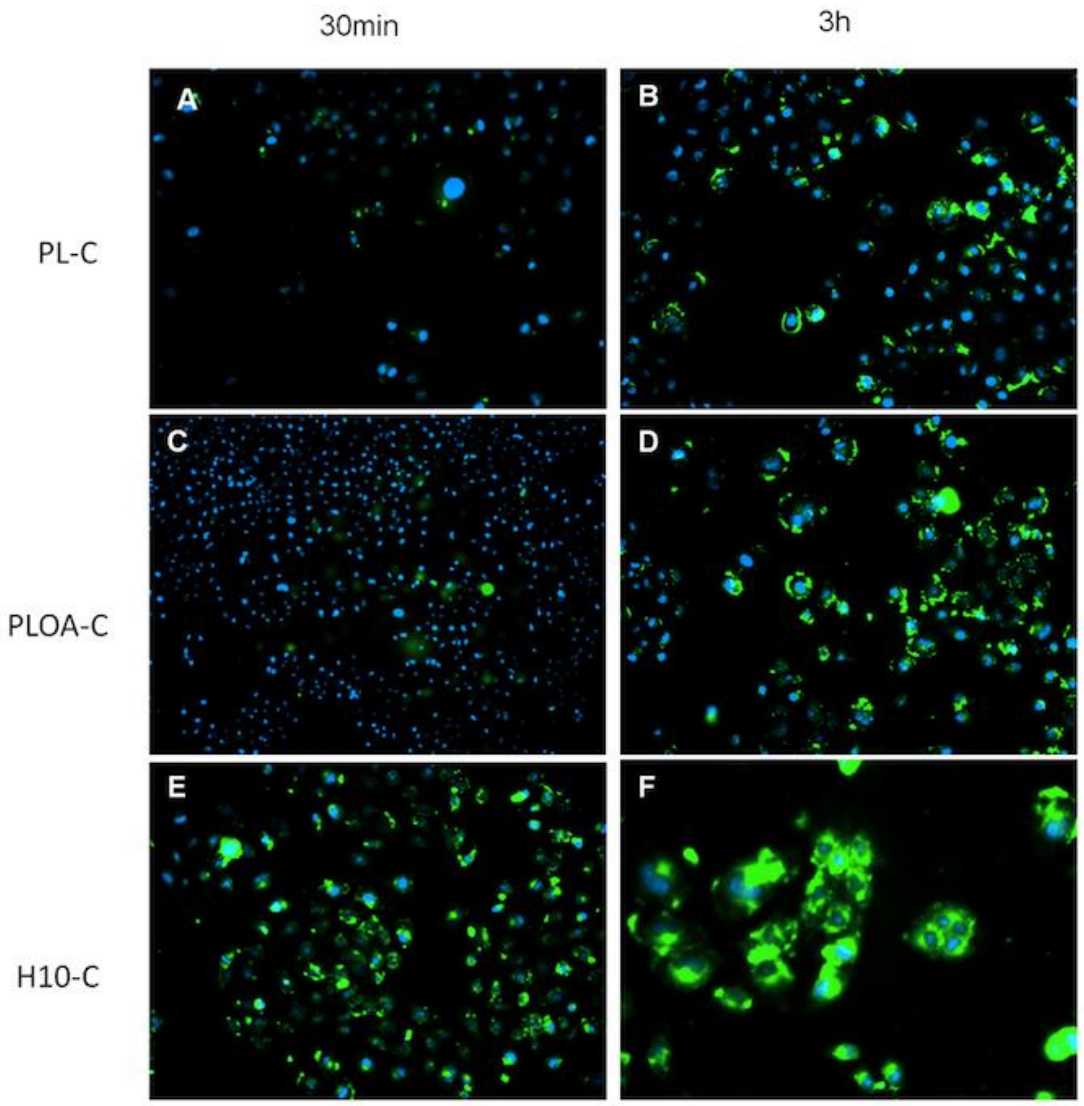

Figure 38. Uptake assays of MCF-7 cells treated with coumarin 6-LLNCs during 30 min (left) and 3 h (right): (A) and (B) PL-C sample; (C) and (D) PLOA-C sample; (E) and (F) H10-C sample. Cell nuclei are stained with DAPI. All images ×10 magnification, except (F) ×20.

5. Cellular uptake of curcumin-LLNCs

To further elucidate the capabilities of albumin-covered LLNCs entering MCF-7 cells, and recognize the possible influence of the protein cross-linking procedure, we undertook confocal fluorescence microscopy observations after a very short incubation time (1 min) and a long one (3 h) with both kinds of nanocapsules, namely HSA-coated LLNCs with and without GAD treatment. In these experiments coumarin 6 was not included in the LLN formulation, since the model drug used, curcumin, displayed enough

fluorescence to be detected in the confocal microscopy. The results are shown in **Figure 39.**

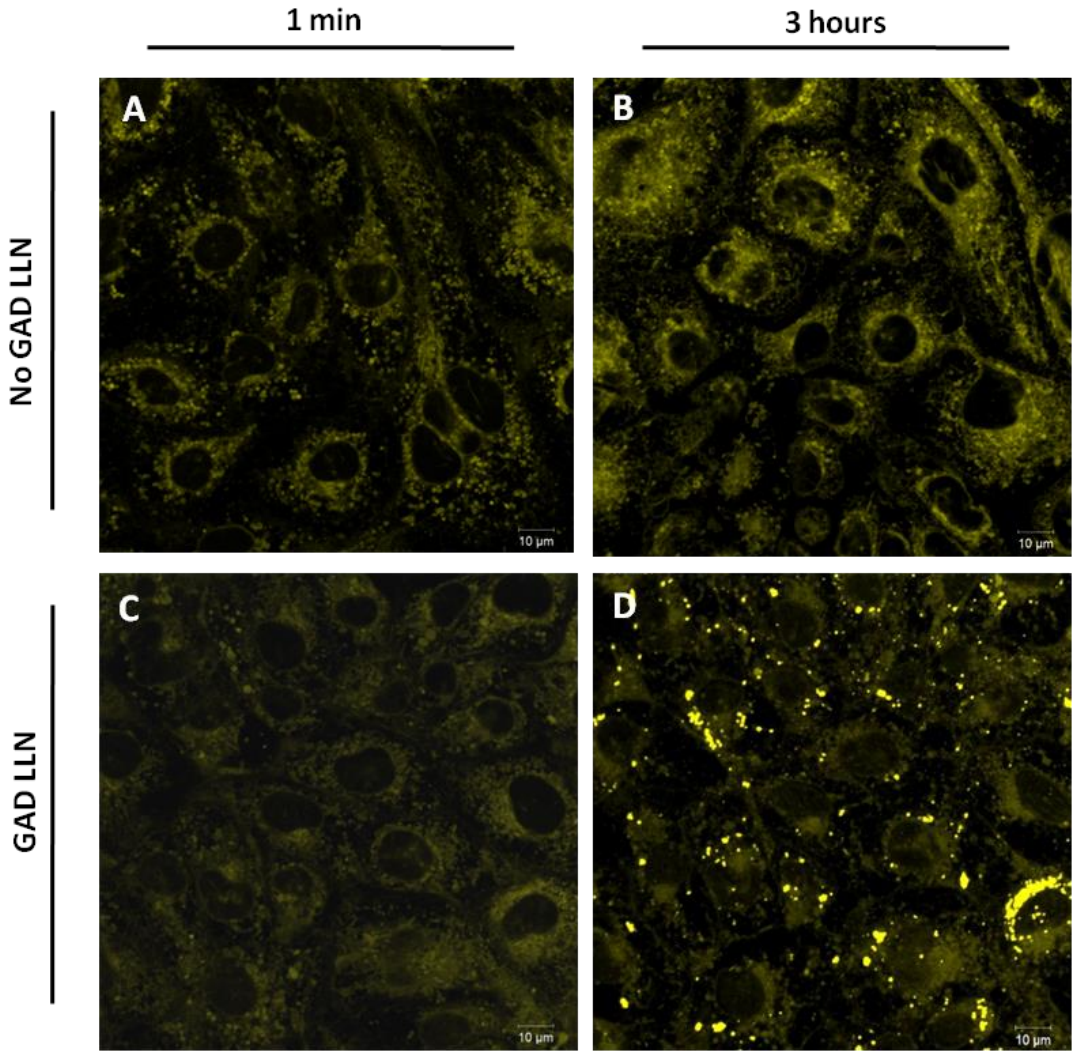

Figure 39. Confocal fluorescence microscopy after 1 min and 3 h exposure of cells to nanocapsules. LLNCs without GAD: (A) 1 min (B) 3 h; LLN cross-linked with GAD: (C) 1 min (D) 3 h.

As can be seen in this figure, the uptake evaluation reveals an outstanding performance of both types of LLNCs (with and without GAD cross-linking) entering massively and efficiently the cells in less than 1 min of exposure, and accumulating in the perinuclear zone. Only a slight difference in fluorescence intensity was detected between the two kinds of nanocapsules within this short time. After 3 h of exposure,

nevertheless, LLNCs treated with GAD (**Figure 39D**) displayed a clear increase in fluorescence intensity with respect to LLNCs not treated with GAD (**Figure 39B**).

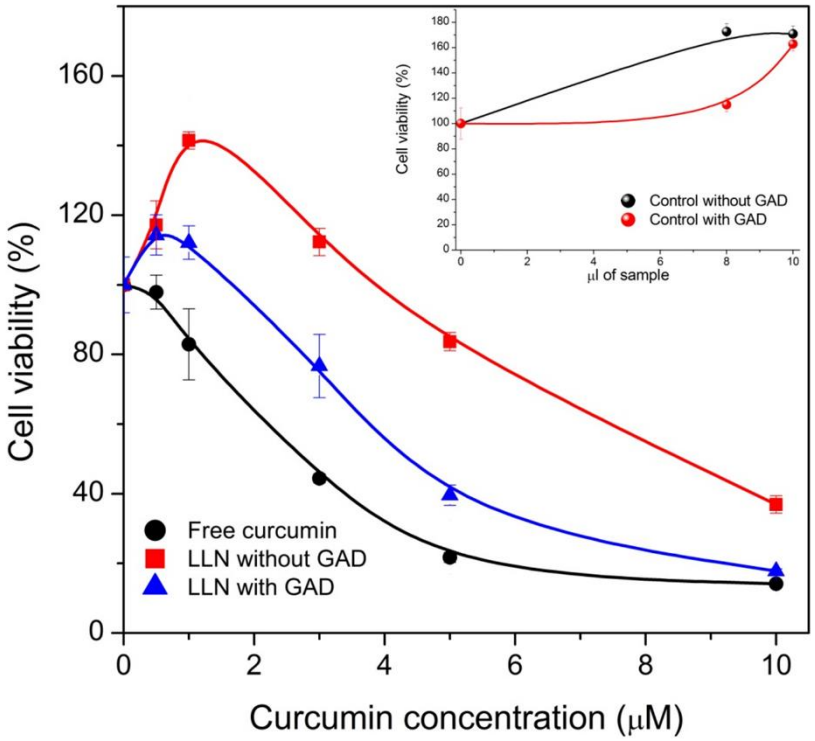

Figure 40. Cell viability of MCF-7 cells upon treatment with free curcumin and albumin-coated LLNCs. Insert: Cell viability upon treatment with blank nanocapsules (no curcumin).

Figure 40 summarizes the cell-viability data from the MTT assay after treating MCF cells with free curcumin and curcumin-loaded LLNCs with and without GAD cross-linking. This figure shows that blank (control) LLNCs, i.e. nanocapsules without curcumin, displayed no toxicity to MCF-7 cells even in the case of the GAD-treated ones. However, curcumin-loaded nanocapsules decreased cell viability in all samples tested. In the case of free curcumin, we found an IC_{50} value of 3.4±0.2 μM, whereas curcumin-LLNCs with and without GAD cross-linking gave IC_{50} values of 4.3±0.2 and 8.7±0.1 μM, respectively.

6. Cell-viability assay using confocal fluorescence microscopy

With the aim of gaining insight into the cell-killing process taking place upon exposure to curcumin-loaded nanocapsules, cell viability was visually analyzed by

confocal fluorescence microscopy (**Figure 41**). Data compiled by this technique show that curcumin-LLNCs caused cell death after three days of treatment in the MCF-7 human breast-cancer cell line. For LLNCs not cross-linked with GAD, cells began to die at 24 h after the addition of the nanocapsules (**Figure 41D**). After 48 and 72 h (**Figures 41E to 41F**), cell death increased. In the case of the GAD cross-linked LLN, cell viability significantly decreased after 24 h of treatment (**Figure 41G**). At 48 and 72 h (**Figures 41H and 41I**) the effect persisted and the number of apoptotic cells even rose, which showed extended formation of large vacuoles, as well as increased cell and nuclear shrinkage, rounding, and detachment among others.

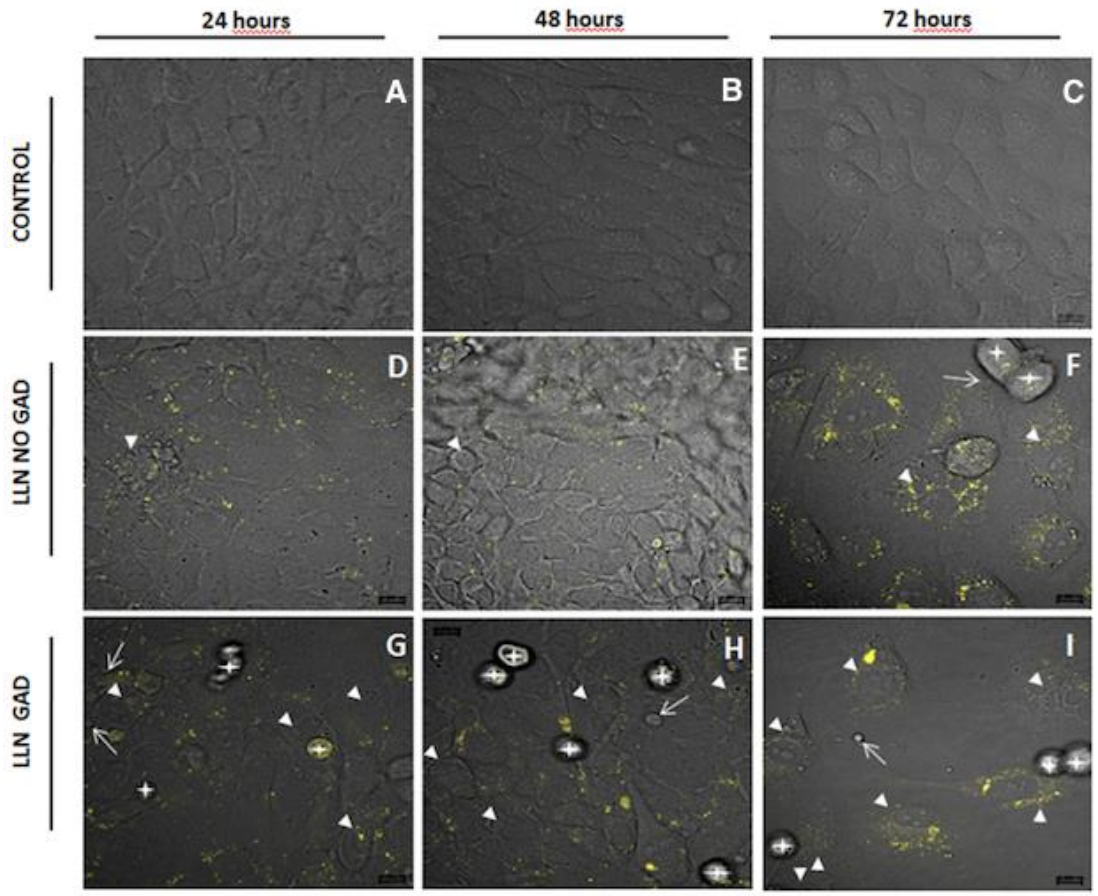

Figure 41. Confocal fluorescence microscopy of MCF-7 cells in culture: (A-C) control; (D-F) non-cross-linked LLNCs; (G-I) GAD-cross-linked LLN. Columns: 24 h, 48 h, and 72 h, respectively. ▶ Apoptotic cells, ⟶ Apoptotic vesicles, ✦ Detached cells.

DISCUSSION

DISCUSSION

In the present study, we have developed colloidally stable nanocapsules with an olive-oil core surrounded by a GAD cross-linked HSA shell. The presence of this shell was confirmed by Cryo-TEM and zeta potential studies. *In vitro* release experiments of encapsulated curcumin showed that the drug:oil relation was key in controlling the drug release from the nanocapsules, and a higher ratio resulted in a higher percentage of discharged curcumin with time. The drug released from LLNCs not treated with GAD was clearly faster than from cross-linked HSA, while an increase in the HSA amount used in the preparation of the nanocapsule shell appeared to decrease the rate of curcumin release. A higher protein concentration resulted in a nanocapsule shell with higher density and thickness, and therefore the amount of HSA could be an effective way to control the release of curcumin from LLNCs.

The *in vitro* studies carried out to determine the internalization capacity of three kinds of LLNCs with different surface coverage (HSA, Poloxamer F127, and a mixture of Poloxamer F127 and oleic acid, **Figure 38**), clearly shows a better performance of protein-covered LLNCs. This difference in internalization among the nanocapsules may be ascribed to a combination of surface charge and hydrophilicity, which play a major role in the membrane affinity prior to the endocytosis process.[347,348] It has been shown that greater hydrophilicity decreases particle uptake by macrophages as well as nonphagocytic HeLa cells.[349] This is consistent with our results, since the HSA-covered particles (H10-C) present a more hydrophobic surface than do the samples with Poloxamer F127 (namely, PL-C and PLOA-C) and a definitely higher uptake, probably by avoiding the multi-drug resistance (MDR) efflux mechanism by cell-membrane transport proteins such as p-glycoprotein (P-gp).[350,351] Moreover, as in the case of nab-paclitaxel (an albumin-bound form of paclitaxel), it may be hypothesized that these albumin-covered nanocapsules probably utilizes receptor-mediated albumin endocytosis to internalize cells.[352] Taking into account these different uptake properties attributed to the particle surface, it is noteworthy to mention the possibility of tailoring NP to either prevent or encourage membrane penetration.

In our case, upon observing the enhanced performance of albumin-coated nanocapsules, we continued the study focusing on these systems. The uptake evaluation

presented in Figure 39 reveals an outstanding performance of both types of LLNCs (with and without GAD cross-linking) entering the cells massively and efficiently in less than 1 min of exposure, and accumulating in the perinuclear zone. It suggests that the cross-linking procedure does not influence the (fast) recognition and internalization of the LLNCs, with cell membranes quickly integrating the nanocapsules into the cytoplasm. As mentioned earlier, this prominent velocity entering cells should be ascribed to the albumin molecules attached to the nanocapsule surface and their natural role as molecular carriers in the mammal bloodstream.[352] Nevertheless, after 3 h of exposure, LLNCs treated with GAD (Figure 39D) displayed a clear increase in fluorescence intensity with respect to LLNCs not treated with GAD. To explain this difference at longer exposure times, we return to the results previously presented for the curcumin-release profiles of both LLNCs. As stated above, LLNCs cross-linked with GAD showed a slower discharge of curcumin at 37ºC (as well as at 4ºC), suggesting that the protein cross-linking facilitates the retention of the drug in the nanocapsules or, in other words, they display a steadier (and more prolonged) release profile. This slower drug discharge, together with the protection against cytoplasmic digestion afforded by the "hardness" of the cross-linked protein wall, could be responsible for the observed increase in fluorescence intensity. These two characteristics showed by GAD cross-linked LLNCs, i.e. fast internalization and sustained drug delivery, may represent a great advantage in intracellular uptake and effectiveness compared to other systems that need more time and concentration to be internalized by the cells while offering similar therapeutic response.[353]

In the MTT assay, nanocapsules without curcumin displayed no toxicity to MCF-7 cells even in the case of the GAD-treated ones. Although GAD is strongly toxic to living organisms, the extremely low concentration used (0.004%), the chemical reaction with protein amine groups, and the cleaning process performed thereafter, renders nanocapsules without any appreciable toxicity to cells. In fact, they thrive upon exposure to the LLNCs. Mahanta et al. have reported that a concentration up to 0.1% GAD does not affect viability in normal (HaCaT) and MCF-7 cells.[354]

The IC_{50} value of curcumin-LLNCs with GAD is similar to the IC_{50} of free curcumin. Although the capacity to kill cells decreased slightly in the encapsulated formulation

with respect to the (DMSO dissolved) free form, the undoubted advantage of nanocapsules is their ease of dispersion at any concentration in water, and consequently the safety for being administered intravenously, thus avoiding adverse effects of excipients such as Cremophor EL©.[355,356] In this way, the encapsulated formulation would allow the administration of higher amounts of curcumin or other hydrophobic drugs without additional secondary side effects, facilitating a better therapeutic effect and the possibility of greater administration frequency, improving the treatment guidelines. Moreover, as we have previously demonstrated,[357] LLNCs allow high functionalization for vehiculization of targeting molecules like antibodies and other cell-surface active compounds. Other authors have also demonstrated the safety and great utility of these lipid-based nanosystems.[358,359]

Moreover, MCF-7 cells treated with GAD cross-linked LLNCs show the extended formation of large vacuoles, as well as increased cell and nuclear shrinkage, rounding, and detachment. These apoptotic morphological changes induced by curcumin have been previously described for MCF-7 breast-cancer cells[360] which are deficient in the caspase-activation mechanisms.[361] In accordance with the previously described uptake assay, this superior performance of GAD cross-linked LLNCs may be ascribed to the more continuous and sustained release of curcumin displayed by these kinds of nanocapsules.

CHAPTER 3

ANTI-CD44-CONJUGATED OLIVE OIL LIQUID NANOCAPSULES FOR TARGETING PANCREATIC CANCER STEM CELLS

BACKGROUND

The development of targeted therapies, especially for cancer, is one of the main goals of nanomedicine today.[362–364] Conventional chemotherapy usually prompts modest tumor response and provokes undesirable side effects due to the nonspecific action of drugs on proliferating tissues.[365] To avoid these and other disadvantages, drug nanocarriers should be formulated to deliver the antitumor drug directly to the cancerous cells. This is a complex interdisciplinary task with too many variables to be properly controlled. These variables include the use of biocompatible materials, with simple but robust processes for biomaterial assembly, usually requiring different conjugation chemistries followed by some purification processes.[223]

Therefore, current formulations based on complex nanostructures such as polymer conjugates, polymeric micelles, liposomes, carbon nanotubes, or nanoparticles,[201,366–368] must be superficially modified to provide carriers with vectorization properties. In recent years, LLNCs have been developed as potential nanocarriers. The inner hydrophobic domain, encased in a hydrophilic outer shell, has been used to encapsulate hydrophobic drugs that are protected during their transport to the target cells.[369] Additionally, the external shell can be physico-chemically modified by ligands such as antibodies, which can be linked to the surface of the nanocarriers to deliver the given drug, specifically inside the cells that overexpress the corresponding antigen receptor. These tailor-made vehicles could improve the effectiveness of the drug, while minimizing undesirable side effects in healthy cells.[164,370] With regard to the nature of the ligands, monoclonal antibodies have been extensively employed to develop targeted nanocarriers, referred to as immuno-nanocarriers.[371] Some advantages of immuno-nanocarriers include the improvement of drug selectivity, high drug-loading efficiency, minor drug leakage, and protection of drugs from enzymatic degradation.[372] The design of immuno-nanocapsules requires not only the creation of well-defined structures, but also the optimization of appropriate antibody-conjugation chemistry.

Despite recent progress in cancer therapy and increased knowledge of tumor biology, cancer remains a very common and lethal disease worldwide. Cancer-associated aggressiveness and mortality is primarily caused by cancer recurrence and

metastasis. Recent advances in cancer research indicate that this is mainly due to a small subpopulation of cells known as cancer stem cells (CSCs, or tumor initiating cells), which possess stem-like functional properties such as self-renewal ability and multipotency, and have the ability to differentiate into bulk tumor cells. Although current treatments can reduce size or eliminate the tumor, however, in several cases these effects are transient and generally do not improve patient survival outcomes. In fact, during chemotherapy most of the cells of the primary tumor can be destroyed, but if CSCs are not totally eradicated, they can lead to the reappearance of the tumor in the same organ or in metastatic sites.[373–376] Therapies that specifically target CSCs hold great promise for improving survival rates and quality of life for cancer patients.

On the other hand, CD44 has attracted considerable attention because of its important functions in mediating cell-cell and cell-matrix interactions and association with malignant processes, particularly in cancer dissemination.[377,378] Recent work has revealed that CD44 is the most common CSC surface marker and plays a pivotal role in CSCs in communicating with the microenvironment and regulating CSC stemness properties. Increasing evidence suggests that CD44 is a promising prognostic biomarker and therapeutic target for many cancers. In fact, it has been demonstrated that populations enriched in CSCs of prostate cancer, uterine adenocarcinoma and pancreatic cancer (PC) among others, have a high expression of CD44.[379]

Specifically, PC is the 12th most commonly occurring cancer in men and the 11th most commonly occurring cancer in women. In 2018, there were 460,000 new cases diagnosed around the world.[380] Although there are different types of treatment available for patients with PC, most patients have no recognizable symptoms, making early diagnosis difficult, and chemotherapies or radiation therapies often show poor results.[381] The biochemical and physiological characteristics of PC appear to limit the effectiveness of these standard forms of therapy, mainly due to the highly enriched CSC subpopulations present in this tumor that explains the resistance to treatments.[66,382]

Starting from our previous works,[357,383] in the present study we have formulated and optimized a new immuno-nanosystem by covalent linking of a specific immuno-γ-globulin (IgG) to the surface of olive oil liquid NCs (O^2LNCs). The chemical procedure for such linkage requires the presence of carboxylic acid functional groups on the solvent-

exposed face of the NC surface. Among the wide variety of chemical groups described in the literature for this purpose, carboxylic acids play a leading role in covalently binding proteins to the surface of colloidal particles. Thus, our group has developed a novel system in which the NC's shell was enriched with deoxycholic acid (DCA).[357] This amphiphilic molecule has been previously used as a component of different types of nanoparticles. Chemically conjugated with oligosaccharides, it has shown great potential to form both drug and gene carriers,[384] and it increases the efficacy of oral bioavailability of different nanoparticles that encapsulate drugs.[385] In this way, using DCA-NC with a core constituted of olive oil prepared by a simple process using a solvent-displacement technique (O^2LNC), we achieved the optimal experimental conditions to covalently link the anti-CD44-FITC clone REA690 onto their carboxylic acid rich surfaces, by means of a reproducible and simple method based on a carbodiimide catalyst.[231,383] The antibody is a recombinant humanized IgG1 that specifically recognizes the CD44 antigen overexpressed on the surface of pancreatic CSCs (PCSCs). Subsequently, the obtained olive oil immuno-NCs (αCD44-O^2LNC) were physico-chemically characterized, which included size analysis, gel electrophoresis measurements, electro-kinetic behavior, and colloidal stability.

Moreover, both bare O^2LNC and αCD44-O^2LNC labeled with a fluorescent molecule (Nile Red or IR-780 iodide) were evaluated *in vitro*, analyzing the uptake efficiency by differentiated pancreatic cancer cells (PCCs) growing in monolayer (low expression of CD44) and PCSCs (high expression of CD44). In addition, a cytotoxicity assay (IC_{50}) was performed using αCD44-O^2LNC loaded with paclitaxel, a drug used as a first-line treatment for advanced PC in patients. Finally, we evaluated the biodistribution and targeting properties of αCD44-O^2LNC in a PCSC orthotopic xenotransplant *in vivo* model.

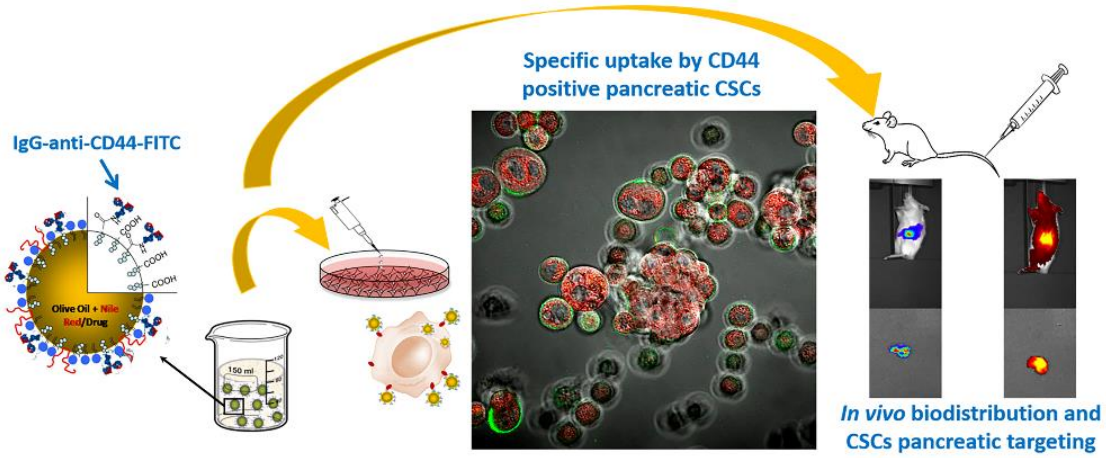
IgG-anti-CD44-FITC
Olive Oil + Nile Red/Drug
150 ml
Specific uptake by CD44 positive pancreatic CSCs
In vivo biodistribution and CSCs pancreatic targeting

MATERIALS AND METHODS

MATERIALS AND METHODS

1. Reagents.

Reagents. Poloxamer 188 (Pluronic F-68), deoxycholic acid (DC), Nile Red (RN), IR-780 iodide (i780), N-(3-Dimethylaminopropyl)-N'-ethylcarbodiimide hydrochloride (ECDI), β-Mercapto-ethanol, Brilliant Blue R250, Paclitaxel (PTX) with a purity ≥97.0% and olive oil were purchased from Sigma-Aldrich (Spain). All of them, except the olive oil, were used as received. Olive oil was previously purified in our laboratories with activated magnesium silicate (Florisil, Fluka) to eliminate free fatty acids. Epikuron® 145 V, which is a phosphatidylcholine-enriched fraction of soybean lecithin, was supplied by Cargill (Barcelona, Spain). Human anti-CD44-FITC (αCD44) (clone REA690), anti-CD44-APC (clone REA690), anti-CXCR4-APC and anti-CXCR4-PE (clone REA649) monoclonal antibodies were obtained from Miltenyi Biotech (Spain). Their isoelectric point (IEP) was 6.8 ± 0.5. 3-(4,5-Dimethylthiazol-2-yl)-2,5-diphenol tetrazolium bromide (MTT) cell-proliferation kit was obtained from Promega (U.S.A.), Cell Counting Kit-8 (CCK8) cell-proliferation assay was purchased from Dojindo (Europe). Water was purified in a Milli-Q Academic Millipore system. NMR solvents (D2O, CDCl3 and CD3OD) were purchased from Eurisotop (France). Other solvents and chemicals used were of the highest grade commercially available.

2. Cell Lines and Culture Conditions.

293T human kidney cancer cell line (CRL11268) and BxPC-3 human pancreatic cancer cell line was obtained from American Type Culture Collection (ATCC), and cultured following ATCC recommendations. 293T cell line was cultured in DMEM (Biowest) and BxPC-3 pancreatic cancer (PC) cell line was cultured in RPMI-1640 Medium (RPMI) (Gibco, Grand Island, NY, USA) supplemented with 10% (v/v) heat-inactivated fetal bovine serum (FBS) (Gibco) 1% L-glutamine, 2.7% sodium bicarbonate, 1% Hepes buffer, and 1% penicillin/streptomycin solution (GPS, Sigma). Both cell lines were grown at 37 °C in an atmosphere containing 5% CO2.

Cancer stem-like cells from BxPC3 PC (adenocarcinoma) cell line were isolated using the methodology previously described by us.52 Briefly, the BxPC-3 cell line was cultured into Ultra-Low Attachment 6-well plates (Corning) with DMEM-F12 (Sigma-Aldrich), 1% streptomycin-penicillin (Sigma-Aldrich), 1 mg/mL hydrocortisone (Sigma-

Aldrich), 4 ng/mL heparin (Sigma-Aldrich), 1X ITS (Gibco); 1X B27 (Gibco), 10 ng/mL EGF (Sigma-Aldrich), 10 ng/mL FGF (Sigma-Aldrich), 10 ng / mL of IL-6 (Sigma-Aldrich) and 10 ng / mL of HGF (Sigma-Aldrich). To obtain the second generation of PCSCs used in the experiments, spheres were collected by centrifugation at 1500 rpm for 5 min, incubated 5 min at 37 °C with trypsin-EDTA(Sigma-Aldrich), disaggregated with a 30G needle and washed with 1X PBS. The cells were seeded again in the same type plates and with the same medium mentioned above. After three days, the spheres were collected and used in the different trials.[386] All cell cultures tested were negative for mycoplasma infection.

3. Preparation of Olive Oil Lipid Nanocapsules (O^2LNC).

O^2LNC were prepared by using a modified solvent-displacement technique of Calvo et al.[387] Briefly, an organic phase composed of 125 µL of olive oil, 10 mg of deoxycholic acid, 40 mg of Epikuron 145 V dissolved in 1 mL of ethanol, and 9 mL of acetone was strongly added to 20 mL of an aqueous phase containing 50 mg Pluronic F68 under magnetic stirring. The mixture turned milky immediately due to the formation of a nanoemulsion. Organic solvents (acetone and ethanol) plus a portion of the volume of water were evaporated in a rotary evaporator at 35 °C, giving a final volume of 16 mL. In some cases, we dissolved PTX or/and NR or i780 iodide dye in the olive-oil phase in order to synthesize O^2LNC loaded with these compounds inside.[383] These different O^2LNCs were used depending on the experiment carried out.

4. HNMR and HRMS Characterization of the Nanocapsules.

NMR spectra were recorded on a Bruker Avance III spectrometer (500 MHz for 1H) equipped with a 1.7mm MicroCryoprobe, using external acetone referencing for the analysis of intact nanocapsules in H_2O/D_2O or the signal of the residual solvent as internal reference (δH 7.26 for $CDCl_3$, δH 3.31 for CD_3OD) for the analysis of disintegrated nanocapsules reconstituted in these deuterated organic solvents. For nanocapsule disintegration, a clean aliquot (80µl) of sample was dissolved in 2-propanol (2 mL), mixed, sonicated for 20 minutes and split into two further aliquots which were concentrated to dryness before reconstitution in organic deuterated solvent (ca. 50 µl of $CDCl_3$ or CD_3OD) for NMR analyses.

5. Preparation of Antibody Coated Nanocapsules.

Antibodies were immobilized on the O^2LNC surface by an optimized carbodiimide method previously described,26 which permits an efficient covalent binding of protein molecules to the carboxylic groups supplied by deoxycholic molecules. The antibody-coupling protocol was conducted at pH value, depending on the IEP of the IgG, in such a way that the O^2LNCs were first centrifuged in a Vivaspin 20 centrifugal concentrator MWCO 1000 kDa (Sartorius) at 2500xG for 15 min, replacing the medium with a phosphate buffer (PB pH 7.4) for αCD44-FITC; in order to eliminate the non-reactive products coming from the synthesis protocol. Once the centrifugation was finished, 1 mg of a solution in phosphate buffer (pH 7.4) of ECDI at 15 mg/ml was added to the O^2LNC solution having a total particle surface equal to 0.29 m^2 for the covalent binding of αCD44-FITC (αCD44). Subsequently, the antibody coverage was performed by adding αCD44 concentration of 0.18 mg/m^2, and then the solution was incubated at room temperature for 2 h. Finally, the αCD44-O^2LNCs were centrifugated in the Vivaspin tubes with its corresponding buffer to remove any IgG molecules that were not coupled to the O^2LNC. The final αCD44-O^2LNC stock was stored at 4°C for further use.

6. Protein Separation by SDS-PAGE.

In order to verify that the covalence of the antibody was effective, a gel chromatography test was performed. The immune-nanocapsule complexes were separated and denatured by boiling 20 µl of each sample for 5 min in the following buffer: 62.5 mM Tris-HCl (pH 6.8 at 25 °C), 2% (w/v) sodium dodecyl sulfate (SDS), 10% glycerol, 0.01% (w/v) bromophenol blue, and 40 mM dithiothreitol (DTT). Samples were then separated by size in porous 12% polyacrylamide gel (1D SDS polyacrylamide gel electrophoresis), under the effect of an electric field. The electrophoresis was run under constant voltage (130 V, 45 min) and the gels were stained using a Coomassie Blue solution (0.1% Coomassie Brilliant Blue R-250, 50% methanol, and 10% glacial acetic acid) and faded with the same solution lacking the dye.

7. Physico-Chemical Characterization.

The hydrodynamic mean diameter of the NC was determined by photon correlation spectroscopy (PCS), using a 4700C light-scattering device (Malvern Instruments, U.K.) and working with a He−Ne laser (10 mW). The light scattered by the

samples was detected at 173°, and the temperature was set at 25 °C. The diffusion coefficient measured by dynamic light scattering can be used to calculate the size of the O^2LNC by means of the Stokes−Einstein equation. The homogeneity of the size distribution is expressed as polydispersity index (PDI), which was calculated from the analysis of the intensity autocorrelation function.[388] Electrophoretic mobility (μe) as a function of pH was measured after diluting a small volume of the O^2LNC stock (with a total surface equal to 0.05 m^2) in 1 mL of the desired buffered solution. It should be noted that all the buffers used in the μe studies had identical ionic strengths, being equal to 0.002 M except for measurements with PBS (pH 7,4 and 150mM) and with RPMI cultured medium supplemented with 10% FBS (pH 7,4 and 150 mM). The μe measurements were made in triplicate using a nanozeta dynamic light-scattering analyzer (Zeta-Sizer NanoZ, Malvern Instruments, U.K.).

8. In Vitro Cellular Uptake.

1.5×10^5 cells from both BxPC-3 cells growing in monolayer and BxPC-3 PCSCs were seeded into Corning® cell culture flasks (VWR, Spain) and into Ultra-Low Attachment 6-well plates (Corning, Spain) respectively. In this study, O^2LNCs were formulated by adding NR into the olive oil at a concentration of 0.025% (w/w). Subsequently, the same protocol described above was used to coat the O^2LNC surface by our antibody. The membrane binding and cell internalization of both labeled naked NR-O^2LNC and NR-αCD44-O^2LNC were examined by laser-scanning confocal microscopy. Briefly, the two types of cell populations (3×10^3/well) were seeded in Slide 8-Well chambers (ibiTreat, IBIDI) with RPMI medium and F12 spheres medium supplemented as described above, for the differentiated PCCs and the PCSCs respectively. After 24 h, $4.4x10^{11}$ of NR-O^2LNC and NR-αCD44-O^2LNC were added to the cells. The images were taken after 3 hours of incubation. Imaging experiments were conducted with a Zeiss LSM 710 laser-scanning microscope using the tissue culture chamber (5% CO_2, 37◦C) with a Plan-Apochromat 63×/1.40 Oil DIC m27. Images were processed with Zen Lite 2012 software.

Additionally, to quantitatively analyze the uptake of the O^2LNCin the two PC cell populations, a flow cytometry assay was performed. Once the different cell populations were obtained, these were washed and centrifuged at 1500 rpm for 5 min in tubes and

resuspended in a 1% BSA (Bovine Serum Albumin) solution to block the possible non-specific binding of antibodies Next, $1x10^6$ cells per sample were incubated with $4.4x10^{11}$ NR-O^2LNC and NR-αCD44-O^2LNC. The incubation times of the cells with the O^2LNC were 15, 30 and 60 min. Then, the cells were washed with 1X PBS and centrifuged at 1500 x G for 5 min twice to remove the non-internalized NCs. Finally, the cells were resuspended in 300 µl of 1X PBS and analyzed for red and green fluorescence by flow cytometry (FACS CANTO II (BD Biosciences)) using the FACS DIVA software. Moreover, we performed a characterization of BxPC-3 PCCs and BxPC-3 PCSCs in order to corroborate their stemness properties. Briefly, cell surface marker levels of BxPC-3 PCSC were determined with human antibodies anti CD44-FITC and anti CXCR4-APC; and ALDEFLUOR assay (Stem Cell Technologies) to detect ALDH1 enzyme activity was performed to complete the characterization. Samples were measured and analyzed by flow cytometry on a FACS CANTO II (BD Biosciences). All experiments were performed in triplicate and replicated at least twice. Sterility evaluations of all nanosystems were performed prior to develop O^2LNC uptake studies in order to exclude possible biological contamination. Cells treated with naked O^2LNC were used as controls.

9. Encapsulation Efficiency, Drug loading and Retention Time of O^2LNC-PTX.

In order to know if our O^2LNCs are a good drug vehicle nanosystem, two parameters were calculated, such as drug loading (DL) (1) and encapsulation efficiency (EE) (2). Then, a defined amount of PTX was dissolved in the olive oil and the synthesis of the O^2LNC was performed. Briefly, PTX was dissolved in olive oil at different concentrations and EE, as well as the permanence over time within the oil core of the O^2LNC, was calculated. After the synthesis and the covalence protocol, O^2LNC, O^2LNC-PTX and αCD44-O^2LNC-PTX were stored at 4°C and aliquots were collected at different times (0, 1, 2, 3 and 4 weeks). These aliquots were centrifuged in Vivaspin 20® tubes with a pore size of 300 KDa at 2500xG for 15 minutes. Then, each aliquot was dissolved in 2-propanol, mixed by vortex and sonicated for 30 mins and centrifuged at 14000 rpm for 20 minutes. The supernatant was collected and analyzed by MS with a mobile phase of acetonitrile-water.

$$\%DL = \frac{Drug\ \ encapsulated\ \ (g)}{Total\ \ Nanocapsule\ \ \ weig\ ht(g)}\ x\ 100 \quad (1)$$

$$\%EE = \frac{Drug\ \ encapsulated\ \ (g)}{Theoretical\ \ drug\ (g)}\ x\ 100 \quad (2)$$

10. In Vitro Antitumor Performance.

The effect of PTX-loaded O^2LNC on cell viability was assessed using the MTT or CCK8 kit assay, depending on the cell population. In the case of differentiated BxPC-3 PCCs, cells were seeded into culture flasks with 15 ml RPMI supplemented 10% of FBS. When confluence was optimal (80%), cells were detached with trypsin/EDTA and seeded into 96-well plates at a concentration of 3000 cells per well. The cells were then treated with O^2LNC-PTX, αCD44-O^2LNC-PTX and free PTX for three days. Free PTX was dissolved in DMSO, and PTX-loaded O^2LNCs were diluted in RPMI medium. The cytotoxicity evaluation was performed by MTT assay according to the protocol. Briefly, the MTT solution was prepared at 5 mg/ml in 1X PBS and then diluted to 0.5 mg/ml in MEM without phenol red. The sample solution in the wells was removed and 100 µl of MTT dye was added to each well. Plates were shaken and incubated for 3 h at 37◦C. The supernatant was removed and 100 µl of pure DMSO was added. The plates were gently shaken to solubilize the formazan that was formed. The absorbance was measured using a plate reader at a wavelength of 570 nm. In the case of BxPC-3 PCSCs, cells were seeded into Ultra-Low Attachment 96-well plates at a concentration of 5000 cells per well. After 3 days, cells were treated with free PTX, O^2LNC-PTX and αCD44-O^2LNC-PTX and the culture medium used was F12 supplemented as described above. The toxicity evaluation was performed by CCK8 assay according to the protocol. Briefly, 15 µl of the CCK 8 kit was added to each well. Plates were shaken and incubated for 3 h at 37◦C. The absorbance was measured using a plate reader at a wavelength of 492 nm. The inhibitory concentration 50 (IC_{50}) values were calculated from dose-response curves by linear interpolation. All of the experiments, plated in triplicate wells, were carried out at least three times.

11. Dual GFP-NanoLuc LVs Production.

The SELWP is a self-inactivated (SIN) LV expressing GFP-2A-NanoLuc under the control of an internal spleen focus-forming virus (SFFV) promoter. SELWP was generated previously (Tristán-Manzano et al, unpublished) based on the SEWP LV.[389] LV particles were generated by transient co-transfection of 293T cells using eGFP-NanoLuc vector plasmid together with the packaging plasmid pCMVDR8.91 (http://www.addgene.org/Didier_Trono) and the p-MD-G plasmid encoding the vesicular stomatitis virus (VSV-G) envelope gene (http://www.addgene.org/Didier_Trono). Vector production was performed as previously described.[390] Briefly, 293 T cells were planted on petri-dishes (Sarsted, Newton, NC), in order to unsure 80% of confluence for transfection. The vectors, the packaging and envelope plasmid (in proportion 3-2-1) were resuspended in 45 µl of LipoD293 (SignaGen, Gainthersburg, MD, USA). The plasmid-LipoD293 mixture was added to pre-washed cells and incubated for 6–8 h. After 48 hours viral supernatants were collected, filtered through 0.45 µm filter (Nalgen, Rochester, NY), aliquoted, and storage at -80ºC. Viral titers were determined by transducing 293T cells with different volumes of supernatant. The percentage of $eGFP^+$ cells was determined by flow cytometry 72h later and transducing units per ml (TU/ml) were estimated according to the formula: [(105plated cells ×% GFP^+ cells) ×1000]/µl of LVs.

12. BxPC-3 Cells Transduction.

100 000 BxPC-3 PCCs were seeded in a 24-well plate and incubated with SELWP LV supernatant at a Multiplicity of Infection (MOI) of 3 during 5h at 37ºC and 5%CO_2. eGFP expression was determined by flow cytometry (FACS Canto II, Becton Dickinson, New Jersey, US) at 72h after transduction. Additionally, cells were stained with anti-CD44-APC and CXCR4-PE for 20 min at room temperature.

13. In vivo Assay for Targeted PCSCs.

All in vivo experiments were performed in male NOD scid gamma mice (NSG, NOD. Cg-Prkdcscid Il2rgtm1Wjl/SzJ). Animal welfare and experimental procedures were carried out in accordance with institutional (Research Ethics Committee of the University of Granada, Spain) and international standards (European Communities Council directive 86/609). All animals (n= 5 per group) were maintained in a micro-

ventilated cage system with a 12h light/dark cycle, and they were manipulated in a laminar air-flow cabinet to keep to the specific pathogen-free conditions. To establish orthotopic xenograft tumors, six- to eight-week old male mice were used. Mice were anesthetized by intraperitoneal administration of ketamine (4 mg/kg) and midazolam (80 mg/kg), we performed a medial laparotomy from the xiphoid appendix to the lower left third of the abdomen. The retrogastric space was accessed and the tumors were generated into the tail of the pancreas by injections of 2×10^5 BxPC-3-SELWP PCSCs/mouse mixed with Corning ®Matrigel® Matrix and using 26-gauge needles. Then, the mice were sewn with 5/0 thread and administered analgesics and antibiotics. Once the generated tumor had a size of around 0.5 cm^3, intravenous administration in the vein tail of the mice of 100µl of PBS, O^2LNC-i780 and αCD44-O^2LNC-i780 was performed in a single dose and then the mice were evaluated by IVIS® (Perkin Elmer). The mice were left for a week in order to eliminate the O^2LNCs that were not specifically bound to the tumor tissue. During that week, the bioluminescence with a previous intraperitoneal administration of NanoGlo substrate (Promega) in PBS and the fluorescence of the mice was analyzed in the IVIS® on three alternate days. Finally, mice were euthanized by cervical dislocation and tumors and organs were excised, photographed and analyzed by IVIS®.

14. Statistical analysis

The data are presented as the mean ± the standard deviation in the error bars. The sample size (n) indicates the experimental repeats of a single representative experiment, with 3 being unless otherwise specified. The results of the experiments were validated by independent repetitions. Graphs and statistical difference data were made with GraphPad Prism 6.0 (Graphpad software Inc.). Statistical significance was determined using Student's t-test in paired groups of samples with known median A p-value of ≤ 0.01 was considered significant.

RESULTS

RESULTS

1. Preparation and Physico-Chemical Characterization of Nanocapsules and Immuno-Nanocapsules.

1.1. Preparation of Nanocapsules.

O^2LNC were prepared by using a modified protocol based on the solvent-displacement technique reported by Calvo et al.[387] Briefly, it consists of the formation of a nanoemulsion by incorporating, with a high mechanical force, an organic phase into an aqueous phase under stirring. This produces a nanoemulsion of a certain size due to the addition of a defined amount of olive oil to the organic phase (**Figure 42**).

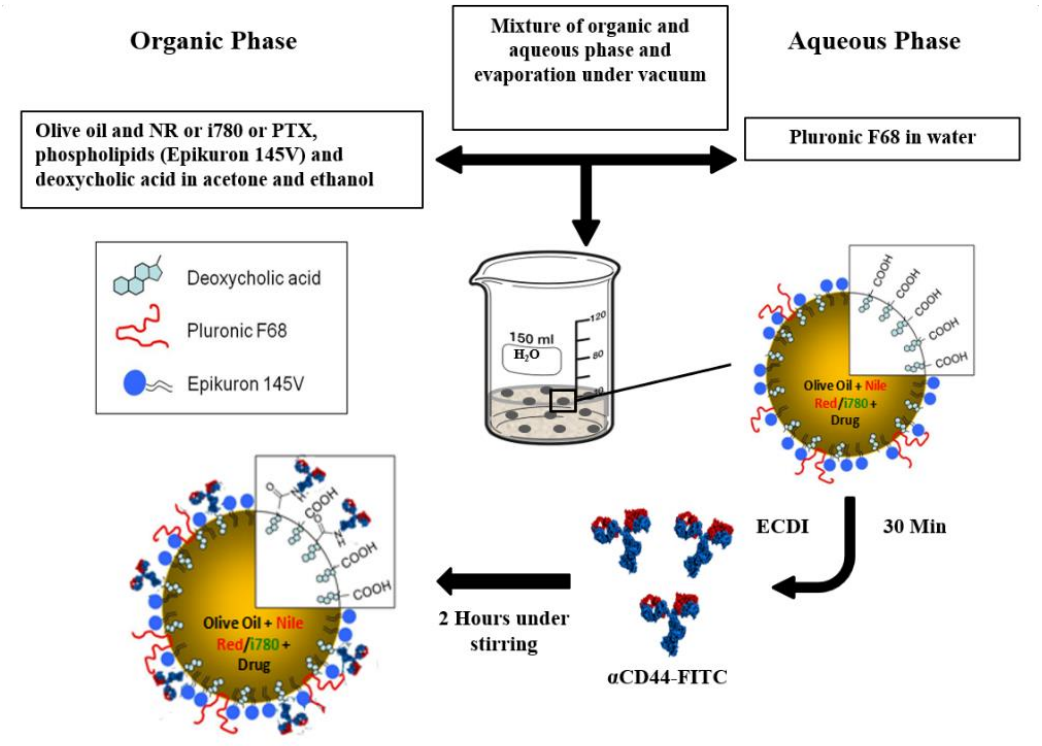

Figure 42: Scheme of synthesis and functionalization of O^2LNC and αCD44-O^2LNC.

1.2. Particle Size and Stability Over Time.

The synthesis method produced a homogeneous population of O^2LNC with an average diameter of around 111 ± 18 nm and a polydispersity index (PDI) of around 0.10 ± 0.02. Additionally, it is important to remark that the size reduction does not affect the

colloidal stability of the sample and the O^2LNC size remained at a constant value under storage conditions, i.e. pure water or phosphate buffer (PB) and 4 °C for at least 4 months. Each week for at least 4 months, the size and PDI of the same O^2LNC samples were analyzed, obtaining a similar size to those taken after synthesis (data not shown).

1.3 Chemical Characterization of O^2LNC by Nuclear Magnetic Resonance Spectroscopy.

Various Nuclear Magnetic Resonance (NMR) spectroscopy experiments were performed in order to verify that all the components used in the synthesis of the O^2LNC were integrated in the nanocapsule entities comprising the colloidal nanoemulsion solution. Before analysis, O^2LNC was further cleaned by centrifugation in Vivaspin 20® tubes with a pore size membrane of 300 KDa to ensure an essentially complete elimination of the organic solvents (ethanol and acetone) employed in their synthesis. The 1H NMR spectrum of intact O^2LNC (**see Annexes, S.I. Chapter 3. Figure S9 and S10**), diluted to a final 13 % content of D_2O, is clearly dominated by the signals of the olive oil core of the O^2LNC, as can clearly be seen by direct comparison with the NMR spectrum of olive oil in $CDCl_3$ (**see Annexes, S.I. Chapter 1. Figure S11**). The observation of olive oil signals NMR in an aqueous sample provides, by itself, direct evidence of the naonoemulsion nature of the sample since olive oil is completely immiscible with water. On the other hand, the linewidth of the observed olive oil signals in the O^2LNC sample is much broader than the linewidth of olive oil signals in $CDCl_3$. This feature is partially the consequence of the higher viscosity of the nanoemulsion but, more importantly, is the result of a reduced transverse relaxation time (T2) product of a much slower tumbling rate of the triglyceride molecules of olive oil, when confined in the nanoparticle core, compared to the tumbling of the same molecules when freely dissolved in $CDCl_3$.[391]

Additionally, and as final evidence, qualitative diffusion NMR experiments proved that the olive oil signals do not diffuse at the expected rate for free triglyceride molecules in solution but rather at a very slow rate, only compatible with a nanometer-size entity[391] (**see Annexes, S.I. Chapter 1. Figure S12**). Once again this is a consequence of the confinement of olive oil in the core of the O^2LNC. Regarding the other chemical constituents of the O^2LNC, only the signals from the surfactant Pluronic F-68 could be observed in the 1H NMR spectrum of intact O^2LNC (**see Annexes, S.I. Chapter 1. Figure S12**), while no signals related to Epikuron or deoxycholic acid are detected in the

spectrum. These three components (surfactant, phospholipid and deoxycholic acid) comprise the shell of the O^2LNC and as such conform to a rather rigid supramolecular structure expected to display a very short T2 broadening the corresponding NMR signals beyond detection. The fact that the signals of the oligomeric surfactant Pluronic F-68 can still be observed is a consequence of the inherent flexibility of the part of these molecules not rigidly embedded in the O^2LNC shell but rather exposed to the bulk water.

To further demonstrate the chemical nature of the components integrated in the O^2LNC, these were disintegrated by dilution with isopropanol and sonication. After the disintegration of the O^2LNC, the sample was split into two aliquots which were concentrated to dryness and resuspended, one in $CDCl_3$ and the other in CD_3OD for 1H NMR analyses. Comparison with the corresponding reference spectra of olive oil, Pluronic F-68, Epikuron and deoxycholic acid acquired in these two solvents unambiguously demonstrated the presence of these components in the original O^2LNC sample (**see Annexes, S.I. Chapter 1. Figure S13-23**).

1.4. Synthesis of the Olive Oil Immuno-Nanocapsules.

In order to produce the immuno-NCs, a defined amount of anti-CD44-FITC (αCD44) antibody equal to 0.18 mg/m2 was initially incubated with the O^2LNC. This amount of antibody, corresponding to a low coverage degree, was used due to the limited protein concentration commercially available. The covalent coupling was developed by means of the ECDI procedure, described in detail in the experimental section. **Figure 43A** shows a schematic representation of the coupling process to produce the immuno-O^2LNC after incubation time, the αCD44-O^2LNC complex was separated from unbound protein by a dialysis procedure. The size of the formulation (αCD44-O^2LNC) with the initial theoretical antibody coverage (low) at pH7.4 and low-ionic-strength medium remained similar to those of the original O^2LNC-systems. A protein quantification analysis of the dialysis elution volumes did not detect any presence of antibody molecules, which means a total coupling of the initial antibody amount. The presence of IgG on the αCD44-O^2LNC surface was estimated by SDS gel chromatography under reducing conditions that confirmed the immobilization of the antibody on the O^2LNC surface. As shown in **Figure 43A**, the intensity of the band

corresponding to αCD44-O²LNC (lane 2) was similar to that of a free αCD44 antibody (lane 1).

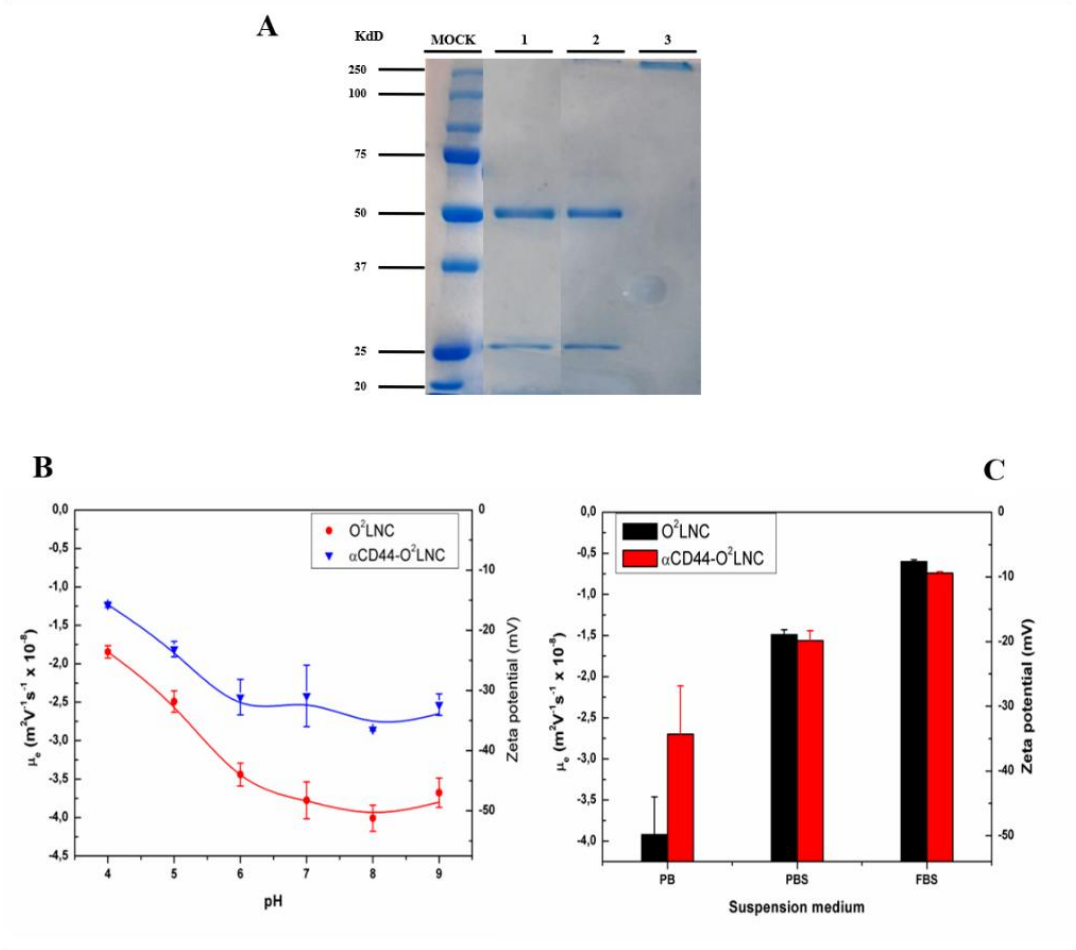

Figure 43: Physico-chemical characterization of O²LNC and αCD44-O²LNC. A) SDS-PAGE of αCD44 (lane 1), αCD44-O²LNC (lane 2) and bare O²LNC (lane 3). B) Electrophoretic mobility and Z potential of O²LNC and αCD44-O²LNC in a pH range from 4 to 9. C) Electrophoretic mobility and Z potential of O²LNC and αCD44-O²LNC incubated in phosphate buffer at pH 7.4 (PB), phosphate buffered saline (PBS) and RPMI culture medium supplemented with 10% Fetal Bovine Serum (FBS).

1.5. Electrophoretic Mobility

Electrophoretic mobility, μ_e, is an experimental parameter directly related to the zeta potential in the shear plane of the particles and it is normally used to obtain information concerning the surface electrical state of colloidal systems.[392,393] μ_e was

determined in low-ionic-strength media at different pH values from 4.0 to 9.0 (**Figure 43B**). Nevertheless, the most important aspects of the μ_e results are related to the presence of IgG molecules immobilized onto the αCD44-O^2LNC surface, which significantly alter the mobility data and indicate a clear correspondence with the adhered antibody and its isoelectric point[394] (IEP) (**Figure 43B**). The Z potential of the O^2LNC and αCD44-O^2LNC measured at pH 7.4 was around -50 and -35 mV respectively (**Figure 43B**). This fact demonstrates that the covalent binding of the αCD44 antibody was carried out satisfactorily and positive antibody molecules at acid pH partially screen the negative surface charge of the O^2LNC, reducing the absolute Z potential values under the IEP of protein.

On the other hand, colloidal stability of delivery nanosystems in physiological media is crucial to successfully achieve their biological applications. As can be observed in **Figure 43B**, O^2LNC and αCD44-O^2LNC have electrokinetic behavior in mediums with low ionic strength, from neutral to basic pH, without variations in the negative surface charge. Thus, the size for both O^2LNC and αCD44-O^2LNC nanosystems remained constant throughout this pH range.

Table 4: Size and PDI of O^2LNC and αCD44-O^2LNC incubated with different mediums.

	O^2LNC-PB	αCD44-O^2LNC-PB	O^2LNC-PBS	αCD44-O^2LNC-PBS	O^2LNC-FBS	αCD44-O^2LNC-FBS
Size (nm)	110±20	110±20	110±20	110±20	120±10	110±20
PDI	0.10±0.02	0.09±0.01	0.15±0.01	0.16±0.01	0.19±0.04	0.25±0.01

Additionally, the colloidal stability was checked in mediums for physiological conditions. Therefore, electrokinetic parameters, hydrodynamic size, and PDI, were measured for O^2LNCand αCD44-O^2LNC by incubating them in physiological medium (PBS) and in cell culture medium (FBS) (RPMI supplemented with 10% FBS). When both nanosystems were in contact with PBS and FBS, the Z potential decreased their negative absolute values (**Figure 43C**) as a consequence of the salinity of the medium (150 mM),

which could mean the aggregation of the NCs. However, as can be seen in **Table 4**, neither NCs did change their sizes and both remained stable in these media. Furthermore, both NC systems also keep a narrow size distribution (PDI ≤ 0.2).

2. In vitro Cellular Uptake of Immuno-Nanocapsules.

The cellular uptake of both O^2LNCs and αCD44-O^2LNCs was investigated on BxPC-3 PCCs growing in monolayer (low expression of CD44) and on BxPC-3 PCSCs secondary spheres (high expression of CD44) by both confocal microscopy and flow cytometry. O^2LNCs were labeled with Nile Red (NR) to investigate the cellular entry of our nanosystems. First, we performed a characterization of the expression levels of CD44 and CXCR4 markers in our tumor cell line ((monolayer and PCSCs) **(Figure 44A**)) as well as the determination of the ALDH1 enzymatic activity. The expression percentages obtained were 6,6%, 16,7% and 68,7% in monolayer and 50,3%, 97,8% and 86,4% in secondary spheres for ALDH1, CD44 and CXCR4 respectively (**Figures 44B and 44C**).

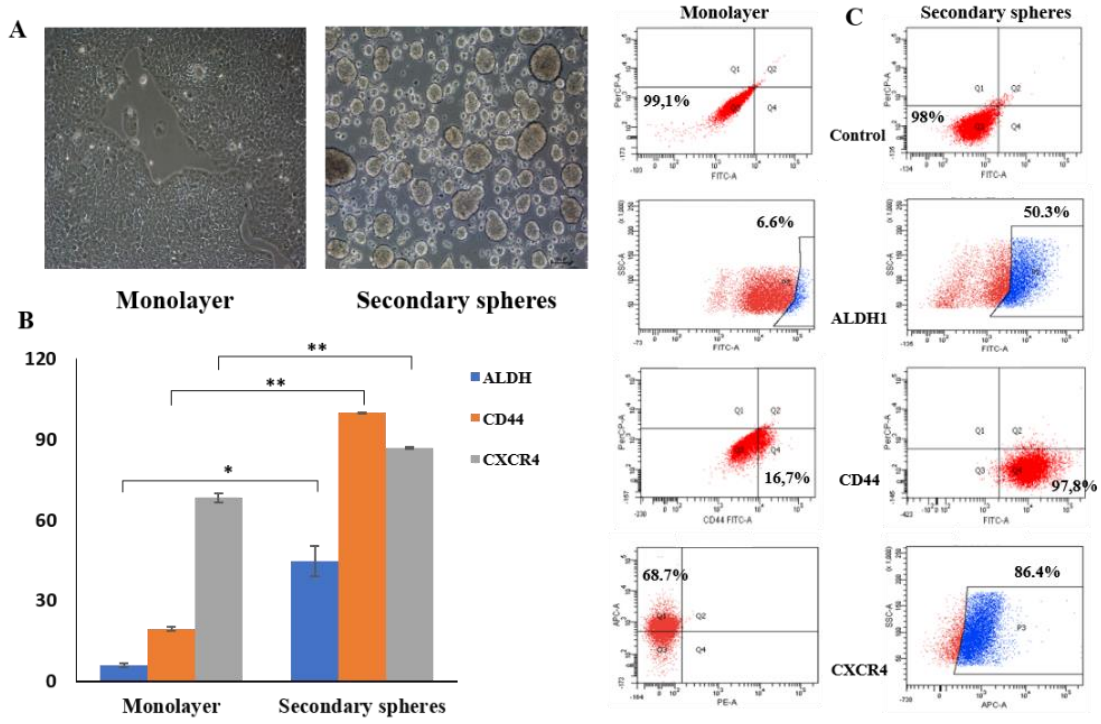

Figure 44: Characterization of BxPC-3 PCCs and PCSCs. A) Representative images of BxPC-3 PCCs (monolayer) and BxPC-3 PCSCs (secondary spheres). B) ALDH1 activity, CD44 and CXCR4 surface expression in monolayer and secondary spheres cell cultures. Data are graphed as

mean ± SEM and the significant values are calculated using t-test. (*p<0.01; **p<0.001). C) Representative DOT PLOTS of BxPC-3 PCCs and PCSCs analysed by flow cytometry.

In addition, a flow cytometry assay was performed to quantitatively evaluate the uptake of our O^2LNC-based nanosystems in the two BxPC-3 PC cell populations. The analysis showed the differential uptake efficiency for NR-O^2LNCs in monolayer BxPC-3 PCCs and BxPC-3 PCSCs subpopulation depending on whether they were functionalized or not with the αCD44 antibody. Moreover, since there were differences in the expression levels of CD44 membrane receptor for both PC cell populations we also found a different behavior for each type of nanosystem. Thus, only around 17% of PCCs growing in monolayer were positive for CD44, and almost all the PCSCs (about 98%) overexpressed this specific surface antigen (**Figure 44C**). However, most bare NR-O^2LNCs entered into both monolayer PCCs and PCSCs regardless of their CD44 expression level (**Figure 45A and 45B**). In contrast, for NR-αCD44-O^2LNCs the entry was dependent on the CD44 expression in the membrane of the PC cells, with uptake values in PCSCs around 80%, 86% and 85% at 15, 30 and 60 min respectively and only around 5% in PCCs growing in monolayer (**Figure 45A and 45B**).

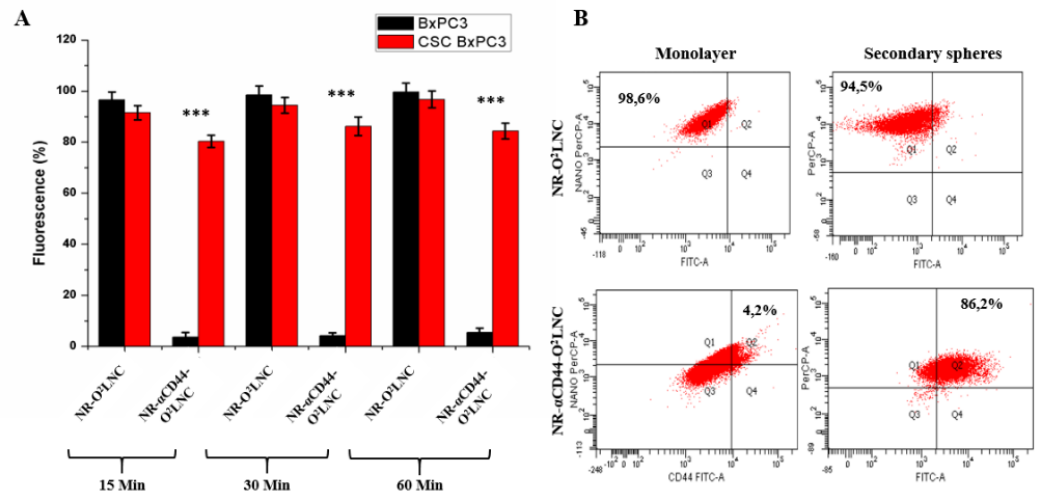

Figure 45: In vitro uptake of O^2LNCs and αCD44-O^2LNCs in BxPC-3 PCCs and PCSCs by flow cytometry. A) Uptake of NR-O^2LNCs and NR-αCD44-O^2LNCs in BxPC-3 PCCs and BxPC-3 PCSCs analyzed by flow cytometry. Data are mean values ± SEM. *** p < 0.001 shows the significant

values calculated using t-test. B) Representative DOT PLOTS of NR-O^2LNCs and NR-αCD44-O^2LNCs uptake in BxPC-3 PCCs and BxPC-3 PCSCs at 30 minutes analyzed by flow cytometry.

Confocal microscopy images show how NR-O^2LNCs enter into both types of cell populations after 3 hours of accumulating NR in the cytoplasm (**Figure 46**). In the case of NR-αCD44-O^2LNCs, where CD44 was labeled with FITC, we observed the specific recognition of CD44 membrane receptors by these NCs and the release into the cells of NR after 3 hours of incubation (**Figure 46**). We incubated the cells with our O^2LNC-based nanosystems for 3 hours, because it was the optimal time to visualize the fluorescence by confocal microscopy.

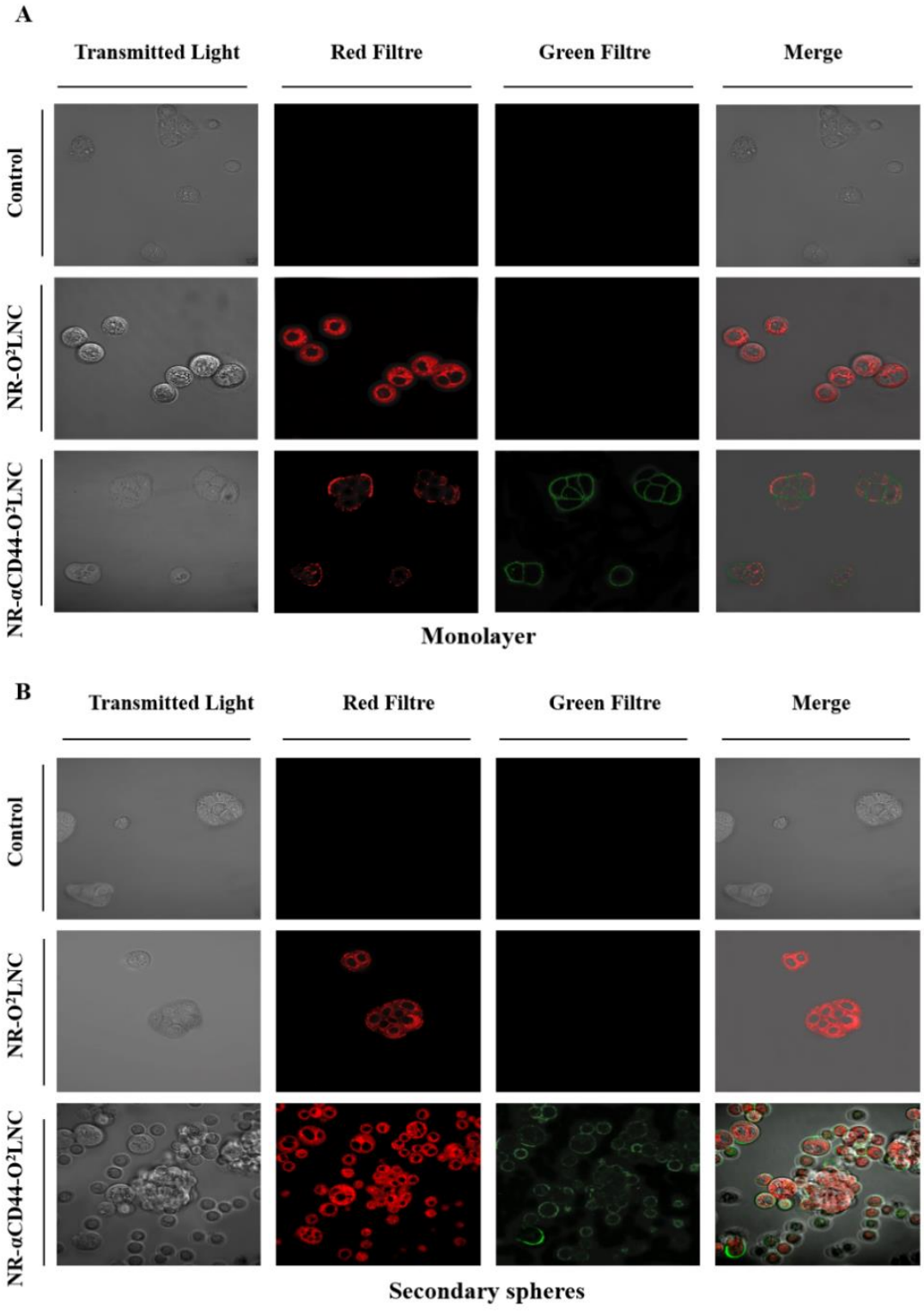
A
Transmitted Light
Red Filtre
Green Filtre
Merge
Control
NR-O²LNC
NR-aCD44-O²LNC
Monolayer
B
Transmitted Light
Red Filtre
Green Filtre
Merge
Control
NR-O²LNC
NR-aCD44-O²LNC
Secondary spheres

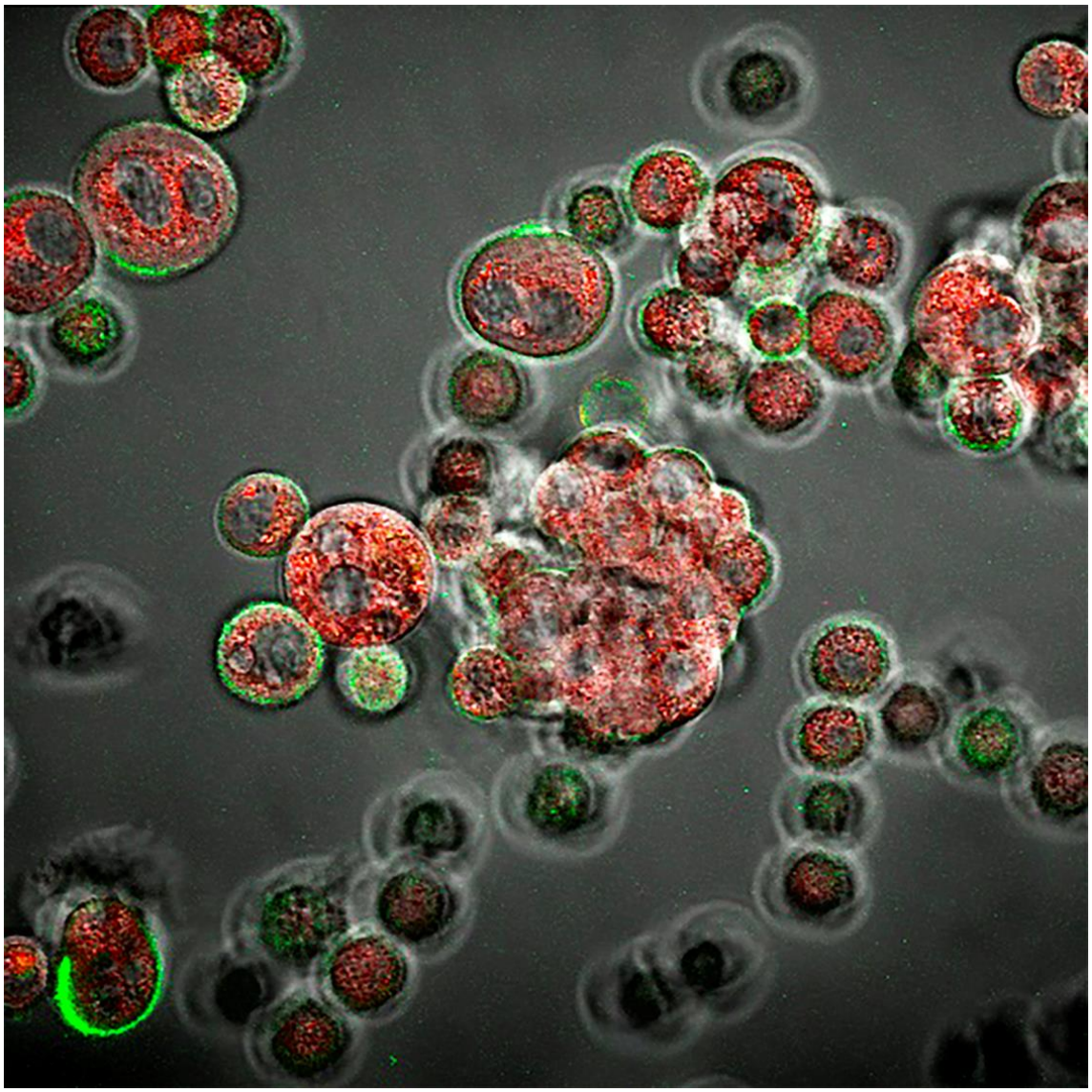

Figure 46: In vitro uptake of O^2LNCs and αCD44-O^2LNCs in BxPC-3 PCCs and PCSCs by confocal microscopy. A-B) Confocal microscopy of BxPC-3 PCCs (monolayer) and BxPC-3 PCSCs (secondary spheres) respectively (scale bar =10µm) incubated 3 hours with NR-O^2LNCs and NR-αCD44-O^2LNCs respectively. Bare O^2LNCs were used as control.

3. Drug loading and encapsulation efficiency

Drug loading (DL) and encapsulation efficiency (EE) were calculated to know whether O^2LNCs are good drug delivery vehicle nanosystems. In order to quantify these parameters, a defined amount of paclitaxel (PTX) was dissolved in the olive oil and the synthesis of the O^2LNC-PTX and αCD44-O^2LNC-PTX was performed. Then, the real amount of PTX inside the NCs measured by MS showed that our NCs had 2.2% of DL and

81.1% of EE. In addition, a 4-week test was conducted to observe the amount of PTX remaining within our O^2LNCs before and after they undergo the covalence process with the αCD44 antibody (**details in the methodology section**). In this way, at time 0 the real amount of PTX within the O^2LNC oily core was around 80% and after the covalence process this amount was reduced to around 40% (**Figure 47**).This decrease is due to the loss of PTX during the stirring of the covalence protocol and in the number of O^2LNCs during the dialysis process by centrifugation in Vivaspin 20 tubes. It should be noted that as the weeks progress, the amount of PTX in both types of O^2LNC remains practically constant, with a difference of 10% between week 0 and week 4 (**Figure 47**).

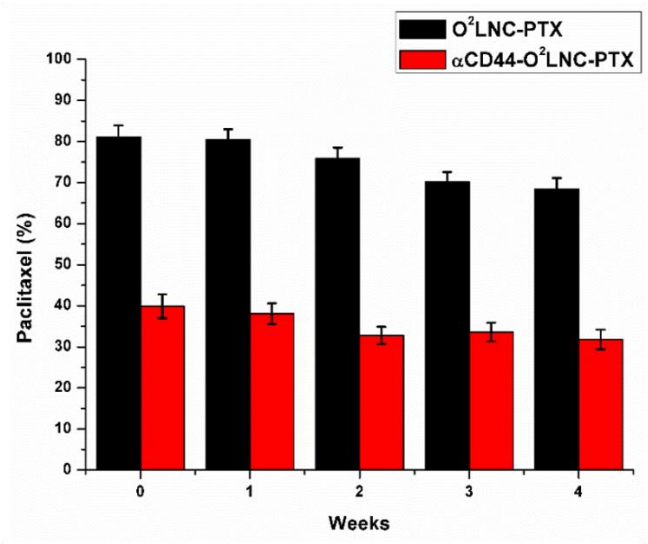

Figure 47: Graphical representation of the amount of paclitaxel (%) remained within O^2LNC-PTX and αCD44-O^2LNC-PTX during 4 weeks.

4. In vitro antitumor cytotoxicity of paclitaxel-loaded O^2LNC and αCD44-O^2LNC.

A cell viability assay was assessed to check the improvement of the antitumor activity of PTX by our functionalized O^2LNCs against differentiated PCCs and PCSCs. This test was performed comparing the effects of free PTX, O^2LNC-PTX or αCD44-O^2LNC-PTX. Results showed that free PTX displayed significant differential antitumor potency depending on the PC cell population (**Figure 48A and 48B**). Thus, in BxPC-3 adherent PCCs the IC_{50} of free PTX was 1.7 nM; however, in BxPC-3 PCSCs the IC_{50} value was 133.4 nM (**Figure 48A**). Moreover, we observed that in monolayer BxPC-3 PCCs, neither O^2LNC-PTX nor αCD44-O^2LNC-PTX improved their antitumor effect but instead increased

their IC_{50} slightly (**Figure 48A**). In contrast, although the O^2LNC-PTX in the population of PCSCs very slightly reduced the IC_{50} value to 113.8 nM; however, αCD44-O^2LNC-PTXs were able to reduce the IC_{50} down to 34.2 nM (**Figure 48A**). The increased potency of up to 4 times of αCD44-O^2LNC-PTX on PCSCs in comparison to free PTX, and up to 3.3 times with respect to O^2LNC-PTX, indicate the targeted activity against PCSCs overexpressing CD44, which facilitates the internalizing, favoring the bioavailability and cytotoxic effect of PTX. Additionally, in **Figure 48C** we can see the cytotoxic effect of free PTX, O^2LNC-PTX and αCD44-O^2LNC-PTX in monolayer BxPC-3 PCCs and in secondary sphere BxPC-3 PCSCs.

A

	IC_{50} (nM) BxPC3	IC_{50} (nM) BxPC-3 P-CSC
PTX	1.7 ± 0.2	133.4 ± 0.3
O^2LNC-PTX	4.3 ± 0.1	113.8 ± 0.3
αCD44-O^2LNC-PTX	3.8 ± 0.2	34.2 ± 0.4

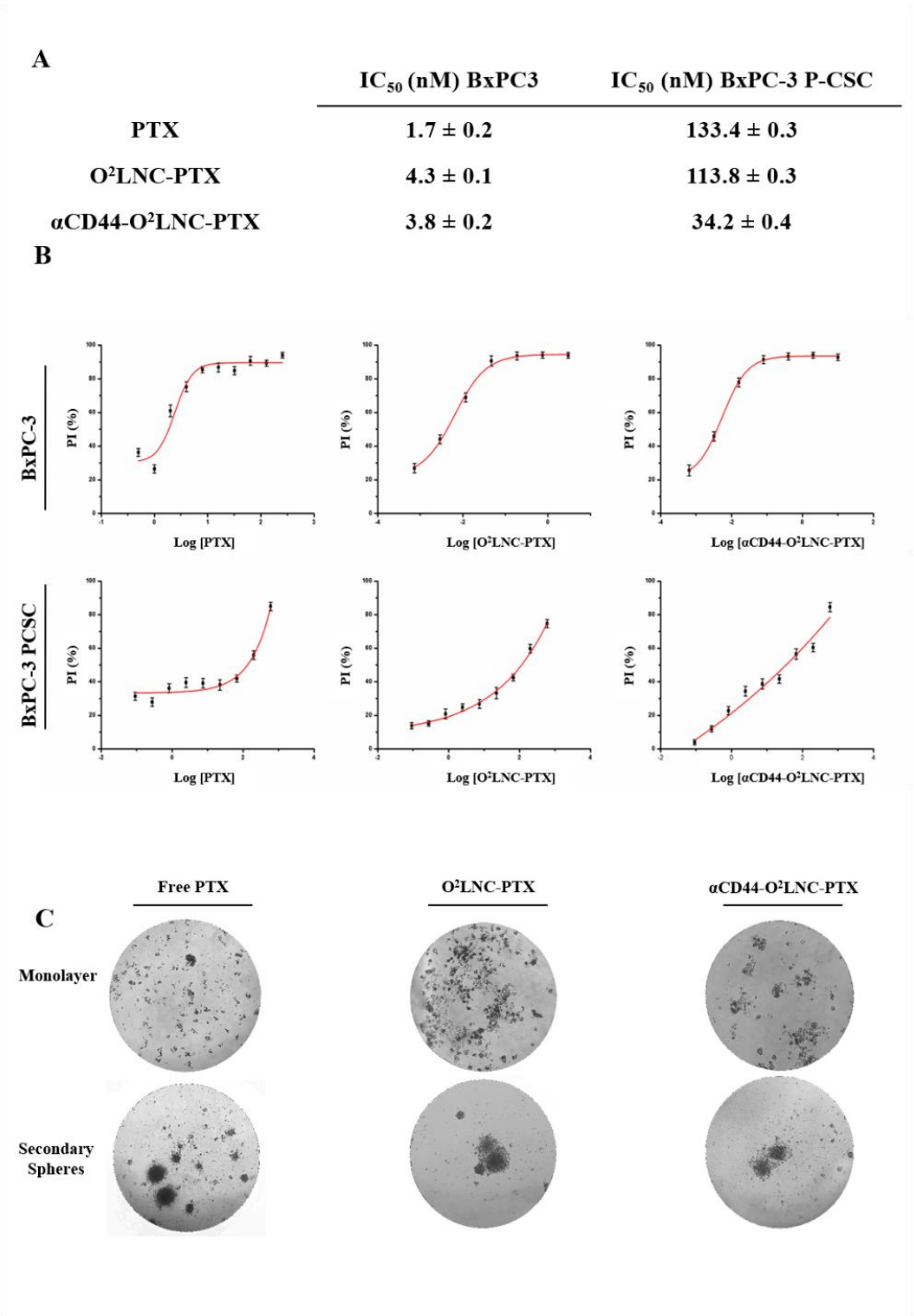

Figure 48: Cytotoxic effect of free PTX, O^2LNC-PTX and αCD44-O^2LNC-PTX on BxPC-3 PCCs and PCSCs. A) Half maximal inhibitory concentration (IC_{50}) values of free PTX, O^2LNC-PTX and αCD44-O^2LNC-PTX on BxPC-3 PCCs and PCSCs. B) Graphical representation of IC_{50} of free PTX, O^2LNC-PTX and αCD44-O^2LNC-PTX on BxPC-3 PCCs and PCSCs. C) Representative images of the cytotoxic effect of free PTX, O^2LNC-PTX and αCD44-O^2LNC-PTX on BxPC-3 monolayer PCCs and PCSCs taken by optical microscopy.

5. Luminescence Stable modification of BxPC-3 cancer cells for in vivo monitoring of αCD44-O^{2}LNC-targeted efficacy.

There is a need to create clinically relevant models for studying treatments directed against PC in established human PC orthotopic xenografts by the visualization of tumor growth in early stages and tracking tumor behavior and progression Thus, our aim was to generate a stable cell model that would allow monitoring pancreatic tumor growth in vivo and the characterization of potential phenotypic changes on the tumor cells. We produced lentiviral vector (LV) particles using the SELWPLV (Tristán-Manzano et al, unpublished) that allow both in vitro and in vivo monitoring of transduced cells by flow cytometry (eGFP) and bioluminescence imaging (NanoLuc) respectively (**Figure 49A**). BxPC-3 PCCs were transduced with SEWLP LVs at a multiplicity of infection (MOI) of 3, to generate BxPC-3-SELWP cell lines expressing both eGFP and NanoLuc. Inoculation of BxPC-3-SELWP in the left flank of immune-deficient NSG mice allowed the in vivo monitoring of tumor growth (**Figure 49 B-D**). We observed increased bioluminescence along time that correlates with tumor size by tumor palpation (data not shown). The analysis of BxPC3-SELWP cells after disaggregation of the tumors generated in the transplanted mice showing stable eGFP expression (**Figure 49E and 49F**), allowing the study of potential changes in the BxPC-3-SELWP phenotype after tumor generation. Interestingly, the expression of eGFP and NanoLuc in BxPC-3-SELWP cells did not significantly alter the expression pattern of both CD44 and CXCR4 PCSC markers (**Figure 49G**).

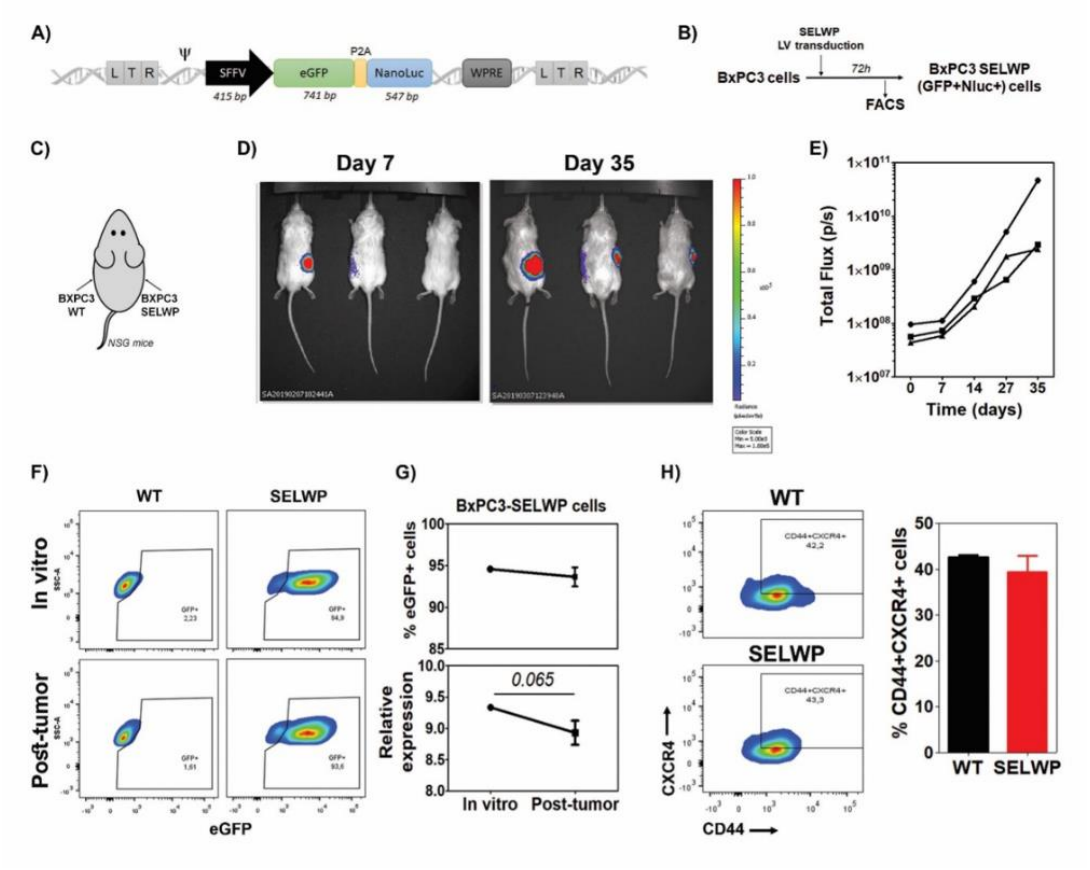

Figure 49: BxPC-3 cells efficiently transduced with SELWP constitute a valid model for monitoring tumor growth in vitro and in vivo. A) Representation of the SELWP LV encoding enhanced GFP and NanoLuc under SFFV promoter in a self-inactivated LV backbone. B) Scheme showing the procedure to generate BxPC-3-eGFP$^+$/NanoLuc$^+$ cells (BxPC-3-SELWP). C) Scheme indicating the injection site of BxPC-3-WT and BxPC-3-SELWP to monitor tumor growth. 300 000 cells in PBS were mixed with Matrigel (proportion 1:1) and inoculated in the left (BxPC-3-WT) and right (BxPC-3-SELWP) flank of 16-week-old NSG mice. D) Representative images of IVIS bioluminescence acquired at days 7 and 35 post-inoculation after the administration of NanoGlo substrate intraperitoneally. E) Total photon flux analysis along time. F) Representative plots showing eGFP expression in BxPC-3-WT (left plots) and BxPC-3-SELWP cells (right plots), before (top plots) and after (bottom plots) transplantation into mice for tumor generation. G) Graph showing percentage (top) and relative expression levels (bottom) of eGFP$^+$ before (In vitro) and after (Post-tumor) transplantation into mice. Relative expression was calculated as the Median of FITC intensity of transduced eGFP$^+$ cells / Median of FITC intensity of non-transduced population. No significant P value, Paired T-test, two tails. H) Representative plots (right) and graph showing the percentage of CD44$^+$CXCR4$^+$ BxPC-3 cells isolated from WT and SELWP tumors (N=3). CD44 and CXCR4 expression was determined by flow cytometry 7 days after sacrifice. No significant P value, Paired T-test, two tails.

6. In vivo biodistribution and targeting assay.

In order to verify that our functionalized αCD44-O^{2}LNCs were specifically directed to the tumor area, an in vivo assay was performed. In this experiment, an orthotopic xenotransplant was performed in the pancreas of the mice and the tumor was generated as described64 but with a modification in the protocol by implanting PCSCs instead of patient tumor samples. BxPC-3 PCSCs transduced with the SELWP LVs were used to generate the tumor and the αCD44-O^{2}LNCs were loaded with IR 780-iodide dye dissolved in the oily core. We choose this dye because it emits in the near infrared and can be easily detected by the in vivo imaging systems (IVIS®), also avoiding background noise caused by the mouse's own auto-florescence.[395] When tumors reached a size of 0.5 cm^3, 100 µl of O^{2}LNC-i780 and αCD44-O^{2}LNC-i780 were administered in the tail vein of the mice in a single dose. After one week, the mice were analyzed, euthanized and the tumors were removed as well as all the organs. As shown in **Figure 50A**, 2×10^5 BxPC-3-SELWP PCSCs were able to engraft in the pancreases of mice only two weeks after inoculation and the growth was easily monitored by bioluminescence (**Figure 50B**).

In addition, we were able to detect micrometastatic sites in organs close to the pancreas, such as stomach, kidneys or spleen among others (**Figure 51, top panel**). An additional advantage of our dual vector is that the targeting properties of O^{2}LNC-i780 and αCD44-O^{2}LNC-i780 were also visualized by fluorescence in the same mice. As can be observed in Figure 50C, O^{2}LNC-i780 were distributed evenly throughout the mice one-week post-inoculation. On the contrary, although the αCD44-O^{2}LNC-i780 also showed a diffuse distribution in the mice, however, they were strongly accumulated in the tumor area (**Figure 50C**). This fact was confirmed in the excised PCSC tumors in concordance with the signal intensity emitted by eGFP in the tumors. (**Figure 50B and 50C, down panel**) as well as in the organs excised from the mice (**Figure 51**). For all this, here we show an enhanced targeting ability of our olive oil-based nanosystem on a PCSC orthotopic xenotransplant in vivo model.

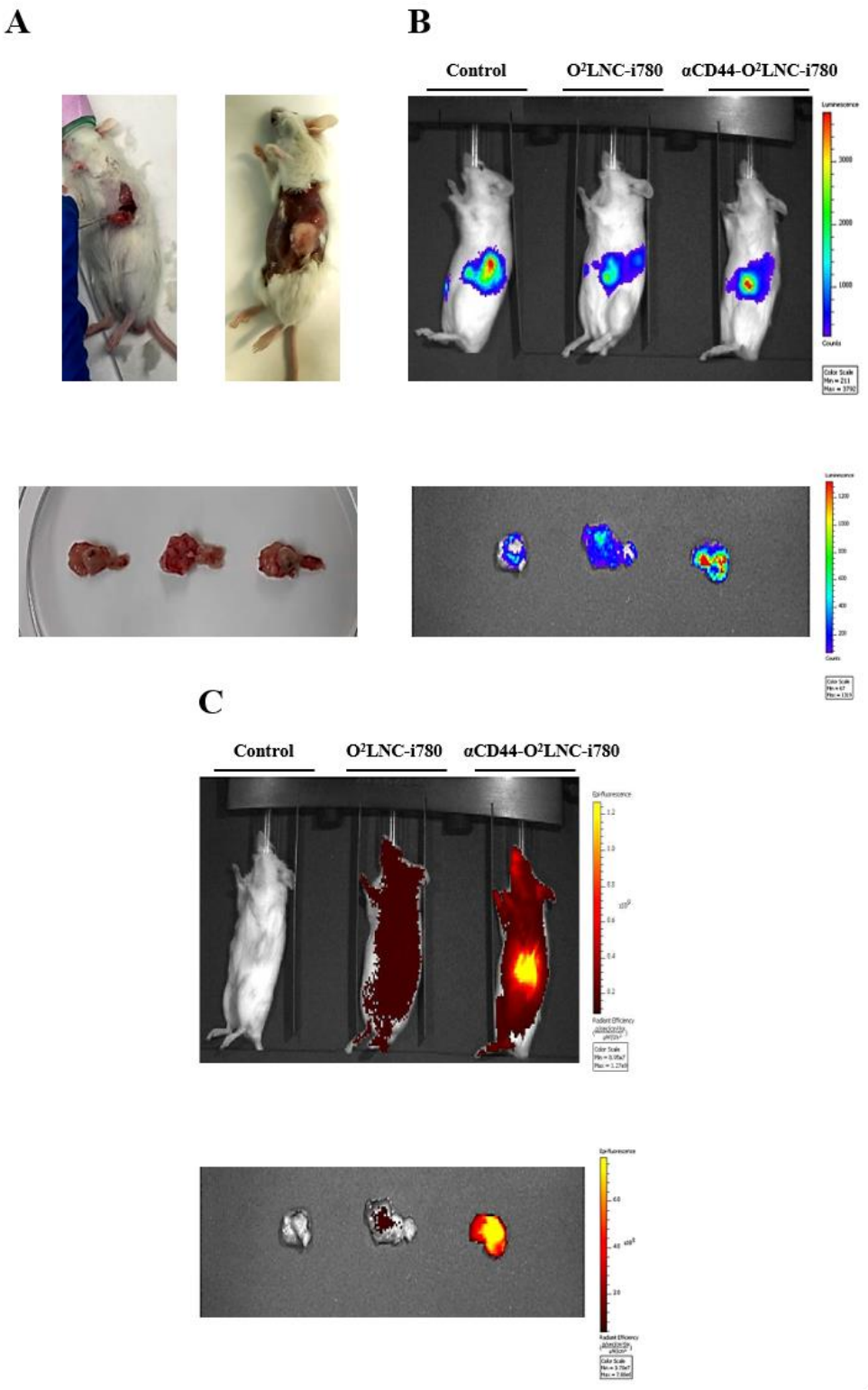

Figure 50: In vivo assay of O^2LNC-i780 and αCD44-O^2LNC-i780 targeting tumor. A) Representative images of the orthotopic xenograft pancreatic tumor generation inoculating the cells (left image) and once the tumor was generated (right image); and excised tumor ex vivo (bottom image). B) Representatives images of mice (top image) and tumors (bottom

image) with Nano-Luc measured by bioluminescence. C) Representatives images of mice and tumors treated with PBS, O^2LNC-i780 and αCD44-O^2LNC-i780 measured by fluorescence.

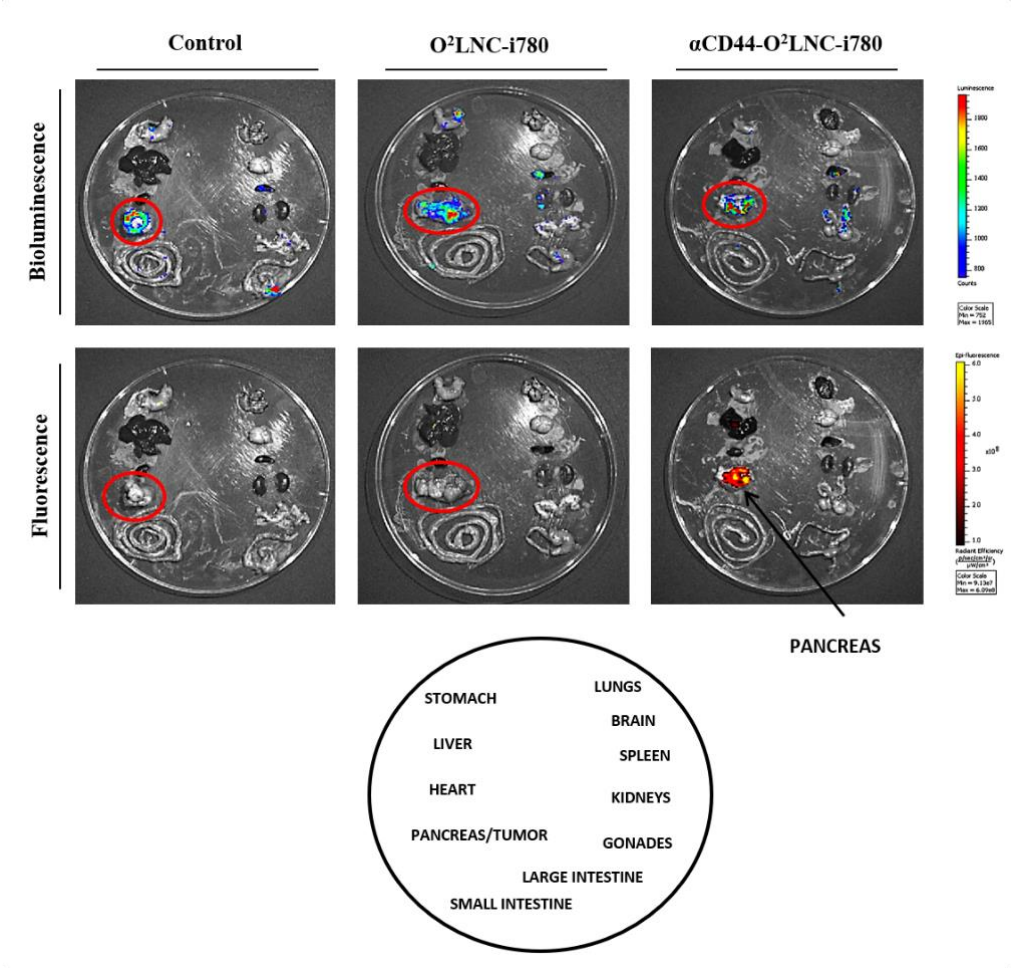

Figure 51: Representative images of the mice organs after treatment with PBS, O^2LNC-i780 and αCD44-O^2LNC-i780 measured by both bioluminescence and by fluorescence.

DISCUSSION

DISCUSION

In the present study, we have developed colloidally stable olive oil immune-nanocapsules (αCD44-O^2LNCs) for targeting PCSCs. The size of nanosystem was lower than those previously reported using a similar technique and similar shell components.[357] The size reduction is related to the increase of the mechanical energy applied when organic and aqueous phases are mixed. The use of high-speed homogenization to produce small particle sizes has already been reported.[396] Furthermore, the diameter of O^2LNC is optimal for *in vivo* applications where the size and size distribution is a decisive variable in ensuring adequate biodistribution by crossing biological barriers and minimizing the macrophage uptake.[397]

After obtaining the αCD44-O^2LNC-based nanosystem, no aggregation was observed during the experimental period, in spite of the well-established idea about the immobilization of antibody molecules on the surface of nanoparticles that strongly alters their surface properties, notably affecting the colloidal stability of the nanosystem. Although the surface antibody layers drive a change in the physico-chemical properties of the O^2LCN's original surface, the low coverage degree and the optimization of the medium conditions throughout the coupling process prevent O^2LCN aggregation.[357,398] The αCD44-O^2LNC complex was separated from unbound protein by a dialysis procedure, which is normally used when working with nanoemulsions and soft-particle systems,[399] and has previously shown their efficacy working with the same type of nanocapsules.[383] Gel electrophoresis shows a migration response typical for IgG antibodies, with two heavy and two light chains corresponding to an upper band at ∼50 kDa (for the Fc fragment) as well as a lower band at ∼25 kDa (for the Fab moieties). In previous studies carried out in our research group with similar type of NCs, the coupling-efficiency reached values of around 50−70% for the initial theoretical coverage of 2.5 mg/m^2.[357] Moreover, Goldstein, D. et al. showed low coupling efficiency when working with monoclonal antibodies and Fab' fragment on functionalized NCs as a consequence of the presence of PEG chains on the surface.[399] It is amply documented how the presence of PEO layers is frequently employed to reduce protein binding,[400,401] and the effect on the protein adsorption processes is clearly reflected by a reduction in the amount of adsorbed proteins mediated by the presence of surface poloxamer

molecules.[402] Nonetheless, we have optimized the methodology and have achieved a coupling of almost 100% of the antibody molecules to the surface of the O^2LNC using a very low protein coverage (0.18 mg/m2) rendering a stable nanoemulsion.

Electrophoretic mobility, μ_e, is an experimental parameter directly related to the zeta potential in the shear plane of the particles and it is normally used to obtain information concerning the surface electrical state of colloidal systems.[392,393] Thus, the μe data reflects the composition of the O^2LNC surface and is influenced by both the pH and the ionic strength of the dispersion medium. Usually, when colloidal particles are coated by protein molecules, the μ_e values change markedly compared to the same bare surfaces. In terms of the electrokinetic behavior of bare O^2LNC, the μe results were in agreement with the nature of the shell of these NCs in which carboxylic groups predominate on the surface, showing the typical behavior of colloids with weak acid groups, that is, constant μ_e values at basic and neutral pH values that begin to fall to acidic pH around the pKa (4.8).[398] Additionally, it is well-known that when a protein covers colloidal particles, the IEP of such complexes also depends on the degree of protein coverage, so that it gradually tends to the pure protein IEP when the protein load on the nanoparticles increases.[399,403] Our results demonstrate that the covalent binding of the αCD44 antibody was carried out satisfactorily and positive antibody molecules at acid pH partially screen the negative surface charge of the O^2LNC, reducing the absolute Z potential values under the IEP of protein.

On the other hand, colloidal stability of delivery nanosystems in physiological media is crucial to successfully achieve their biological applications. Our NCs have electrokinetic behavior in mediums with low ionic strength, from neutral to basic pH, without variations in the negative surface charge, which can be correlated to stable nanosystems due to an electrostatic repulsion mechanism.[404] Thus, the size for both O^2LNC and αCD44-O^2LNC nanosystems remained constant throughout this pH range. Additionally, the colloidal stability was checked in mediums for physiological conditions. Our NCs did not change their sizes and remaining stable in these media. Furthermore, both NC systems also keep a narrow size distribution (PDI ≤ 0.2). A stabilization mechanism mediated by hydration forces could be responsible of these results. This stabilization phenomenon is typical for hydrophilic colloidal systems at high salt

concentrations.[405] In our nanosystems, PEO chains from poloxamers and antibody molecules supply the hydrophilic character to the surface shell and this behavior has been previously revealed by NCs with similar shell composition[406,407] in complex mediums with different electrolytes.

The cellular uptake of both O^2LNC and αCD44-O^2LNC was investigated on BxPC-3 PCCs growing in monolayer (low expression of CD44) and on BxPC-3 PCSC secondary spheres (high expression of CD44) by both confocal microscopy and flow cytometry. It is well known that the levels of CD44 expression in BxPC3 PCSCs are much higher than in their tumor counterpart.[408–410] First, we performed a characterization of the expression levels of CD44 and CXCR4 markers in our tumor cell line (monolayer and PCSCs) as well as the determination of the ALDH1 enzymatic activity. The overexpression of these markers, as well as the increase in ALDH1 enzymatic activity, is an indication that tumor cells have stem properties.[386] The expression percentages obtained were satisfactory and can thus conclude that a population of BxPC-3 PCSCs obtained was valid for the study. The results obtained from confocal microscopy and flow cytometry are in concordance with previous studies showing targeted killing of PCSCs overexpressing CD44 surface marker by NCs functionalized with hyaluronic acid (HA), the most common and immediate ligand for CD44.[411,412] Then, we can confirm that our αCD44-O^2LNCs were able to selectively bind to CD44 receptors releasing their content inside the PCSCs. It is worth highlighting the high uptake efficiency of NR-αCD44-O^2LNC in the BxPC3 PCSCs as opposed to the more differentiated tumor and attached cell population. Recently, Trabulo et al. published a study where they covalently attached an anti-CD47 antibody to the surface of iron oxide nanoparticles for the recognition of this membrane receptor overexpressed in PCSCs, obtaining very similar results to those described in this study.[413] Moreover, since the interaction of HA and CD44 promotes EGFR-mediated pathways, consequently leading to tumor cell growth, tumor cell migration, and chemotherapy resistance in solid cancers,[414] the ability of our O^2LNC functionalized with αCD44 antibody could bind and neutralize the receptor by competitive inhibition of its HA-ligand and consequently prevent the receptor-signaling cascade activation. All this makes our nanosystem a good candidate for targeted therapy against PCSCs.

In the cell viability assay, the difference of the effect of free PTX between BxPC-3 PCCs and PCSCs is due to the fact that PTX has a very high efficacy on differentiated and replicative tumor cells[415], but this efficiency drastically decreases in CSCs. The increased potency of up to 4 times of αCD44-O^{2}LNC-PTX on PCSCs in comparison to free PTX, and up to 3.3 times with respect to O^{2}LNC-PTX, indicate the targeted activity against PCSCs overexpressing CD44, which facilitates the internalizing, favoring the bioavailability and cytotoxic effect of PTX. Recent studies have tried to encapsulate chemotherapeutic drugs into NPs and then functionalize the particle surface with monoclonal antibodies to maintain targeting efficacy.[204] The conjugated antibodies enhance uptake and cytotoxic potency of the NPs. The significant reduction in cell viability provoked by αCD44-O^{2}LNC-PTX compared to naked O^{2}LNC-PTX is also in agreement with other studies conducted with NPs of a different nature, which are modified to be specifically targeted against PCCs.[416–418]

On the other hand, there is a need to create clinically relevant models for studying treatments directed against PC in established human PC orthotopic xenografts by the visualization of tumor growth in early stages and tracking tumor behavior and progression. Previous results indicate that the model is advantageous and several PCCs, including BxPC-3 PCCs, have been modified to express luciferase.[419].We produced lentiviral vector (LV) particles using the SELWPLV (Tristán-Manzano et al, unpublished) that allow both in vitro and in vivo monitoring of transduced cells by flow cytometry (eGFP) and bioluminescence imaging (NanoLuc) respectively. In addition, we generated and validated a suitable pancreatic tumor model based on BxPC-3 PCC that stably expressed both eGFP and NanoLuc, which can be useful for in vitro phenotypic analysis and in vivo tracking.

Finally, in order to verify that our functionalized αCD44-O^{2}LNCs were specifically directed to the tumor area, an *in vivo* assay was performed. In this experiment, an orthotopic xenotransplant was performed in the pancreas of the mice and the tumor was generated as described[420] but with a modification in the protocol by implanting PCSCs instead of patient tumor samples. BxPC-3 PCSCs transduced with the SELWP LVs were used to generate the tumor. In agreement with other studies using targeted tumor NPs,[421,422] our olive oil-based nanosystem specifically targets PC tumors which could

serve as a non-invasive imaging modality for molecular and cellular tracing and specific carrier of hydrophobic drugs against PCSCs. More specifically, Han, Y. et al. demonstrated the targeting ability of anti-CD326-grafted Gadolinium ion-doped upconversion NP-based micelles on BxPC-3 PCCs overexpressing this transmembrane glycoprotein.[423] In addition to these studies, here we show an enhanced targeting ability of our olive oil-based nanosystem on a PCSC orthotopic xenotransplant *in vivo* model.

CONCLUSIONS

1) A theranostic nanodevice based on orthogonal conjugation strategies for the multifunctionalization of polystyrene NPs has been successfully developed. Theranostic NPs (HP-Cy7-DOX-NPs) containing controlled amount of each one of the components (Cy7 dye, Doxorubicin and CRGDK peptide) have been successfully prepared and evaluated *in vitro* and *in vivo*.

2) Doxorubicin bound to the NPs through a pH labile hydrazone bond allowed its release inside the tumor cells. The sustained drug release of HP-Cy7-DOX-NPs validates the drug release strategy selected for this study. Thanks to this, it has been possible to avoid the systemic and physical toxicity of free Doxorubicin in the *in vivo* models.

3) CRGDK (Cys-Arg-Gly-Aps-Lys) homing peptide was coupled to the NPs via chemo-selective conjugation to target TNBC cells overexpressing Nrp-1.

4) Cytotoxicity assays showed three-fold reduction of the amount of Doxorubicin required to have the same effect than soluble Doxorubicin in MDA-MB-231 TNBC cells.

5) The *in vivo* experiments demonstrated the efficient targeted delivery and enhanced therapeutic activity of the theranostic NPs in Nrp-1 overexpressing TNBC tumors.

6) Colloidally stable nanocapsules with an olive-oil core surrounded by a GAD cross-linked HSA shell have been successfully developed. LLNCs cross-linked with GAD showed a fast internalization and a sustained drug delivery.

7) The curcumin-LLNCs with GAD cross-linking nanocapsules displayed an outstanding uptake performance and exhibited a tumor cell killing capacity (IC_{50}) similar to that of free curcumin.

8) An optimizing procedure to develop immuno-nanocapsules (O^2LNCs functionalized with an anti-CD44 antibody) with specific recognition properties against PCSCs have been successfully developed. The successful optimization in the anti-CD44 antibody functionalization procedure using a simple and reproducible ECDI method was demonstrated.

9) A complete physico-chemical characterization of the O^2LNCs has been carried out, revealing the presence of each of the components used in the synthesis procedure as well as the characterization of the immuno-O^2LNCs showing the

accurate bound of the antibody molecules to the carboxyl surface groups of bare O^2LNCs.

10) The specific immunological recognition of the CD44 cell membrane receptors has been reveal *in vitro*.

11) *In vitro* results supported the enhanced targeting activity and receptor-mediated binding mechanism of αCD44-O^2LNCs against CD44 overexpressing PCSCs and the increased cytotoxicity up to 4 times of PTX loaded αCD44-O^2LNC in comparison to free PTX.

12) Both the efficient targeted delivery on PCSCs and the noninvasive imaging cell tracking of αCD44-O^2LNCs has been demonstrated *in vivo* by generating a PC orthotopic xenotransplant model by direct inoculation of BxPC-3 PCSCs transduced with the SELWP LVs.

CONCLUSIONES

1) Se ha desarrollado con éxito un nano dispositivo teranóstico basado en estrategias de conjugación ortogonal para la multifuncionalización de NPs de poliestireno. Las NPs teranósticas (HP-Cy7-DOX-NP) se han preparado conteniendo una cantidad controlada de cada uno de los componentes (colorante Cy7, doxorrubicina y péptido CRGDK) y se han evaluado con éxito *in vitro* e *in vivo*.

2) La doxorrubicina unida a las NPs a través de un enlace de hidrazona lábil a pH permitió su liberación dentro de las células tumorales. La liberación sostenida de fármaco por parte de las HP-Cy7-DOX-NP valida la estrategia de liberación seleccionada para este estudio. Gracias a esto, ha sido posible evitar la toxicidad sistémica y local de la doxorrubicina libre en modelos *in vivo*.

3) El péptido de referencia CRGDK (Cys-Arg-Gly-Aps-Lys) se acopló a las NPs mediante conjugación quimio-selectiva para dirigirlas hacia células TNBC que sobreexpresan la Nrp-1.

4) Los ensayos de citotoxicidad mostraron una reducción de hasta tres veces la cantidad de doxorrubicina requerida para tener el mismo efecto que la doxorrubicina soluble sobre las células TNBC MDA-MB-231.

5) Los experimentos *in vivo* demostraron la entrega dirigida eficiente y la actividad terapéutica mejorada de las NPs teranósticas en tumores TNBC que sobreexpresan Nrp-1.

6) Se han desarrollado con éxito nanocápsulas coloidales estables con un núcleo de aceite de oliva rodeado por una cubierta de HSA reticulada con GAD. Las LLNCs reticuladas con GAD mostraron una rápida internalización y una entrega sostenida de fármaco.

7) Las LLNCs con curcumina reticuladas con GAD mostraron un excelente rendimiento de absorción y exhibieron una capacidad para matar células tumorales (IC_{50}) similar a la de la curcumina libre.

8) Se ha desarrollado con éxito un procedimiento de optimización para desarrollar O^2LNC funcionalizadas con el anticuerpo anti-CD44 con propiedades de reconocimiento específicas contra PCSC. Se demostró la optimización exitosa en el procedimiento de funcionalización de anticuerpo anti-CD44 usando un método ECDI simple y reproducible.

9) Se ha llevado a cabo una caracterización fisicoquímica completa de las O^2LNC, que revela la presencia de cada uno de los componentes utilizados en el procedimiento de síntesis, así como la caracterización de las inmuno-O^2LNC que muestran la unión precisa de las moléculas de anticuerpo a los grupos carboxilo de superficie de las O^2LNC desnudas.

10) Se ha demostrado *in vitro* el reconocimiento inmunológico específico de las α-CD44-O^2LNC por los receptores de membrana celular CD44.

11) Los resultados *in vitro* respaldaron la actividad de direccionamiento mejorada y el mecanismo de unión mediado por receptor de las αCD44-O^2LNC contra PCSCs que sobreexpresan CD44 y el aumento de la citotoxicidad hasta 4 veces de las αCD44-O^2LNC cargadas con PTX en comparación con PTX libre.

12) Se ha demostrado *in vivo* tanto la entrega eficiente dirigida en PCSCs como el rastreo por imagen no invasiva de las αCD44-O^2LNCs al generar un modelo de xenotrasplante ortotópico de PC mediante la inoculación de PCSC BxPC-3 transducidas con LV SELWP.

GLOSSARY

GLOSSARY

AFM: Atomic Force Microscopy.

AgNPs: Silver Nanoparticles.

ALDH: Aldehyde Dehydrogenase.

AR: Androgen.

AuNPs: Gold Nanoparticles.

BC: Breast Cancer.

BCSC: Breast Cancer Stem Cell.

BSA: Bovine Serum Albumin.

CASP: Caspase.

CNT: Carbon Nanotubes.

CSC: Cancer Stem Cell.

DIPEA: Diisopropide ethyl amine.

DLS: Dynamic Light Scattering.

DMEM: Dulbecco Modified Essential Medium.

DMF: Dimethyl Formamide.

DMSO: Dimethyl Sulfoxide.

DOX: Doxorubicin.

ECDI: Dimethylaminopropyl Ethyl-carbodiimide.

ECM: Extracellular Matrix.

EGF: Epidermal Growth Factor.

EMT: Epithelial-to-Mesenchymal Transition.

EPC: Endothelial Progenitor Cell.

EPR: Enhanced Permeability and Retention Effect.

ER: Estrogen.

ESC: Embryonic Stem Cell.

FBS: Fetal Bovine Serum.

FGF: Fibroblast Growth Factor.

FGF: Fibroblast Growth Factor.

GAD: Glutaraldehyde.

GFP: Green Fluorescent Protein.

HGF: Hepatocyte Growth Factor.

HP: Homing peptide.

HPLC: High Performance Liquid Chromatography.

HSA: Human Serum Albumin.

HSC: Hematopoietic Stem Cell.

IC_{50}: Half Maximal Inhibitory Concentration.

IEP: Isoelectric Point.

IgG: Immunoglobulin.

ITS: Insulin-Transferrin-Selenium.

LLN: Lipid Liquid Nanoparticles.

LV: Lentiviral Vector.

mAbs: Monoclonal Antibodies.

MDR: Multi-drug Resistance Mechanism.

MEM: Minimum Essential Medium.

MMP: Matrix Metalloproteinase Receptor.

MOI: Multiplicity of Infection.

MPS: Mononuclear Phagocyte System.

mRNA: Micro RNA.

MS: Mass Spectrometry.

NCs: Nanocapsules.

NMR: Nuclear Magnetic resonance.

NPs: Nanoparticles.

NR: Nile Red.

Nrp-1: Neuropilin-1.

O^2LNC: Olive oil Liquid Nanocapsules.

PACA: Polyalkylcyanoacrylate.

PB: Phosphate Buffer.

PBS: Phosphate Buffer Saline.

PC: Pancreatic Cancer.

PDI: Polydispersity Index.

PEG: Polyethylene Glycol.

PLGA: Poli lactic-co-glycolic acid.

PR: Progesterone.

PTX: Paclitaxel.

SC: Stem Cell.

TEM: Transmission Electron Microscopy.

TGF-β: Tumor Growth Factor β.

TIC: Tumor initiating cell.

TME: Tumor Microenvironment.

TNBC: Triple Negative Breast Cancer.

TNF: Tumor Necrosis Factor.

TP53: Tumor Protein 53.

UV: Ultraviolet.

VCAM: Vascular Cell Adhesion Molecule.

VEGF: Vascular Endothelial Cell Growth Factor.

VEGFR: Vascular Endothelial Cell Growth Factor Receptor.

WHO: World Health Organization.

WOS: Web of Science.

BIBLIOGRAPHY

BIOBLIOGRAPHY

(1) Boyle, P. and Levin, B. *World Cancer Report 2008*; Lyon, 2008.

(2) Chung, D.C., Haber, D. A. and M. G. H. *Principles of Clinical Cancer Genetics: A Handbook from the Massachusetts General Hospital.*; Springer US: New York.

(3) Roy, D., Dorak, M. T. *Environmental Factors, Genes, and the Development of Human Cancers.*; Springer US: New York.

(4) Baba, A.I. and Câtoi, C. *Comparative Oncology*; The Publishing House of the Romanian Academy.: Bucharest, 2007.

(5) Plummer, M.; de Martel, C.; Vignat, J.; Ferlay, J.; Bray, F.; Franceschi, S. Global Burden of Cancers Attributable to Infections in 2012: A Synthetic Analysis. *Lancet Glob. Heal.* **2016**, *4* (9), e609–e616. https://doi.org/10.1016/S2214-109X(16)30143-7.

(6) Davies, N. J.; Batehup, L.; Thomas, R. The Role of Diet and Physical Activity in Breast, Colorectal, and Prostate Cancer Survivorship: A Review of the Literature. *Br. J. Cancer* **2011**, *105* (SUPPL. 1), S52–S72. https://doi.org/10.1038/bjc.2011.423.

(7) Dong, L. M.; Potter, J. D.; White, E.; Ulrich, C. M.; Cardon, L. R.; Peters, U. Genetic Susceptibility to Cancer: The Role of Polymorphisms in Candidate Genes. *JAMA - J. Am. Med. Assoc.* **2008**, *299* (20), 2423–2436. https://doi.org/10.1001/jama.299.20.2423.

(8) Merlo, L. M. F.; Pepper, J. W.; Reid, B. J.; Maley, C. C. Cancer as an Evolutionary and Ecological Process. *Nat. Rev. Cancer* **2006**, *6* (12), 924–935. https://doi.org/10.1038/nrc2013.

(9) Hanahan, D.; Weinberg, R. A. Hallmarks of Cancer: The next Generation. *Cell* **2011**, *144* (5), 646–674. https://doi.org/10.1016/j.cell.2011.02.013.

(10) Kroemer, G.; Pouyssegur, J. Tumor Cell Metabolism: Cancer's Achilles' Heel. *Cancer Cell* **2008**, *13* (6), 472–482. https://doi.org/10.1016/j.ccr.2008.05.005.

(11) Negrini, S.; Gorgoulis, V. G.; Halazonetis, T. D. Genomic Instability an Evolving Hallmark of Cancer. *Nat. Rev. Mol. Cell Biol.* **2010**, *11* (3), 220–228. https://doi.org/10.1038/nrm2858.

(12) Grivennikov, S. I.; Greten, F. R.; Karin, M. Immunity, Inflammation, and Cancer. *Cell* **2010**, *140* (6), 883–899. https://doi.org/10.1016/j.cell.2010.01.025.

(13) Heldin, C. H. Autocrine PDGF Stimulation in Malignancies. *Ups. J. Med. Sci.* **2012**, *117* (2), 83–91. https://doi.org/10.3109/03009734.2012.658119.

(14) Aharinejad S., Sioud M., Lucas T., A. D. *Targeting Stromal-Cancer Cell Interactions with SiRNAs. In: Sioud M. (Eds) SiRNA and MiRNA Gene Silencing.*; Springer US, 2009. https://doi.org/https://doi.org/10.1007/978-1-60327-547-7_12.

(15) Newsholme, E.A. and Leech, A. R. *Functional Biochemistry in Health and Disease.*; Wiley- Blackwell: Chichester, 2009.

(16) Valeri, N.; Gasparini, P.; Fabbri, M.; Braconi, C.; Veronese, A.; Lovat, F.; Adair, B.; Vannini, I.; Fanini, F.; Bottoni, A.; et al. Modulation of Mismatch Repair and Genomic Stability by MiR-155. *Proc. Natl. Acad. Sci. U. S. A.* **2010**, *107* (15), 6982–6987. https://doi.org/10.1073/pnas.1002472107.

(17) Plati, J.; Bucur, O.; Khosravi-Far, R. Apoptotic Cell Signaling in Cancer Progression and Therapy. *Integr. Biol.* **2011**, *3* (4), 279–296. https://doi.org/10.1039/c0ib00144a.

(18) Adams, J. M.; Cory, S. The Bcl-2 Apoptotic Switch in Cancer Development and Therapy. *Oncogene* **2007**, *26* (9), 1324–1337. https://doi.org/10.1038/sj.onc.1210220.

(19) Jin, Z.; El-Deiry, W. S. Overview of Cell Death Signaling Pathways. *Cancer Biol. Ther.* **2005**, *4* (2), 147–171. https://doi.org/10.4161/cbt.4.2.1508.

(20) Nagy, J. A.; Dvorak, H. F. Heterogeneity of the Tumor Vasculature: The Need for New Tumor Blood Vessel Type-Specific Targets. *Clin. Exp. Metastasis* **2012**, *29* (7), 657–662. https://doi.org/10.1007/s10585-012-9500-6.

(21) Talmadge, J. E.; Fidler, I. J. AACR Centennial Series: The Biology of Cancer Metastasis: Historical Perspective. *Cancer Res.* **2010**, *70* (14), 5649–5669. https://doi.org/10.1158/0008-5472.CAN-10-1040.

(22) Valastyan, S.; Weinberg, R. A. Tumor Metastasis: Molecular Insights and Evolving Paradigms. *Cell* **2011**, *147* (2), 275–292. https://doi.org/10.1016/j.cell.2011.09.024.

(23) Gao, D.; Nolan, D. J.; Mellick, A. S.; Bambino, K.; McDonnell, K.; Mittal, V. Endothelial Progenitor Cells Control the Angiogenic Switch in Mouse Lung Metastasis. *Science (80-.).* **2008**, *319* (5860), 195–198. https://doi.org/10.1126/science.1150224.

(24) Martínez, P.; Blasco, M. A. Telomeric and Extra-Telomeric Roles for Telomerase and the Telomere-Binding Proteins. *Nat. Rev. Cancer* **2011**, *11* (3), 161–176. https://doi.org/10.1038/nrc3025.

(25) Colotta, F.; Allavena, P.; Sica, A.; Garlanda, C.; Mantovani, A. Cancer-Related Inflammation, the Seventh Hallmark of Cancer: Links to Genetic Instability. *Carcinogenesis* **2009**, *30* (7), 1073–1081. https://doi.org/10.1093/carcin/bgp127.

(26) Murphy, J. F. Clinical Medicine Insights : Oncology Trends in Cancer Immunotherapy. *Clin. Med. Insights Oncol.* **2010**, *4*, 67–80.

(27) Visvader, J. E. Cells of Origin in Cancer. *Nature* **2011**, *469* (7330), 314–322. https://doi.org/10.1038/nature09781.

(28) Pardee, A.B., Stein, G. S. *The Biology and Treatment of Cancer Understanding Cancer*; Wiley-Blackwell, Ed.; Hoboken, 2009.

(29) Cogliano, V. J.; Baan, R.; Straif, K.; Grosse, Y.; Lauby-Secretan, B.; Ghissassi, F. El; Bouvard, V.; Benbrahim-Tallaa, L.; Guha, N.; Freeman, C.; et al. Preventable Exposures Associated with Human Cancers. *J. Natl. Cancer Inst.* **2010**, *103* (24), 1827–1839. https://doi.org/10.1093/jnci/djr483.

(30) Fanale, D.; Amodeo, V.; Corsini, L. R.; Rizzo, S.; Bazan, V.; Russo, A. Breast Cancer

Genome-Wide Association Studies: There Is Strength in Numbers. *Oncogene* **2012**, *31* (17), 2121–2128. https://doi.org/10.1038/onc.2011.408.

(31) Tavassoli, F.A., Devilee, P. *Pathology and Genetics of Tumours of the Breast and Female Genital Organs*; 2003.

(32) Prat, A.; Perou, C. M. Mammary Development Meets Cancer Genomics. *Nat. Med.* **2009**, *15* (8), 842–844. https://doi.org/10.1038/nm0809-842.

(33) Haibe-Kains, B.; Desmedt, C.; Loi, S.; Culhane, A. C.; Bontempi, G.; Quackenbush, J.; Sotiriou, C. A Three-Gene Model to Robustly Identify Breast Cancer Molecular Subtypes. *J. Natl. Cancer Inst.* **2012**, *104* (4), 311–325. https://doi.org/10.1093/jnci/djr545.

(34) Melchor, L.; Benítez, J. An Integrative Hypothesis about the Origin and Development of Sporadic and Familial Breast Cancer Subtypes. *Carcinogenesis* **2008**, *29* (8), 1475–1482. https://doi.org/10.1093/carcin/bgn157.

(35) Wiechmann, L.; Sampson, M.; Stempel, M.; Jacks, L. M.; Patil, S. M.; King, T.; Morrow, M. Presenting Features of Breast Cancer Differ by Molecular Subtype. *Ann. Surg. Oncol.* **2009**, *16* (10), 2705–2710. https://doi.org/10.1245/s10434-009-0606-2.

(36) Parkin, D. M.; Boyd, L.; Walker, L. C. The Fraction of Cancer Attributable to Lifestyle and Environmental Factors in the UK in 2010. *Br. J. Cancer* **2011**, *105* (S2), S77–S81. https://doi.org/10.1038/bjc.2011.489.

(37) Bosetti, C.; Bertuccio, P.; Negri, E.; La Vecchia, C.; Zeegers, M. P.; Boffetta, P. Pancreatic Cancer: Overview of Descriptive Epidemiology. *Mol. Carcinog.* **2012**, *51* (1), 3–13. https://doi.org/10.1002/mc.20785.

(38) Anand, P.; Kunnumakara, A. B.; Sundaram, C.; Harikumar, K. B.; Tharakan, S. T.; Lai, O. S.; Sung, B.; Aggarwal, B. B. Cancer Is a Preventable Disease That Requires Major Lifestyle Changes. *Pharm. Res.* **2008**, *25* (9), 2097–2116. https://doi.org/10.1007/s11095-008-9661-9.

(39) Rastogi, T.; Devesa, S.; Mangtani, P.; Mathew, A.; Cooper, N.; Kao, R.; Sinha, R.

Cancer Incidence Rates among South Asians in Four Geographic Regions: India, Singapore, UK and US. *Int. J. Epidemiol.* **2008**, *37* (1), 147–160. https://doi.org/10.1093/ije/dym219.

(40) Vrieling, A.; Bueno-de-Mesquita, H. B.; Boshuizen, H. C.; Michaud, D. S.; Severinsen, M. T.; Overvad, K.; Olsen, A.; Tjønneland, A.; Clavel-Chapelon, F.; Boutron-Ruault, M. C.; et al. Cigarette Smoking, Environmental Tobacco Smoke Exposure and Pancreatic Cancer Risk in the European Prospective Investigation into Cancer and Nutrition. *Int. J. Cancer* **2010**, *126* (10), 2394–2403. https://doi.org/10.1002/ijc.24907.

(41) Aune, D.; Greenwood, D. C.; Chan, D. S. M.; Vieira, R.; Vieira, A. R.; Navarro Rosenblatt, D. A.; Cade, J. E.; Burley, V. J.; Norat, T. Body Mass Index, Abdominal Fatness and Pancreatic Cancer Risk: A Systematic Review and Non-Linear Dose-Response Meta-Analysis of Prospective Studies. *Ann. Oncol.* **2012**, *23* (4), 843–852. https://doi.org/10.1093/annonc/mdr398.

(42) Ilic, M.; Ilic, I. Epidemiology of Pancreatic Cancer. *World J. Gastroenterol.* **2016**, *22* (44), 9694–9705. https://doi.org/10.3748/wjg.v22.i44.9694.

(43) Ekbom, A.; Mclaughlin, J. K.; Karlsson, B. M.; Nyrén, O.; Gridley, G.; Adami, H. O.; Fraumeni, J. F. Pancreatitis and Pancreatic Cancer: A Population-Based Study. *J. Natl. Cancer Inst.* **1994**, *86* (8), 625–627. https://doi.org/10.1093/jnci/86.8.625.

(44) Kudo, Y.; Kamisawa, T.; Anjiki, H.; Takuma, K.; Egawa, N. Incidence of and Risk Factors for Developing Pancreatic Cancer in Patients with Chronic Pancreatitis. *Hepatogastroenterology.* **2011**, *58* (106), 609–611.

(45) Rohrmann, S.; Linseisen, J.; Nöthlings, U.; Overvad, K.; Egeberg, R.; Tjønneland, A.; Boutron-Ruault, M. C.; Clavel-Chapelon, F.; Cottet, V.; Pala, V.; et al. Meat and Fish Consumption and Risk of Pancreatic Cancer: Results from the European Prospective Investigation into Cancer and Nutrition. *Int. J. Cancer* **2013**, *132* (3), 617–624. https://doi.org/10.1002/ijc.27637.

(46) Larsson, S. C.; Wolk, A. Red and Processed Meat Consumption and Risk of Pancreatic Cancer: Meta-Analysis of Prospective Studies. *Br. J. Cancer* **2012**, *106*

(3), 603–607. https://doi.org/10.1038/bjc.2011.585.

(47) Maisonneuve, P.; Lowenfels, A. B. Risk Factors for Pancreatic Cancer: A Summary Review of Meta-Analytical Studies. *Int. J. Epidemiol.* **2015**, *44* (1), 186–198. https://doi.org/10.1093/ije/dyu240.

(48) Hemminki, K.; Li, X.; Sundquist, J.; Sundquist, K. Cancer Risks in Crohn Disease Patients. *Ann. Oncol.* **2009**, *20* (3), 574–580. https://doi.org/10.1093/annonc/mdn595.

(49) Collisson, E. A.; Bailey, P.; Chang, D. K.; Biankin, A. V. Molecular Subtypes of Pancreatic Cancer. *Nat. Rev. Gastroenterol. Hepatol.* **2019**, *16* (4), 207–220. https://doi.org/10.1038/s41575-019-0109-y.

(50) Luo, G.; Fan, Z.; Gong, Y.; Jin, K.; Yang, C.; Cheng, H.; Huang, D.; Ni, Q.; Liu, C.; Yu, X. Characteristics and Outcomes of Pancreatic Cancer by Histological Subtypes. *Pancreas* **2019**, *48* (6), 817–822. https://doi.org/10.1097/MPA.0000000000001338.

(51) Torres, C.; Grippo, P. J. Pancreatic Cancer Subtypes: A Roadmap for Precision Medicine. *Ann. Med.* **2018**, *50* (4), 277–287. https://doi.org/10.1080/07853890.2018.1453168.

(52) Durrett, R.; Foo, J.; Leder, K.; Mayberry, J.; Michor, F. Intratumor Heterogeneity in Evolutionary Models of Tumor Progression. *Genetics* **2011**, *188* (2), 461–477. https://doi.org/10.1534/genetics.110.125724.

(53) Nowell, P. C. The Clonal Evolution of Tumor Cell Populations. *Science (80-.).* **1976**, *194* (4260), 23–28. https://doi.org/10.1126/science.959840.

(54) Dick, J. E. Looking Ahead in Cancer Stem Cell Research. *Nature Biotechnology*. January 25, 2009, pp 44–46. https://doi.org/10.1038/nbt0109-44.

(55) O'Brien, C. A.; Kreso, A.; Dick, J. E. Cancer Stem Cells in Solid Tumors: An Overview. *Seminars in Radiation Oncology*. April 2009, pp 71–77. https://doi.org/10.1016/j.semradonc.2008.11.001.

(56) Vermeulen, L.; de Sousa e Melo, F.; Richel, D. J.; Medema, J. P. The Developing

Cancer Stem-Cell Model: Clinical Challenges and Opportunities. *Lancet Oncol.* **2012**, *13* (2), e83–e89. https://doi.org/10.1016/S1470-2045(11)70257-1.

(57) Southam, C. M.; Brunschwig, A. Quantitative Studies of Autotransplantation of Human Cancer. Preliminary Report. *Cancer* **1961**, *14* (5), 971–978. https://doi.org/10.1002/1097-0142(196109/10)14:5<971::AID-CNCR2820140510>3.0.CO;2-O.

(58) Lapidot, T.; Sirard, C.; Vormoor, J.; Murdoch, B.; Hoang, T.; Caceres-Cortes, J.; Minden, M.; Paterson, B.; Caligiuri, M. A.; Dick, J. E. A Cell Initiating Human Acute Myeloid Leukaemia after Transplantation into SCID Mice. *Nature* **1994**, *367* (6464), 645–648. https://doi.org/10.1038/367645a0.

(59) Reya, T.; Morrison, S. J.; Clarke, M. F.; Weissman, I. L. Stem Cells, Cancer, and Cancer Stem Cells. *Nature*. November 1, 2001, pp 105–111. https://doi.org/10.1038/35102167.

(60) Al-Hajj, M.; Wicha, M. S.; Benito-Hernandez, A.; Morrison, S. J.; Clarke, M. F. Prospective Identification of Tumorigenic Breast Cancer Cells. *Proc. Natl. Acad. Sci. U. S. A.* **2003**, *100* (7), 3983–3988. https://doi.org/10.1073/pnas.0530291100.

(61) Shackleton, M.; Quintana, E.; Fearon, E. R.; Morrison, S. J. Heterogeneity in Cancer: Cancer Stem Cells versus Clonal Evolution. *Cell*. September 4, 2009, pp 822–829. https://doi.org/10.1016/j.cell.2009.08.017.

(62) Chaffer, C. L.; Brueckmann, I.; Scheel, C.; Kaestli, A. J.; Wiggins, P. A.; Rodrigues, L. O.; Brooks, M.; Reinhardt, F.; Suc, Y.; Polyak, K.; et al. Normal and Neoplastic Nonstem Cells Can Spontaneously Convert to a Stem-like State. *Proc. Natl. Acad. Sci. U. S. A.* **2011**, *108* (19), 7950–7955. https://doi.org/10.1073/pnas.1102454108.

(63) Mani, S. A.; Guo, W.; Liao, M. J.; Eaton, E. N.; Ayyanan, A.; Zhou, A. Y.; Brooks, M.; Reinhard, F.; Zhang, C. C.; Shipitsin, M.; et al. The Epithelial-Mesenchymal Transition Generates Cells with Properties of Stem Cells. *Cell* **2008**, *133* (4), 704–715. https://doi.org/10.1016/j.cell.2008.03.027.

(64) Scheel, C.; Eaton, E. N.; Li, S. H. J.; Chaffer, C. L.; Reinhardt, F.; Kah, K. J.; Bell, G.; Guo, W.; Rubin, J.; Richardson, A. L.; et al. Paracrine and Autocrine Signals Induce and Maintain Mesenchymal and Stem Cell States in the Breast. *Cell* **2011**, *145* (6), 926–940. https://doi.org/10.1016/j.cell.2011.04.029.

(65) Vermeulen, L.; De Sousa E Melo, F.; Van Der Heijden, M.; Cameron, K.; De Jong, J. H.; Borovski, T.; Tuynman, J. B.; Todaro, M.; Merz, C.; Rodermond, H.; et al. Wnt Activity Defines Colon Cancer Stem Cells and Is Regulated by the Microenvironment. *Nat. Cell Biol.* **2010**, *12* (5), 468–476. https://doi.org/10.1038/ncb2048.

(66) Hernández-Camarero, P.; Jiménez, G.; López-Ruiz, E.; Barungi, S.; Marchal, J. A.; Perán, M. Revisiting the Dynamic Cancer Stem Cell Model: Importance of Tumour Edges. *Crit. Rev. Oncol. Hematol.* **2018**, *131* (June), 35–45. https://doi.org/10.1016/j.critrevonc.2018.08.004.

(67) Vaiopoulos, A. G.; Kostakis, I. D.; Koutsilieris, M.; Papavassiliou, A. G. Concise Review: Colorectal Cancer Stem Cells. *Stem Cells*. March 2012, pp 363–371. https://doi.org/10.1002/stem.1031.

(68) Verga Falzacappa, M. V.; Ronchini, C.; Reavie, L. B.; Pelicci, P. G. Regulation of Self-Renewal in Normal and Cancer Stem Cells. *FEBS J.* **2012**, *279* (19), 3559–3572. https://doi.org/10.1111/j.1742-4658.2012.08727.x.

(69) Roy, S.; Majumdar, A. P. N. Signaling in Colon Cancer Stem Cells. *J. Mol. Signal.* **2012**, *7* (1), 11. https://doi.org/10.1186/1750-2187-7-11.

(70) Subramaniam, D.; Ramalingam, S.; Houchen, C. W.; Anant, S. Cancer Stem Cells: A Novel Paradigm for Cancer Prevention and Treatment. *Mini-Reviews Med. Chem.* **2010**, *10* (5), 359–371. https://doi.org/10.2174/138955710791330954.

(71) Hermann, P. C.; Bhaskar, S.; Cioffi, M.; Heeschen, C. Cancer Stem Cells in Solid Tumors. *Seminars in Cancer Biology*. April 2010, pp 77–84. https://doi.org/10.1016/j.semcancer.2010.03.004.

(72) La Porta, C. A. Thoughts about Cancer Stem Cells in Solid Tumors. *World J. Stem Cells* **2012**, *4* (3), 17. https://doi.org/10.4252/wjsc.v4.i3.17.

(73) Ma, I.; Allan, A. L. The Role of Human Aldehyde Dehydrogenase in Normal and Cancer Stem Cells. *Stem Cell Reviews and Reports*. June 2011, pp 292–306. https://doi.org/10.1007/s12015-010-9208-4.

(74) Visvader, J. E.; Lindeman, G. J. Cancer Stem Cells in Solid Tumours: Accumulating Evidence and Unresolved Questions. *Nature Reviews Cancer*. October 2008, pp 755–768. https://doi.org/10.1038/nrc2499.

(75) Willis, N. D.; Przyborski, S. A.; Hutchison, C. J.; Wilson, R. G. Colonic and Colorectal Cancer Stem Cells: Progress in the Search for Putative Biomarkers. *Journal of Anatomy*. July 2008, pp 59–65. https://doi.org/10.1111/j.1469-7580.2008.00917.x.

(76) Zabierowski, S. E.; Herlyn, M. Melanoma Stem Cells: The Dark Seed of Melanoma. *Journal of Clinical Oncology*. June 10, 2008, pp 2890–2894. https://doi.org/10.1200/JCO.2007.15.5465.

(77) Elsaba, T. M. A.; Martinez-Pomares, L.; Robins, A. R.; Crook, S.; Seth, R.; Jackson, D.; McCart, A.; Silver, A. R.; Tomlinson, I. P. M.; Ilyas, M. The Stem Cell Marker CD133 Associates with Enhanced Colony Formation and Cell Motility in Colorectal Cancer. *PLoS One* **2010**, *5* (5), e10714. https://doi.org/10.1371/journal.pone.0010714.

(78) Kusumbe, A. P.; Mali, A. M.; Bapat, S. A. CD133-Expressing Stem Cells Associated with Ovarian Metastases Establish an Endothelial Hierarchy and Contribute to Tumor Vasculature. *Stem Cells* **2009**, *27* (3), 498–508. https://doi.org/10.1634/stemcells.2008-0868.

(79) O'Brien, C. A.; Pollett, A.; Gallinger, S.; Dick, J. E. A Human Colon Cancer Cell Capable of Initiating Tumour Growth in Immunodeficient Mice. *Nature* **2007**, *445* (7123), 106–110. https://doi.org/10.1038/nature05372.

(80) Rowehl, R. A.; Crawford, H.; Dufour, A.; Ju, J.; Botchkina, G. I. Genomic Analysis of Prostate Cancer Stem Cells Isolated from a Highly Metastatic Cell Line. *Cancer Genomics and Proteomics* **2008**, *5* (6), 301–310.

(81) Shmelkov, S. V; Butler, J. M.; Hooper, A. T.; Hormigo, A.; Kushner, J.; Milde, T.;

St, C. R.; Baljevic, M.; White, I.; Jin, D. K.; et al. CD133 Expression Is Not Restricted to Stem Cells, and Both CD133+ and C. *J.Clin.Invest* **2008**, *118* (0021-9738 (Print)), 2111–2120.

(82) Liu, H.; Patel, M. R.; Prescher, J. A.; Patsialou, A.; Qian, D.; Lin, J.; Wen, S.; Chang, Y. F.; Bachmann, M. H.; Shimono, Y.; et al. Cancer Stem Cells from Human Breast Tumors Are Involved in Spontaneous Metastases in Orthotopic Mouse Models. *Proc. Natl. Acad. Sci. U. S. A.* **2010**, *107* (42), 18115–18120. https://doi.org/10.1073/pnas.1006732107.

(83) Lorico, A.; Rappa, G. Phenotypic Heterogeneity of Breast Cancer Stem Cells. *Journal of Oncology*. 2011, p 135039. https://doi.org/10.1155/2011/135039.

(84) Uchino, M.; Kojima, H.; Wada, K.; Imada, M.; Onoda, F.; Satofuka, H.; Utsugi, T.; Murakami, Y. Nuclear β-Catenin and CD44 Upregulation Characterize Invasive Cell Populations in Non-Aggressive MCF-7 Breast Cancer Cells. *BMC Cancer* **2010**, *10*, 414. https://doi.org/10.1186/1471-2407-10-414.

(85) Chikamatsu, K.; Takahashi, G.; Sakakura, K.; Ferrone, S.; Masuyama, K. Immunoregulatory Properties of CD44+ Cancer Stem-like Cells in Squamous Cell Carcinoma of the Head and Neck. *Head Neck* **2011**, *33* (2), 208–215. https://doi.org/10.1002/hed.21420.

(86) Dalerba, P.; Dylla, S. J.; Park, I. K.; Liu, R.; Wang, X.; Cho, R. W.; Hoey, T.; Gurney, A.; Huang, E. H.; Simeone, D. M.; et al. Phenotypic Characterization of Human Colorectal Cancer Stem Cells. *Proc. Natl. Acad. Sci. U. S. A.* **2007**, *104* (24), 10158–10163. https://doi.org/10.1073/pnas.0703478104.

(87) Li, C.; Lee, C. J.; Simeone, D. M. Identification of Human Pancreatic Cancer Stem Cells. *Methods Mol. Biol.* **2009**, *568*, 161–173. https://doi.org/10.1007/978-1-59745-280-9_10.

(88) Maitland, N. J.; Collins, A. T. Prostate Cancer Stem Cells: A New Target for Therapy. *Journal of Clinical Oncology*. June 10, 2008, pp 2862–2870. https://doi.org/10.1200/JCO.2007.15.1472.

(89) Meng, E.; Long, B.; Sullivan, P.; McClellan, S.; Finan, M. A.; Reed, E.; Shevde, L.;

Rocconi, R. P. CD44+/CD24- Ovarian Cancer Cells Demonstrate Cancer Stem Cell Properties and Correlate to Survival. *Clin. Exp. Metastasis* **2012**, *29* (8), 939–948. https://doi.org/10.1007/s10585-012-9482-4.

(90) Hurt, E. M.; Kawasaki, B. T.; Klarmann, G. J.; Thomas, S. B.; Farrar, W. L. CD44+CD24- Prostate Cells Are Early Cancer Progenitor/Stem Cells That Provide a Model for Patients with Poor Prognosis. *Br. J. Cancer* **2008**, *98* (4), 756–765. https://doi.org/10.1038/sj.bjc.6604242.

(91) Moreb, J. S.; Ucar, D.; Han, S.; Amory, J. K.; Goldstein, A. S.; Ostmark, B.; Chang, L. J. The Enzymatic Activity of Human Aldehyde Dehydrogenases 1A2 and 2 (ALDH1A2 and ALDH2) Is Detected by Aldefluor, Inhibited by Diethylaminobenzaldehyde and Has Significant Effects on Cell Proliferation and Drug Resistance. *Chem. Biol. Interact.* **2012**, *195* (1), 52–60. https://doi.org/10.1016/j.cbi.2011.10.007.

(92) Ginestier, C.; Hur, M. H.; Charafe-Jauffret, E.; Monville, F.; Dutcher, J.; Brown, M.; Jacquemier, J.; Viens, P.; Kleer, C. G.; Liu, S.; et al. ALDH1 Is a Marker of Normal and Malignant Human Mammary Stem Cells and a Predictor of Poor Clinical Outcome. *Cell Stem Cell* **2007**, *1* (5), 555–567. https://doi.org/10.1016/j.stem.2007.08.014.

(93) Huang, E. H.; Hynes, M. J.; Zhang, T.; Ginestier, C.; Dontu, G.; Appelman, H.; Fields, J. Z.; Wicha, M. S.; Boman, B. M. Aldehyde Dehydrogenase 1 Is a Marker for Normal and Malignant Human Colonic Stem Cells (SC) and Tracks SC Overpopulation during Colon Tumorigenesis. *Cancer Res.* **2009**, *69* (8), 3382–3389. https://doi.org/10.1158/0008-5472.CAN-08-4418.

(94) Nishida, S.; Hirohashi, Y.; Torigoe, T.; Kitamura, H.; Takahashi, A.; Masumori, N.; Tsukamoto, T.; Sato, N. Gene Expression Profiles of Prostate Cancer Stem Cells Isolated by Aldehyde Dehydrogenase Activity Assay. *J. Urol.* **2012**, *188* (1), 294–299. https://doi.org/10.1016/j.juro.2012.02.2555.

(95) Feng, J.; Qi, Q.; Khanna, A.; Todd, N. W.; Deepak, J.; Lingxiao, X.; Huijun, W.; Zhenqiu, L.; Yun, S.; Stass, S. A.; et al. Aldehyde Dehydrogenase 1 Is a Tumor Stem Cell-Associated Marker in Lung Cancer. *Mol. Cancer Res.* **2009**, *7* (3), 330–

338. https://doi.org/10.1158/1541-7786.MCR-08-0393.

(96) Clay, M. R.; Tabor, M.; Owen, J. H.; Carey, T. E.; Bradford, C. R.; Wolf, G. T.; Wicha, M. S.; Prince, M. E. Single-Marker Identification of Head and Neck Squamous Cell Carcinoma Cancer Stem Cells with Aldehyde Dehydrogenase. *Head Neck* **2010**, *32* (9), 1195–1201. https://doi.org/10.1002/hed.21315.

(97) Lohberger, B.; Rinner, B.; Stuendl, N.; Absenger, M.; Liegl-Atzwanger, B.; Walzer, S. M.; Windhager, R.; Leithner, A. Aldehyde Dehydrogenase 1, a Potential Marker for Cancer Stem Cells in Human Sarcoma. *PLoS One* **2012**, *7* (8). https://doi.org/10.1371/journal.pone.0043664.

(98) Croker, A. K.; Goodale, D.; Chu, J.; Postenka, C.; Hedley, B. D.; Hess, D. A.; Allan, A. L. High Aldehyde Dehydrogenase and Expression of Cancer Stem Cell Markers Selects for Breast Cancer Cells with Enhanced Malignant and Metastatic Ability. *J. Cell. Mol. Med.* **2009**, *13* (8 B), 2236–2252. https://doi.org/10.1111/j.1582-4934.2008.00455.x.

(99) Saini, V.; Shoemaker, R. H. Potential for Therapeutic Targeting of Tumor Stem Cells. *Cancer Science*. January 2010, pp 16–21. https://doi.org/10.1111/j.1349-7006.2009.01371.x.

(100) Rappa, G.; Mercapide, J.; Anzanello, F.; Prasmickaite, L.; Xi, Y.; Ju, J.; Fodstad, O.; Lorico, A. Growth of Cancer Cell Lines under Stem Cell-like Conditions Has the Potential to Unveil Therapeutic Targets. *Exp. Cell Res.* **2008**, *314* (10), 2110–2122. https://doi.org/10.1016/j.yexcr.2008.03.008.

(101) Hwang-Verslues, W. W.; Kuo, W. H.; Chang, P. H.; Pan, C. C.; Wang, H. H.; Tsai, S.; Jeng, Y. M.; Shew, J. Y.; Kung, J. T.; Chen, C. H.; et al. Multiple Lineages of Human Breast Cancer Stem/Progenitor Cells Identified by Profiling with Stem Cell Markers. *PLoS One* **2009**, *4* (12), e8377. https://doi.org/10.1371/journal.pone.0008377.

(102) Walia, V.; Elble, R. C. Enrichment for Breast Cancer Cells with Stem/Progenitor Properties by Differential Adhesion. *Stem Cells Dev.* **2010**, *19* (8), 1175–1182. https://doi.org/10.1089/scd.2009.0430.

(103) Lee, C. J.; Dosch, J.; Simeone, D. M. Pancreatic Cancer Stem Cells. *Journal of Clinical Oncology*. June 10, 2008, pp 2806–2812. https://doi.org/10.1200/JCO.2008.16.6702.

(104) Klonisch, T.; Wiechec, E.; Hombach-Klonisch, S.; Ande, S. R.; Wesselborg, S.; Schulze-Osthoff, K.; Los, M. Cancer Stem Cell Markers in Common Cancers - Therapeutic Implications. *Trends in Molecular Medicine*. October 2008, pp 450–460. https://doi.org/10.1016/j.molmed.2008.08.003.

(105) Li, C.; Heidt, D. G.; Dalerba, P.; Burant, C. F.; Zhang, L.; Adsay, V.; Wicha, M.; Clarke, M. F.; Simeone, D. M. Identification of Pancreatic Cancer Stem Cells. *Cancer Res.* **2007**, *67* (3), 1030–1037. https://doi.org/10.1158/0008-5472.CAN-06-2030.

(106) Bao, B.; Ahmad, A.; Azmi, A. S.; Ali, S.; Sarkar, F. H. Implications for Cancer Therapy. *Natl. Institutes Heal.* **2014**, 1–18. https://doi.org/10.1002/0471141755.ph1425s61.Cancer.

(107) Dosch, J. S.; Ziemke, E. K.; Shettigar, A.; Rehemtulla, A.; Sebolt-Leopold, J. S. Cancer Stem Cell Marker Phenotypes Are Reversible and Functionally Homogeneous in a Preclinical Model of Pancreatic Cancer. *Cancer Res.* **2015**, *75* (21), 4582–4592. https://doi.org/10.1158/0008-5472.CAN-14-2793.

(108) Yechiel, E.; Coste, R. L. *From Ancient Potions To Modern Lotions: A Technology Overview and Introduction to Topical Delivery Systems*.

(109) Porter, C. J. H.; Trevaskis, N. L.; Charman, W. N. Lipids and Lipid-Based Formulations: Optimizing the Oral Delivery of Lipophilic Drugs. *Nature Reviews Drug Discovery*. March 2007, pp 231–248. https://doi.org/10.1038/nrd2197.

(110) Williams, R. O., Watts, A. B., and Miller, D. A. *Formulating Poorly Water Soluble Drugs*; Williams III, Robert O., Watts, Alan B., Miller, D. A., Ed.; Springer US, 2012.

(111) Wong, K. K. Y.; Liu, X. Silver Nanoparticles - The Real “Silver Bullet” in Clinical Medicine? *Medchemcomm* **2010**, *1* (2), 125–131. https://doi.org/10.1039/c0md00069h.

(112) Boulaiz, H.; Alvarez, P. J.; Ramirez, A.; Marchal, J. A.; Prados, J.; Rodríguez-Serrano, F.; Perán, M.; Melguizo, C.; Aranega, A. Nanomedicine: Application Areas and Development Prospects. *International Journal of Molecular Sciences*. May 2011, pp 3303–3321. https://doi.org/10.3390/ijms12053303.

(113) Wong, K. K. Y.; Liu, X. L. Nanomedicine: A Primer for Surgeons. *Pediatric Surgery International*. Springer October 2012, pp 943–951. https://doi.org/10.1007/s00383-012-3162-y.

(114) APPENZELLER, T. The Man Who Dared to Think Small. *Science (80-.).* **1991**, *254* (5036), 1300–1300. https://doi.org/10.1126/science.254.5036.1300.

(115) Feynman, R. P. There's Plenty of Room at the Bottom - Caltech Magazine http://calteches.library.caltech.edu/1976/ (accessed Feb 8, 2020).

(116) Soriano, M. L.; Rodríguez-Benot, A.; Valcárcel, M. Nanotechnological Foundations of a "New" Nephrology. *Nefrologia*. Elsevier Espana S.L. July 1, 2018, pp 362–372. https://doi.org/10.1016/j.nefroe.2018.06.004.

(117) Atala, A.; Lanza, R.; Thomson, J. A.; Nerem, R. M. *Principles of Regenerative Medicine*; Elsevier Inc., 2008. https://doi.org/10.1016/B978-0-12-369410-2.X5001-3.

(118) Liu, X.; Lee, P. Y.; Ho, C. M.; Lui, V. C. H.; Chen, Y.; Che, C. M.; Tam, P. K. H.; Wong, K. K. Y. Silver Nanoparticles Mediate Differential Responses in Keratinocytes and Fibroblasts during Skin Wound Healing. *ChemMedChem* **2010**, *5* (3), 468–475. https://doi.org/10.1002/cmdc.200900502.

(119) Kwan, K. H. L.; Liu, X.; To, M. K. T.; Yeung, K. W. K.; Ho, C. ming; Wong, K. K. Y. Modulation of Collagen Alignment by Silver Nanoparticles Results in Better Mechanical Properties in Wound Healing. *Nanomedicine Nanotechnology, Biol. Med.* **2011**, *7* (4), 497–504. https://doi.org/10.1016/j.nano.2011.01.003.

(120) Hu, N. M.; Chen, Z.; Liu, X.; Liu, H.; Lian, X.; Wang, X.; Cui, F. Z. Mechanical Properties and in Vitro Bioactivity of Injectable and Self-Setting Calcium Sulfate/Nano-HA/Collagen Bone Graft Substitute. *J. Mech. Behav. Biomed. Mater.* **2012**, *12*, 119–128. https://doi.org/10.1016/j.jmbbm.2011.12.007.

(121) Smith, L. A.; Ma, P. X. Nano-Fibrous Scaffolds for Tissue Engineering. *Colloids Surfaces B Biointerfaces* **2004**, *39* (3), 125–131. https://doi.org/10.1016/j.colsurfb.2003.12.004.

(122) Kavya, K. C.; Dixit, R.; Jayakumar, R.; Nair, S. V.; Chennazhi, K. P. Synthesis and Characterization of Chitosan/Chondroitin Sulfate/Nano- SiO2composite Scaffold for Bone Tissue Engineering. *J. Biomed. Nanotechnol.* **2012**, *8* (1), 149–160. https://doi.org/10.1166/jbn.2012.1363.

(123) Polini, A.; Pisignano, D.; Parodi, M.; Quarto, R.; Scaglione, S. Osteoinduction of Human Mesenchymal Stem Cells by Bioactive Composite Scaffolds without Supplemental Osteogenic Growth Factors. *PLoS One* **2011**, *6* (10), e26211. https://doi.org/10.1371/journal.pone.0026211.

(124) Zhu, W. Z.; Li, X.; Qi, J. P.; Tang, Z. P.; Wang, W.; Wei, L.; Lei, H. Experimental Study of Cell Migration and Functional Differentiation of Transplanted Neural Stem Cells Co-Labeled with Superparamagnetic Iron Oxide and Brdu in an Ischemic Rat Model. *Biomed. Environ. Sci.* **2008**, *21* (5), 420–424. https://doi.org/10.1016/S0895-3988(08)60063-X.

(125) Ortega-Oller, I.; Padial-Molina, M.; Galindo-Moreno, P.; O'Valle, F.; Jódar-Reyes, A. B.; Peula-García, J. M. Bone Regeneration from PLGA Micro-Nanoparticles. *BioMed Research International*. 2015. https://doi.org/10.1155/2015/415289.

(126) Alexis, F.; Pridgen, E.; Molnar, L. K.; Farokhzad, O. C. Factors Affecting the Clearance and Biodistribution of Polymeric Nanoparticles. In *Molecular Pharmaceutics*; 2008; Vol. 5, pp 505–515. https://doi.org/10.1021/mp800051m.

(127) Jain, K. K. Nanodiagnostics: Application of Nanotechnology in Molecular Diagnostics. *Expert Review of Molecular Diagnostics*. March 2003, pp 153–161. https://doi.org/10.1586/14737159.3.2.153.

(128) Zuo, H.; Chen, W.; Li, B.; Xu, K.; Cooper, H.; Gu, Z.; Xu, Z. P. MnAl Layered Double Hydroxide Nanoparticles as a Dual-Functional Platform for Magnetic Resonance Imaging and SiRNA Delivery. *Chem. - A Eur. J.* **2017**, *23* (57), 14299–14306. https://doi.org/10.1002/chem.201702835.

(129) Lux, F.; Sancey, L.; Bianchi, A.; Crémillieux, Y.; Roux, S.; Tillement, O. Gadolinium-Based Nanoparticles for Theranostic MRI-Radiosensitization. *Nanomedicine*. Future Medicine Ltd. June 1, 2015, pp 1801–1815. https://doi.org/10.2217/nnm.15.30.

(130) Cancino-Bernardi, J.; Marangoni, V. S.; Besson, J. C. F.; Cancino, M. E. C.; Natali, M. R. M.; Zucolotto, V. Gold-Based Nanospheres and Nanorods Particles Used as Theranostic Agents: An in Vitro and in Vivo Toxicology Studies. *Chemosphere* **2018**, *213*, 41–52. https://doi.org/10.1016/j.chemosphere.2018.09.012.

(131) Rajkumar, S.; Prabaharan, M. Theranostics Based on Iron Oxide and Gold Nanoparticles for Imaging- Guided Photothermal and Photodynamic Therapy of Cancer. *Curr. Top. Med. Chem.* **2017**, *17* (16), 1858–1871. https://doi.org/10.2174/1568026617666161122120537.

(132) Wang, L.; Zhao, W.; Tan, W. Bioconjugated Silica Nanoparticles: Development and Applications. *Nano Res.* **2008**, *1* (2), 99–115. https://doi.org/10.1007/s12274-008-8018-3.

(133) Masayuki, Y.; Mizue, M.; Noriko, Y.; Teruo, O.; Yasuhisa, S.; Kazunori, K.; Shohei, I. Polymer Micelles as Novel Drug Carrier: Adriamycin-Conjugated Poly(Ethylene Glycol)-Poly(Aspartic Acid) Block Copolymer. *J. Control. Release* **1990**, *11* (1–3), 269–278. https://doi.org/10.1016/0168-3659(90)90139-K.

(134) Yokoyama, M.; Okano, T.; Sakurai, Y.; Ekimoto, H.; Shibazaki, C.; Kataoka, K. Toxicity and Antitumor Activity against Solid Tumors of Micelle-Forming Polymeric Anticancer Drug and Its Extremely Long Circulation in Blood. *Cancer Res.* **1991**, *51* (12), 3229–3236.

(135) Guo, J. H.; Skinner, G. W.; Harcum, W. W.; Barnum, P. E. Pharmaceutical Applications of Naturally Occurring Water-Soluble Polymers. *Pharmaceutical Science and Technology Today*. Elsevier Current Trends September 1, 1998, pp 254–261. https://doi.org/10.1016/S1461-5347(98)00072-8.

(136) Park, J. H.; Lee, S.; Kim, J. H.; Park, K.; Kim, K.; Kwon, I. C. Polymeric Nanomedicine for Cancer Therapy. *Progress in Polymer Science (Oxford)*.

Pergamon January 1, 2008, pp 113–137. https://doi.org/10.1016/j.progpolymsci.2007.09.003.

(137) Farokhzad, O. C.; Langer, R. Impact of Nanotechnology on Drug Delivery. *ACS Nano* **2009**, *3* (1), 16–20. https://doi.org/10.1021/nn900002m.

(138) Merisko-Liversidge, E.; Liversidge, G. G.; Cooper, E. R. Nanosizing: A Formulation Approach for Poorly-Water-Soluble Compounds. *European Journal of Pharmaceutical Sciences*. Elsevier February 1, 2003, pp 113–120. https://doi.org/10.1016/S0928-0987(02)00251-8.

(139) Jokerst, J. V.; Lobovkina, T.; Zare, R. N.; Gambhir, S. S. Nanoparticle PEGylation for Imaging and Therapy. *Nanomedicine*. June 2011, pp 715–728. https://doi.org/10.2217/nnm.11.19.

(140) Jain, T. K.; Morales, M. A.; Sahoo, S. K.; Leslie-Pelecky, D. L.; Labhasetwar, V. Iron Oxide Nanoparticles for Sustained Delivery of Anticancer Agents. *Mol. Pharm.* **2005**, *2* (3), 194–205. https://doi.org/10.1021/mp0500014.

(141) Üner, M.; Yener, G. Importance of Solid Lipid Nanoparticles (SLN) in Various Administration Routes and Future Perspective. *International Journal of Nanomedicine*. 2007, pp 289–300.

(142) Ye, D.; Raghnaill, M. N.; Bramini, M.; Mahon, E.; Åberg, C.; Salvati, A.; Dawson, K. A. Nanoparticle Accumulation and Transcytosis in Brain Endothelial Cell Layers. *Nanoscale* **2013**, *5* (22), 11153–11165. https://doi.org/10.1039/c3nr02905k.

(143) Davis, M. E. Design and Development of IT-101, a Cyclodextrin-Containing Polymer Conjugate of Camptothecin. *Advanced Drug Delivery Reviews*. November 12, 2009, pp 1189–1192. https://doi.org/10.1016/j.addr.2009.05.005.

(144) Vizirianakis, I. S. Nanomedicine and Personalized Medicine toward the Application of Pharmacotyping in Clinical Practice to Improve Drug-Delivery Outcomes. *Nanomedicine Nanotechnology, Biol. Med.* **2011**, *7* (1), 11–17. https://doi.org/10.1016/j.nano.2010.11.002.

(145) Jabr-Milane, L. S.; van Vlerken, L. E.; Yadav, S.; Amiji, M. M. Multi-Functional Nanocarriers to Overcome Tumor Drug Resistance. *Cancer Treatment Reviews*. November 2008, pp 592–602. https://doi.org/10.1016/j.ctrv.2008.04.003.

(146) Shapira, A.; Livney, Y. D.; Broxterman, H. J.; Assaraf, Y. G. Nanomedicine for Targeted Cancer Therapy: Towards the Overcoming of Drug Resistance. *Drug Resist. Updat.* **2011**, *14* (3), 150–163. https://doi.org/10.1016/j.drup.2011.01.003.

(147) Sahoo, S. K.; Labhasetwar, V. Nanotech Approaches to Drug Delivery and Imaging. *Drug Discovery Today*. December 15, 2003, pp 1112–1120. https://doi.org/10.1016/S1359-6446(03)02903-9.

(148) Cho, K.; Wang, X.; Nie, S.; Chen, Z.; Shin, D. M. Therapeutic Nanoparticles for Drug Delivery in Cancer. *Clinical Cancer Research*. March 1, 2008, pp 1310–1316. https://doi.org/10.1158/1078-0432.CCR-07-1441.

(149) Hervella, P.; Lozano, V.; Garcia-Fuentes, M.; Alonso, M. J. Nanomedicine: New Challenges and Opportunities in Cancer Therapy. In *Journal of Biomedical Nanotechnology*; 2008; Vol. 4, pp 276–292. https://doi.org/10.1166/jbn.2008.339.

(150) Navya, P. N.; Kaphle, A.; Srinivas, S. P.; Bhargava, S. K.; Rotello, V. M.; Daima, H. K. Current Trends and Challenges in Cancer Management and Therapy Using Designer Nanomaterials. *Nano Converg.* **2019**, *6* (1). https://doi.org/10.1186/s40580-019-0193-2.

(151) Duncan, R. Polymer Conjugates as Anticancer Nanomedicines. *Nature Reviews Cancer*. September 2006, pp 688–701. https://doi.org/10.1038/nrc1958.

(152) Garcia-Fuentes, M.; Alonso, M. J. Chitosan-Based Drug Nanocarriers: Where Do We Stand? *Journal of Controlled Release*. July 20, 2012, pp 496–504. https://doi.org/10.1016/j.jconrel.2012.03.017.

(153) Pinto Reis, C.; Neufeld, R. J.; Ribeiro, A. J.; Veiga, F. Nanoencapsulation I. Methods for Preparation of Drug-Loaded Polymeric Nanoparticles. *Nanomedicine: Nanotechnology, Biology, and Medicine*. 2006, pp 8–21.

https://doi.org/10.1016/j.nano.2005.12.003.

(154) Brigger, I.; Dubernet, C.; Couvreur, P. Nanoparticles in Cancer Therapy and Diagnosis. *Advanced Drug Delivery Reviews*. September 13, 2002, pp 631–651. https://doi.org/10.1016/S0169-409X(02)00044-3.

(155) Lee, J. H.; Nan, A. Combination Drug Delivery Approaches in Metastatic Breast Cancer. *J. Drug Deliv.* **2012**, *2012*, 1–17. https://doi.org/10.1155/2012/915375.

(156) Hoffman, A. S. Hydrogels for Biomedical Applications. *Adv. Drug Deliv. Rev.* **2002**, *54* (1), 3–12. https://doi.org/10.1016/S0169-409X(01)00239-3.

(157) Bettinger, C. J.; Weinberg, E. J.; Kulig, K. M.; Vacanti, J. P.; Wang, Y.; Borenstein, J. T.; Langer, R. Three-Dimensional Microfluidic Tissue-Engineering Scaffolds Using a Flexible Biodegradable Polymer. *Adv. Mater.* **2006**, *18* (2), 165–169. https://doi.org/10.1002/adma.200500438.

(158) Cheng, Y.; He, C.; Ding, J.; Xiao, C.; Zhuang, X.; Chen, X. Thermosensitive Hydrogels Based on Polypeptides for Localized and Sustained Delivery of Anticancer Drugs. *Biomaterials* **2013**, *34* (38), 10338–10347. https://doi.org/10.1016/j.biomaterials.2013.09.064.

(159) Kesharwani, P.; Jain, K.; Jain, N. K. Dendrimer as Nanocarrier for Drug Delivery. *Progress in Polymer Science*. Pergamon February 1, 2014, pp 268–307. https://doi.org/10.1016/j.progpolymsci.2013.07.005.

(160) Lee, C. C.; Gillies, E. R.; Fox, M. E.; Guillaudeu, S. J.; Fréchet, J. M. J.; Dy, E. E.; Szoka, F. C. A Single Dose of Doxorubicin-Functionalized Bow-Tie Dendrimer Cures Mice Bearing C-26 Colon Carcinomas. *Proc. Natl. Acad. Sci. U. S. A.* **2006**, *103* (45), 16649–16654. https://doi.org/10.1073/pnas.0607705103.

(161) Ren, Y.; Kang, C. S.; Yuan, X. B.; Zhou, X.; Xu, P.; Han, L.; Wang, G. X.; Jia, Z.; Zhong, Y.; Yu, S.; et al. Co-Delivery of as-MiR-21 and 5-FU by Poly(Amidoamine) Dendrimer Attenuates Human Glioma Cell Growth in Vitro. *J. Biomater. Sci. Polym. Ed.* **2010**, *21* (3), 303–314. https://doi.org/10.1163/156856209X415828.

(162) Wang, T.; Petrenko, V. A.; Torchilin, V. P. Paclitaxel-Loaded Polymeric Micelles

Modified with MCF-7 Cell-Specific Phage Protein: Enhanced Binding to Target Cancer Cells and Increased Cytotoxicity. *Mol. Pharm.* **2010**, *7* (4), 1007–1014. https://doi.org/10.1021/mp1001125.

(163) Ke, X. Y.; Lin Ng, V. W.; Gao, S. J.; Tong, Y. W.; Hedrick, J. L.; Yang, Y. Y. Co-Delivery of Thioridazine and Doxorubicin Using Polymeric Micelles for Targeting Both Cancer Cells and Cancer Stem Cells. *Biomaterials* **2014**, *35* (3), 1096–1108. https://doi.org/10.1016/j.biomaterials.2013.10.049.

(164) Torchilin, V. P. Recent Advances with Liposomes as Pharmaceutical Carriers. *Nat. Rev. Drug Discov.* **2005**, *4* (2), 145–160. https://doi.org/10.1038/nrd1632.

(165) Zhang, L.; Gu, F. X.; Chan, J. M.; Wang, A. Z.; Langer, R. S.; Farokhzad, O. C. Nanoparticles in Medicine: Therapeutic Applications and Developments. *Clinical Pharmacology and Therapeutics*. May 30, 2008, pp 761–769. https://doi.org/10.1038/sj.clpt.6100400.

(166) Northfelt, D. W.; Dezube, B. J.; Thommes, J. A.; Miller, B. J.; Fischl, M. A.; Friedman-Kien, A.; Kaplan, L. D.; Du Mond, C.; Mamelok, R. D.; Henry, D. H. Pegylated-Liposomal Doxorubicin versus Doxorubicin, Bleomycin, and Vincristine in the Treatment of AIDS-Related Kaposi's Sarcoma: Results of a Randomized Phase III Clinical Trial. *J. Clin. Oncol.* **1998**, *16* (7), 2445–2451. https://doi.org/10.1200/JCO.1998.16.7.2445.

(167) Lim, S. B.; Banerjee, A.; Önyüksel, H. Improvement of Drug Safety by the Use of Lipid-Based Nanocarriers. In *Journal of Controlled Release*; J Control Release, 2012; Vol. 163, pp 34–45. https://doi.org/10.1016/j.jconrel.2012.06.002.

(168) Joshi, M. D.; Müller, R. H. Lipid Nanoparticles for Parenteral Delivery of Actives. *European Journal of Pharmaceutics and Biopharmaceutics*. Eur J Pharm Biopharm February 2009, pp 161–172. https://doi.org/10.1016/j.ejpb.2008.09.003.

(169) Parveen, S.; Misra, R.; Sahoo, S. K. Nanoparticles: A Boon to Drug Delivery, Therapeutics, Diagnostics and Imaging. *Nanomedicine: Nanotechnology, Biology, and Medicine*. Nanomedicine February 2012, pp 147–166.

https://doi.org/10.1016/j.nano.2011.05.016.

(170) Harivardhan Reddy, L.; Sharma, R. K.; Chuttani, K.; Mishra, A. K.; Murthy, R. S. R. Influence of Administration Route on Tumor Uptake and Biodistribution of Etoposide Loaded Solid Lipid Nanoparticles in Dalton's Lymphoma Tumor Bearing Mice. *J. Control. Release* **2005**, *105* (3), 185–198. https://doi.org/10.1016/j.jconrel.2005.02.028.

(171) Paliwal, R.; Rai, S.; Vaidya, B.; Khatri, K.; Goyal, A. K.; Mishra, N.; Mehta, A.; Vyas, S. P. Effect of Lipid Core Material on Characteristics of Solid Lipid Nanoparticles Designed for Oral Lymphatic Delivery. *Nanomedicine Nanotechnology, Biol. Med.* **2009**, *5* (2), 184–191. https://doi.org/10.1016/j.nano.2008.08.003.

(172) Zara, G. P.; Bargoni, A.; Cavalli, R.; Fundarò, A.; Vighetto, D.; Gasco, M. R. Pharmacokinetics and Tissue Distribution of Idarubicin-Loaded Solid Lipid Nanoparticles after Duodenal Administration to Rats. *J. Pharm. Sci.* **2002**, *91* (5), 1324–1333. https://doi.org/10.1002/jps.10129.

(173) Cai, S.; Yang, Q.; Bagby, T. R.; Forrest, M. L. Lymphatic Drug Delivery Using Engineered Liposomes and Solid Lipid Nanoparticles. *Advanced Drug Delivery Reviews*. Adv Drug Deliv Rev September 10, 2011, pp 901–908. https://doi.org/10.1016/j.addr.2011.05.017.

(174) Fernandez, P.; André, V.; Rieger, J.; Kühnle, A. Nano-Emulsion Formation by Emulsion Phase Inversion. *Colloids Surfaces A Physicochem. Eng. Asp.* **2004**, *251* (1–3), 53–58. https://doi.org/10.1016/j.colsurfa.2004.09.029.

(175) Savage, D. J.; Liu, X.; Curley, S. A.; Ferrari, M.; Serda, R. E. Porous Silicon Advances in Drug Delivery and Immunotherapy. *Current Opinion in Pharmacology*. Elsevier Ltd 2013, pp 834–841. https://doi.org/10.1016/j.coph.2013.06.006.

(176) Faraji, A. H.; Wipf, P. Nanoparticles in Cellular Drug Delivery. *Bioorganic and Medicinal Chemistry*. Bioorg Med Chem April 15, 2009, pp 2950–2962. https://doi.org/10.1016/j.bmc.2009.02.043.

(177) Kar, M.; Tiwari, N.; Tiwari, M.; Lahiri, M.; Gupta, S. Sen. Poly-L-Arginine Grafted

Silica Mesoporous Nanoparticles for Enhanced Cellular Uptake and Their Application in DNA Delivery and Controlled Drug Release. *Part. Part. Syst. Charact.* **2013**, *30* (2), 166–179. https://doi.org/10.1002/ppsc.201200089.

(178) Ferris, D. P.; Lu, J.; Gothard, C.; Yanes, R.; Thomas, C. R.; Olsen, J. C.; Stoddart, J. F.; Tamanoi, F.; Zink, J. I. Synthesis of Biomolecule-Modified Mesoporous Silica Nanoparticles for Targeted Hydrophobic Drug Delivery to Cancer Cells. *Small* **2011**, *7* (13), 1816–1826. https://doi.org/10.1002/smll.201002300.

(179) Lu, J.; Li, Z.; Zink, J. I.; Tamanoi, F. In Vivo Tumor Suppression Efficacy of Mesoporous Silica Nanoparticles-Based Drug-Delivery System: Enhanced Efficacy by Folate Modification. *Nanomedicine Nanotechnology, Biol. Med.* **2012**, *8* (2), 212–220. https://doi.org/10.1016/j.nano.2011.06.002.

(180) Kumar, A.; Ma, H.; Zhang, X.; Huang, K.; Jin, S.; Liu, J.; Wei, T.; Cao, W.; Zou, G.; Liang, X. J. Gold Nanoparticles Functionalized with Therapeutic and Targeted Peptides for Cancer Treatment. *Biomaterials* **2012**, *33* (4), 1180–1189. https://doi.org/10.1016/j.biomaterials.2011.10.058.

(181) Arruebo, M.; Fernández-Pacheco, R.; Ibarra, M. R.; Santamaría, J. Magnetic Nanoparticles for Drug Delivery. **2007**, *2* (3), 22–32.

(182) Chen, F. H.; Zhang, L. M.; Chen, Q. T.; Zhang, Y.; Zhang, Z. J. Synthesis of a Novel Magnetic Drug Delivery System Composed of Doxorubicin-Conjugated Fe3O4 Nanoparticle Cores and a PEG-Functionalized Porous Silica Shell. *Chem. Commun.* **2010**, *46* (45), 8633–8635. https://doi.org/10.1039/c0cc02577a.

(183) Wagstaff, A. J.; Brown, S. D.; Holden, M. R.; Craig, G. E.; Plumb, J. A.; Brown, R. E.; Schreiter, N.; Chrzanowski, W.; Wheate, N. J. Cisplatin Drug Delivery Using Gold-Coated Iron Oxide Nanoparticles for Enhanced Tumour Targeting with External Magnetic Fields. *Inorganica Chim. Acta* **2012**, *393*, 328–333. https://doi.org/10.1016/j.ica.2012.05.012.

(184) Rieter, W. J.; Pott, K. M.; Taylor, K. M. L.; Lin, W. Nanoscale Coordination Polymers for Platinum-Based Anticancer Drug Delivery. *J. Am. Chem. Soc.* **2008**, *130* (35), 11584–11585. https://doi.org/10.1021/ja803383k.

(185) Sun, Y.; Mayers, B. T.; Xia, Y. Template-Engaged Replacement Reaction: A One-Step Approach to the Large-Scale Synthesis of Metal Nanostructures with Hollow Interiors. *Nano Lett.* **2002**, *2* (5), 481–485. https://doi.org/10.1021/nl025531v.

(186) Chen, M. L.; He, Y. J.; Chen, X. W.; Wang, J. H. Quantum Dots Conjugated with Fe3O4-Filled Carbon Nanotubes for Cancer-Targeted Imaging and Magnetically Guided Drug Delivery. *Langmuir* **2012**, *28* (47), 16469–16476. https://doi.org/10.1021/la303957y.

(187) Probst, C. E.; Zrazhevskiy, P.; Bagalkot, V.; Gao, X. Quantum Dots as a Platform for Nanoparticle Drug Delivery Vehicle Design. *Advanced Drug Delivery Reviews*. Elsevier B.V. 2013, pp 703–718. https://doi.org/10.1016/j.addr.2012.09.036.

(188) Sahithi, K.; Swetha, M.; Ramasamy, K.; Srinivasan, N.; Selvamurugan, N. Polymeric Composites Containing Carbon Nanotubes for Bone Tissue Engineering. *International Journal of Biological Macromolecules*. Elsevier April 1, 2010, pp 281–283. https://doi.org/10.1016/j.ijbiomac.2010.01.006.

(189) Bianco, A.; Kostarelos, K.; Prato, M. Applications of Carbon Nanotubes in Drug Delivery. *Current Opinion in Chemical Biology*. Curr Opin Chem Biol December 2005, pp 674–679. https://doi.org/10.1016/j.cbpa.2005.10.005.

(190) Meng, L.; Zhang, X.; Lu, Q.; Fei, Z.; Dyson, P. J. Single Walled Carbon Nanotubes as Drug Delivery Vehicles: Targeting Doxorubicin to Tumors. *Biomaterials* **2012**, *33* (6), 1689–1698. https://doi.org/10.1016/j.biomaterials.2011.11.004.

(191) Liu, Z.; Chen, K.; Davis, C.; Sherlock, S.; Cao, Q.; Chen, X.; Dai, H. Drug Delivery with Carbon Nanotubes for in Vivo Cancer Treatment. *Cancer Res.* **2008**, *68* (16), 6652–6660. https://doi.org/10.1158/0008-5472.CAN-08-1468.

(192) Zhao, J.; Castranova, V. Toxicology of Nanomaterials Used in Nanomedicine. *Journal of Toxicology and Environmental Health - Part B: Critical Reviews*. J Toxicol Environ Health B Crit Rev 2011, pp 593–632. https://doi.org/10.1080/10937404.2011.615113.

(193) Maeda, H.; Nakamura, H.; Fang, J. The EPR Effect for Macromolecular Drug

Delivery to Solid Tumors: Improvement of Tumor Uptake, Lowering of Systemic Toxicity, and Distinct Tumor Imaging in Vivo. *Advanced Drug Delivery Reviews*. Adv Drug Deliv Rev January 2013, pp 71–79. https://doi.org/10.1016/j.addr.2012.10.002.

(194) Jain, R. K.; Stylianopoulos, T. Delivering Nanomedicine to Solid Tumors. *Nature Reviews Clinical Oncology*. Nat Rev Clin Oncol November 2010, pp 653–664. https://doi.org/10.1038/nrclinonc.2010.139.

(195) Hobbs, S. K.; Monsky, W. L.; Yuan, F.; Roberts, W. G.; Griffith, L.; Torchilin, V. P.; Jain, R. K. Regulation of Transport Pathways in Tumor Vessels: Role of Tumor Type and Microenvironment. *Proc. Natl. Acad. Sci. U. S. A.* **1998**, *95* (8), 4607–4612. https://doi.org/10.1073/pnas.95.8.4607.

(196) Bertrand, N.; Wu, J.; Xu, X.; Kamaly, N.; Farokhzad, O. C. Cancer Nanotechnology: The Impact of Passive and Active Targeting in the Era of Modern Cancer Biology. *Advanced Drug Delivery Reviews*. Adv Drug Deliv Rev 2014, pp 2–25. https://doi.org/10.1016/j.addr.2013.11.009.

(197) Rosenblum, D.; Joshi, N.; Tao, W.; Karp, J. M.; Peer, D. Progress and Challenges towards Targeted Delivery of Cancer Therapeutics. *Nature Communications*. Nature Publishing Group December 1, 2018, pp 1–12. https://doi.org/10.1038/s41467-018-03705-y.

(198) Byrne, J. D.; Betancourt, T.; Brannon-Peppas, L. Active Targeting Schemes for Nanoparticle Systems in Cancer Therapeutics. *Advanced Drug Delivery Reviews*. Adv Drug Deliv Rev December 14, 2008, pp 1615–1626. https://doi.org/10.1016/j.addr.2008.08.005.

(199) Mout, R.; Moyano, D. F.; Rana, S.; Rotello, V. M. Surface Functionalization of Nanoparticles for Nanomedicine. *Chemical Society Reviews*. Chem Soc Rev April 7, 2012, pp 2539–2544. https://doi.org/10.1039/c2cs15294k.

(200) Weissleder, R.; Kelly, K.; Sun, E. Y.; Shtatland, T.; Josephson, L. Cell-Specific Targeting of Nanoparticles by Multivalent Attachment of Small Molecules. *Nat. Biotechnol.* **2005**, *23* (11), 1418–1423. https://doi.org/10.1038/nbt1159.

(201) Peer, D.; Karp, J. M.; Hong, S.; Farokhzad, O. C.; Margalit, R.; Langer, R. Nanocarriers as an Emerging Platform for Cancer Therapy. *Nature Nanotechnology*. Nat Nanotechnol December 2007, pp 751–760. https://doi.org/10.1038/nnano.2007.387.

(202) Gao, J.; Feng, S. S.; Guo, Y. Antibody Engineering Promotes Nanomedicine for Cancer Treatment. *Nanomedicine*. Future Medicine Ltd London, UK October 1, 2010, pp 1141–1145. https://doi.org/10.2217/nnm.10.94.

(203) Taheri, A.; Dinarvand, R.; Atyabi, F.; Ghahremani, M. H.; Ostad, S. N. Trastuzumab Decorated Methotrexate-Human Serum Albumin Conjugated Nanoparticles for Targeted Delivery to HER2 Positive Tumor Cells. *Eur. J. Pharm. Sci.* **2012**, *47* (2), 331–340. https://doi.org/10.1016/j.ejps.2012.06.016.

(204) Wang, L.; Su, W.; Liu, Z.; Zhou, M.; Chen, S.; Chen, Y.; Lu, D.; Liu, Y.; Fan, Y.; Zheng, Y.; et al. CD44 Antibody-Targeted Liposomal Nanoparticles for Molecular Imaging and Therapy of Hepatocellular Carcinoma. *Biomaterials* **2012**, *33* (20), 5107–5114. https://doi.org/10.1016/j.biomaterials.2012.03.067.

(205) Abdelghany, S. M.; Schmid, D.; Deacon, J.; Jaworski, J.; Fay, F.; McLaughlin, K. M.; Gormley, J. A.; Burrows, J. F.; Longley, D. B.; Donnelly, R. F.; et al. Enhanced Antitumor Activity of the Photosensitizer Meso -Tetra(N -Methyl-4-Pyridyl) Porphine Tetra Tosylate through Encapsulation in Antibody-Targeted Chitosan/Alginate Nanoparticles. *Biomacromolecules* **2013**, *14* (2), 302–310. https://doi.org/10.1021/bm301858a.

(206) Molek, P.; Strukelj, B.; Bratkovic, T. Peptide Phage Display as a Tool for Drug Discovery: Targeting Membrane Receptors. *Molecules*. Molecules January 2011, pp 857–887. https://doi.org/10.3390/molecules16010857.

(207) Pan, L.; He, Q.; Liu, J.; Chen, Y.; Ma, M.; Zhang, L.; Shi, J. Nuclear-Targeted Drug Delivery of Tat Peptide-Conjugated Monodisperse Mesoporous Silica Nanoparticles. *J. Am. Chem. Soc.* **2012**, *134* (13), 5722–5725. https://doi.org/10.1021/ja211035w.

(208) Shroff, K.; Pearce, T. R.; Kokkoli, E. Peptide Targeted Lipid Nanoparticles for

Anticancer Drug Delivery. *Advanced Materials*. Adv Mater July 24, 2012, pp 3803–3822. https://doi.org/10.1002/adma.201200832.

(209) Shi, J.; Xiao, Z.; Kamaly, N.; Farokhzad, O. C. Self-Assembled Targeted Nanoparticles: Evolution of Technologies and Bench to Bedside Translation. *Accounts of Chemical Research*. Acc Chem Res October 18, 2011, pp 1123–1134. https://doi.org/10.1021/ar200054n.

(210) Kamaly, N.; Xiao, Z.; Valencia, P. M.; Radovic-Moreno, A. F.; Farokhzad, O. C. Targeted Polymeric Therapeutic Nanoparticles: Design, Development and Clinical Translation. *Chemical Society Reviews*. Chem Soc Rev April 7, 2012, pp 2971–3010. https://doi.org/10.1039/c2cs15344k.

(211) Wang, J.; Tian, S.; Petros, R. A.; Napier, M. E.; Desimone, J. M. The Complex Role of Multivalency in Nanoparticles Targeting the Transferrin Receptor for Cancer Therapies. *J. Am. Chem. Soc.* **2010**, *132* (32), 11306–11313. https://doi.org/10.1021/ja1043177.

(212) Mammen, M.; Choi, S.-K.; Whitesides, G. M. Polyvalent Interactions in Biological Systems: Implications for Design and Use of Multivalent Ligands and Inhibitors. *Angew. Chemie Int. Ed.* **1998**, *37* (20), 2754–2794. https://doi.org/10.1002/(sici)1521-3773(19981102)37:20<2754::aid-anie2754>3.0.co;2-3.

(213) Wu, Y.; Phillips, J. A.; Liu, H.; Yang, R.; Tan, W. Carbon Nanotubes Protect DNA Strands during Cellular Delivery. *ACS Nano* **2008**, *2* (10), 2023–2028. https://doi.org/10.1021/nn800325a.

(214) Mukherjee, S.; Ghosh, R. N.; Maxfield, F. R. Endocytosis. *Physiological Reviews*. American Physiological Society 1997, pp 759–803. https://doi.org/10.1152/physrev.1997.77.3.759.

(215) Stefanick, J. F.; Ashley, J. D.; Kiziltepe, T.; Bilgicer, B. A Systematic Analysis of Peptide Linker Length and Liposomal Polyethylene Glycol Coating on Cellular Uptake of Peptide-Targeted Liposomes. *ACS Nano* **2013**, *7* (4), 2935–2947. https://doi.org/10.1021/nn305663e.

(216) Elias, D. R.; Poloukhtine, A.; Popik, V.; Tsourkas, A. Effect of Ligand Density, Receptor Density, and Nanoparticle Size on Cell Targeting. *Nanomedicine Nanotechnology, Biol. Med.* **2013**, *9* (2), 194–201. https://doi.org/10.1016/j.nano.2012.05.015.

(217) Rizvi, S. A. A.; Saleh, A. M. Applications of Nanoparticle Systems in Drug Delivery Technology. *Saudi Pharmaceutical Journal*. Elsevier B.V. January 1, 2018, pp 64–70. https://doi.org/10.1016/j.jsps.2017.10.012.

(218) Moradi, E.; Vllasaliu, D.; Garnett, M.; Falcone, F.; Stolnik, S. Ligand Density and Clustering Effects on Endocytosis of Folate Modified Nanoparticles. *RSC Adv.* **2012**, *2* (7), 3025. https://doi.org/10.1039/c2ra01168a.

(219) Geng, Y.; Dalhaimer, P.; Cai, S.; Tsai, R.; Tewari, M.; Minko, T.; Discher, D. E. Shape Effects of Filaments versus Spherical Particles in Flow and Drug Delivery. *Nat. Nanotechnol.* **2007**, *2* (4), 249–255. https://doi.org/10.1038/nnano.2007.70.

(220) Petros, R. A.; Desimone, J. M. Strategies in the Design of Nanoparticles for Therapeutic Applications. *Nature Reviews Drug Discovery*. Nat Rev Drug Discov August 2010, pp 615–627. https://doi.org/10.1038/nrd2591.

(221) Vincent, A.; Babu, S.; Heckert, E.; Dowding, J.; Hirst, S. M.; Inerbaev, T. M.; Self, W. T.; Reilly, C. M.; Masunov, A. E.; Rahman, T. S.; et al. Protonated Nanoparticle Surface Governing Ligand Tethering and Cellular Targeting. *ACS Nano* **2009**, *3* (5), 1203–1211. https://doi.org/10.1021/nn9000148.

(222) Patil, Y. B.; Toti, U. S.; Khdair, A.; Ma, L.; Panyam, J. Single-Step Surface Functionalization of Polymeric Nanoparticles for Targeted Drug Delivery. *Biomaterials* **2009**, *30* (5), 859–866. https://doi.org/10.1016/j.biomaterials.2008.09.056.

(223) Gu, F.; Zhang, L.; Teply, B. A.; Mann, N.; Wang, A.; Radovic-Moreno, A. F.; Langer, R.; Farokhzad, O. C. Precise Engineering of Targeted Nanoparticles by Using Self-Assembled Biointegrated Block Copolymers. *Proc. Natl. Acad. Sci. U. S. A.* **2008**, *105* (7), 2586–2591. https://doi.org/10.1073/pnas.0711714105.

(224) Wu, J.; Chu, C. C. Block Copolymer of Poly(Ester Amide) and Polyesters: Synthesis, Characterization, and in Vitro Cellular Response. *Acta Biomater.* **2012**, *8* (12), 4314–4323. https://doi.org/10.1016/j.actbio.2012.07.027.

(225) Moghimi SM, Hunter AC, M. J. Long-Circulating and Target-Specific Nanoparticles: Theory to Practice. *Pharmacol Rev.* **2001**, *53* (2), 283–318.

(226) Stoddart, A. Corona Creation. *Nat. Mater.* **2013**, *12* (11), 946–946. https://doi.org/10.1038/nmat3799.

(227) Lynch, I.; Salvati, A.; Dawson, K. A. Protein-Nanoparticle Interactions: What Does the Cell See? *Nature Nanotechnology*. Nature Publishing Group 2009, pp 546–547. https://doi.org/10.1038/nnano.2009.248.

(228) Oh, J. Y.; Kim, H. S.; Palanikumar, L.; Go, E. M.; Jana, B.; Park, S. A.; Kim, H. Y.; Kim, K.; Seo, J. K.; Kwak, S. K.; et al. Cloaking Nanoparticles with Protein Corona Shield for Targeted Drug Delivery. *Nat. Commun.* **2018**, *9* (1), 1–9. https://doi.org/10.1038/s41467-018-06979-4.

(229) Thiele, L.; Diederichs, J. E.; Reszka, R.; Merkle, H. P.; Walter, E. Competitive Adsorption of Serum Proteins at Microparticles Affects Phagocytosis by Dendritic Cells. *Biomaterials* **2003**, *24* (8), 1409–1418. https://doi.org/10.1016/S0142-9612(02)00525-2.

(230) Karmali, P. P.; Simberg, D. Interactions of Nanoparticles with Plasma Proteins: Implication on Clearance and Toxicity of Drug Delivery Systems. *Expert Opinion on Drug Delivery*. Expert Opin Drug Deliv March 2011, pp 343–357. https://doi.org/10.1517/17425247.2011.554818.

(231) Salvati, A.; Pitek, A. S.; Monopoli, M. P.; Prapainop, K.; Bombelli, F. B.; Hristov, D. R.; Kelly, P. M.; Åberg, C.; Mahon, E.; Dawson, K. A. Transferrin-Functionalized Nanoparticles Lose Their Targeting Capabilities When a Biomolecule Corona Adsorbs on the Surface. *Nat. Nanotechnol.* **2013**, *8* (2), 137–143. https://doi.org/10.1038/nnano.2012.237.

(232) Moghimi, S. M.; Hunter, A. C. Poloxamers and Poloxamines in Nanoparticle Engineering and Experimental Medicine. *Trends in Biotechnology*. Trends

Biotechnol October 1, 2000, pp 412–420. https://doi.org/10.1016/S0167-7799(00)01485-2.

(233) Moghimi, S. M.; Muir, I. S.; Illum, L.; Davis, S. S.; Kolb-Bachofen, V. Coating Particles with a Block Co-Polymer (Poloxamine-908) Suppresses Opsonization but Permits the Activity of Dysopsonins in the Serum. *BBA - Mol. Cell Res.* **1993**, *1179* (2), 157–165. https://doi.org/10.1016/0167-4889(93)90137-E.

(234) Owens, D. E.; Peppas, N. A. Opsonization, Biodistribution, and Pharmacokinetics of Polymeric Nanoparticles. *International Journal of Pharmaceutics*. Int J Pharm January 3, 2006, pp 93–102. https://doi.org/10.1016/j.ijpharm.2005.10.010.

(235) Abuchowski, A.; Van Es, T.; Palczuk, N. C.; Davis, F. F. Alteration of Immunological Properties of Bovine Serum Albumin by Covalent Attachment of Polyethylene Glycol. *J. Biol. Chem.* **1977**, *252* (11), 3578–3581.

(236) Perry, J. L.; Reuter, K. G.; Kai, M. P.; Herlihy, K. P.; Jones, S. W.; Luft, J. C.; Napier, M.; Bear, J. E.; Desimone, J. M. PEGylated PRINT Nanoparticles: The Impact of PEG Density on Protein Binding, Macrophage Association, Biodistribution, and Pharmacokinetics. *Nano Lett.* **2012**, *12* (10), 5304–5310. https://doi.org/10.1021/nl302638g.

(237) Lee, H. Molecular Dynamics Studies of PEGylated Single-Walled Carbon Nanotubes: The Effect of PEG Size and Grafting Density. *J. Phys. Chem. C* **2013**, *117* (49), 26334–26341. https://doi.org/10.1021/jp4093749.

(238) DiMasi, J. A.; Hansen, R. W.; Grabowski, H. G. The Price of Innovation: New Estimates of Drug Development Costs. *J. Health Econ.* **2003**, *22* (2), 151–185. https://doi.org/10.1016/S0167-6296(02)00126-1.

(239) Wang, A. Z.; Langer, R.; Farokhzad, O. C. Nanoparticle Delivery of Cancer Drugs. *Annu. Rev. Med.* **2012**, *63* (1), 185–198. https://doi.org/10.1146/annurev-med-040210-162544.

(240) Wang, R.; Billone, P. S.; Mullett, W. M. An Overview of Cancer Nanomedicine on the Market and in Clinical Trials. *J. Coast. Life Med.* **2015**, *3* (6). https://doi.org/10.12980/JCLM.3.2015JCLM-2015-0018.

(241) Hofheinz, R. D.; Gnad-Vogt, S. U.; Beyer, U.; Hochhaus, A. Liposomal Encapsulated Anti-Cancer Drugs. *Anti-Cancer Drugs*. Anticancer Drugs August 2005, pp 691–707. https://doi.org/10.1097/01.cad.0000167902.53039.5a.

(242) Miele, E.; Spinelli, G. P.; Miele, E.; Tomao, F.; Tomao, S. Albumin-Bound Formulation of Paclitaxel (Abraxane® ABI-007) in the Treatment of Breast Cancer. *International Journal of Nanomedicine*. Int J Nanomedicine 2009, pp 99–105. https://doi.org/10.2147/ijn.s3061.

(243) Kim, T. Y.; Kim, D. W.; Chung, J. Y.; Shin, S. G.; Kim, S. C.; Heo, D. S.; Kim, N. K.; Bang, Y. J. Phase I and Pharmacokinetic Study of Genexol-PM, a Cremophor-Free, Polymeric Micelle-Formulated Paclitaxel, in Patients with Advanced Malignancies. *Clin. Cancer Res.* **2004**, *10* (11), 3708–3716. https://doi.org/10.1158/1078-0432.CCR-03-0655.

(244) Alexander, L. Micro-Particles as Cellular Delivery Devices, The University of Edinburgh, 2009.

(245) Spicer, C. D.; Jumeaux, C.; Gupta, B.; Stevens, M. M. Peptide and Protein Nanoparticle Conjugates: Versatile Platforms for Biomedical Applications. *Chemical Society Reviews*. Royal Society of Chemistry May 21, 2018, pp 3574–3620. https://doi.org/10.1039/c7cs00877e.

(246) Tsakiridis, A.; Alexander, L. M.; Gennet, N.; Sanchez-Martin, R. M.; Livigni, A.; Li, M.; Bradley, M.; Brickman, J. M. Microsphere-Based Tracing and Molecular Delivery in Embryonic Stem Cells. *Biomaterials* **2009**, *30* (29), 5853–5861. https://doi.org/10.1016/j.biomaterials.2009.06.024.

(247) Alexander, L. M.; Pernagallo, S.; Livigni, A.; Sánchez-Martín, R. M.; Brickman, J. M.; Bradley, M. Investigation of Microsphere-Mediated Cellular Delivery by Chemical, Microscopic and Gene Expression Analysis. *Mol. Biosyst.* **2010**, *6* (2), 399–409. https://doi.org/10.1039/b914428e.

(248) Gennet, N.; Alexander, L. M.; Sánchez-Martín, R. M.; Behrendt, J. M.; Sutherland, A. J.; Brickman, J. M.; Bradley, M.; Li, M. Microspheres as a Vehicle for Biomolecule Delivery to Neural Stem Cells. *N. Biotechnol.* **2009**, *25* (6), 442–

449. https://doi.org/10.1016/j.nbt.2009.05.006.

(249) Pietrovito, L.; Cano-Cortés, V.; Gamberi, T.; Magherini, F.; Bianchi, L.; Bini, L.; Sánchez-Martín, R. M.; Fasano, M.; Modesti, A. Cellular Response to Empty and Palladium-Conjugated Amino-Polystyrene Nanospheres Uptake: A Proteomic Study. *Proteomics* **2015**, *15* (1), 34–43. https://doi.org/10.1002/pmic.201300423.

(250) Sánchez-Martín, R. M.; Cuttle, M.; Mittoo, S.; Bradley, M. Microsphere-Based Real-Time Calcium Sensing. *Angew. Chemie - Int. Ed.* **2006**, *45* (33), 5472–5474. https://doi.org/10.1002/anie.200601242.

(251) Bradley, M.; Alexander, L.; Duncan, K.; Chennaoui, M.; Jones, A. C.; Sánchez-Martín, R. M. PH Sensing in Living Cells Using Fluorescent Microspheres. *Bioorganic Med. Chem. Lett.* **2008**, *18* (1), 313–317. https://doi.org/10.1016/j.bmcl.2007.10.075.

(252) Bradley, M.; Alexander, L.; Sanchez-Martin, R. M. Cellular Uptake of Fluorescent Labelled Biotin-Streptavidin Microspheres. In *Journal of Fluorescence*; J Fluoresc, 2008; Vol. 18, pp 733–739. https://doi.org/10.1007/s10895-008-0334-1.

(253) Alexander, L. M.; Sanchez-Martín, R. M.; Bradley, M. Knocking (Anti)-Sense into Cells: The Microsphere Approach to Gene Silencing. *Bioconjug. Chem.* **2009**, *20* (3), 422–426. https://doi.org/10.1021/bc800529r.

(254) Cardenas-Maestre, J. M.; Sanchez-Martin, R. M. Efficient Solid Phase Strategy for Preparation of Modified Xanthene Dyes for Biolabelling. *Org. Biomol. Chem.* **2011**, *9* (6), 1720–1722. https://doi.org/10.1039/c0ob00875c.

(255) Sanchez-Martin, R. M.; Alexander, L.; Muzerelle, M.; Cardenas-Maestre, J. M.; Tsakiridis, A.; Brickman, J. M.; Bradley, M. Microsphere-Mediated Protein Delivery into Cells. *ChemBioChem* **2009**, *10* (9), 1453–1456. https://doi.org/10.1002/cbic.200900136.

(256) Borger, J. G.; Cardenas-Maestre, J. M.; Zamoyska, R.; Sanchez-Martin, R. M. Novel Strategy for Microsphere-Mediated DNA Transfection. *Bioconjug. Chem.* **2011**, *22* (10), 1904–1908. https://doi.org/10.1021/bc200289n.

(257) Yusop, R. M.; Unciti-Broceta, A.; Johansson, E. M. V.; Sánchez-Martín, R. M.; Bradley, M. Palladium-Mediated Intracellular Chemistry. *Nat. Chem.* **2011**, *3* (3), 239–243. https://doi.org/10.1038/nchem.981.

(258) Cárdenas-Maestre, J. M.; Pérez-Lõpez, A. M.; Bradley, M.; Sánchez-Martín, R. M. Microsphere-Based Intracellular Sensing of Caspase-3/7 in Apoptotic Living Cells. *Macromol. Biosci.* **2014**, *14* (7), 923–928. https://doi.org/10.1002/mabi.201300525.

(259) Madaan, V.; Chanana, A.; Kataria, M. K.; Bilandi, A. EMULSION TECHNOLOGY AND RECENT TRENDS IN EMULSION APPLICATIONS. *Int. Res. J. Pharm.* **2014**, *5* (7), 533–542. https://doi.org/10.7897/2230-8407.0507108.

(260) Fast, J. P.; Mecozzi, S. Nanoemulsions for Intravenous Drug Delivery. In *Nanotechnology in Drug Delivery*; Springer New York, 2009; pp 461–489. https://doi.org/10.1007/978-0-387-77668-2_15.

(261) Solè, I.; Maestro, A.; Pey, C. M.; González, C.; Solans, C.; Gutiérrez, J. M. Nano-Emulsions Preparation by Low Energy Methods in an Ionic Surfactant System. *Colloids Surfaces A Physicochem. Eng. Asp.* **2006**, *288* (1–3), 138–143. https://doi.org/10.1016/j.colsurfa.2006.02.013.

(262) Mason, T. G.; Wilking, J. N.; Meleson, K.; Chang, C. B.; Graves, S. M. Nanoemulsions: Formation, Structure, and Physical Properties. *J. Phys. Condens. Matter* **2007**, *19* (7), 079001. https://doi.org/10.1088/0953-8984/19/7/079001.

(263) Anton, N.; Vandamme, T. F. The Universality of Low-Energy Nano-Emulsification. *Int. J. Pharm.* **2009**, *377* (1–2), 142–147. https://doi.org/10.1016/j.ijpharm.2009.05.014.

(264) Tadros, T.; Izquierdo, P.; Esquena, J.; Solans, C. Formation and Stability of Nano-Emulsions. *Adv. Colloid Interface Sci.* **2004**, *108–109*, 303–318. https://doi.org/10.1016/j.cis.2003.10.023.

(265) Izquierdo, P.; Esquena, J.; Tadros, T. F.; Dederen, C.; Garcia, M. J.; Azemar, N.; Solans, C. Formation and Stability of Nano-Emulsions Prepared Using the Phase Inversion Temperature Method. *Langmuir* **2002**, *18* (1), 26–30.

https://doi.org/10.1021/la010808c.

(266) Floyd, A. G. Top Ten Considerations in the Development of Parenteral Emulsions. *Pharmaceutical Science and Technology Today*. Pharm Sci Technolo Today April 1, 1999, pp 134–143. https://doi.org/10.1016/S1461-5347(99)00141-8.

(267) Driscoll, D. F.; Ling, P. R.; Bistrian, B. R. Pharmacopeial Compliance of Fish Oil-Containing Parenteral Lipid Emulsion Mixtures: Globule Size Distribution (GSD) and Fatty Acid Analyses. *Int. J. Pharm.* **2009**, *379* (1–2), 125–130. https://doi.org/10.1016/j.ijpharm.2009.06.021.

(268) Wooster, T. J.; Golding, M.; Sanguansri, P. Impact of Oil Type on Nanoemulsion Formation and Ostwald Ripening Stability. *Langmuir* **2008**, *24* (22), 12758–12765. https://doi.org/10.1021/la801685v.

(269) Izquierdo, P.; Esquena, J.; Tadros, T. F.; Dederen, J. C.; Feng, J.; Garcia-Celma, M. J.; Azemar, N.; Solans, C. Phase Behavior and Nano-Emulsion Formation by the Phase Inversion Temperature Method. *Langmuir* **2004**, *20* (16), 6594–6598. https://doi.org/10.1021/la049566h.

(270) Piacentini, E. Emulsion. In *Encyclopedia of Membranes*; Springer Berlin Heidelberg, 2014; pp 1–4. https://doi.org/10.1007/978-3-642-40872-4_1066-1.

(271) Jumaa, M.; Müller, B. W. Parenteral Emulsions Stabilized with a Mixture of Phospholipids and PEG-660-12-Hydroxy-Stearate: Evaluation of Accelerated and Long-Term Stability. *Eur. J. Pharm. Biopharm.* **2002**, *54* (2), 207–212. https://doi.org/10.1016/S0939-6411(02)00057-7.

(272) Young, T. J.; Johnston, K. P.; Pace, G. W.; Mishra, A. K. Phospholipid-Stabilized Nanoparticles of Cyclosporine A by Rapid Expansion from Supercritical to Aqueous Solution. *AAPS PharmSciTech* **2004**, *5* (1). https://doi.org/10.1208/pt050111.

(273) Ortega-Vinuesa, J. L.; Bastos-González, D. A Review of Factors Affecting the Performances of Latex Agglutination Tests. *J. Biomater. Sci. Polym. Ed.* **2001**, *12* (4), 379–408. https://doi.org/10.1163/156856201750195289.

(274) Hidalgo-Álvarez, R.; Martín, A.; Fernández, A.; Bastos, D.; Martínez, F.; De Las Nieves, F. J. Electrokinetic Properties, Colloidal Stability and Aggregation Kinetics of Polymer Colloids. *Advances in Colloid and Interface Science*. Elsevier September 2, 1996, pp 1–118. https://doi.org/10.1016/0001-8686(96)00297-7.

(275) López-León, T.; Carvalho, E. L. S.; Seijo, B.; Ortega-Vinuesa, J. L.; Bastos-González, D. Physicochemical Characterization of Chitosan Nanoparticles: Electrokinetic and Stability Behavior. *J. Colloid Interface Sci.* **2005**, *283* (2), 344–351. https://doi.org/10.1016/j.jcis.2004.08.186.

(276) Lazaridis, N.; Alexopoulos, A. H.; Chatzi, E. G.; Kiparissides, C. Steric Stabilization in Emulsion Polymerization Using Oligomeric Nonionic Surfactants. *Chem. Eng. Sci.* **1999**, *54* (15–16), 3251–3261. https://doi.org/10.1016/S0009-2509(98)00336-4.

(277) Mollet, H.; Grubenmann, A. Formulation Technology: Emulsions, Suspensions, Solid Forms. **2008**.

(278) Grigoriev, D. O.; Miller, R. Mono- and Multilayer Covered Drops as Carriers. *Current Opinion in Colloid and Interface Science*. February 2009, pp 48–59. https://doi.org/10.1016/j.cocis.2008.03.003.

(279) Porter, C. J. H.; Pouton, C. W.; Cuine, J. F.; Charman, W. N. Enhancing Intestinal Drug Solubilisation Using Lipid-Based Delivery Systems. *Advanced Drug Delivery Reviews*. Adv Drug Deliv Rev March 17, 2008, pp 673–691. https://doi.org/10.1016/j.addr.2007.10.014.

(280) Müller, R. H.; Schmidt, S.; Buttle, I.; Akkar, A.; Schmitt, J.; Brömer, S. SolEmuls® - Novel Technology for the Formulation of i.v. Emulsions with Poorly Soluble Drugs. *Int. J. Pharm.* **2004**, *269* (2), 293–302. https://doi.org/10.1016/j.ijpharm.2003.09.019.

(281) Cevc, G.; Vierl, U. Nanotechnology and the Transdermal Route. A State of the Art Review and Critical Appraisal. *Journal of Controlled Release*. J Control Release February 2010, pp 277–299. https://doi.org/10.1016/j.jconrel.2009.10.016.

(282) Souto, E. B.; Nayak, A. P.; Murthy, R. S. R. Lipid Nanoemulsions for Anti-Cancer Drug Therapy. *Pharmazie* **2011**, *66* (7), 473–478.

(283) Elsabahy, M.; Heo, G. S.; Lim, S. M.; Sun, G.; Wooley, K. L. Polymeric Nanostructures for Imaging and Therapy. *Chem. Rev.* **2015**, *115* (19), 10967–11011. https://doi.org/10.1021/acs.chemrev.5b00135.

(284) Lim, E. K.; Kim, T.; Paik, S.; Haam, S.; Huh, Y. M.; Lee, K. Nanomaterials for Theranostics: Recent Advances and Future Challenges. *Chem. Rev.* **2015**, *115* (1), 327–394. https://doi.org/10.1021/cr300213b.

(285) Ang, C. Y.; Tan, S. Y.; Teh, C.; Lee, J. M.; Wong, M. F. E.; Qu, Q.; Poh, L. Q.; Li, M.; Zhang, Y.; Korzh, V.; et al. Redox and PH Dual Responsive Polymer Based Nanoparticles for In Vivo Drug Delivery. *Small* **2017**, *13* (7), 1–10. https://doi.org/10.1002/smll.201602379.

(286) Ponzoni, M.; Curnis, F.; Brignole, C.; Bruno, S.; Guarnieri, D.; Sitia, L.; Marotta, R.; Sacchi, A.; Bauckneht, M.; Buschiazzo, A.; et al. Enhancement of Tumor Homing by Chemotherapy-Loaded Nanoparticles. *Small* **2018**, *14* (45). https://doi.org/10.1002/smll.201802886.

(287) Unciti-Broceta, A.; Díaz-Mochón, J. J.; Sánchez-Martín, R. M.; Bradley, M. The Use of Solid Supports to Generate Nucleic Acid Carriers. *Acc. Chem. Res.* **2012**, *45* (7), 1140–1152. https://doi.org/10.1021/ar200263c.

(288) Cardenas-Maestre, J. M.; Panadero-Fajardo, S.; Perez-Lopez, A. M.; Sanchez-Martin, R. M. Sulfhydryl Reactive Microspheres for the Efficient Delivery of Thiolated Bioactive Cargoes. *J. Mater. Chem.* **2011**, *21* (34), 12735–12743. https://doi.org/10.1039/c1jm11948f.

(289) Loos, C.; Syrovets, T.; Musyanovych, A.; Mailänder, V.; Landfester, K.; Ulrich Nienhaus, G.; Simmet, T. Functionalized Polystyrene Nanoparticles as a Platform for Studying Bio-Nano Interactions. *Beilstein J. Nanotechnol.* **2014**, *5* (1), 2403–2412. https://doi.org/10.3762/bjnano.5.250.

(290) Borger, J. G.; Cardenas-Maestre, J. M.; Zamoyska, R.; Sanchez-Martin, R. M. Novel Strategy for Microsphere-Mediated DNA Transfection. *Bioconjug. Chem.*

2011, *22* (10), 1904–1908. https://doi.org/10.1021/bc200289n.

(291) Yusop, R. M.; Unciti-Broceta, A.; Johansson, E. M. V.; Sánchez-Martín, R. M.; Bradley, M. Palladium-Mediated Intracellular Chemistry. *Nat. Chem.* **2011**, *3* (3), 239–243. https://doi.org/10.1038/nchem.981.

(292) Cárdenas-Maestre, J. M.; Pérez-Lõpez, A. M.; Bradley, M.; Sánchez-Martín, R. M. Microsphere-Based Intracellular Sensing of Caspase-3/7 in Apoptotic Living Cells. *Macromol. Biosci.* **2014**, *14* (7), 923–928. https://doi.org/10.1002/mabi.201300525.

(293) Altea-Manzano, P.; Unciti-Broceta, J. D.; Cano-Cortes, V.; Ruiz-Blas, M. P.; Valero-Griñan, T.; Diaz-Mochon, J. J.; Sanchez-Martin, R. Tracking Cell Proliferation Using a Nanotechnology-Based Approach. *Nanomedicine* **2017**, *12* (13), 1591–1605. https://doi.org/10.2217/nnm-2017-0118.

(294) Valero, T.; Delgado-González, A.; Unciti-Broceta, J. D.; Cano-Cortés, V.; Pérez-López, A. M.; Unciti-Broceta, A.; Sánchez Martín, R. M. Drug "Clicking" on Cell-Penetrating Fluorescent Nanoparticles for in Cellulo Chemical Proteomics. *Bioconjug. Chem.* **2018**, *29* (9), 3154–3160. https://doi.org/10.1021/acs.bioconjchem.8b00481.

(295) Naik, A.; Al-Zeheimi, N.; Bakheit, C. S.; Al Riyami, M.; Al Jarrah, A.; Al Moundhri, M. S.; Al Habsi, Z.; Basheer, M.; Adham, S. A. Neuropilin-1 Associated Molecules in the Blood Distinguish Poor Prognosis Breast Cancer: A Cross-Sectional Study. *Sci. Rep.* **2017**, *7* (1), 1–14. https://doi.org/10.1038/s41598-017-03280-0.

(296) Unciti-Broceta, A.; Johansson, E. M. V.; Yusop, R. M.; Sánchez-Martín, R. M.; Bradley, M. Synthesis of Polystyrene Microspheres and Functionalization with Pd0 Nanoparticles to Perform Bioorthogonal Organometallic Chemistry in Living Cells. *Nat. Protoc.* **2012**, *7* (6), 1207–1218. https://doi.org/10.1038/nprot.2012.052.

(297) Picon-Ruiz, M.; Pan, C.; Drews-Elger, K.; Jang, K.; Besser, A. H.; Zhao, D.; Morata-Tarifa, C.; Kim, M.; Ince, T. A.; Azzam, D. J.; et al. Interactions between Adipocytes and Breast Cancer Cells Stimulate Cytokine Production and Drive

Src/Sox2/MiR-302b-Mediated Malignant Progression. *Cancer Res.* **2016**, *76* (2), 491–504. https://doi.org/10.1158/0008-5472.CAN-15-0927.

(298) Unciti-Broceta, J. D.; Cano-Cortés, V.; Altea-Manzano, P.; Pernagallo, S.; Díaz-Mochón, J. J.; Sánchez-Martín, R. M. Number of Nanoparticles per Cell through a Spectrophotometric Method - A Key Parameter to Assess Nanoparticle-Based Cellular Assays. *Sci. Rep.* **2015**, *5* (March), 1–10. https://doi.org/10.1038/srep10091.

(299) Kaiser E, Colescott RL, Bossinger CD, C. P. Color Test for Detection of Free Terminal Amino Groups in the Solid-Phase Synthesis of Peptides. *Anal Biochem.* **1970**, *24* (2), 595–598. https://doi.org/10.1016/0003-2697(70)90146-6.

(300) FIELDS, G. B.; NOBLE, R. L. Solid Phase Peptide Synthesis Utilizing 9-fluorenylmethoxycarbonyl Amino Acids. *Int. J. Pept. Protein Res.* **1990**, *35* (3), 161–214. https://doi.org/10.1111/j.1399-3011.1990.tb00939.x.

(301) Díaz-Mochón, J. J.; Bialy, L.; Bradley, M. Full Orthogonality between Dde and Fmoc: The Direct Synthesis of PNA-Peptide Conjugates. *Org. Lett.* **2004**, *6* (7), 1127–1129. https://doi.org/10.1021/ol049905y.

(302) Barrie W. Bycroft, Weng C. Chan, S. R. C. and N. D. H. A Novel Lysine-Protecting Procedure for Continuous Flow Solid Phase Synthesis of Branched Peptides. *J. Chem. Soc., Chem. Commun.* **1993**, No. 9, 778–779. https://doi.org/10.1039/C39930000778.

(303) Yang, K.; Ma, Y. Q. Computer Simulation of the Translocation of Nanoparticles with Different Shapes across a Lipid Bilayer. *Nat. Nanotechnol.* **2010**, *5* (8), 579–583. https://doi.org/10.1038/nnano.2010.141.

(304) Thielbeer, F.; Johansson, E. M. V.; Chankeshwara, S. V.; Bradley, M. Influence of Spacer Length on the Cellular Uptake of Polymeric Nanoparticles. *Macromol. Biosci.* **2013**, *13* (6), 682–686. https://doi.org/10.1002/mabi.201200455.

(305) Smith, P. K.; Krohn, R. I.; Hermanson, G. T.; Mallia, A. K.; Gartner, F. H.; Provenzano, M. D.; Fujimoto, E. K.; Goeke, N. M.; Olson, B. J.; Klenk, D. C. Measurement of Protein Using Bicinchoninic Acid. *Anal. Biochem.* **1985**, *150* (1),

76–85. https://doi.org/10.1016/0003-2697(85)90442-7.

(306) Taherian, A.; Li, X.; Liu, Y.; Haas, T. A. Differences in Integrin Expression and Signaling within Human Breast Cancer Cells. *BMC Cancer* **2011**, *11*. https://doi.org/10.1186/1471-2407-11-293.

(307) Chalakur-Ramireddy, N. K. R.; Pakala, S. B. *Combined Drug Therapeutic Strategies for the Effective Treatment of Triple Negative Breast Cancer*; 2018; Vol. 38. https://doi.org/10.1042/BSR20171357.

(308) O'Brien J, Wilson I, Orton T, P. F. Investigation of the Alamar Blue (Resazurin) Fluorescent Dye for the Assessment of Mammalian Cell Cytotoxicity. *Eur J Biochem* **2000**, *267* (17), 5421–5426. https://doi.org/10.1046/j.1432-1327.2000.01606.x.

(309) Liu, P.; Qin, L.; Wang, Q.; Sun, Y.; Zhu, M.; Shen, M.; Duan, Y. CRGD-Functionalized MPEG-PLGA-PLL Nanoparticles for Imaging and Therapy of Breast Cancer. *Biomaterials* **2012**, *33* (28), 6739–6747. https://doi.org/10.1016/j.biomaterials.2012.06.008.

(310) Jin, G.; Feng, G.; Qin, W.; Tang, B. Z.; Liu, B.; Li, K. Multifunctional Organic Nanoparticles with Aggregation-Induced Emission (AIE) Characteristics for Targeted Photodynamic Therapy and RNA Interference Therapy. *Chem. Commun.* **2016**, *52* (13), 2752–2755. https://doi.org/10.1039/c5cc07818k.

(311) Minotti, G.; Menna, P.; Salvatorelli, E.; Cairo, G.; Gianni, L. Anthracyclines: Molecular Advances and Pharmacologie Developments in Antitumor Activity and Cardiotoxicity. *Pharmacol. Rev.* **2004**, *56* (2), 185–229. https://doi.org/10.1124/pr.56.2.6.

(312) Shafei, A.; El-Bakly, W.; Sobhy, A.; Wagdy, O.; Reda, A.; Aboelenin, O.; Marzouk, A.; El Habak, K.; Mostafa, R.; Ali, M. A.; et al. A Review on the Efficacy and Toxicity of Different Doxorubicin Nanoparticles for Targeted Therapy in Metastatic Breast Cancer. *Biomed. Pharmacother.* **2017**, *95* (June), 1209–1218. https://doi.org/10.1016/j.biopha.2017.09.059.

(313) Manchun, S.; Dass, C. R.; Sriamornsak, P. Targeted Therapy for Cancer Using PH-

Responsive Nanocarrier Systems. *Life Sci.* **2012**, *90* (11–12), 381–387. https://doi.org/10.1016/j.lfs.2012.01.008.

(314) Arpel, A.; Gamper, C.; Spenlé, C.; Fernandez, A.; Jacob, L.; Baumlin, N.; Laquerriere, P.; Orend, G.; Crémel, G.; Bagnard, D. Inhibition of Primary Breast Tumor Growth and Metastasis Using a Neuropilin-1 Transmembrane Domain Interfering Peptide. *Oncotarget* **2016**, *7* (34), 54723–54732. https://doi.org/10.18632/oncotarget.10101.

(315) Kumar, A.; Huo, S.; Zhang, X.; Liu, J.; Tan, A.; Li, S.; Jin, S.; Xue, X.; Zhao, Y.; Ji, T.; et al. Neuropilin-1-Targeted Gold Nanoparticles Enhance Therapeutic Efficacy of Platinum (IV) Drug For. *ACS Nano* **2014**, No. 5, 4205–4220.

(316) Fan, X.; Zhang, W.; Hu, Z.; Li, Z. Facile Synthesis of RGD-Conjugated Unimolecular Micelles Based on a Polyester Dendrimer for Targeting Drug Delivery. *J. Mater. Chem. B* **2017**, *5* (5), 1062–1072. https://doi.org/10.1039/C6TB02234K.

(317) Yang, M.; Yu, L.; Guo, R.; Dong, A.; Lin, C.; Zhang, J. A Modular Coassembly Approach to All-in-One Multifunctional Nanoplatform for Synergistic Codelivery of Doxorubicin and Curcumin. *Nanomaterials* **2018**, *8* (3), 1–18. https://doi.org/10.3390/nano8030167.

(318) Liu, X.; Si, J.; Zhang, Q.; Huang, Q.; Gu, D.; Yang, H.; Chen, X.; Shen, Y.; Sui, M. Functionalized Nanoparticles Efficiently Enhancing the Targeted Delivery, Tumor Penetration, and Anticancer Activity of 7-Ethyl-10-Hydroxycamptothecin. *Adv. Healthc. Mater.* **2018**, *7* (7), 1–12. https://doi.org/10.1002/adhm.201701140.

(319) Liu, H.; Shi, X.; Wu, D.; Kahsay Khshen, F.; Deng, L.; Dong, A.; Wang, W.; Zhang, J. Injectable, Biodegradable, Thermosensitive Nanoparticles-Aggregated Hydrogel with Tumor-Specific Targeting, Penetration, and Release for Efficient Postsurgical Prevention of Tumor Recurrence. *ACS Appl. Mater. Interfaces* **2019**, *11* (22), 19700–19711. https://doi.org/10.1021/acsami.9b01987.

(320) Wei, T.; Liu, J.; Ma, H.; Cheng, Q.; Huang, Y.; Zhao, J.; Huo, S.; Xue, X.; Liang, Z.; Liang, X. J. Functionalized Nanoscale Micelles Improve Drug Delivery for Cancer Therapy in Vitro and in Vivo. *Nano Lett.* **2013**, *13* (6), 2528–2534.

https://doi.org/10.1021/nl400586t.

(321) Escobedo, J. O.; Rusin, O.; Lim, S.; Strongin, R. M. NIR Dyes for Bioimaging Applications. *Curr. Opin. Chem. Biol.* **2010**, *14* (1), 64–70. https://doi.org/10.1016/j.cbpa.2009.10.022.

(322) Madureira, A. R.; Campos, D. A.; Fonte, P.; Nunes, S.; Reis, F.; Gomes, A. M.; Sarmento, B.; Pintado, M. M. Characterization of Solid Lipid Nanoparticles Produced with Carnauba Wax for Rosmarinic Acid Oral Delivery. *RSC Adv.* **2015**, *5* (29), 22665–22673. https://doi.org/10.1039/c4ra15802d.

(323) Lamprecht, A.; Bouligand, Y.; Benoit, J. P. New Lipid Nanocapsules Exhibit Sustained Release Properties for Amiodarone. *J. Control. Release* **2002**, *84* (1–2), 59–68. https://doi.org/10.1016/S0168-3659(02)00258-4.

(324) Ourique, A. F.; Pohlmann, A. R.; Guterres, S. S.; Beck, R. C. R. Tretinoin-Loaded Nanocapsules: Preparation, Physicochemical Characterization, and Photostability Study. *Int. J. Pharm.* **2008**, *352* (1–2), 1–4. https://doi.org/10.1016/j.ijpharm.2007.12.035.

(325) Singh, S.; Sharma, A.; Robertson, G. P. Realizing the Clinical Potential of Cancer Nanotechnology by Minimizing Toxicologic and Targeted Delivery Concerns. *Cancer Res.* **2012**, *72* (22), 5663–5668. https://doi.org/10.1158/0008-5472.CAN-12-1527.

(326) Camner, P.; Lundborg, M.; Låstbom, L.; Gerde, P.; Gross, N.; Jarstrand, C. Experimental and Calculated Parameters on Particle Phagocytosis by Alveolar Macrophages. *J. Appl. Physiol.* **2002**, *92* (6), 2608–2616. https://doi.org/10.1152/japplphysiol.01067.2001.

(327) Ogawara, K. I.; Furumoto, K.; Nagayama, S.; Minato, K.; Higaki, K.; Kai, T.; Kimura, T. Pre-Coating with Serum Albumin Reduces Receptor-Mediated Hepatic Disposition of Polystyrene Nanosphere: Implications for Rational Design of Nanoparticles. *J. Control. Release* **2004**, *100* (3), 451–455. https://doi.org/10.1016/j.jconrel.2004.07.028.

(328) Pignatta, S.; Orienti, I.; Falconi, M.; Teti, G.; Arienti, C.; Medri, L.; Zanoni, M.;

Carloni, S.; Zoli, W.; Amadori, D.; et al. Albumin Nanocapsules Containing Fenretinide: Pre-Clinical Evaluation of Cytotoxic Activity in Experimental Models of Human Non-Small Cell Lung Cancer. *Nanomedicine Nanotechnology, Biol. Med.* **2015**, *11* (2), 263–273. https://doi.org/10.1016/j.nano.2014.10.004.

(329) Bolling, C.; Graefe, T.; Lübbing, C.; Jankevicius, F.; Uktveris, S.; Cesas, A.; Meyer-Moldenhauer, W. H.; Starkmann, H.; Weigel, M.; Burk, K.; et al. Phase II Study of MTX-HSA in Combination with Cisplatin as First Line Treatment in Patients with Advanced or Metastatic Transitional Cell Carcinoma. *Invest. New Drugs* **2006**, *24* (6), 521–527. https://doi.org/10.1007/s10637-006-8221-6.

(330) Unger, C.; Häring, B.; Medinger, M.; Drevs, J.; Steinbild, S.; Kratz, F.; Mross, K. Phase I and Pharmacokinetic Study of the (6-Maleimidocaproyl)Hydrazone Derivative of Doxorubicin. *Clin. Cancer Res.* **2007**, *13* (16), 4858–4866. https://doi.org/10.1158/1078-0432.CCR-06-2776.

(331) Ibrahim, N. K.; Samuels, B.; Page, R.; Doval, D.; Patel, K. M.; Rao, S. C.; Nair, M. K.; Bhar, P.; Desai, N.; Hortobagyi, G. N. Multicenter Phase II Trial of ABI-007, an Albumin-Bound Paclitaxel, in Women with Metastatic Breast Cancer. *J. Clin. Oncol.* **2005**, *23* (25), 6019–6026. https://doi.org/10.1200/JCO.2005.11.013.

(332) Hsin-I Chang and Ming-Kung Yeh. Clinical Dev Liposome. *Int. J. Nanomed.* **2012**, *7*, 49–60. https://doi.org/http://dx.doi.org/10.2147/IJN.S26766.

(333) Thanki, K.; Gangwal, R. P.; Sangamwar, A. T.; Jain, S. Oral Delivery of Anticancer Drugs: Challenges and Opportunities. *J. Control. Release* **2013**, *170* (1), 15–40. https://doi.org/10.1016/j.jconrel.2013.04.020.

(334) Mora-Huertas, C. E.; Fessi, H.; Elaissari, A. Polymer-Based Nanocapsules for Drug Delivery. *Int. J. Pharm.* **2010**, *385* (1–2), 113–142. https://doi.org/10.1016/j.ijpharm.2009.10.018.

(335) Sánchez-Moreno, P.; Buzón, P.; Boulaiz, H.; Peula-García, J. M.; Ortega-Vinuesa, J. L.; Luque, I.; Salvati, A.; Marchal, J. A. Balancing the Effect of Corona on Therapeutic Efficacy and Macrophage Uptake of Lipid Nanocapsules. *Biomaterials* **2015**, *61*, 266–278.

https://doi.org/10.1016/j.biomaterials.2015.04.049.

(336) Fang, C.; Bhattarai, N.; Sun, C.; Zhang, M. Functionalized Nanoparticles with Long-Term Stability in Biological Media. *Small* **2009**, *5* (14), 1637–1641. https://doi.org/10.1002/smll.200801647.

(337) Walkey, C. D.; Olsen, J. B.; Guo, H.; Emili, A.; Chan, W. C. W. Nanoparticle Size and Surface Chemistry Determine Serum Protein Adsorption and Macrophage Uptake. *J. Am. Chem. Soc.* **2012**, *134* (4), 2139–2147. https://doi.org/10.1021/ja2084338.

(338) Zhang, S.; Li, J.; Lykotrafitis, G.; Bao, G.; Suresh, S. Size-Dependent Endocytosis of Nanoparticles. *Adv. Mater.* **2009**, *21* (4), 419–424. https://doi.org/10.1002/adma.200801393.

(339) Chithrani, B. D.; Ghazani, A. A.; Chan, W. C. W. Determining the Size and Shape Dependence of Gold Nanoparticle Uptake into Mammalian Cells. *Nano Lett.* **2006**, *6* (4), 662–668. https://doi.org/10.1021/nl052396o.

(340) Molina-Bolívar, J. A.; Galisteo-González, F. Olive-Oil Nanocapsules Stabilized by HSA: Influence of Processing Variables on Particle Properties. *J. Nanoparticle Res.* **2015**, *17* (10), 1–13. https://doi.org/10.1007/s11051-015-3192-1.

(341) Patel, A.; Hu, Y.; Tiwari, J. K.; Velikov, K. P. Synthesis and Characterisation of Zein-Curcumin Colloidal Particles. *Soft Matter* **2010**, *6* (24), 6192–6199. https://doi.org/10.1039/c0sm00800a.

(342) Srivastava, R. M.; Singh, S.; Dubey, S. K.; Misra, K.; Khar, A. Immunomodulatory and Therapeutic Activity of Curcumin. *Int. Immunopharmacol.* **2011**, *11* (3), 331–341. https://doi.org/10.1016/j.intimp.2010.08.014.

(343) Hamaguchi, T.; Ono, K.; Yamada, M. Curcumin and Alzheimer's Disease. *CNS Neurosci. Ther.* **2010**, *16* (5), 285–297. https://doi.org/10.1111/j.1755-5949.2010.00147.x.

(344) Liu J, Chen S, Lv L, Song L, Guo S, H. S. Recent Progress in Studying Curcumin and Its Nano-Preparations for Cancer Therapy. *Curr Pharm Des.* **2013**, *19* (11), 1974–

1993. https://doi.org/10.2174/1381612811319110003.

(345) Raffin Pohlmann, A.; Weiss, V.; Mertins, O.; Pesce da Silveira, N.; Stanisçuaski Guterres, S. Spray-Dried Indomethacin-Loaded Polyester Nanocapsules and Nanospheres: Development, Stability Evaluation and Nanostructure Models. *Eur. J. Pharm. Sci.* **2002**, *16* (4–5), 305–312. https://doi.org/10.1016/S0928-0987(02)00127-6.

(346) Abdel-Mottaleb, M. M. A.; Neumann, D.; Lamprecht, A. In Vitro Drug Release Mechanism from Lipid Nanocapsules (LNC). *Int. J. Pharm.* **2010**, *390* (2), 208–213. https://doi.org/10.1016/j.ijpharm.2010.02.001.

(347) Florence, A. T.; Hussain, N. Transcytosis of Nanoparticle and Dendrimer Delivery Systems: Evolving Vistas. *Adv. Drug Deliv. Rev.* **2001**, *50* (SUPPL. 1). https://doi.org/10.1016/S0169-409X(01)00184-3.

(348) Sánchez-Moreno, P.; Boulaiz, H.; Ortega-Vinuesa, J. L.; Peula-García, J. M.; Aránega, A. Novel Drug Delivery System Based on Docetaxel-Loaded Nanocapsules as a Therapeutic Strategy against Breast Cancer Cells. *Int. J. Mol. Sci.* **2012**, *13* (4), 4906–4919. https://doi.org/10.3390/ijms13044906.

(349) Kettler, K.; Veltman, K.; van de Meent, D.; van Wezel, A.; Hendriks, A. J. Cellular Uptake of Nanoparticles as Determined by Particle Properties, Experimental Conditions, and Cell Type. *Environ. Toxicol. Chem.* **2014**, *33* (3), 481–492. https://doi.org/10.1002/etc.2470.

(350) Sahu, A.; Kasoju, N.; Goswami, P.; Bora, U. Encapsulation of Curcumin in Pluronic Block Copolymer Micelles for Drug Delivery Applications. *J. Biomater. Appl.* **2011**, *25* (6), 619–639. https://doi.org/10.1177/0885328209357110.

(351) Anbharasi, V.; Cao, N.; Feng, S. S. Doxorubicin Conjugated to D-α-Tocopheryl Polyethylene Glycol Succinate and Folic Acid as a Prodrug for Targeted Chemotherapy. *J. Biomed. Mater. Res. - Part A* **2010**, *94* (3), 730–743. https://doi.org/10.1002/jbm.a.32734.

(352) Loong, H. H.; Chan, A. C. Y.; Wong, A. C. Y. Evolving Evidence of the Efficacy and Safety of Nab-Paclitaxel in the Treatment of Cancers with Squamous Histologies.

J. Cancer **2016**, *7* (3), 268–275. https://doi.org/10.7150/jca.12986.

(353) Wang, J.; Zhu, R.; Sun, D.; Sun, X.; Geng, Z.; Liu, H.; Wang, S. L. Intracellular Uptake of Curcumin-Loaded Solid Lipid Nanoparticles Exhibit Anti-Inflammatory Activities Superior to Those of Curcumin through the NF-KB Signaling Pathway. *J. Biomed. Nanotechnol.* **2015**, *11* (3), 403–415. https://doi.org/10.1166/jbn.2015.1925.

(354) Mahanta, S.; Paul, S. Stable Self-Assembly of Bovine α-Lactalbumin Exhibits Target-Specific Antiproliferative Activity in Multiple Cancer Cells. *ACS Appl. Mater. Interfaces* **2015**, *7* (51), 28177–28187. https://doi.org/10.1021/acsami.5b06076.

(355) Gelderblom, H.; Verweij, J.; Nooter, K.; Sparreboom, A. Cremophor EL: The Drawbacks and Advantages of Vehicle Selection for Drug Formulation. *Eur. J. Cancer* **2001**, *37* (13), 1590–1598. https://doi.org/10.1016/S0959-8049(01)00171-X.

(356) Muley, P.; Kumar, S.; El Kourati, F.; Kesharwani, S. S.; Tummala, H. Hydrophobically Modified Inulin as an Amphiphilic Carbohydrate Polymer for Micellar Delivery of Paclitaxel for Intravenous Route. *Int. J. Pharm.* **2016**, *500* (1–2), 32–41. https://doi.org/10.1016/j.ijpharm.2016.01.005.

(357) Sánchez-Moreno, P.; Ortega-Vinuesa, J. L.; Boulaiz, H.; Marchal, J. A.; Peula-García, J. M. Synthesis and Characterization of Lipid Immuno-Nanocapsules for Directed Drug Delivery: Selective Antitumor Activity against HER2 Positive Breast-Cancer Cells. *Biomacromolecules* **2013**, *14* (12), 4248–4259. https://doi.org/10.1021/bm401103t.

(358) He, Z.; Huang, J.; Xu, Y.; Zhang, X.; Teng, Y.; Huang, C.; Wu, Y.; Zhang, X.; Zhang, H.; Sun, W. Co-Delivery of Cisplatin and Paclitaxel by Folic Acid Conjugated Amphiphilic PEG-PLGA Copolymer Nanoparticles for the Treatment of Non-Small Lung Cancer. *Oncotarget* **2015**, *6* (39), 42150–42168. https://doi.org/10.18632/oncotarget.6243.

(359) Wang, X.; Chen, X.; Yang, X.; Gao, W.; He, B.; Dai, W.; Zhang, H.; Wang, X.; Wang,

J.; Zhang, X.; et al. A Nanomedicine Based Combination Therapy Based on QLPVM Peptide Functionalized Liposomal Tamoxifen and Doxorubicin against Luminal A Breast Cancer. *Nanomedicine Nanotechnology, Biol. Med.* **2016**, *12* (2), 387–397. https://doi.org/10.1016/j.nano.2015.12.360.

(360) Akkoç, Y.; Berrak, Ö.; Arisan, E. D.; Obakan, P.; Çoker-Gürkan, A.; Palavan-Ünsal, N. Inhibition of PI3K Signaling Triggered Apoptotic Potential of Curcumin Which Is Hindered by Bcl-2 through Activation of Autophagy in MCF-7 Cells. *Biomed. Pharmacother.* **2015**, *71*, 161–171. https://doi.org/10.1016/j.biopha.2015.02.029.

(361) García-Rubiño ME, Conejo-García A, Núñez MC, Carrasco E, García MA, Choquesillo-Lazarte D, García-Ruiz JM, Gallo MA, Marchal JA, C. J. Enantiospecific Synthesis of Heterocycles Linked to Purines: Different Apoptosis Modulation of Enantiomers in Breast Cancer Cells. *Curr Med Chem.* **2013**, *20* (38), 4924–4934. https://doi.org/10.2174/09298673113206660263.

(362) Duncan, R. Nanomedicines in Action. *Pharm. J.* **2004**, *273*, 485–488.

(363) Sorg, C. Scientific Forward Look on Nanomedicine. *Eur. Sci. Found. Policy Brief.* **2005**, *23* (February), 1–6. https://doi.org/10.1017/CBO9781107415324.004.

(364) Ferrari, M. Cancer Nanotechnology: Opportunities and Challenges. *Nat. Rev. Cancer* **2005**, *5* (3), 161–171. https://doi.org/10.1038/nrc1566.

(365) Zhukov, N. V.; Tjulandin, S. A. Targeted Therapy in the Treatment of Solid Tumors: Practice Contradicts Theory. *Biochem.* **2008**, *73* (5), 605–618. https://doi.org/10.1134/S000629790805012X.

(366) James R. Heath and Mark E. Davis. Nanotechnology and Cancer. *Annu Rev Med.* **2013**, *59*, 251–265. https://doi.org/10.1146/annurev.med.59.061506.185523.

(367) Delogu, L. G.; Venturelli, E.; Manetti, R.; Pinna, G. A.; Carru, C.; Madeddu, R.; Murgia, L.; Sgarrella, F.; Dumortier, H.; Bianco, A. Ex Vivo Impact of Functionalized Carbon Nanotubes on Human Immune Cells. *Nanomedicine* **2012**, *7* (2), 231–243. https://doi.org/10.2217/nnm.11.101.

(368) Pescatori, M.; Bedognetti, D.; Venturelli, E.; Ménard-Moyon, C.; Bernardini, C.; Muresu, E.; Piana, A.; Maida, G.; Manetti, R.; Sgarrella, F.; et al. Functionalized Carbon Nanotubes as Immunomodulator Systems. *Biomaterials* **2013**, *34* (18), 4395–4403. https://doi.org/10.1016/j.biomaterials.2013.02.052.

(369) Yoo, H. S.; Park, T. G. Biodegradable Polymeric Micelles Composed of Doxorubicin Conjugated PLGA-PEG Block Copolymer. *J. Control. Release* **2001**, *70* (1–2), 63–70. https://doi.org/10.1016/S0168-3659(00)00340-0.

(370) Allen, T. M. Ligand-Targeted Therapeutics in Anticancer Therapy. *Nat. Rev. Cancer* **2002**, *2* (10), 750–763. https://doi.org/10.1038/nrc903.

(371) Thierry, B. Drug Nanocarriers and Functional Nanoparticles: Applications in Cancer Therapy. *Curr. Drug Deliv.* **2009**, *6* (4), 391–403. https://doi.org/10.2174/156720109789000474.

(372) Moghimi, S. M.; Hunter, A. C.; Murray, J. C. Long-Circulating and Target-Specific Nanoparticles: Theory to Practice. *Pharmacological Reviews*. Pharmacol Rev June 2001, pp 283–318.

(373) Stockler, M.; Wilcken, N. R. C.; Ghersi, D.; Simes, R. J. Systematic Reviews of Chemotherapy and Endocrine Therapy in Metastatic Breast Cancer. *Cancer Treatment Reviews*. 2000. https://doi.org/10.1053/ctrv.1999.0161.

(374) Jordan, C. T.; Guzman, M. L. Mechanisms Controlling Pathogenesis and Survival of Leukemic Stem Cells. *Oncogene* **2004**, *23* (43 REV. ISS. 6), 7178–7187. https://doi.org/10.1038/sj.onc.1207935.

(375) Jordan, C. T.; Guzman, M. L.; Noble, M. Cancer Stem Cells. *N. Engl. J. Med.* **2006**, *355* (12), 1253–1261. https://doi.org/10.1056/NEJMra061808.

(376) Liu, H. G.; Chen, C.; Yang, H.; Pan, Y. F.; Zhang, X. H. Cancer Stem Cell Subsets and Their Relationships. *J. Transl. Med.* **2011**, *9* (1), 50. https://doi.org/10.1186/1479-5876-9-50.

(377) Naor, D.; Wallach-Dayan, S. B.; Zahalka, M. A.; Sionov, R. V. Involvement of CD44, a Molecule with a Thousand Faces, in Cancer Dissemination. *Semin.*

Cancer Biol. **2008**, *18* (4), 260–267. https://doi.org/10.1016/j.semcancer.2008.03.015.

(378) Naor, D.; Nedvetzki, S.; Golan, I.; Melnik, L.; Faitelson, Y. CD44 in Cancer. *Crit. Rev. Clin. Lab. Sci.* **2002**, *39* (6), 527–579. https://doi.org/10.1080/10408360290795574.

(379) Yan, Y.; Zuo, X.; Wei, D. Concise Review: Emerging Role of CD44 in Cancer Stem Cells: A Promising Biomarker and Therapeutic Target. *Stem Cells Transl. Med.* **2015**, *4* (9), 1033–1043. https://doi.org/10.5966/sctm.2015-0048.

(380) Bray, F.; Ferlay, J.; Soerjomataram, I.; Siegel, R. L.; Torre, L. A.; Jemal, A. Global Cancer Statistics 2018: GLOBOCAN Estimates of Incidence and Mortality Worldwide for 36 Cancers in 185 Countries. *CA. Cancer J. Clin.* **2018**, *68* (6), 394–424. https://doi.org/10.3322/caac.21492.

(381) Boulaiz, H.; Ramos, M. C.; Griñán-Lisón, C.; García-Rubiño, M. E.; Vicente, F.; Marchal, J. A. What's New in the Diagnosis of Pancreatic Cancer: A Patent Review (2011-Present). *Expert Opin. Ther. Pat.* **2017**, *27* (12), 1319–1328. https://doi.org/10.1080/13543776.2017.1379991.

(382) Ramos, M. C.; Boulaiz, H.; Griñan-Lison, C.; Marchal, J. A.; Vicente, F. What's New in Treatment of Pancreatic Cancer: A Patent Review (2010–2017). *Expert Opin. Ther. Pat.* **2017**, *27* (11), 1251–1266. https://doi.org/10.1080/13543776.2017.1349106.

(383) Sánchez-Moreno, P.; Ortega-Vinuesa, J. L.; Martín-Rodríguez, A.; Boulaiz, H.; Marchal-Corrales, J. A.; Peula-García, J. M. Characterization of Different Functionalized Lipidic Nanocapsules as Potential Drug Carriers. *Int. J. Mol. Sci.* **2012**, *13* (2), 2405–2424. https://doi.org/10.3390/ijms13022405.

(384) Zhou, H.; Yu, W.; Guo, X.; Liu, X.; Li, N.; Zhang, Y.; Ma, X. Synthesis and Characterization of Amphiphilic Glycidol-Chitosan-Deoxycholic Acid Nanoparticles as a Drug Carrier for Doxorubicin. *Biomacromolecules* **2010**, *11* (12), 3480–3486. https://doi.org/10.1021/bm100989x.

(385) Samstein, R. M.; Perica, K.; Balderrama, F.; Look, M.; Fahmy, T. M. The Use of

Deoxycholic Acid to Enhance the Oral Bioavailability of Biodegradable Nanoparticles. *Biomaterials* **2008**, *29* (6), 703–708. https://doi.org/10.1016/j.biomaterials.2007.10.026.

(386) Jiménez, G.; Hackenberg, M.; Catalina, P.; Boulaiz, H.; Griñán-Lisón, C.; García, M. Á.; Perán, M.; López-Ruiz, E.; Ramírez, A.; Morata-Tarifa, C.; et al. Mesenchymal Stem Cell's Secretome Promotes Selective Enrichment of Cancer Stem-like Cells with Specific Cytogenetic Profile. *Cancer Lett.* **2018**, *429* (March), 78–88. https://doi.org/10.1016/j.canlet.2018.04.042.

(387) Calvo, P.; Remuñán-López, C.; Vila-Jato, J. L.; Alonso, M. J. Novel Hydrophilic Chitosan-Polyethylene Oxide Nanoparticles as Protein Carriers. *J. Appl. Polym. Sci.* **1997**, *63* (1), 125–132. https://doi.org/10.1002/(SICI)1097-4628(19970103)63:1<125::AID-APP13>3.0.CO;2-4.

(388) Delgado-Calvo-Flores, J. M.; Peula-García, J. M.; Martínez-García, R.; Callejas-Fernández, J. Experimental Evidence of Hydration Forces between Polymer Colloids Obtained by Photon Correlation Spectroscopy Measurements. *J. Colloid Interface Sci.* **1997**, *189* (1), 58–65. https://doi.org/10.1006/jcis.1997.4815.

(389) Demaison, C.; Parsley, K.; Brouns, G.; Scherr, M.; Battmer, K.; Kinnon, C.; Grez, M.; Thrasher, A. J. High-Level Transduction and Gene Expression in Hematopoietic Repopulating Cells Using a Human Imunodeficiency Virus Type 1-Based Lentiviral Vector Containing an Internal Spleen Focus Forming Virus Promoter. *Hum. Gene Ther.* **2002**, *13* (7), 803–813. https://doi.org/10.1089/10430340252898984.

(390) Benabdellah, K.; Gutierrez-Guerrero, A.; Cobo, M.; Muñoz, P.; Martín, F. A Chimeric HS4-SAR Insulator (IS2) That Prevents Silencing and Enhances Expression of Lentiviral Vectors in Pluripotent Stem Cells. *PLoS One* **2014**, *9* (1). https://doi.org/10.1371/journal.pone.0084268.

(391) Garcia-Fuentes, M.; Torres, D.; Martín-Pastor, M.; Alonso, M. J. Application of NMR Spectroscopy to the Characterization of PEG-Stabilized Lipid Nanoparticles. *Langmuir* **2004**, *20* (20), 8839–8845. https://doi.org/10.1021/la049505j.

(392) Gupta, A. K.; Curtis, A. S. G. Lactoferrin and Ceruloplasmin Derivatized Superparamagnetic Iron Oxide Nanoparticles for Targeting Cell Surface Receptors. *Biomaterials* **2004**, *25* (15), 3029–3040. https://doi.org/10.1016/j.biomaterials.2003.09.095.

(393) Couvreur P, Barratt G, Fattal E, Legrand P, V. C. Nanocapsule Technology: A Review. *Crit. Rev. Ther. Drug Carrier Syst.* **2002**, *19*, 99–134. https://doi.org/10.1615/critrevtherdrugcarriersyst.v19.i2.10.

(394) Martin, A.; Puig, J.; Galisteo, F.; Serra, J.; Hidalgo-Alvarez, R. On Some Aspect of the Adsorption of Immunoglobulin-G Molecules on Polystyrene Microspheres. *J. Dispers. Sci. Technol.* **1992**, *13*, 399–416.

(395) Yi, X.; Zhang, J.; Yan, F.; Lu, Z.; Huang, J.; Pan, C.; Yuan, J.; Zheng, W.; Zhang, K.; Wei, D.; et al. Synthesis of IR-780 Dye-Conjugated Abiraterone for Prostate Cancer Imaging and Therapy. *Int. J. Oncol.* **2016**, *49* (5), 1911–1920. https://doi.org/10.3892/ijo.2016.3693.

(396) Urbaniak, T.; Musiał, W. Influence of Solvent Evaporation Technique Parameters on Diameter of Submicron Lamivudine-Poly-ε-Caprolactone Conjugate Particles. *Nanomaterials* **2019**, *9* (9). https://doi.org/10.3390/nano9091240.

(397) Panyam, J.; Labhasetwar, V. Biodegradable Nanoparticles for Drug and Gene Delivery to Cells and Tissue. *Adv. Drug Deliv. Rev.* **2003**, *55* (3), 329–347. https://doi.org/10.1016/S0169-409X(02)00228-4.

(398) Peula, J. M.; Hidalgo-Alvarez, R.; De Las Nieves, F. J. Covalent Binding of Proteins to Acetal-Functionalized Latexes. I. Physics and Chemical Adsorption and Electrokinetic Characterization. *J. Colloid Interface Sci.* **1998**, *201* (2), 132–138. https://doi.org/10.1006/jcis.1997.5388.

(399) Goldstein, D.; Gofrit, O.; Nyska, A.; Benita, S. Anti-HER2 Cationic Immunoemulsion as a Potential Targeted Drug Delivery System for the Treatment of Prostate Cancer. *Cancer Res.* **2007**, *67* (1), 269–275. https://doi.org/10.1158/0008-5472.CAN-06-2731.

(400) Pop-Georgievski, O.; Popelka, Š.; Houska, M.; Chvostová, D.; Proks, V.; Rypáček,

F. Poly(Ethylene Oxide) Layers Grafted to Dopamine-Melanin Anchoring Layer: Stability and Resistance to Protein Adsorption. *Biomacromolecules* **2011**, *12* (9), 3232–3242. https://doi.org/10.1021/bm2007086.

(401) Delcroix, M. F.; Huet, G. L.; Conard, T.; Demoustier-Champagne, S.; Du Prez, F. E.; Landoulsi, J.; Dupont-Gillain, C. C. Design of Mixed PEO/PAA Brushes with Switchable Properties toward Protein Adsorption. *Biomacromolecules* **2013**, *14* (1), 215–225. https://doi.org/10.1021/bm301637h.

(402) Torcello-Gómez, A.; Santander-Ortega, M. J.; Peula-García, J. M.; Maldonado-Valderrama, J.; Gálvez-Ruiz, M. J.; Ortega-Vinuesa, J. L.; Martín-Rodríguez, A. Adsorption of Antibody onto Pluronic F68-Covered Nanoparticles: Link with Surface Properties. *Soft Matter* **2011**, *7* (18), 8450–8461. https://doi.org/10.1039/c1sm05570d.

(403) Peula, J. M.; Hidalgo-Alvarez, R.; De Las Nieves, F. J. Coadsorption of IgG and BSA onto Sulfonated Polystyrene Latex: I. Sequential and Competitive Coadsorption Isotherms. *J. Biomater. Sci. Polym. Ed.* **1995**, *7* (3), 231–240. https://doi.org/10.1163/156856295X00274.

(404) Peula-Garcia, J. M.; Hidaldo-Alvarez, R.; De las Nieves, F. J. Protein Co-Adsorption on Different Polystyrene Latexes: Electrokinetic Characterization and Colloidal Stability. *Colloid Polym. Sci.* **1997**, *275* (2), 198–202. https://doi.org/10.1007/s003960050072.

(405) Molina-Bolívar, J. A.; Ortega-Vinuesa, J. L. How Proteins Stabilize Colloidal Particles by Means of Hydration Forces. *Langmuir* **1999**, *15* (8), 2644–2653. https://doi.org/10.1021/la981445s.

(406) Santander-Ortega, M. J.; Lozano-López, M. V.; Bastos-González, D.; Peula-García, J. M.; Ortega-Vinuesa, J. L. Novel Core-Shell Lipid-Chitosan and Lipid-Poloxamer Nanocapsules: Stability by Hydration Forces. *Colloid Polym. Sci.* **2010**, *288* (2), 159–172. https://doi.org/10.1007/s00396-009-2132-y.

(407) Farace, C.; Sánchez-Moreno, P.; Orecchioni, M.; Manetti, R.; Sgarrella, F.; Asara, Y.; Peula-García, J. M.; Marchal, J. A.; Madeddu, R.; Delogu, L. G. Immune Cell

Impact of Three Differently Coated Lipid Nanocapsules: Pluronic, Chitosan and Polyethylene Glycol. *Sci. Rep.* **2016**, *6* (July 2015), 1–14. https://doi.org/10.1038/srep18423.

(408) Xu, Z.; Jia, Y.; Huang, X.; Feng, N.; Li, Y. Rapid Induction of Pancreatic Cancer Cells to Cancer Stem Cells via Heterochromatin Modulation. *Cell Cycle* **2018**, *17* (12), 1487–1495. https://doi.org/10.1080/15384101.2018.1489180.

(409) Ning, X.; Du, Y.; Ben, Q.; Huang, L.; He, X.; Gong, Y.; Gao, J.; Wu, H.; Man, X.; Jin, J.; et al. Bulk Pancreatic Cancer Cells Can Convert into Cancer Stem Cells(CSCs) in Vitro and 2 Compounds Can Target These CSCs. *Cell Cycle* **2016**, *15* (3), 403–412. https://doi.org/10.1080/15384101.2015.1127471.

(410) Hernández-Camarero, P.; López-Ruiz, E.; Griñán-Lisón, C.; García, M. Á.; Chocarro-Wrona, C.; Marchal, J. A.; Kenyon, J.; Perán, M. Pancreatic (pro)Enzymes Treatment Suppresses BXPC-3 Pancreatic Cancer Stem Cell Subpopulation and Impairs Tumour Engrafting. *Sci. Rep.* **2019**, *9* (1), 1–17. https://doi.org/10.1038/s41598-019-47837-7.

(411) Kesharwani, P.; Banerjee, S.; Padhye, S.; Sarkar, F. H.; Iyer, A. K. Hyaluronic Acid Engineered Nanomicelles Loaded with 3,4-Difluorobenzylidene Curcumin for Targeted Killing of CD44+ Stem-Like Pancreatic Cancer Cells. *Biomacromolecules* **2015**, *16* (9), 3042–3053. https://doi.org/10.1021/acs.biomac.5b00941.

(412) Qian, C.; Wang, Y.; Chen, Y.; Zeng, L.; Zhang, Q.; Shuai, X.; Huang, K. Suppression of Pancreatic Tumor Growth by Targeted Arsenic Delivery with Anti-CD44v6 Single Chain Antibody Conjugated Nanoparticles. *Biomaterials* **2013**, *34* (26), 6175–6184. https://doi.org/10.1016/j.biomaterials.2013.04.056.

(413) Trabulo, S.; Aires, A.; Aicher, A.; Heeschen, C.; Cortajarena, A. L. Multifunctionalized Iron Oxide Nanoparticles for Selective Targeting of Pancreatic Cancer Cells. *Biochim. Biophys. Acta - Gen. Subj.* **2017**, *1861* (6), 1597–1605. https://doi.org/10.1016/j.bbagen.2017.01.035.

(414) Thapa, R.; Wilson, G. D. The Importance of CD44 as a Stem Cell Biomarker and Therapeutic Target in Cancer. *Stem Cells Int.* **2016**, *2016* (Figure 1).

https://doi.org/10.1155/2016/2087204.

(415) Liebmann, J. E.; Cook, J. A.; Lipschultz, C.; Teague, D.; Fisher, J.; Mitchell, J. B. Cytotoxic Studies of Pacfitaxel (Taxol®) in Human Tumour Cell Lines. *Br. J. Cancer* **1993**, *68* (6), 1104–1109. https://doi.org/10.1038/bjc.1993.488.

(416) Okamoto, Y.; Taguchi, K.; Sakuragi, M.; Imoto, S.; Yamasaki, K.; Otagiri, M. Preparation, Characterization, and in Vitro/in Vivo Evaluation of Paclitaxel-Bound Albumin-Encapsulated Liposomes for the Treatment of Pancreatic Cancer. *ACS Omega* **2019**, *4* (5), 8693–8700. https://doi.org/10.1021/acsomega.9b00537.

(417) Wu, S. ta; Fowler, A. J.; Garmon, C. B.; Fessler, A. B.; Ogle, J. D.; Grover, K. R.; Allen, B. C.; Williams, C. D.; Zhou, R.; Yazdanifar, M.; et al. Treatment of Pancreatic Ductal Adenocarcinoma with Tumor Antigen Specific-Targeted Delivery of Paclitaxel Loaded PLGA Nanoparticles. *BMC Cancer* **2018**, *18* (1), 1–13. https://doi.org/10.1186/s12885-018-4393-7.

(418) Dubey, N.; Shukla, J.; Hazari, P. P.; Varshney, R.; Ganeshpurkar, A.; Mishra, A. K.; Trivedi, P.; Bandopadhaya, G. P. Preparation and Biological Evaluation of Paclitaxel Loaded Biodegradable PCL/PEG Nanoparticles for the Treatment of Human Neuroendocrine Pancreatic Tumor in Mice. *Hell. J. Nucl. Med.* **2012**, *15* (1).

(419) Lee, C. J.; Spalding, A. C.; Ben-Josef, E.; Wang, L.; Simeone, D. M. In Vivo Bioluminescent Imaging of Irradiated Orthotopic Pancreatic Cancer Xenografts in Nonobese Diabetic-Severe Combined Immunodeficient Mice: A Novel Method for Targeting and Assaying Efficacy of Ionizing Radiation. *Transl. Oncol.* **2010**, *3* (3), 153–159. https://doi.org/10.1593/tlo.09184.

(420) Rubio-Viqueira, B.; Jimeno, A.; Cusatis, G.; Zhang, X.; Iacobuzio-Donahue, C.; Karikari, C.; Shi, C.; Danenberg, K.; Danenberg, P. V.; Kuramochi, H.; et al. An in Vivo Platform for Translational Drug Development in Pancreatic Cancer. *Clin. Cancer Res.* **2006**, *12* (15), 4652–4661. https://doi.org/10.1158/1078-0432.CCR-06-0113.

(421) Cano-Cortes, M. V.; Navarro-Marchal, S. A.; Ruiz-Blas, M. P.; Diaz-Mochon, J. J.; Marchal, J. A.; Sanchez-Martin, R. M. A Versatile Theranostic Nanodevice Based on an Orthogonal Bioconjugation Strategy for Efficient Targeted Treatment and Monitoring of Triple Negative Breast Cancer. *Nanomedicine Nanotechnology, Biol. Med.* **2020**, *24*. https://doi.org/10.1016/j.nano.2019.102120.

(422) Miller, A. D. Lipid-Based Nanoparticles in Cancer Diagnosis and Therapy. *J. Drug Deliv.* **2013**, *2013* (Figure 1), 1–9. https://doi.org/10.1155/2013/165981.

(423) Han, Y.; An, Y.; Jia, G.; Wang, X.; He, C.; Ding, Y.; Tang, Q. Facile Assembly of Upconversion Nanoparticle-Based Micelles for Active Targeted Dual-Mode Imaging in Pancreatic Cancer. *J. Nanobiotechnology* **2018**, *16* (1), 1–13. https://doi.org/10.1186/s12951-018-0335-4.

(424) Immordino, M. L.; Brusa, P.; Arpicco, S.; Stella, B.; Dosio, F.; Cattel, L. Preparation, Characterization, Cytotoxicity and Pharmacokinetics of Liposomes Containing Docetaxel. *J. Control. Release* **2003**, *91* (3), 417–429. https://doi.org/10.1016/S0168-3659(03)00271-2.

(425) Valle-Delgado, J. J.; Molina-Bolívar, J. A.; Galisteo-González, F.; Gálvez-Ruiz, M. J.; Feiler, A.; Rutland, M. W. Existence of Hydration Forces in the Interaction between Apoferritin Molecules Adsorbed on Silica Surfaces. *Langmuir* **2005**, *21* (21), 9544–9554. https://doi.org/10.1021/la050825s.

(426) Valle-Delgado, J. J.; Molina-Bolívar, J. A.; Galisteo-González, F.; Gálvez-Ruiz, M. J. Evidence of Hydration Forces between Proteins. *Current Opinion in Colloid and Interface Science*. Elsevier December 1, 2011, pp 572–578. https://doi.org/10.1016/j.cocis.2011.04.004.

ANNEXES

SUPLEMENTARY INFORMATION CHAPTER 1

1. Supplementary Figures.

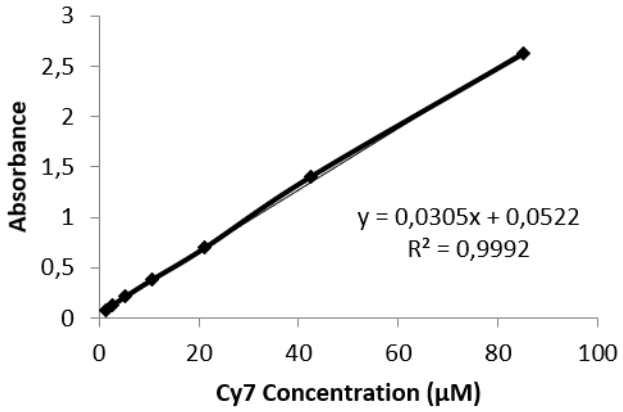

Figure S1. Calibration curve of absorbance vs concentration for Cy7 at 750 nm.

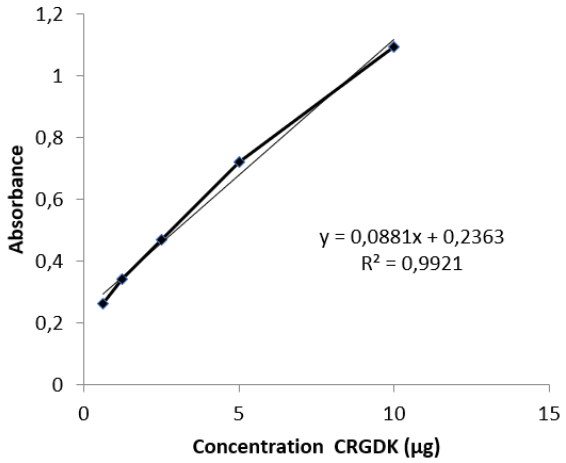

Figure S2. Calibration curve of CRGDK homing peptide by BCA assay.

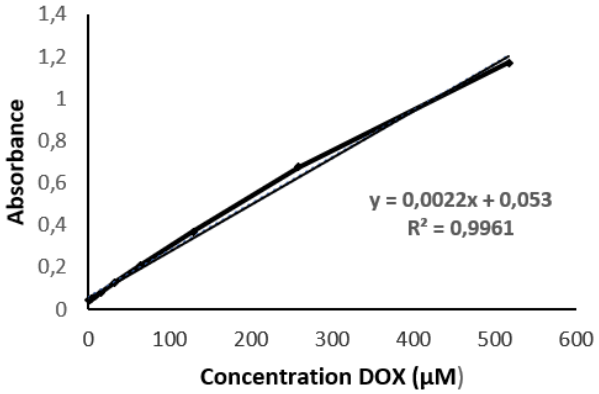

Figure S3. Calibration curve of absorbance vs concentration for doxorubicin at 481 nm.

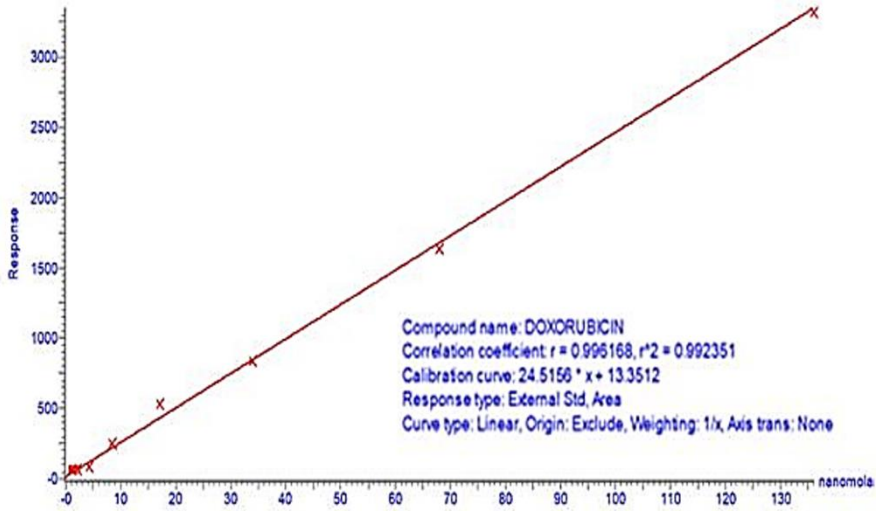

Figure S4. Calibration curve of doxorubicin by HPLC method.

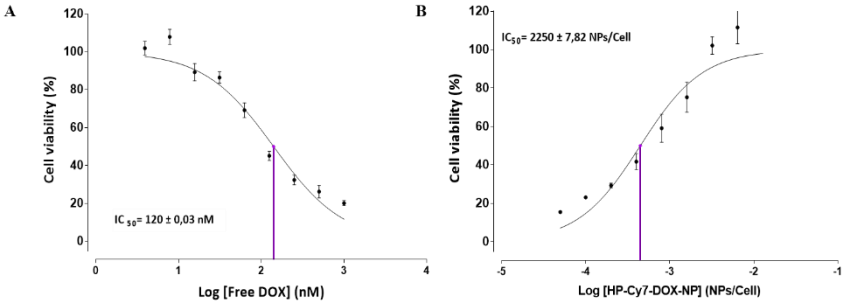

Figure S5. A) Dose-response curves (percentage of cell viability versus DOX concentration) of DOX free treatment and B) of HP-Cy7-DOX-NP (14) (NPs/Cell) treatment in MDA MB 231 cell line.

2. General experimental methods

2.1. General information

Chemistry equipment:

The HPLC analysis was performed on an Agilent 1200 series HPLC system coupled to a PL-ELS 1000 evaporative light scattering detector (ELS) from Polymer Lab with UV detection at 220, 254, 260, 282 and 495 nm, Discovery® C 18 of Supelco (50 mm x 2.1 mm x 5 µm), method S50D. The elution was carried out with Solvent A (0.1% formic acid in deionized HPLC grade water) and Solvent B (0.1% formic acid in HPLC grade methanol)

at 1 ml x min with a gradient of 5 to 95% B for 3 minutes, followed by 1 minute isocratic to 95% of B and ending with a gradient of 95 to 5% of B for 1 minute, then 1 min of isocratic to 95% of A.

Low resolution mass spectra were obtained using an Agilent Technologies 1200 HPLC-MS (6110 Quadrupole LC / MS) with ESR LRMS mass detector.

The high-resolution mass spectra were obtained using a LCT-TOF Premier XE High Resolution Mass Spectrometer, Micromass Technology.

The dynamic light scattering (DLS) and the Zeta potential were measured on a Zetasizer Nano ZS ZEN 3500 in biological grade water in a disposable cuvette for size measurements or in a transparent disposable cuvette for zeta potential measurements.

All conjugations were carried out with an Eppendorf Thermomixer® agitator and the centrifugations were performed in an Eppendorf centrifuge.

Biology equipment:

Cell cultures were performed in a NU-4750E US AutoFlow incubator from NUAIRE.

Cell experiments were carried out in a laminar flow cabinet Bio II A of TELSTAR Class II A.

Flow cytometry was performed on a FACS Canto II system (Becton Dickinson & Co., NJ, USA) using the Flowjo® 10 software for analysis.

Cell viability was assayed using a M200 Nanoquan microplate reader to measure absorbance.

Confocal microscopy was performed on a Zeiss LSM 710 confocal laser scanning microscope and Zeiss ZEN 2010 software for image acquisition. Transmission electron microscopy was performed on a FEI Titan G2 high resolution microscope. Atomic force microscopy was performed on a Nx20 atomic force microscope (Park Systems) and analysed using Xei data acquisition software.

2.2. Synthesis of CRGDK homing peptide.

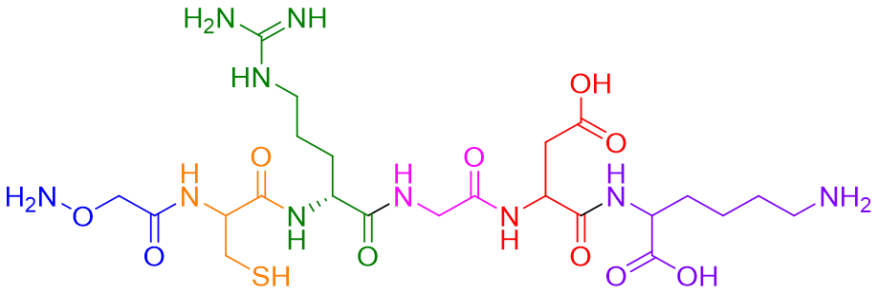

2-chlorotryl chloride resin (300 mg) was placed in a Solid Phase Extraction (SPE) cartridge, suspended in 6 ml of anhydrous DCM and stirred for 15 minutes to swell the resin. After that, the solvent was removed and a solution containing 2 equivuivalents of Fmoc-Lys-L-OH (Boc) (0.672 mmol) and DIPEA (456 ml, 262 mmol) in 6 ml of anhydrous DCM was added to the resin. The SPE cartridge with the reaction mixture was placed in a wheel and allowed to react for 15 hours at room temperature. Then, the resin was drained under vacuo and washed with DMF (5x1min) and DCM (5x1min). After that, a ninhydrin test was carried out to check if the reaction had procceed completely. Once the reaction had finished, the Fmoc group was deprotected by treating the resin with 20% piperidine in DMF at room temperature (3 x 10 min). The remaining L-aminoacids, Fmoc-Asp (OtBu) -OH, Fmoc-Gly-OH, Fmoc-Arg (Pbf) -OH and Fmoc-D-Cys-(TRT) -OH were sequentially coupled to the resin. To do so, oxyma (3.5 equiv) was added to a solution of the corresponding Fmoc-protected L-aminoacids (3.5 equiv) in DMF (3.9 mL) and, after mixing for 4 minutes at room temperature, DIC (3.5 equiv) was added and the solution was stirred for another 8-10 minutes at room temperature. This mixture was then added to the resin and left to react stirring in the wheel for 2 hours at room temperature. Coupling of Fmoc-protected aminoacids followed by Fmoc deprotection procedure was sequentially done as described above until the peptide sequence was complete. Once the last Fmoc group was removed, oxyma (3.5 equiv) was added to a Boc-aminooxyacetic acid (3.5 equiv) solution in DMF and left to react for 2 hours. Finally, acidic cleavage of the aminoxy peptide was carried out by treatment with an acidolytic mixture of trifluoroacetic acid (TFA), trimethylsilane (TIS) and dichloromethane (DCM) (90:5:5) for 4 hours at room temperature. The solution was then evaporated in the rotary evaporator and the crude peptide was precipitated by the addition of cold Et_2O (2 x 15 ml). Finally, the mixture was centrifuged and the supernatant removed the crude peptide (35mg, 27% yield).

CRGDK

MW = 650.7056 mmol / g

Exact mass = 650.2806

Resin loading = 0.65 mmol / g

Mass = 300 mg

Theoretical mass: 126.89 mg (0.192mmol)

2.3. Synthesis of cross-linked polystyrene aminomethyl NPs (Naked-NPs (1)).

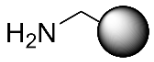

1

PVP (Mw 29,000, 0.05g, 1.7 µmol, Sigma-Aldrich) was dissolved in 92% ethanol/8% water for a final volume of 10 mL, and deoxygenated via argon bubbling. AIBN (7 mg, 42.4 µmol) was dissolved in styrene (freshly washed, 0.5 mL) with VBAH (7 mg, 41.3 µmol) and DVB (freshly washed, 4.65 µL).[296] The dispersion was deoxygenated with argon bubbling before addition to the PVP/Ethanol solution.

The mixture was stirred under argon for 1 hours before heating to 68 °C for 15 hours. NPs were obtained by centrifugation (11,000 G, 15 minutes) and washed with methanol (2 x 10 mL) and water (2 x 10 mL). Finally, NPs were stored in water (10 mL) at 4°C.

Particle size distribution: mean diameter: 460 nm, PDI: 0.042.

Loading (Ninhydrin): 0.057 mmol / g.

Number of particles per gram: 1.96 x 1013.

2.3.1. Characterization of Naked-NPs (1)

2.3.1.1. Solid content (SC) of the emulsion (%)

A known mass of a suspension of polystyrene NPs (0.5-1mg, suspended in water) was placed in a watch glass, covered with aluminum foil, dried at 25 °C for 15 hours, weighed and reweighed to give the mass of NPs. The solid content was then calculated according

to the following equation: % SC = (m/Vs) x 100, where m = mass of NPs (mg), Vs = Volume of suspension (µL).

SC: 2%, 2 mg of NPs in 100 µL of solution.

2.3.1.2. Transmission electron microscopy (TEM)

A sample of 5 µL of NPs was suspended in absolute ethanol, treated with copper and deposited on a grid lined with carbon.

2.3.1.3. Atomic force microscopy (AFM)

A sample of 1 µL of NPs was dispersed in distilled water by sonication, placed on a mica disk (1 cm^2) and dried for a few minutes (5-10).

2.3.1.4. Calculation of number of particles per gram

N= 6 x 1012/(π x ρs x d^3) Where: N = Number of particles/g for dry powder, ρs= Density of solid spheres (g/cm^3), which is 1 g/cm^3 for polystyrene, d= Mean diameter (nm).

Result: N= 1.96 x 1013 NPs per gram.

2.3.1.5. Calculation of loading of n using Fmoc NPs test

Fmoc-(x)-NPs (where x is Fmoc-PEG-OH or Fmoc-Lys(Dde)-OH, etc) were resuspended in 1 mL of 20% piperidine in DMF (3 x 20 min) after which the beads were washed by centrifugation three times, the supernatants combined and the loading was calculated according to the following equation:

Loading (mmol/g) = (A302 x V) / (Ɛ302 x d x W) x 1000

A302: Absorbance measured at 302 nm, VmL: Volume of combined supernatants, ε302: Molar Extinction Coefficient (7800 $M^{-1}cm^{-1}$) and Wmg: Mass of beads.

Result: Loading (Fmoc test): 0.054 mmol/g

2.3.1.6. Qualitative ninhydrin test

The reaction control was determined by qualitative ninhydrin test. Small samples of NPs in methanol (12 µL, 2% SC) in a 0.5 mL capacity eppendorf were washed with methanol and centrifuged after which 6 µL of reagent A and 2 µL of reagent B were added. Mix

well and heat to 100 ºC for 3 min. Blue stained resin beads indicate the presence of primary amines.

2.4. Determination of NPs concentration (NPs/µL) by spectrophotometric method.

NPs concentration (NPs per microliter) was determined by a spectrophotometric method as described previously.[298] Briefly, measurement of turbidity optical density at 600 nm of polystyrene NP suspensions was performed, based on nephelometric principals. Light going through NP suspensions is scattered via reflection, refraction and diffraction phenomena and the intensity of the scattered light, which are proportional to number of NPs in suspension, is recorded by standard spectrophotometers. In this way, calibrate standard curves were obtained for amino-methyl cross-linked polystyrene NPs of 460 nm by NP known concentrations. Calibration curves fitted linear regression models by which the number of NPs per microliter corresponding to one unit of OD600 for each size could be determined. Thus, these curves using initial batches of NP suspensions permitted us to estimate the number of NPs in final batches, which underwent multiple handling procedures, by OD600 measurement of 1 µL.

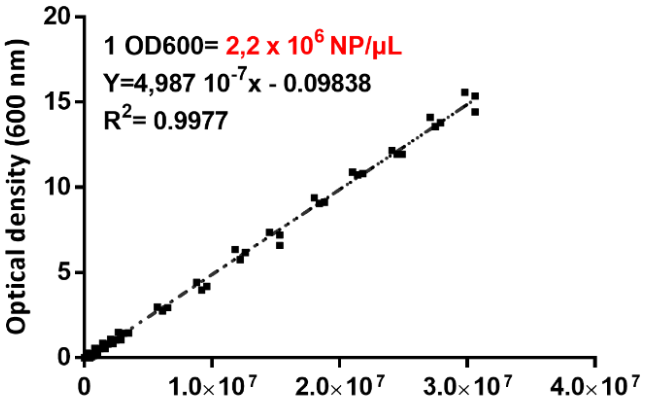

Figure S6. Calibration standard curve of concentration of nanoparticles (OD 600)

2.5. General protocol for Fmoc and Dde deprotection

2.5.1. Fmoc deprotection.

Fmoc deprotection was achieved by treating NPs with 20% piperidine/DMF (1 mL; 3 x 20 min). NPs were obtained by centrifugation and subsequivuently washed with DMF (3 x 1 mL), MeOH (3 x 1 mL), deionised water (3 x 1 mL).

2.5.2. Dde deprotection.

Dde deprotection was facilitated by treating NPs 10 with the Dde deprotection solution mixture (1.25 g (1.80 mmol) of $NH_2OH.HCl$ and 0.918 g (1.35 mmol) of imidazole were suspended in 5 mL of NMP, and the mixture was sonicated until complete dissolution. Just before reaction, 5 volumes of this solution were diluted with 1 volume of DMF (1 mL) for 1 hour at r.t. on a rotary wheel, then NPs were washed with DMF (1 mL). NPs were obtained by centrifugation and subsequivuently washed with DMF (3 x 1 mL), methanol (3 x 1 mL), deionised water (3 x 1 mL) and finally DMF (3 x 1 mL).

3. Preparation of PEGylated and bifunctionalized NPs

3.1. General scheme for synthetic strategy to obtain double PEGylated and bifunctionalized NPs.

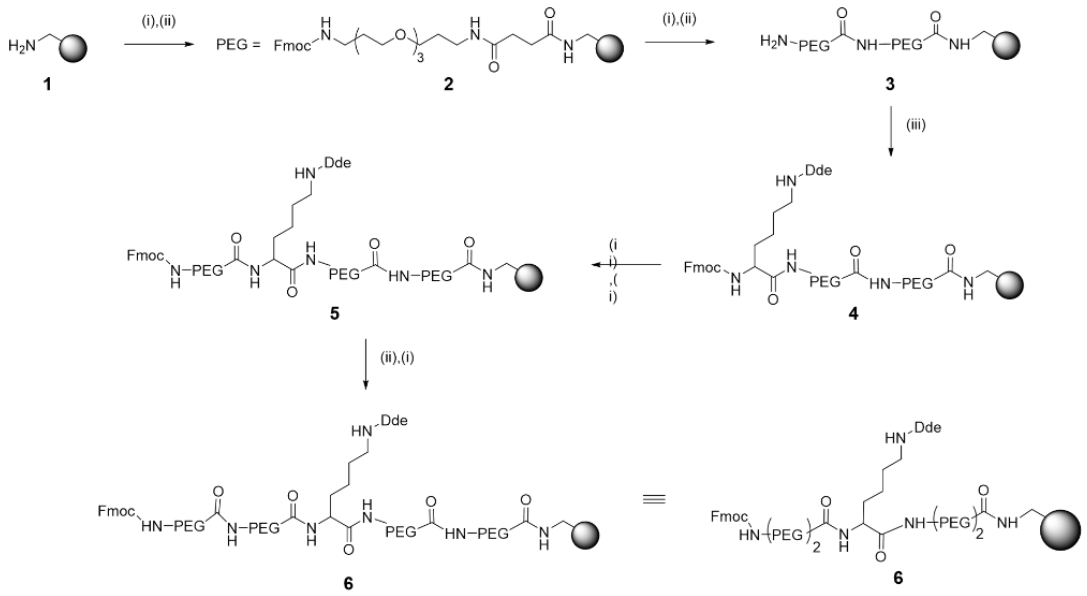

Scheme S1. Synthesis of PEGylated and bifunctionalized NPs. Reagents and conditions: (i) Fmoc-PEG-OH (15 equiv), Oxyma (15 equiv), DIC (15 equiv), DMF. 2 h, 60ºC;(ii) 20% piperidine, DMF. 3 x 20 min; (iii) Fmoc-Lys(Dde)-OH,Oxyma (15 equiv), DIC (15equiv), DMF. 2 h, 60ºC

3.2. Conjugation of PEG spacer to NPs (3).

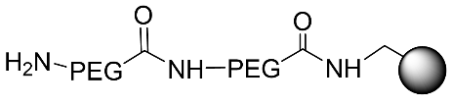

3

Aminomethyl NPs 1 (1 mL, 2% SC, 54 µmol/g, 1 µmol, 1 equiv) were washed in DMF (1 mL x 3 times) and suspended in DMF (1 mL). Separately, the Fmoc-PEG spacer (15 equiv) was dissolved in DMF (1 mL), then oxyma (15 equiv) was added and the solution mixture mixed for 4 minutes at R.T. before the addition of DIC (15 equiv) and mixed for 8-10 minutes at 25ºC. The solution mixture was then added to amino NPs and suspension mixed on the Thermomixer at 1400 rpm for 2 hours at 60°C.[288] Fmoc deprotection was achieved by treating NPs with 20% piperidine/DMF. Next, the whole process is repeated to obtain the double-PEGylated NPs **3.**

3.3. Preparation of bifunctionalised NPs (Fmoc-Dde-NPs, 6).

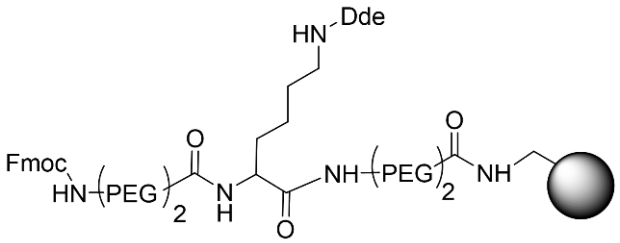

6

PEG functionalised NPs 3 (1 mL; 1 equiv) were washed in DMF (1 mL x 3 times) and suspended in DMF (1 mL). Separately, Fmoc-Lys (Dde)OH (15 equiv) was dissolved in DMF (1 mL), then oxyma (15 equiv) was added and the solution mixture mixed for 4 minutes at R.T. before the addition of DIC (15 equiv) and mixed for 8-10 minutes at R.T.[301] The solution mixture was then added to NPs **3** and suspension mixed on the Thermomixer at 1400 rpm for 2 hours at 60°C. Then this step was repeated to Fmoc deprotection and to introduce two units PEG spacer to obtain NPs 6.

4. Preparation of control NPs (Cy7-DOX-NP (11))

4.1. General scheme for synthetic strategy to obtain control NPs (Cy7-DOX-NP (11)).

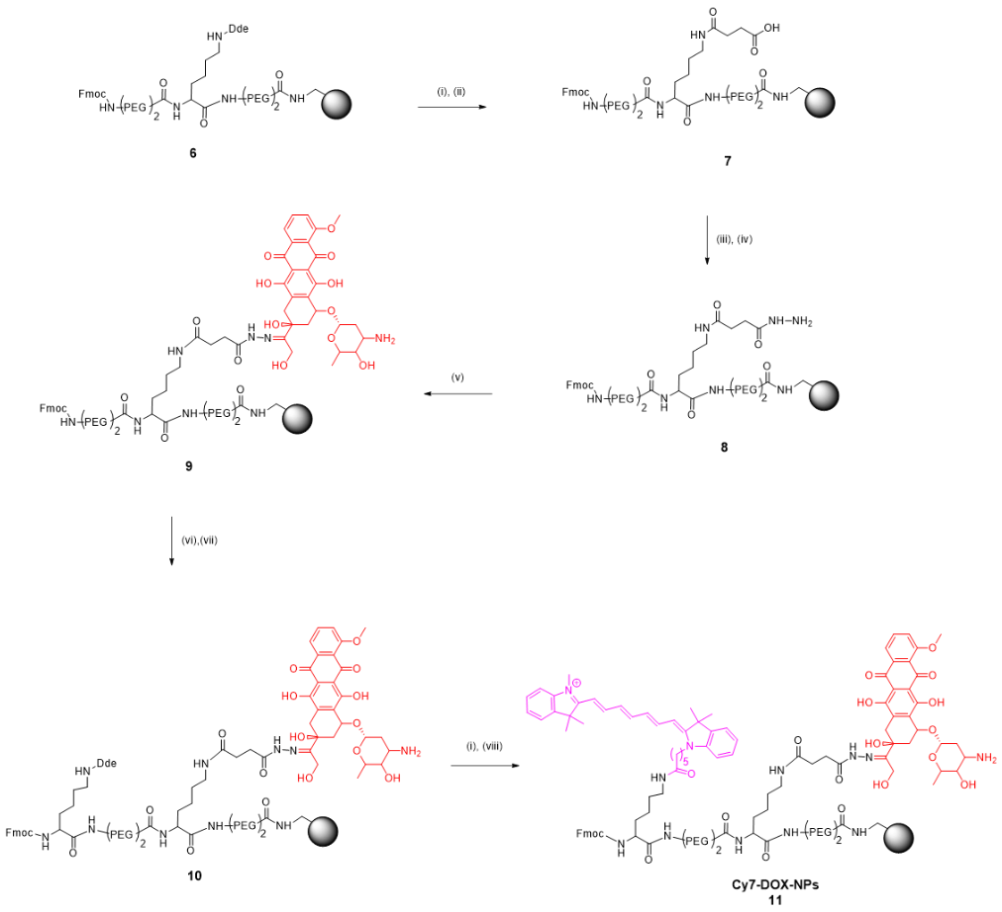

Scheme S2. General scheme of synthesis of control NPs (Cy7-DOX-NP (11)). Reagents and conditions (i) Hydroxylamine HCl, Imidazole, NMP, 2x 1 h, 25 °C; (ii) Succinic anhydride (15 equiv), DIPEA (15 equiv), 2 h., 60 ºC (iii) Activation COOH group with Oxyma (15 equiv), DIC (15 equiv), 2 h, 25 ºC; (iv) Hydrazine, 55% v/v (15 equiv), 15 h, 25 °C; (v) DOX, PBS pH 6, 15 h, 25 °C; (vi) 20% piperidine, DMF, 3 x 20 min; (vii) Fmoc-Lys (Dde) -OH, Oxyma (15 equiv), Oxyma (15 equiv), DIC (15 equiv), DMF. 2 h, 60 °C; (viii) Cy7-NHS (1 equiv), DIPEA (0.1 equiv), 15 h, 25 °C.

4.2. Preparation of Cy7-DOX-NP (11).

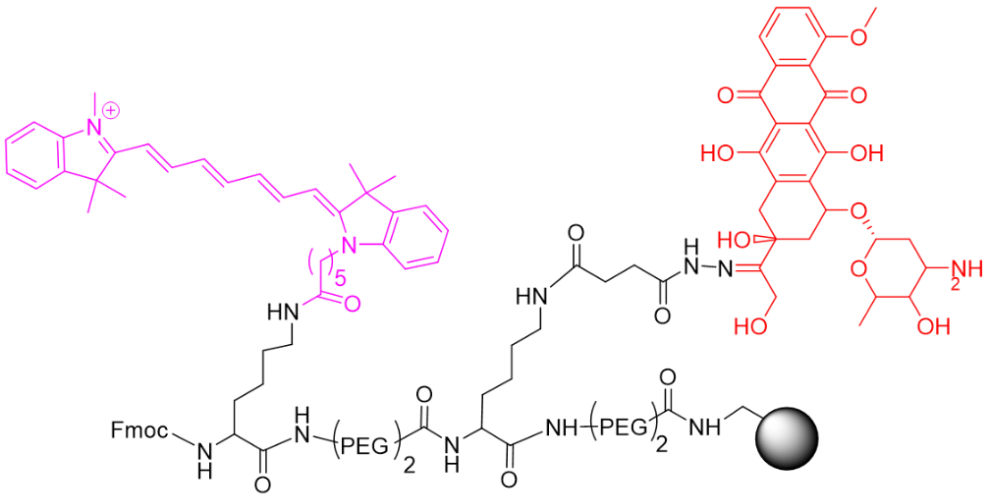

Cy7-DOX-NPs
11

Firstly, Dde deprotection of Fmoc-Dde-NPs (6) was carried out followed by the conjugation of the succinic anhydride (15 equiv) with DIPEA (7.5 equiv) to obtain COOH-Fmoc-NPs (7). Later, carboxi-functionalized COOH-Fmoc-NPs (7) were activated with oxyma (15 equiv) and DIC (15 equiv) during 4 hours and they were centrifuged and a solution of 55% v/v hydrazine in DMF was added and they were left stirring for 15 hours at 25 ° C. Next, the Fmoc-Hydrazide-NPs (8) were washed and conditioned in 1 mL of PBS pH 6. Then, 1 equivalent of DOX was dissolved in PBS at pH 6 and added to the NPs and the resulting mixture was mixed for 15 hours at 50 °C to yield DOX-NPs (9). NPs 9 were washed in DMF (1 mL x 3 times) and suspended in DMF (1 mL) and conjugated with Fmoc-Lys (Dde)OH (15 equiv) with oxyma (15 equiv) and DIC (15 equiv) in DMF as explained in the previous section (section 3.3) to obtain Fmoc-Dde-DOX-NPs (10) after Fmoc deprotection. Following Dde deprotection of Fmoc-Dde-DOX-NPs (10) the conjugation of fluorophore Cy7 was carried out to yield control NPs (11). NPs 10 were washed with anhydrous DMF (3 x 1 mL) and resuspended in anhydrous DMF (1 mL). On the other hand, Cy7-NHS (1.5 equiv) activated with NHS was dissolved in anhydrous DMF (1mL) with DIPEA (1 equiv). Subsequently, the solution was added to NPs and suspension was stirred in the Thermomixer at 1400 rpm for 15 hours at 25 °C. Cy7-DOX-NPs (11) were obtained by centrifugation and subsequently washed with DMF (3 x 1 mL), MeOH (3 x 1 mL) and sterile deionized water (3 x 1 mL).

4.3. Characterization of control NPs (11).

Table S1. Characterization of NPs by DLS.

NPs	Diameter Mean (nm)	PDI
Cy7-DOX-NP (11)	466 ± 1,6	0,013

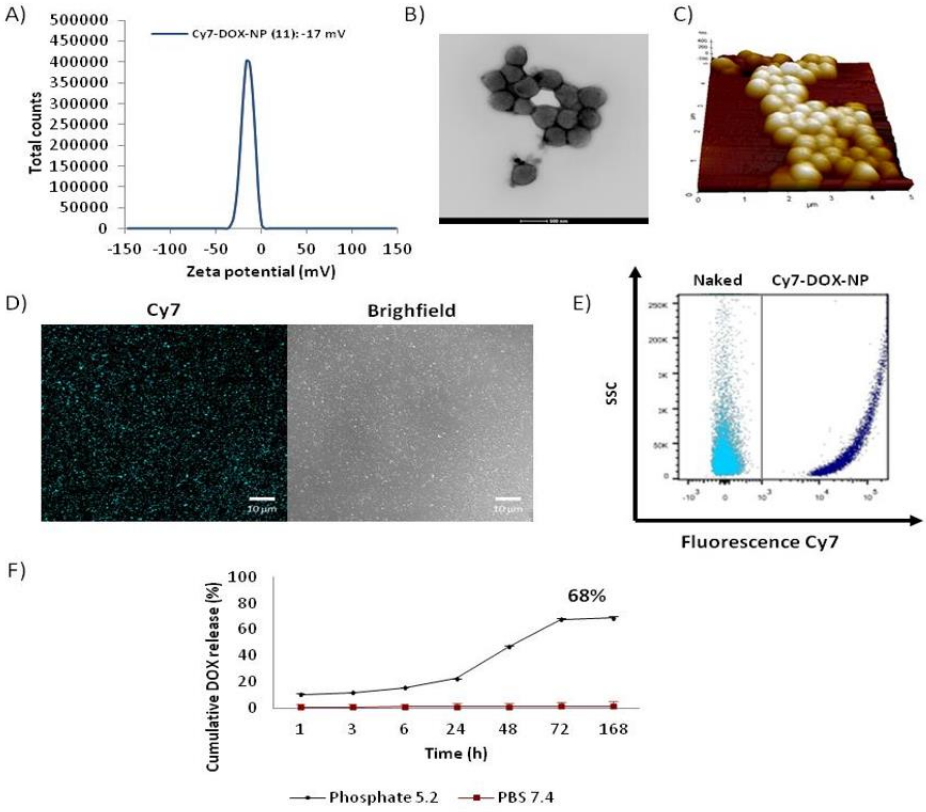

Figure S7. Characterization of Cy7-DOX-NP (11). A) Zeta potential values of Cy7-DOX-NPs (11). B) TEM of Cy7-DOX-NPs (11); C) AFM of Cy7-DOX-NPs (11); D) Confocal microscopy of Cy7-DOX-NPs (11), Scale bar, 10 µm; E) Representative overlay dot plot obtained after flow cytometry analysis of naked NPs (1) (blue) and Cy7-DOX-NPs (11) (blue); F) Cumulative DOX release of Cy7-DOX-NPs (11).

5. Preparation and characterization of theranostic nanoparticles (HP-Cy7-DOX-NPs (14))

5.1. Preparation of theranostic nanoparticles (HP-Cy7-DOX-NPs (14)).

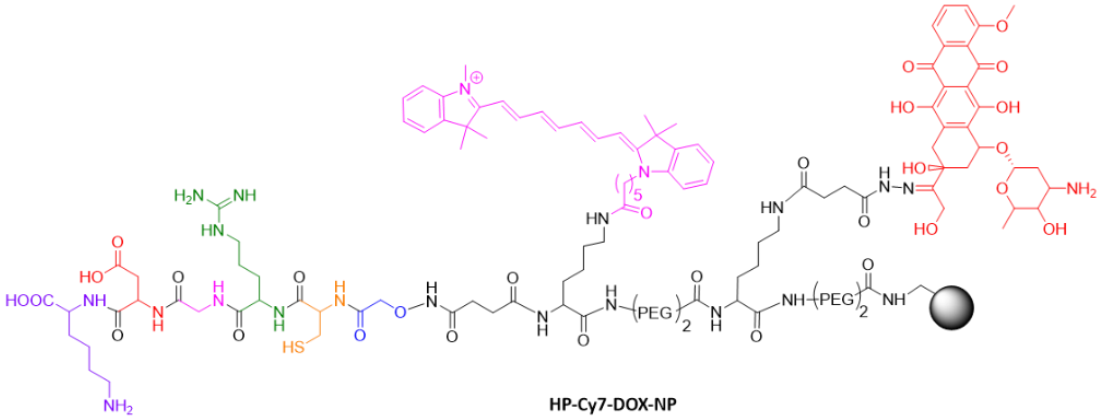

Double PEGylated and bifunctionalized NPs (Fmoc-Dde-NPs, (6)) were obtained by using protocols previously described [17] (see details above). Next, carboxy functionalization was achieved by treatment with succinic anhydride (20 equiv) in DMF for 4 h at 60 ºC. Next, COOH-Fmoc-NPs (7) were activated with oxyma (10 equiv) and DIC (10 equiv.) for 4 hours at 25 °C following by centrifugation. Then, 1 mL of 55% v/v hydrazine in DMF was added and NPs were left stirring for 15 hours at 25 °C to give rise to Fmoc-Hydrazide-NPs (8). Next, Fmoc-Hydrazide-NPs (8) were washed and conditioned in 1 mL of PBS pH 6. DOX (1equiv.) was dissolved in PBS at pH 6 and added to the NPs and the resulting mixture was mixed for 15 hours at 50°C to yield DOX-NPs (9). To generate trifunctionalized NPs Fmoc-lysine-Dde(OH) (15 equiv) was conjugated to DOX-NPs (9) after Fmoc deprotection and the fluorophore conjugation step was carried out using a sulfo-Cy7 NHS ester solution in DMF with N,N-diisopropylethylamine (DIPEA) (0.1 equiv) at 25 °C for 14 h after deprotection of Dde. Finally, COOH-Cy7-DOX-NPs (13) were activated with oxyma (15 equiv) and DIC (15 equiv) and were functionalized with a solution of CRGDK homing peptide (see peptide synthesis details above) in DMF and DIPEA at 25 °C for 15 hours to obtain theranostic nanoparticles (HP-Cy7-DOX-NPs (14)).

5.2. Characterization of theranostic nanoparticles (HP-Cy7-DOX-NPs (14)).

Size distributions of the NPs were controlled after each key conjugation step by DLS (Figure 2A). It can be observed that this multifunctionalization strategy did not affect the NP size. These results confirm that trifunctionalized NPs were stable and aggregation did not occur. These DLS size results were corroborated by TEM analysis (Figure 2B) and

by AFM (Figure 2C), revealing a spheroidal morphology with irregular contours, without aggregation and with a good dispersion.

NP zeta potentials were measured in aqueous environments at pH 7.4. Figure 2A shows the zeta potential values which shown negative values of Fmoc-Dde-NP (6), COOH-Cy7-DOX-NP (13) and HP-Cy7-DOX-NP (14) as a consequence of the conjugation to the amino groups of NPs so that they cannot be protonated. These results also confirm the ability of zeta potential measurements to monitor the success of the chemical modifications of NPs. Finally, the characteristics of homogeneous size and low polydispersity of NPs populations studied were also confirmed.

In order to measure the labelling level of the theranostic nanoparticles, HP-Cy7-DOX-NPs (14) were analysed by flow cytometry and confocal microscopy. The labelling efficiency was quantified by measuring the remaining fluorophore in the reaction supernatant after the conjugation step by using a calibration curve with lineal ratio between the optic density of the Cy7 dye and its concentration (Figure S1). The conjugation efficiency was 74.1%. Taking into account the number of NPs used in this assay (5.2×10^7 NPs/µL), we can estimate a final concentration of 9.5×10^{-8} nmol of Cy7 per NP that correspond to 5.7×10^7 molecules of Cy7 per NP.

The efficiency of conjugation of the CRGDK homing peptide to the theranostic NPs (HP-Cy7-DOX-NPs (14)) was determined by measuring the initial and final peptide concentration in the reaction vessel by BCA test.[305] The absorbance values obtained at 562 nm were translated into concentration using a standard calibration curve (**Figure S2**). The obtained results show a conjugation efficiency of 80.7%. Taking into account the number of NPs used (1.83×10^8 NPs/µL), we can estimate a final concentration of 8×10^{-9} nmol of CRGDK homing peptide per NP that correspond to a density of 5.23×10^7 CRGDK homing peptide molecules/NP.

In order to evaluate the conjugation efficiency of DOX to theranostic NPs (HP-Cy7-DOX-NPs (14)) the unconjugated drug which remain in the supernatant of the reaction was measured by UV spectroscopy. A calibration curve, with lineal ratio between the optic density of DOX and its concentration, was previously performed (Figure S3). The conjugation efficiency was calculated to be 72%. As the number of NPs used in this assay

were 5.2 x 10^7 NPs/µL, we can estimate a final concentration of 1.4 x 10^8 nmol DOX per NP that correspond to 8.4 x 10^7 molecules of drug per NP.

The efficiency of DOX release from HP-Cy7-DOX-NPs (14) was determined by performing UV spectroscopy of the buffers in which HP-Cy7-DOX-NPs (14) were incubated and using a HPLC system (Figure S4). HP-Cy7-DOX-NPs (14) where incubated at pH 5.2 (phosphate buffer) at which pH sensitive hydrazone bonds are reversible cleaved. A significant drug release of 44% ± 0.1 after 24 hours of incubation at pH 5.2 was observed. Then, a sustained release occurs up to 168 hours incubation, achieving a maximum release value of 73%. In contrast, there is no significant loss of DOX conjugated to NPs when incubation is carried out in 7.4 pH PBS. Consequently, an efficient and selective drug release at acidic pH has been achieved.

6. Doxorubicin release profile

6.1. Calibration curve of doxorubicin by HPLC method of theranostic NPs (HP-Cy7-DOX-NPs (14)).

Analysis of the efficacy of the release of doxorubicin by HPLC: chromatographic conditions: the HPLC system (Acquity UPLC System, Waters) with a C18 column from Waters CORTECS ™ (2.1 mm x 75 mm, 2.7 µm). The detection of PDA eλ for doxorubicin was established at 252 nm. The mobile phase of water: acetonitrile (30:70, pH 3.0, adjusted with 85% phosphoric acid) was supplied at a flow rate of 0.4 ml / min of acetonitrile: 0% B, T8: 95% B, T8.1: 0% B, analysis time 10 minutes. The maximum identification was confirmed by the retention time of doxorubicin hydrochloride at 2.69 min (Figure S4).

7. General protocol for cellular nanofection.

7.1. Cellular nanofection by flow cytometry.

After incubation with NPs, the medium was aspirated and the cells were washed with 1x PBS and separated with trypsin-EDTA at 37 °C for 5 minutes. Then, each sample was fixed in 2% paraformaldehyde (PFA) at room temperature for 10 minutes and protected from light. Samples were analyzed by flow cytometry with a FACS Canto II flow cytometer. Each experiment was performed in duplicate by ratio and time of incubation and was repeated at least three times.

The study of the nanofection of HP-Cy7-DOX-NP (14) and control NPs were carried out using the following ratio of NPs per cell: 1/50; 1/100; 1/250; 1/500; 1/1000; 1/2500; 1/5000; 1/10000. The dot plots and the cytometry statistics were obtained using the FlowJo software. Graphs and statistical difference data were made using the GraphPad software according to the following explanation. The percentages of cell data containing NPs were plotted against the cell/NPs ratio (3.3) in two different chart types. First in an XY representation according to the adjustment model of the hyperbola equation to study the saturation profile NPs of the MDA MB 231 cell line and the specific multiplicity of fifty nanofection (number of NPs to obtain the 50 % of the cells that contain NPs (nanofected)). Second in a bar representation to establish the statistically significant differences mediated by the analysis of the variance of a factor (ANOVA) using the Bonferroni multiple comparison comparing the same treatments between different NPs. In addition, the median fluorescence intensity (MFI) was analyzed comprehensively by comparing the increase of the MFI (ΔMFI, MFI sample/MFI without treatment). The ANOVA multiple comparison test was also used.

7.2. Cellular nanofection by confocal microscopy.

The cells were washed with 1X PBS, separated with trypsin / EDTA, counted and diluted with the corresponding media to a final concentration of 105 cells per mL. 500 µL of each cell line suspension was seeded onto glass coverslips coated with poly-L-lysine in 24-well plates and incubated for 15 h. Then, the media was replaced by a new solution with the medium containing the quantity of NPs corresponding to each experiment. After the corresponding incubation time, the medium was aspirated and the cells were washed with 1X PBS and fixed in 4% paraformaldehyde at room temperature for 30 minutes. The fixed cells were washed with 1X PBS and mounted with ProLong Gold mounting medium with DAPI (Life technologies). The images were collected with the ZEISS LSM 710 confocal laser microscope using a DIC Plan-Apochromat 63X oil immersion objective with 1.40 numerical aperture and the ZEN 2010 software. The image analysis was subsequently carried out with the ZEN 2012 program Blue Edition or the program ImageJ version 1.49b (free software). Samples containing fluorescent NPs and DAPI nuclear staining were excited using a HeNe laser line of 633 nm wavelength (5.0 mW) and 7% power for the NPs, a laser line of 405 nm diode wavelength (30.0 mW)

2.8% power for DAPI and HeNe laser line with wavelength of 543 nm (1.2 mW) 20% power for DIC images and 1.00 Airy unit (AU). Each experiment was performed in duplicate and repeated three times per cell line.

SUPLEMENTARY INFORMATION CHAPTER 2

1. Colloidal Stability of LLNCs

In chemotherapy, most of suggested NP present certain handicaps associated with toxicity, inappropriate drug-release pattern or low colloidal stability.[424] An important requirement for NP to be used as drug carriers is to retain colloidal stability under physiological conditions. Photon correlation spectroscopy is a reliable method to determine the degree of stability of a colloidal system by providing information about the average size of the aggregates. Nanocapsules prepared with and without cross-linked HSA were incubated at pH 7.4 with increasing NaCl concentrations for 24 h to study their colloidal stability (**see Figure S8**).

From this figure it bears mentioning that nanocapsules treated with GAD are completely stable in the range 0-500 mM of NaCl. By contrast, in the case of non-cross linked nanocapsules, the size of aggregates increased steeply with the NaCl concentration to a maximum value reached at 100 mM NaCl. Over that concentration, the extent of aggregation decreased abruptly again at 150 mM, and continued diminishing thereafter, although slightly, with increasing ionic strength. The observed stability of nanocapsules at high electrolyte concentrations can be explained by the presence of hydration forces.[425,426] It has been proposed that the specific adsorption of cations onto protein molecules, with their surrounding hydration layer, is the origin of hydration forces. These repulsive interactions would then be favored by the net negative charge of the protein. The enhanced colloidal stability of nanocapsules with GAD cross-linked HSA could then be ascribed to the increase in the net negative charge due to the GAD reaction with the protein amino groups.

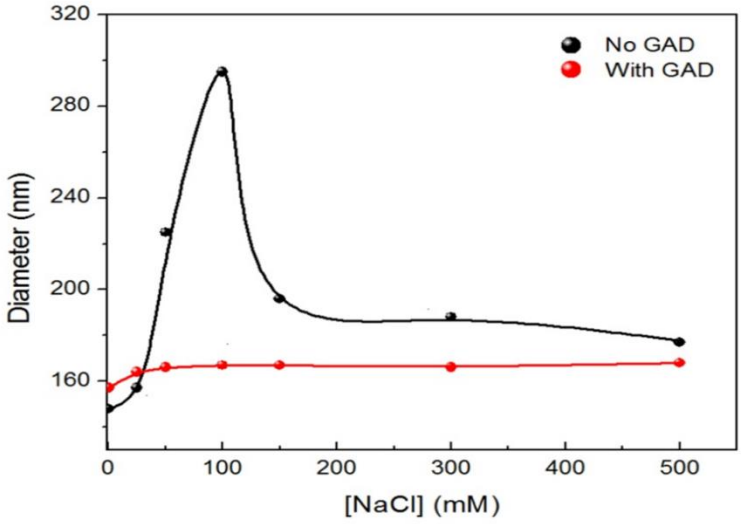

Figure S8. Diameter of LLNCs prepared with and without GAD as a function of NaCl. GAD/HSA 0.16

SUPLEMENTARY INFORMATION. CHAPTER 3

1. Supplementary Figures

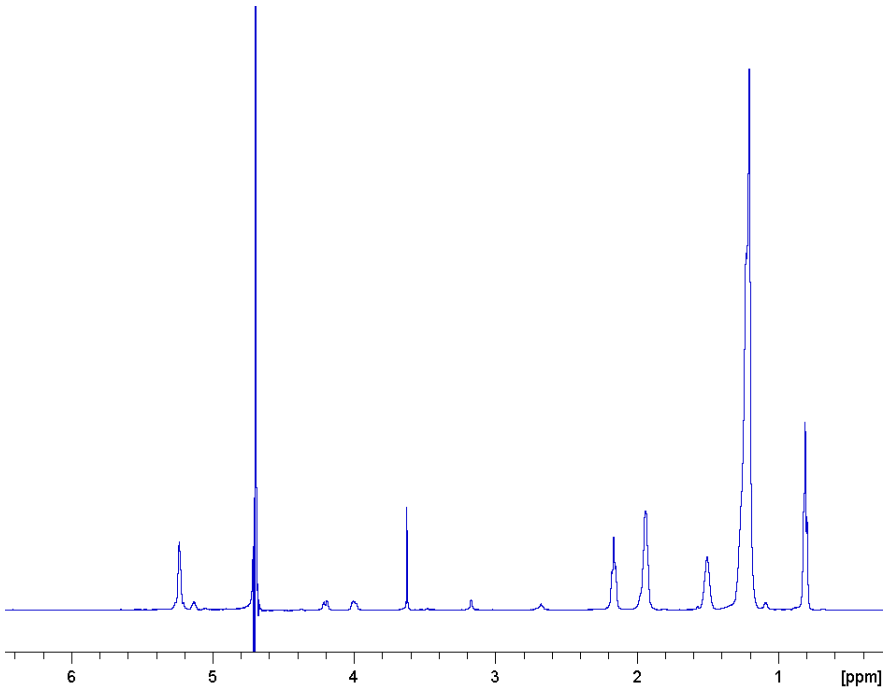

Figure S9. ^{1}H NMR spectrum (water-suppressed) of intact O^{2}LNC in H_2O with 13% D_2O (24 ºC, 500 MHz)

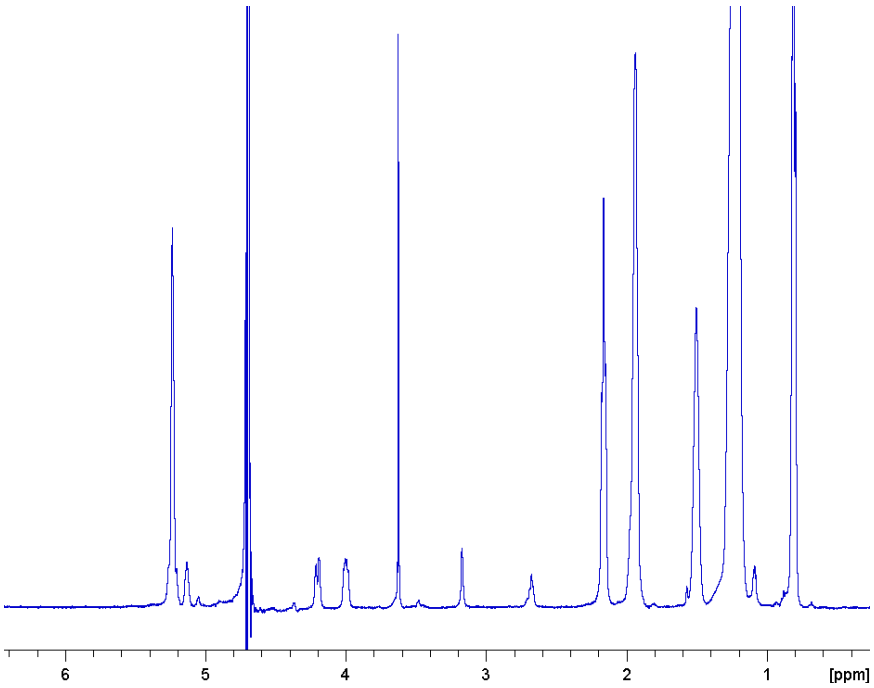

Figure S10. ^{1}H NMR spectrum (water-suppressed) of intact O^{2}LNC in H_2O with 13% D_2O (24 ºC, 500 MHz). The vertical intensity is enhanced compared to Figure IPV1.

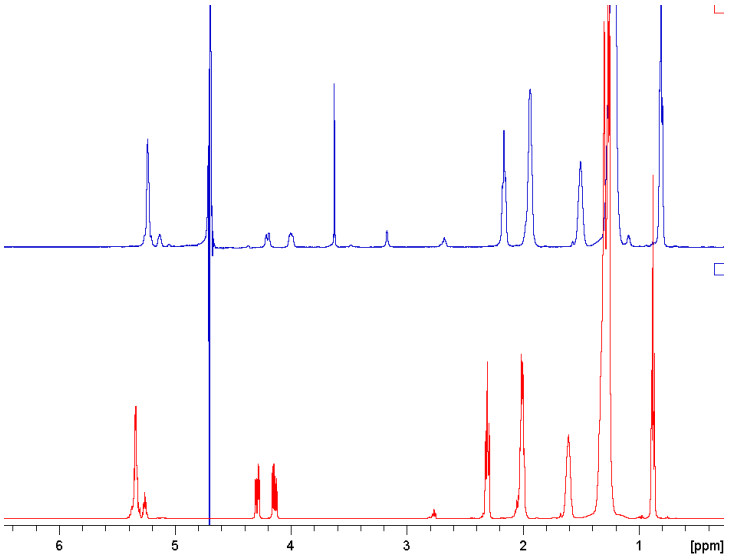

Figure S11. Blue trace: ^{1}H NMR spectrum (water-suppressed) of intact $O^{2}LNC$ in H_2O with 13% D_2O (blue trace). Red trace: ^{1}H NMR spectrum of olive oil in $CDCl_3$. Acquisitions at 24 ºC, 500 MHz.

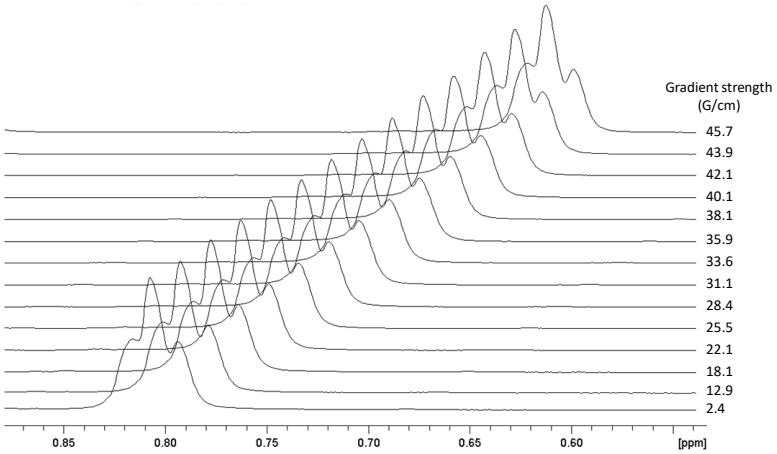

Figure S12. Diffusion NMR experiment with the intact $O^{2}LNC$ sample in H_2O with 13% D_2O (24 ºC, 500 MHz). Expansion of the olive oil triglyceride end methyl triplet signal at each of the effective gradient strengths employed in the diffusion experiment (ledbpgppr2s pulse sequence from Bruker's library, diffusion time was 125 ms). Receiver gain is constant along all traces. It is clearly observed that the NMR signal remains essentially non-attenuated even at the highest effective gradient strength employed (95%, considering the squared gradient shape employed, of the maximum nominal gradient strength which the probe may deliver). This behavior is a consequence of the olive oil triglyceride molecules diffusing at the rate of the nanocapsule vehicle they are confined in.

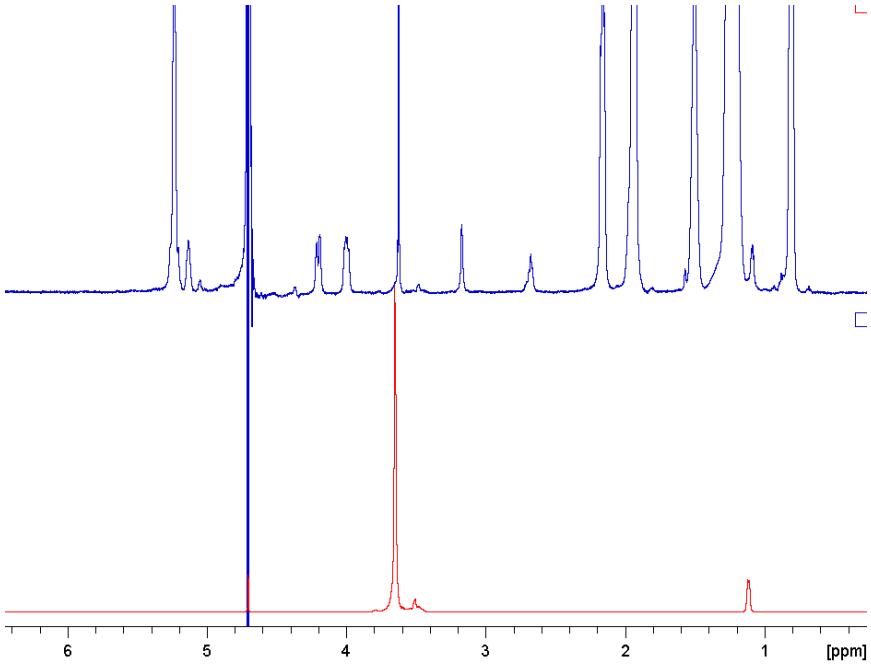

Figure S13. Blue trace: ^{1}H NMR spectrum (water-suppressed) of intact O^{2}LNC in H_2O with 13% D_2O. Red trace: ^{1}H NMR spectrum of Pluronic F-68 in D_2O. Acquisitions at 24 ºC, 500 MHz.

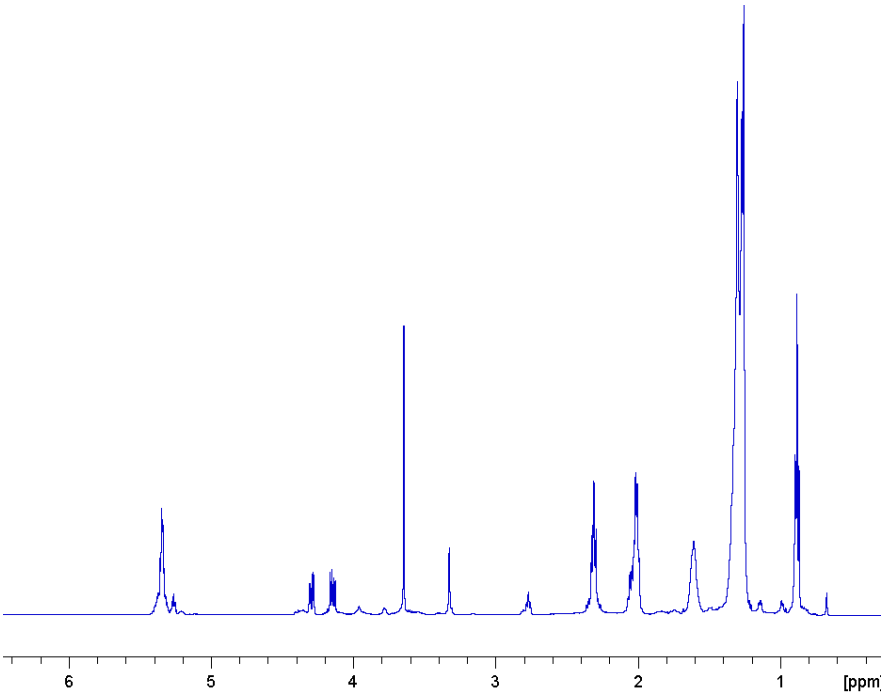

Figure S14. ^{1}H NMR spectrum of disintegrated O^{2}LNC after isopropanol evaporation and further redissolution in $CDCl_3$ (24 ºC, 500 MHz).

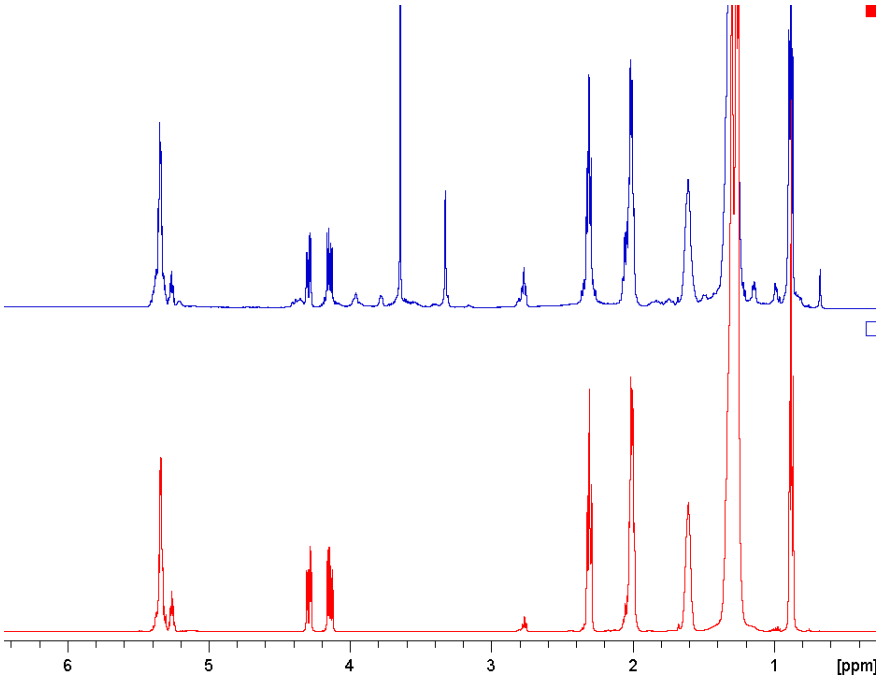

Figure S15. Blue trace: ^{1}H NMR spectrum of disintegrated O^{2}LNC after isopropanol evaporation and further redissolution in $CDCl_3$. Red trace: ^{1}H NMR spectrum of olive oil in $CDCl_3$. Acquisitions at 24 ºC, 500 MHz.

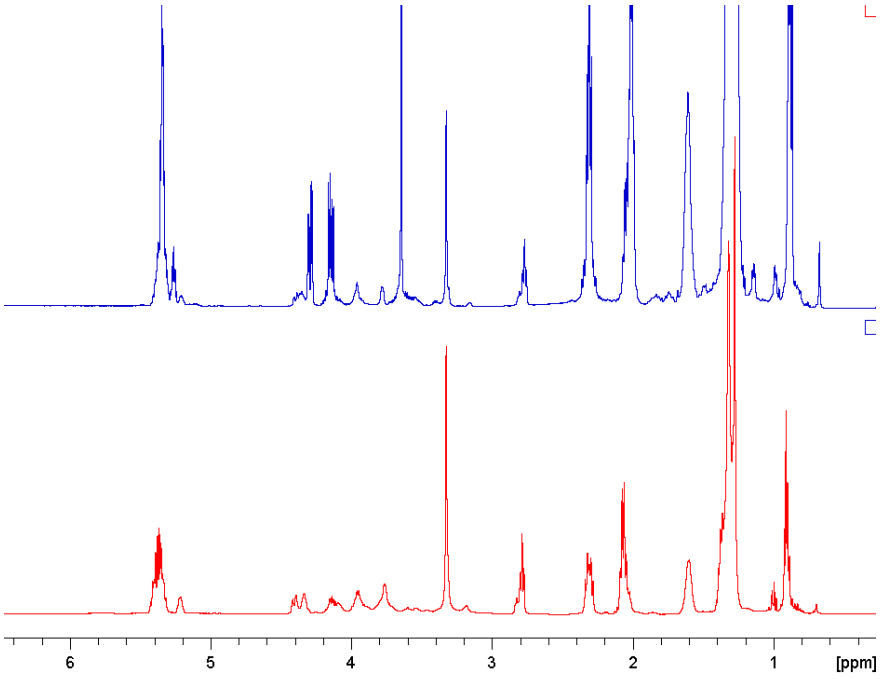

Figure S16. Blue trace: ^{1}H NMR spectrum of disintegrated O^{2}LNC after isopropanol evaporation and further redissolution in $CDCl_3$. Red trace: ^{1}H NMR spectrum of Epikuron 145V in $CDCl_3$. Acquisitions at 24 ºC, 500 MHz.

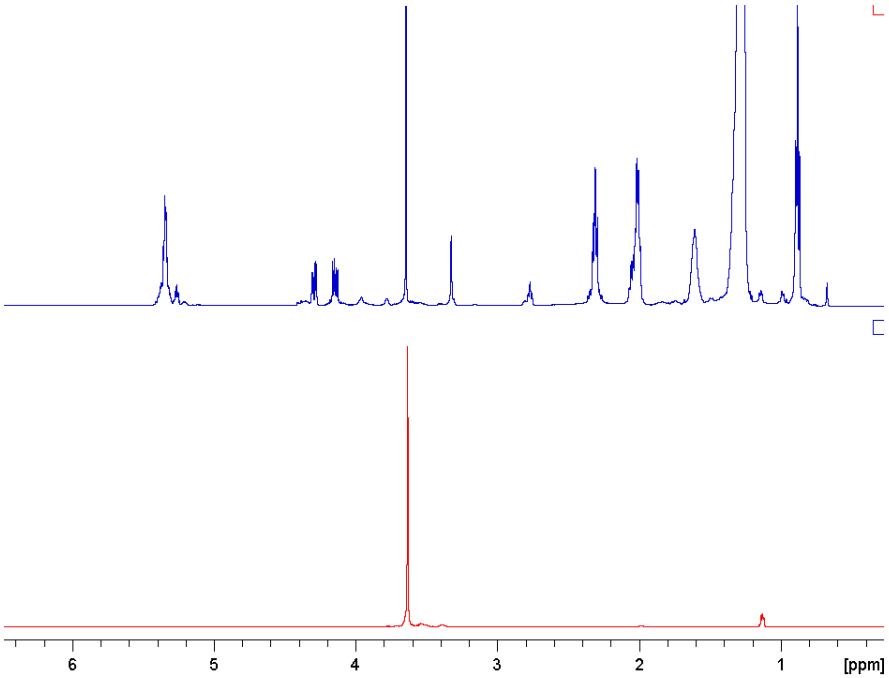

Figure S17. Blue trace: ^{1}H NMR spectrum of disintegrated O^{2}LNC after isopropanol evaporation and further redissolution in $CDCl_3$. Red trace: ^{1}H NMR spectrum of Pluronic F-68 in $CDCl_3$. Acquisitions at 24 ºC, 500 MHz.

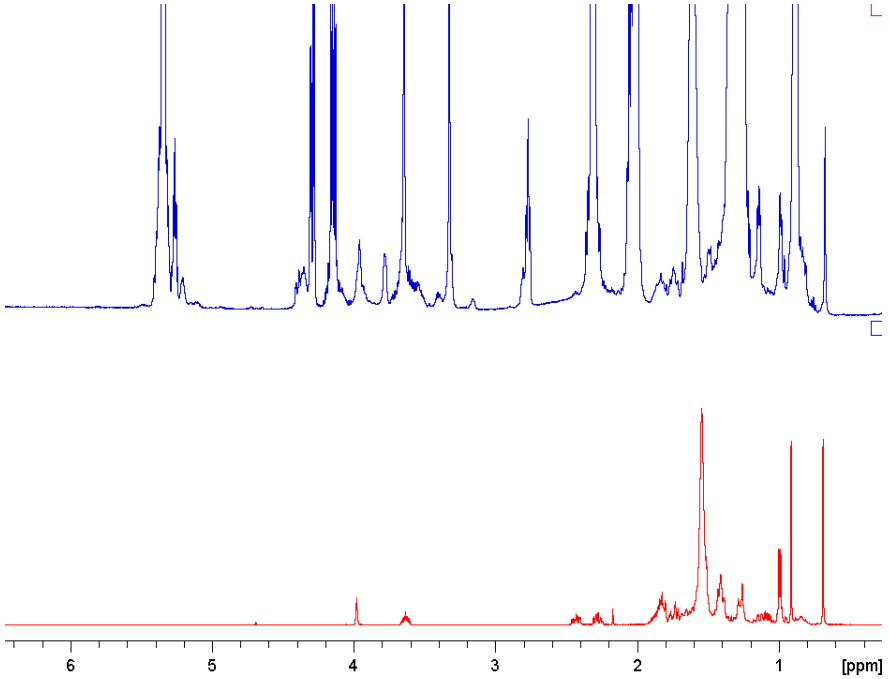

Figure S18. Blue trace: ^{1}H NMR spectrum of disintegrated O^{2}LNC after isopropanol evaporation and further redissolution in $CDCl_3$. Red trace: ^{1}H NMR spectrum of Deoxycholic acid in $CDCl_3$. Acquisitions at 24 ºC, 500 MHz.

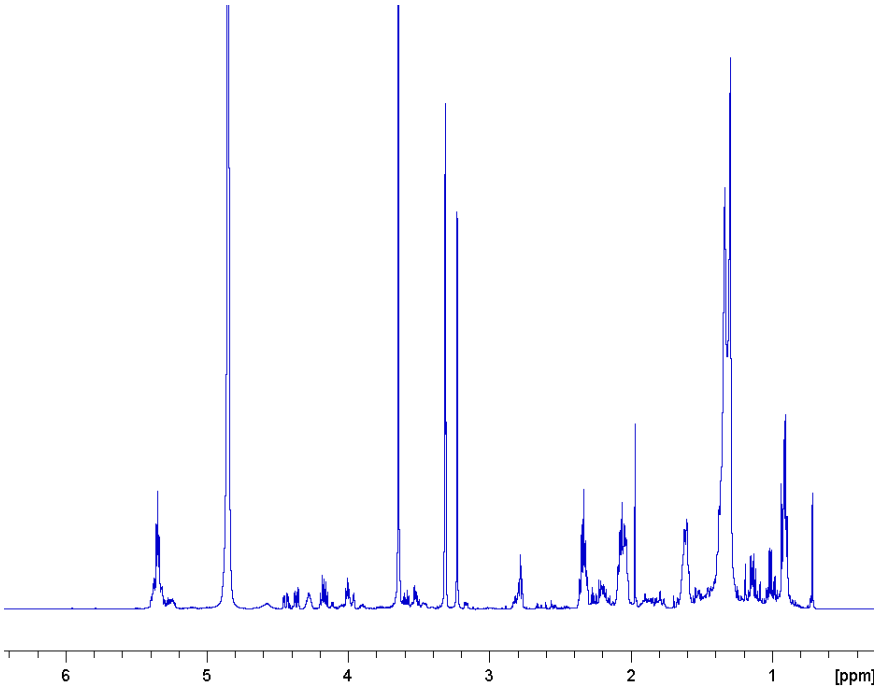

Figure S19. ^{1}H NMR spectrum of disintegrated $O^{2}LNC$ after isopropanol evaporation and further redissolution in CD_3OD (24 ºC, 500 MHz).

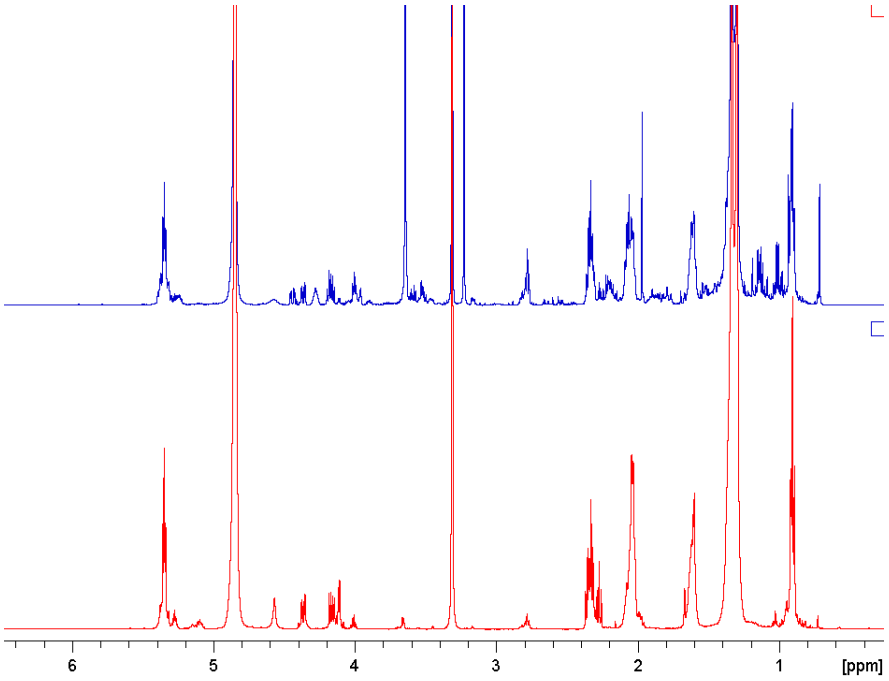

Figure S20. Blue trace: ^{1}H NMR spectrum of $O^{2}LNC$ after isopropanol evaporation and further redissolution in CD_3OD. Red trace: ^{1}H NMR spectrum of olive oil in CD_3OD. Acquisitions at 24 ºC, 500 MHz.

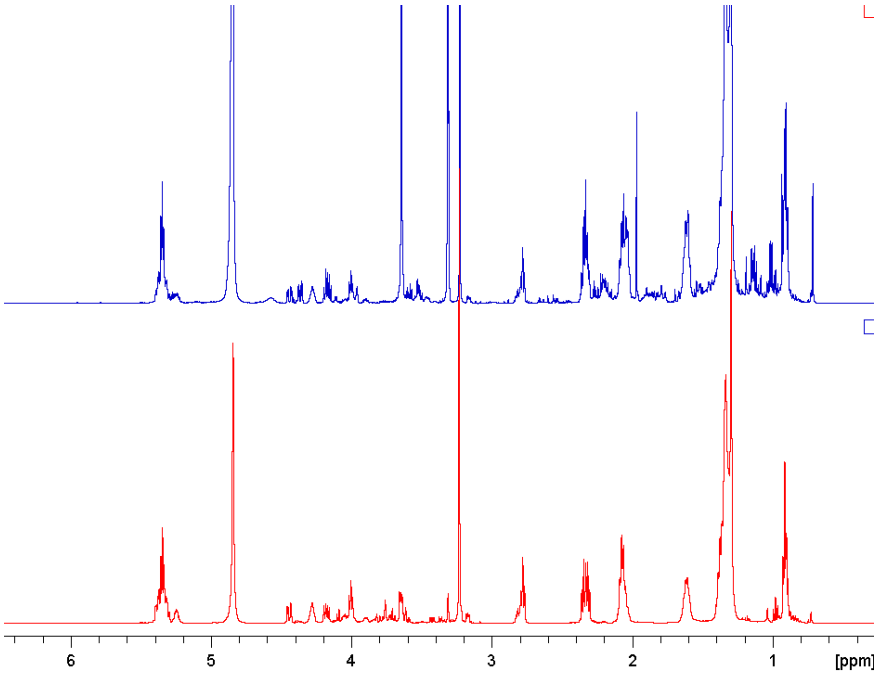

Figure S21. Blue trace: ^{1}H NMR spectrum of O^{2}LNC after isopropanol evaporation and further redissolution in CD_3OD. Red trace: ^{1}H NMR spectrum of Epikuron 145V in CD_3OD. Acquisitions at 24 ºC, 500 MHz.

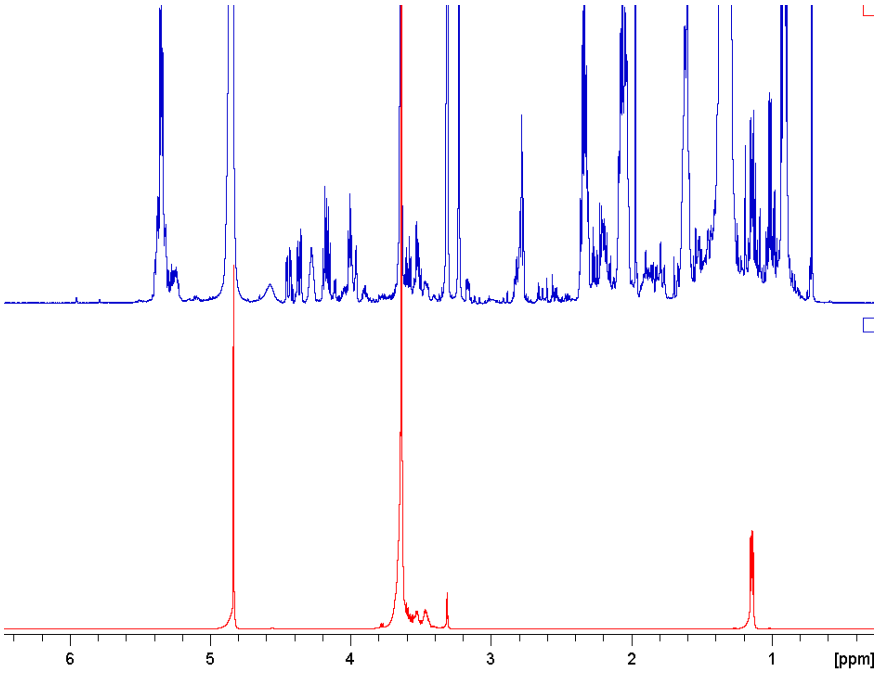

Figure S22. Blue trace: ^{1}H NMR spectrum of O^{2}LNC after isopropanol evaporation and further redissolution in CD_3OD. Red trace: ^{1}H NMR spectrum of Pluronic F-68 in CD_3OD. Acquisitions at 24 ºC, 500 MHz.

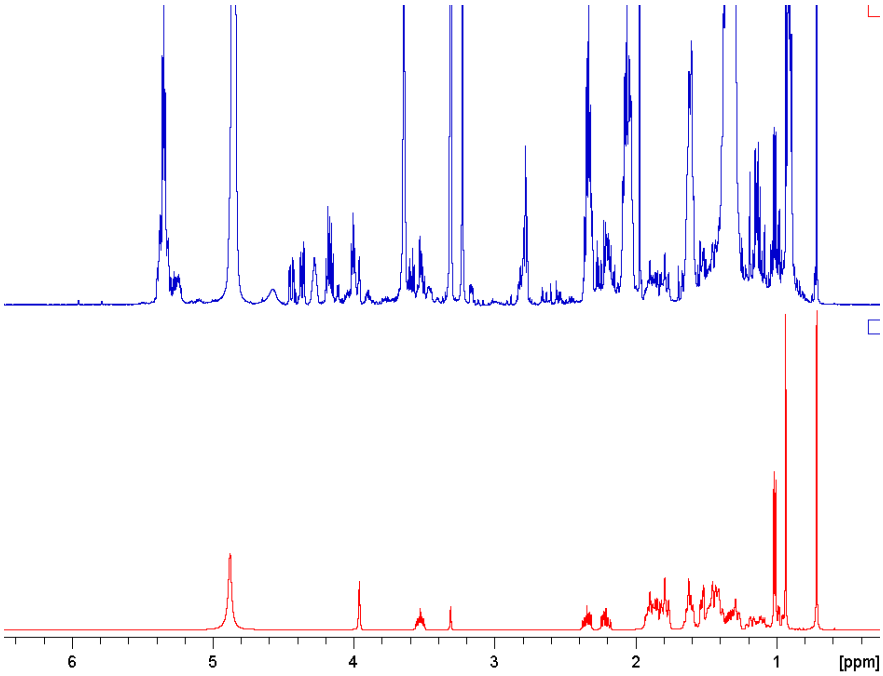

Figure S23. Blue trace: ^{1}H NMR spectrum of O^{2}LNC after isopropanol evaporation and further redissolution in CD_3OD. Red trace: ^{1}H NMR spectrum of Deoxycholic acid in CD_3OD. Acquisitions at 24 ºC, 500 MHz.

CURRICULUM VITAE